Newcastle University

A COMPARISON OF FATIGUE PROPERTIES OF EPOXY COATINGS IN MARINE ENVIRONMENTS

by

Mirjana Vicevic B.Sc.

Thesis submitted in partial requirement for the degree of Doctor of Philosophy
in the School of Chemical Engineering and Advanced Materials of Newcastle University

Corrosion Research Group
School of Chemical Engineering and Advanced Materials
Newcastle University
Newcastle Upon Tyne
U.K.

March 2008

PAGE NUMBERING AS ORIGINAL

ACKNOWLEDGEMENTS

I wish to express my gratitude to Dr Alasdair Charles and Professor Jim White for their supervision, guidance and helpful suggestions throughout this research. I am also indebted to 'International Paint Akzo-Nobel' and 'NECET' for the in-kind and studentship support for the duration of my Ph.D.

This work would not be possible without extremely helpful and skilful technical staff. I would like to thank late Mr Rob Tullin for his technical guidance. Special thanks to Mr Brian Stoker for all his helpful work. Many thanks to Mrs Pauline Carrick and Mr Grant Staines for their constant help and assistance.

My sincere gratitude goes to fellow students and members of staff in the Herschel Building for creating a wonderful place to work.

And finally, thanks to my parents, sister and husband, for always being there for me.

ABSTRACT

Three experimental marine epoxy coatings on steel substrates were tested under four-point bend cyclic-loading in both simulated sea water, at two temperatures, and in air. Freshly prepared and artificially aged coatings were examined. The samples were characterised by sectioning, scanning electron microscopy and EDX elemental analysis. The ageing processes used had multiple stages involving temperature cycles and/or repeated water soaking and drying.

The coatings were loaded at strain amplitudes of 0.15% and 0.22% for 500,000 cycles at frequencies simulating wave action. The coatings showed high fatigue resistance, so slot defects of different depths and widths were introduced to simulate damage in service and to act as crack initiators. This permitted observation of crack propagation under cyclic loading. Additionally, plastic substrates were tried so that tests at higher coating strains of 1.33% could be performed. The results showed that the softest epoxy coating was the most fatigue resistant. An epoxy containing large filler particles (50μm diameter) was the next most resistant while a hard epoxy with small filler particles showed multiple fatigue cracking after 300,000 cycles when tested on steel substrates. No fatigue cracks were observed on aged coatings.

Internal stress measurements were performed that showed the coating which was most resistant to fatigue had the lowest internal stress of around 2 MPa. The other coatings internal stress levels were over 15 MPa. Tensile tests on free-films indicated that the coating most resistant to fatigue showed the lowest tensile strength, approximately 10 MPa, and the highest strain to failure, the latter property being the more important one. Hardness measurements using micro and macro Vickers indentors were performed between stages of an ageing process, along with nano-indentation (to measure Young's modulus) showing that the softest coating exhibited low elasticity. Higher hardness values were observed for coatings after ageing.

TABLE OF CONTENTS

CHAPTER 3:

CHAPTER 4:

TABLE OF FIGURES

CHAPTER 1:

CHAPTER 2:

CHAPTER 3:

CHAPTER 4:

APPENDICES:

LIST OF TABLES

CHAPTER 1.

INTRODUCTION

1.1. STATEMENT OF AIMS AND OBJECTIVES

Premature failure of the protective coating system is a problem that is often noted in the ballast tanks of ships in service. In the past decades a number of ships suffered early failure of protective coatings in the form of cracking [1]. Failures by delamination, blistering and a range of other processes have also been recorded. These failures are costly to the world's shipping business and potentially hazardous to the ship and the crew. An early example of this was the 'Exxon Valdez' accident, Alaska, in March 1989, followed by 'Erika' off the coast of France 1999, 'Castor' in the Mediterranean Sea in 2000 and 'Prestige' more recently near Spain 2002. Once failure occurred, rapid corrosion of the unprotected steel followed soon after with catastrophic consequences. Repair or reinstatement of the failed coating system to the standard that was achieved during the new building stage is extremely difficult.

Following environmental pressures, new cost factors and safety concerns, requirements for anticorrosive protections are changing regardless of the field of application, leading to new trends for both surface preparation and coating type. These needs and corresponding trends have been recognised by numerous authors [2-9].

Since the 90s, increasing attention has been paid to the corrosion of ballast and cargo tanks within the tanker fleet. Several organizations like IMO, IACS, INTERTANKO and SOLAS reacted to those events [10] promoting the study of failure causes and introducing marked changes in the regulatory environment regarding corrosion assessment and control obligations upon ship owners. Further changes have been induced by competitive and consumer pressures to produce environmentally and user friendly coatings without sacrificing ease of application, initial appearance or, most importantly, significantly reducing the expected service life of the coating system.

Guidance that is associated with a requirement for ballast tank coatings is given in number of resolutions by different marine organisations (IMO resolution A.798(19), SOLAS '74 regulation II-I, 3-2-1) and all of them agreed that it is of the utmost importance for coatings to be correctly applied at the ballast tank [6]. The following photographs (Figures 1.1. and 1.2.), [6], show the ballast tanks of two ships of the

same age (13 years). During construction, both ships were coated with an epoxy system; the application of the ballast tank coating for the ship in the first photo was correctly done, whilst that for the ship shown in the second photo was poor. The images show the importance of using correct application procedures (surface preparation and paint system application) and of coating selection.

Figure 1.1. Correct paint application, ballast tank condition after 13 years (a bulk carrier double bottom tank is shown in this example) [6]

Figure 1.2. Poor paint application, ballast tank condition after 13 years (a bulk carrier top side tank is shown in this example) [6]

Coatings are generally applied to ship ballast tank for protection against corrosion. Hard coatings are now mandatory in ballast tanks for all vessels at new building. Coating breakdown in ballast tanks in ships is a well-known phenomenon but very difficult to predict. There are a large number of variables affecting coating breakdown with time, as a result of its application and these influence its service lifetime. The analyses of these variables at various stages of the life of the coating, if identified correctly, may determine the remedial work that is necessary to prolong the coating durability and assure that little corrosion occurs.

Apart from coating failures connected with their application, fatigue cracks, which may occur on all vessel types, not only in ballast tanks, are associated with cyclical stresses and are linked to 'optimised' ship structure, poor design details, corrosion, stress concentration, incorrect use of high tensile steel and a tank's trading

pattern/area of operation. Fatigue cracks are generally found on older vessels although they have been found on vessels within five years of delivery [7]. Fatigue cracks can propagate over time and if no action is taken (repair, renewals or design modification) then a major structural failure may occur. Present practise is for fatigue cracks to be repaired as and when they are found during surveys. The illustration of two ballast tanks with extensive fatigue cracks are shown in Figure 1.3. [6].

Figure 1.3. Fatigue cracks in ballast tanks [6]; structural failure

Currently, most ships are not directly designed for coating fatigue crack control, although there is some underlying consideration of fatigue strength in setting the allowable stress [11, 12]. Structural ship details are selected based on experience with similar details in service. In commercial tankers and bulk carriers fabricated from high-strength steel, the increase in fatigue cracking associated with the use of high-strength steel has become a serious problem. As the allowable primary stress is increased to take advantage of high-strength steel, the magnitude of the stress ranges is also increased. Although the allowable static design stress may be increased, the fatigue strength is essentially unchanged. This is supported by results from fatigue tests which indicate that the fatigue strength of, for example, welded details in air is approximately independent of the type and strength of the steel [13-19]. Therefore, unless the details are upgraded, some areas are more likely to exhibit fatigue

problems. The advanced double-hull ship design is an example of an application of high-strength steel where the fatigue strength of the system is improved through overall design.

The study of cracks propagating extensively in structures has been limited to special applications because of the complexities involved. The fatigue strength of components with various welded details has been studied for decades [15-19] and design curves exist in most structural codes [20-24]. The failure criterion used in these developments is growth of a coating fatigue crack to an easily visible size.

In a "fail-safe" design methodology, cracks are allowed and for this reason structural integrity now depends on inspection procedures to detect fatigue cracks in coatings before they attain a critical length to cause coating failure. In order to establish efficient and reliable inspection intervals, the coating crack growth behaviour must be understood and analytical methods for predicting the rate of growth of fatigue cracks must be developed for both structural details of ship and coatings that protecting those details.

Since the new vessel design and new coating system design as well as comparison of old materials on new structures used in a double-hull ship structure have not been studied before, the fatigue behaviour of this type of coating and structure needs to be investigated.

Despite the acknowledged importance of the fatigue failure of marine coatings, very little research on this area has been reported in the open literature. The research described in this thesis was designed to develop laboratory tests that are relevant to the service conditions experienced by the coatings. The aims of this project were to investigate a range of polymeric coatings on steel substrates under cyclic loading in both wet and dry conditions, to determine the extent and nature of coating failures. Freshly prepared samples as well as artificially aged coatings were tested, the failures were characterised by metallography and scanning electron microscopy. As well as identifying the most fatigue resistant coatings for marine applications, experiments were designed to help devise methods to improve the assessment procedure for

coatings and so to permit acceleration of the introduction of new formulations with extended life.

The aims of this study were:

1. To determine the mechanisms of failure of marine coatings under cyclic loading;
2. To develop test procedures to determine relative rankings of marine coatings of different compositions;
3. To improve the level of understanding of the mechanical properties of epoxy coatings and how they change with time and exposure to various environments related to marine application.

1.2. GENERAL BACKGROUND

As this study had a focus on marine coatings for ballast tanks and their fatigue properties, this part of the introduction will give a general outline for coatings, their definition and typical composition, for fatigue and its mechanism and for ship ballast tanks with explanation of their purpose and some general notes.

1.2.1. COATINGS

A coating can be described as a fluid material capable of being applied or spread over a solid surface which dries or hardens to form a continuous, adherent, cohesive, obliterating skin or film [25]. There are numerous types of surfaces which are painted, such as plastic, metals and alloys and reasons for coating such surfaces fall into three main categories: decoration and/or preservation and/or sanitation (providing a surface which is easily cleaned).

A typical paint composition consists of:
1. Pigment and Extender
2. Binder
3. Solvent
4. Other additives.

The function of each ingredient has an essential part in the performance of the coating.

Pigments and extenders are used in the form of fine powders which are dispersed in the paint binder and are insoluble. The major difference between them is that the pigments are solid and provide colour when dispersed in organic coating whereas extenders have little or no effect on colour or opacity.

In a general classification pigments can be divided conveniently into natural and manufactured products. The latter can be subdivided further into inorganic and organic types.

Natural pigments are usually dull in colour compared with the synthetic products. They are often mixtures and the purity and quality can therefore vary. Chemically they are usually oxides or iron in some form, varying in colour from dull yellows, reds, browns to black. They are all inert or unreactive pigments with good light-fastness.

Organic types of manufactured pigments are available in a wider range of colours, which are much brighter than their inorganic counterparts. However they may vary considerably in light-fastness and opacity. Their molecular structures vary from fairly simple to very complex.

Extenders make no contribution to the colour of the coating, but they have a great influence on its physical properties. These include flow, degree of gloss, pigment suspension, sprayability, water resistance, mechanical strength and hardness, film build (volume solid), hold-up (on vertical surfaces) and chemical resistance. All extenders are inorganic and are chemically inert. They vary considerably in particle size, shape and hardness and mixtures are often used to obtain optimum properties. The vast majority of extenders are much less expensive than pigments and this has the effect of reducing the cost of many coating systems when they are incorporated.

Binders are the film-forming components of coatings and can be considered the most important single ingredient since they control many fundamental properties, both physical and chemical, of the coating. In fact paints are generally named after their binder component (i.e. Chlorinated Rubber paints, Epoxy Paints). Binders used in the manufacture of marine and other protective coating products fall into two classes, convertible types and non-convertible types. The classification relates to how binders change state from liquid to solid or in paint terms how they dry.

Drying is considered to be a two stage process if solvent is required for film formation. Both stages actually occur together but at different rates.

Stage one: Solvent is lost from the film by evaporation and the film may become dry to touch.

Stage two: The film progressively becomes more chemically complex by one of the following mechanisms:

- Reaction with atmospheric oxygen, known as oxidation,
- Reaction with an added chemical curing agent
- Reaction with water.

Whatever method is employed films are formed which are chemically different to the original material and which are not re-soluble in solvent. Types of binders which fall into this category are:

1. Binders dried by oxidation (vegetable drying oils, epoxy ester resins)
2. Binders dried by chemical curing (two-component epoxy resins, two-component polyurethane resins)
3. Binders dried by water absorption (moisture cured polyurethane resins, organic silicate resins)

Non-convertible types of coating binders are simple solutions of various resins in suitable solvent(s). Drying is effected simply by the loss of solvent by evaporation. This is termed physical drying as no chemical change occurs. The resulting film therefore, is always readily soluble in the original solvent and can be softened with heat (thermoplastic). Bitumen and vinyl polymer resins are examples of non-convertible coating binders.

A *solvent* can be defined as a liquid which disperses a solid or semi-solid substance, to give a solution. In the form of paint the solvent(s) dissolves the resin or binders and reduces the viscosity which enables the paint to flow and be applied more easily. The type and quantity of solvent(s) used depends upon the method of coating application, whether it is brush, roller, conventional spray or airless spray. After application, the solvent(s) evaporates and plays no further part in the final coating film. In addition to commercial factors, such as price and availability, the solvent must satisfy a number of different properties, i.e. solvency properties, toxicity, volatility, flammability, odour and legislation on use. All solvent vapours apart from water, are to some degree toxic (some are very toxic). It is therefore necessary to take all the recommended

precautions during painting and cleaning up with particular regard to ventilation and skin protection. Some typical solvent types are water, aliphatic hydrocarbons, aromatic hydrocarbons, alcohols, ketones and esters.

All oil based paints, like epoxy ester and urethane oils, dry when laid out as a film, firstly by solvent evaporation and secondly by oxidation. Driers are added to these types of paint to increase the speed of drying in the second oxidation phase. They act as catalysts by increasing the uptake of oxygen into the film. Modern day driers are compounds of metals, particularly lead, cobalt, manganese, calcium and zinc with fatty or other organic acids such as acids obtained from petroleum. One dryer alone cannot promote good drying and in practice combinations of dryers are used.

To improve the performance of the coating, modern day paints require various *other additives*. The term additive covers a wide range of materials which are essential to good formulation, but which are used in minor proportions of the whole paint. Typical groups of additives are: anti-floating agents, dispersion agents, stabilizers, viscosity controllers, adhesion promoters, antifouling agents and corrosion inhibitors.

1.2.2. SHIP BALLAST TANKS

Ships have always required ballast to operate successfully and safely. For millennia, ships carried solid ballast in the form of rocks, sand, roof tiles, and many other heavy materials. From the 1880s onward, ships increasingly used water for ballast, thereby avoiding time-consuming loading of solid materials and dangerous vessel instabilities resulting from the shifting of solid ballast during a voyage [26]. Today, vessels carry ballast that may be fresh, brackish or salt water. The major purposes of ballasting a vessel for a voyage are to increase its manageability (and safety), particularly under heavy weather conditions; control its draft and trim for maximum efficiency; and control its stability to ensure safe passage [27].

Ballast water is carried by many types of vessels and is held in a variety of tanks or holds. The relative complexity of ballast operations depends on the size, configuration, and requirements of the ship and on the complexity of its pumping and piping systems. Ballast capacity can range from several cubic meters in sailing boats and fishing boats to hundreds of thousands of cubic meters in large cargo carriers. Large tankers can carry in excess of 200,000 m^3 of ballast. Ballasting rates can be as high as 15,000 to 20,000 m^3/h [28].

There is a wide range of ballast tank locations and configurations, as illustrated schematically in Figure 1.4. The capacity, location and flexibility of use of ballast tanks are a focal point in ship design. Consideration of required drafts and trim, hull loading limitations, and required vertical centre of gravity establishes the necessary ballast volume and location [27].

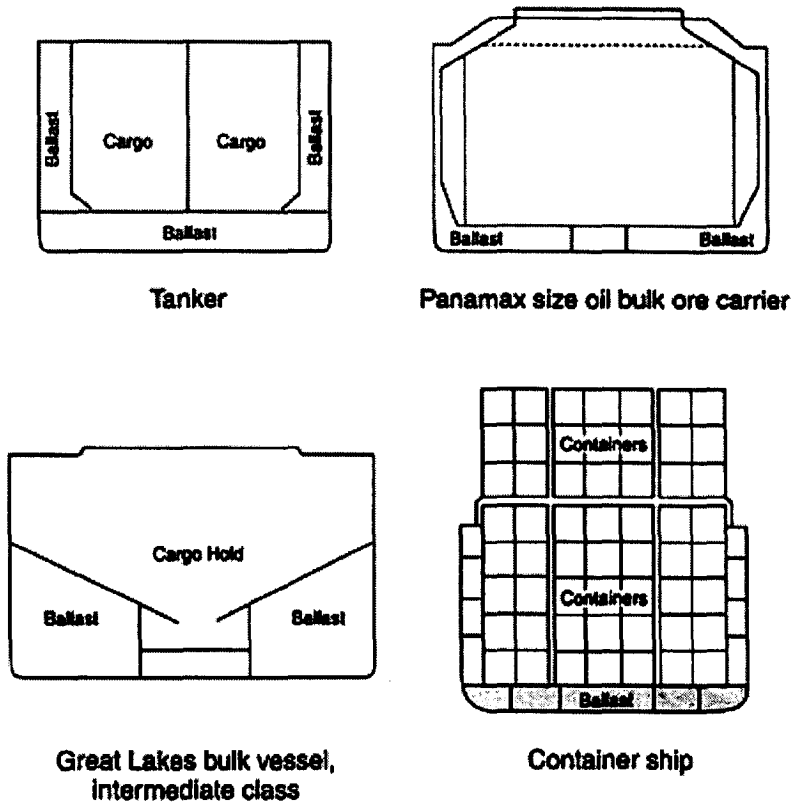

Figure 1.4. Typical ballast tank arrangements [28]

Proper ballasting (in terms of the amount of water taken aboard and its distribution) fulfils the following functions:

- reduces stresses on the hull of the ship;
- provides for transverse stability;
- aids propulsion by controlling the submergence of the propeller;
- aids manoeuvrability by submerging the rudder and reducing the amount of exposed hull surface (freeboard or windage) and
- compensates for weight lost from fuel and water consumption

Ballast condition, including when and how much water is loaded, is determined by ships' officers, based on the specific vessel's operating needs and the national and

international requirements for proper maintenance of the trim and stability of the vessel at sea [26].

Ballast water is taken on board using sea chests with ballast pumps or by gravity feed. Sea chests can be located under the ship, on the turn of the bilge, or on the ship's side and are usually replicated on both sides of the vessel (Figure 1.5.).

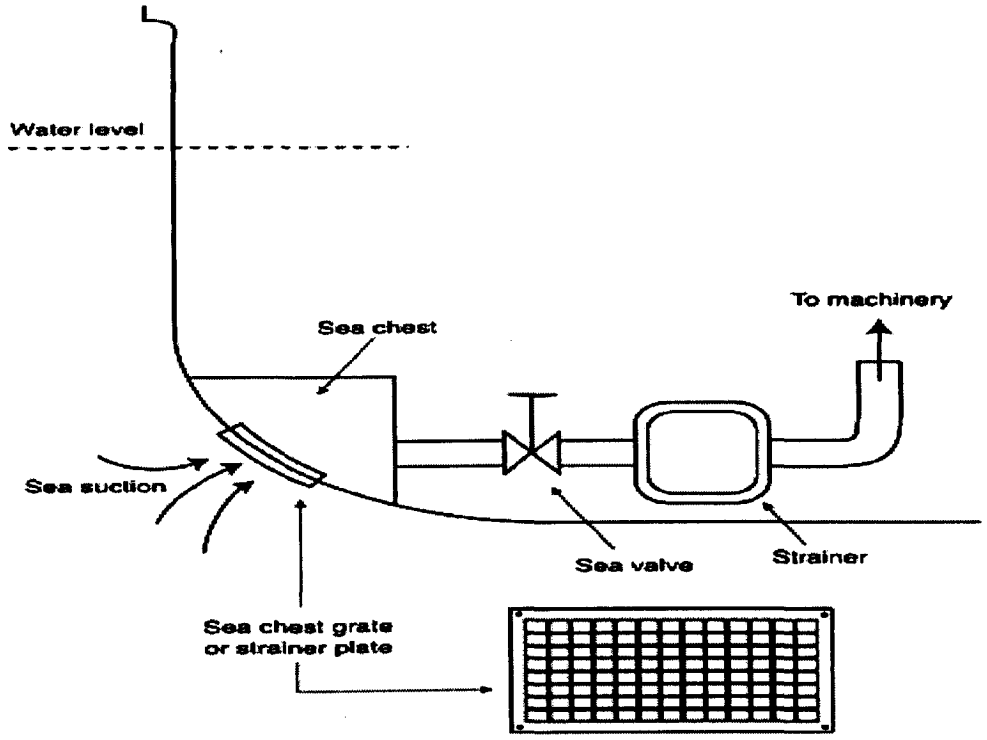

Figure 1.5. Typical ballast system [26]

Ballast water loading and discharging operations are usually controlled from a central ballast monitoring/control station and ballast water can be gravitated in or out of a particular tank or hold, pumped in or out, or a combination of these methods can be used. Ballast pumps remove most of the ballast water. In some cases, separate stripping pumps further reduce the amount of water remaining in the tanks. Trimming of the ship by the stern may also be used to aid ballast removal. Despite these efforts, some ballast water and sediment will always remain on board.

1.2.3. FATIGUE

In materials science, fatigue is the progressive, localised, and permanent structural damage that occurs when a material is subjected to cyclic or fluctuating strains at nominal stresses that have maximum values less than (often much less than) the static yield strength of the material [29]. The low stresses may be still cause catastrophic failure. Under the action of changing stresses a material may become work hardened. Thus, whilst creep is a phenomenon associated with extension under a steady force acting over a long period, usually at high temperatures, fatigue refers to the failure of a material under the action of repeated or fluctuating stresses [30].

Fatigue of materials refers to the changes in properties resulting from the application of cyclic loads. Fatigue failures occur in many different forms. Cyclic loads acting in association with high temperatures cause *creep-fatigue in metals*; when the temperature of the cyclically loaded component also fluctuates, *thermomechanical fatigue* (i.e. a combination of thermal and mechanical fatigue) is induced [31, 32]. Recurring loads imposed in the presence of a chemically aggressive environment give rise to *corrosion-fatigue*. The repeated application of loads in conjunction with rolling contact between materials produces rolling *contact fatigue*, while *fretting fatigue* occurs as a result of pulsating stresses along with oscillatory relative motion and frictional sliding between surfaces. The majority of failures in machinery and structural components can be attributed to one of the above fatigue processes. Such failures generally take place under the influence of cyclic loads, whose peak values are considerably smaller than the 'safe' loads estimated on the basis of static fracture analysis.

1.2.3.1. Basic Mechanisms of Metal Fatigue

Although the stresses and strains may be well below the static resistance level of the metal, damage is accumulating cycle by cycle and after a certain number of load fluctuations a failure will occur. The fatigue process is usually divided into three phases [33]:

1. crack initiation
2. crack growth
3. final fracture.

The crack initiation usually takes place on the surface of the metal in the vicinity of a notch. The mechanism is explained by a slip band mechanism at a microscopic level driven by the maximum shear stress. When the load is imposed, some grains will be subjected to plastic deformation involving the sliding of some of the crystallographic planes. The mechanism is limited to a few grains where these crystallographic planes have an unfavourable orientation with respect to the local maximum shear stress. When the load is reversed, the planes will not slide back to their initial position due to the cyclic stain hardening effect. Hence, in the reversed part of the load cycle, it is the neighbouring planes that will suffer yielding by sliding in the opposite direction. The final result is microscopic extrusions and interference on the metal surface. The interferences act as a micro-crack for further crack extension during the subsequent loading cycles.

After crack initiation has occurred within a few grains, subsequent microscopic growth will extend the crack to pass several grain boundaries. When the crack front reaches over several grains, the crack will continue to grow in a direction perpendicular to the largest tensile principal stress. The initiation phase is related to the surface condition of the metal and governed by the cyclic shear stress whereas the crack growth depends on the material bulk property and the crack is driven by the cyclic principal stresses.

In the growth phase, the crack growth process is explained by a crack opening and front blunting mechanism followed by a subsequent crack closing and front

sharpening mechanism during each load cycle. After one complete cycle, the crack front has advanced a small distance which may be traced by microscopy on the fatigue surface. This advancement corresponding to one load cycle is the distance between so called striations. The magnitude of the advancement depends on the range of the stress intensity factor.

The final fracture in phase three will take place when the crack becomes so large that the remaining ligament of the cross section is too small to transfer the peak of the load cycle or when the local stresses and strains at the crack front inflict a local brittle fracture. In the former case, it is the net section average stresses that are the driving force for the fracture. In the later case, it is a local failure that is driven by the maximum stress intensity factor.

1.2.3.2. Parameters that are Important to the Fatigue Damage Process

1.2.3.2.1. Stress Cycles

Fatigue is caused by repeated cycling of the load. It is a progressive localized damage due to fluctuating stresses and strains on the material. Fatigue cracks initiate and propagate in regions where the strain is most severe [34]. For polymers crack propagation is relatively quick.

It will be advantageous to define briefly the general types of fluctuating stresses which can cause fatigue [35]. Figure 1.6. illustrates a repeated stress cycle in which the maximum stress σ_{max} and minimum stress σ_{min} are not equal. In this illustration they are both tension, but a repeated stress cycle could just as well contain maximum and minimum stresses of opposite signs or both in compression (although fatigue failure is unlikely under compression conditions).

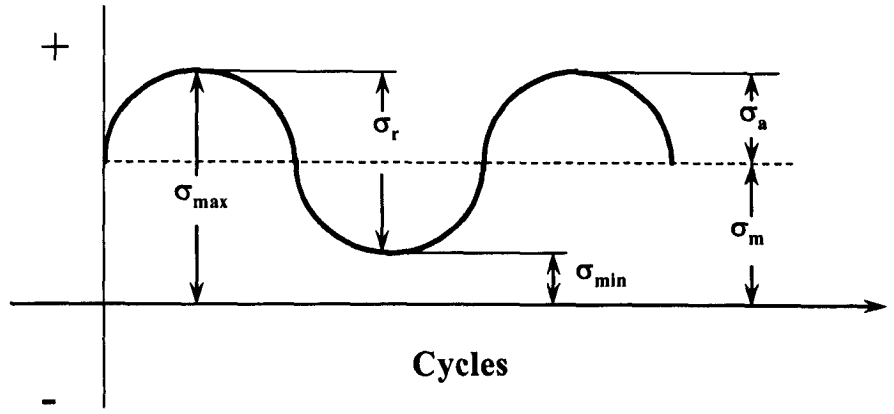

Figure 1.6. Typical fatigue stress cycle, showing cyclic-loading parameters

A fluctuating stress cycle can be considered to be made up of two components, a *mean* or *steady,* stress σ_m and an *alternating* or *variable*, stress σ_a. Another important parameter is the *range of stress* σ_r. The range of stress is the algebraic difference between the maximum and minimum stress in a cycle.

$$\sigma_r = \sigma_{max} - \sigma_{min}$$

The alternating stress, then, in one-half the range of stress.

$$\sigma_a = \frac{\sigma_r}{2} = \frac{\sigma_{max} - \sigma_{min}}{2}$$

The mean stress is the algebraic mean of the maximum and minimum stress in the cycle.

$$\sigma_m = \frac{\sigma_{max} + \sigma_{min}}{2}$$

Two ratios are used in presenting fatigue data:

Amplitude ratio: $$A = \frac{\sigma_a}{\sigma_m} = \frac{1-R}{1+R}$$

1.2.3.2.2. S-N Curve

In fatigue-cycle situations, materials performance is commonly characterised by an *S-N curve*, also known as a *Wöhler curve*. This is a graph of the magnitude of a cyclical stress (*S*) against the cycles to failure (*N*), (Figure 1.7.). A log scale is almost always used for N. The stress values are usually nominal stresses, i.e. there is no adjustment for stress concentration. The S-N relationship is determined for a specified value of σ_a, R or A. Many determinations of the fatigue properties of materials have been made in complete reversed bending, where the mean stress is zero.

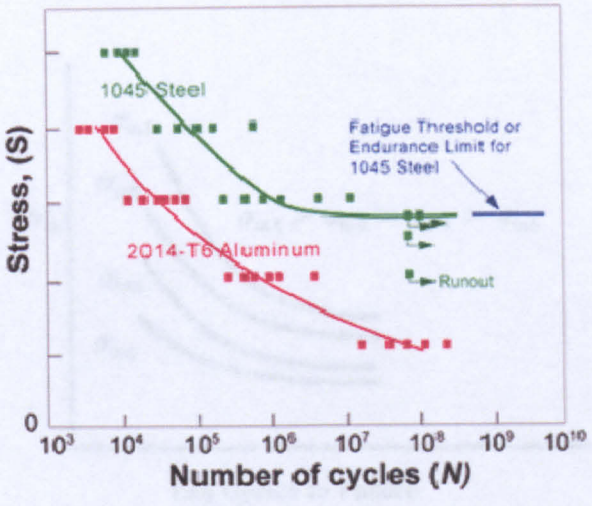

Figure 1.7. Schematic of S-N Curve, showing increase in fatigue life with decreasing stresses [35]

1.2.3.2.3. Stress Ratio

The most commonly used stress ratio is R, the ratio of the minimum stress to the maximum stress ($\sigma_{min}/\sigma_{max}$).

- If the stresses are fully reversed, then **R**= -1;
- If the stresses are partially reversed, **R** is a negative number less than 1;
- If the stress is cycled between a maximum stress and no load, **R**= zero;
- If the stress is cycled between two tensile stresses, **R** is a positive number less than 1.

Variation in the stress ratios can significantly affect fatigue life (Figure 1.8.). The presence of a mean stress component has a substantial effect on fatigue failure. When a tensile mean stress is added to the alternating stresses, a component will fail at lower alternating stress than it does under a fully reversed stress [34].

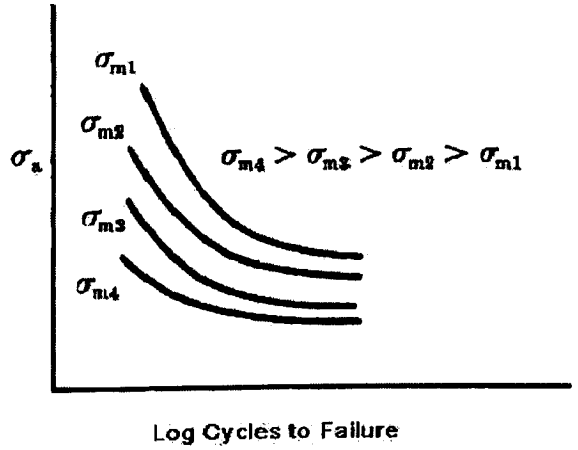

Figure 1.8. Typical effect of stress on fatigue life [34]

1.2.3.2.4. Preventing Fatigue Failure

The most effective method of enhancing fatigue performance of a component is to improve the design:

- Eliminate or reduce stress raisers by streamlining the component;
- Avoid sharp surface tears resulting from punching, stamping, shearing, or other processes;
- Prevent the development of surface discontinuities during processing;
- Reduce or eliminate tensile residual stresses caused by manufacturing;
- Improve the details of fabrication and fastening procedures.

1.2.3.3. Polymer fatigue

In spite of the fundamental differences between metals and polymers, the responses to applied loads appear to be similar. It has been found that some polymers exhibit stress versus cycles to failure curves which are similar to those for metals [36]. Also, a stress below which failure does not occur has been observed.

The deformation resistance of a material may increase (cyclic hardening), decrease (cyclic softening) or remain unchanged (cyclic stability). For most polymers subjected to cyclic strains only cyclic softening has been reported; the extent of this is dependent upon the structure of the polymer. Despite this, it is possible to find exceptions and Beardmore and Rabinowitz in their review of fatigue deformation of polymers [37] illustrate cyclic hardening and cyclic softening under controlled conditions of completely reversed strain cycling. In cyclic hardening, the stress (both tension and compression) required to maintain fixed strain limits increases with increasing number of cycles. Conversely, in cyclic softening, the stress required to maintain fixed strain limits decreases with increasing number of cycles. One of the major distinctions between fatigue of metals and polymers is the degree to which the loading rate influences the stress-strain characteristics and failure modes [38].

Fatigue failure in most polymeric materials occurs basically in the same way. The three stages of fatigue consist of a) reversed plastic deformation, b) crack initiation and c) crack propagation. The molecular mechanism by which the three stages occur depends upon the material. Much work on the examination of fatigue of polymers has been conducted upon glassy polymers (polyethylene, polystyrene, poly(methyl methacrylate) and polycarbonate). In terms of microstructure, these may be classified as single phase polymers.

In the case of semi-crystalline materials, two phases are present-crystalline aggregates in a matrix of amorphous polymer of the same composition [39]. Deformations such as slip, twinning, phase transformations, crystal rotation, unravelling and fibrillation can occur as well.

It may be noted that a major obstacle in the development of life prediction models for fatigue lies in the choice of a definition for crack initiation [38].

The total fatigue life is defined as the sum of the numbers of cycles to initiate a fatigue crack and the number of cycles to propagate it subcritically to some final crack size.

Fatigue cracks can be characterised by the presence of fine striations on the fracture surface. In the polymer fatigue literature, the term striation is exclusively used to represent growth bands on the fracture surface whose spacing equals the rate of crack growth in each stress cycle. The common method of characterising fatigue crack growth in polymers involves use of the Paris law:

$$\frac{da}{dN} = C(\Delta K)^m \quad \text{[m/cycle]} ;$$

where: $\frac{da}{dN}$ is fatigue crack growth rate;

C and m are material constants (m for polymers varies from about 4 to 20);

ΔK is stress intensity factor range.

In polymeric solids only empirical correlations exist between striation spacing and macroscopic crack growth rate. Therefore, no quantitative estimates of ΔK can be derived without recourse to experimental measurements of crack growth rates.

It is known [40, 41] that the variation of fatigue crack growth in a wide variety of amorphous and semicrystalline polymers can be characterised in terms of the stress intensity factor range, ΔK. When characterised in terms of the nominal values of ΔK, polymers exhibit an evidently inferior resistance to fatigue crack growth than metal alloys.

There is a correlation between fatigue crack growth rates and fracture toughness in that polymers with a higher toughness generally show a lower fatigue crack growth

CHAPTER 2

LITERATURE REVIEW

2.1. EPOXY COATINGS

Epoxy resins consist of a linear chain molecule with a reactive epoxy group at each end of the chain. Each particular type of epoxy resin varies in terms of its detailed structure and the length of the chain between the epoxy groups. For example, short chains give liquid resins whereas longer chains give solid epoxy resins [42]. The most commonly used commercially available resins are based on Bisphenol A. The generalized formula for this series is given in Figure 2.1. In this structure, *n*, the number of repeating units, may range from 0 to 24. The resins are liquids at low *n* values (1 or less) and solids of increasing molecular weight and melting point as the value of *n* increases. These resins, therefore, differ in their degree of polymerization, molecular weight, and viscosity.

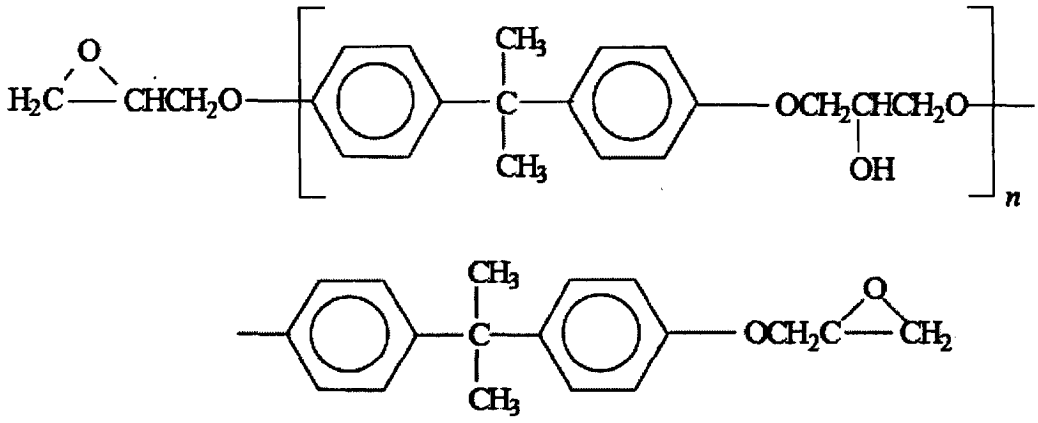

Figure 2.1. Generalised structure for 'Bisphenol A' epoxy resins

A variety of agents can be used to cure epoxies but for marine coating applications the main hardeners are amine based. When mixed with the epoxy resin, the amine 'active site' reacts with the epoxy 'active site' and a chemical bond is formed which links the resin and hardener chains together. Once all the amine sites have reacted with the epoxy sites a three dimensional network is achieved. An important feature of this curing mechanism is that there is a fixed resin-to-hardener ratio [42]. If there is an

excess of either component, a full cross-linked network will not be achieved because some of one or other component will remain unreacted in the polymer network and therefore the mechanical properties of the coating will be degraded. It is for this reason that manufacturers of epoxy systems stress the importance of accurate mixing to the specified ratio.

The actual properties of the final coatings are very much dependent on the type of resin and hardener used. Solid epoxy resins have larger molecules and thereby the distance between cross-linking points is greater, which results in more flexible and resilient films. Liquid resins with shorter chains give harder and stronger films due to more dense cross-linking.

2.1.1. WORKING PROPERTIES OF AN EPOXY

The ambient temperature has a profound affect on the working or handling properties of uncured epoxy as well as its rate and degree of cure. A change in temperature will drastically change an epoxy resin's viscosity [43] and the kinetics of the reaction between the epoxy resin and amine curing agent. The viscosity of water varies little with temperature change until it either boils or freezes. However, the effect of temperature on the viscosity of epoxy is much more continuous. As the temperature drops, the epoxy becomes thicker, reducing its ability to flow. This change has three important consequences when working with epoxies in cold conditions.

First, it is more difficult to meter and mix the resin and hardener. The cold resin and hardener do not flow through the dispensing pumps easily and the thicker material clings to the surface of the pumps, containers and mixing tools [44]. Colder and thicker resin and hardener take much more time and effort to blend thoroughly. The potential for inaccurate metering and incomplete mixing, compounded by a less efficient chemical reaction, greatly increases the possibility of a deficient bond to the substrate when used as a coating.

Second, the epoxy is much harder to apply to a substrate. Cold temperatures make it much more difficult to coat and wet-out surfaces with epoxy [45]. In coating

applications at low temperatures, the epoxy mixture will not flow as easily resulting in thicker, uneven coats. In bonding applications, the thicker epoxy may not wet out or penetrate porous surfaces enough for a reliable bond.

Third, air bubbles may be introduced during mixing or application and held in suspension due to the chilled epoxy's increased viscosity. Air bubbles reduce the epoxy strength in a bond and a coating's effectiveness as a moisture barrier. In addition, air bubbles show through clear coating applications.

2.1.2. THE FUNCTION OF POLYMERIC COATINGS AS CORROSION PROTECTION

The perfect protective coating system, from primer to top coating, must fulfil many functions [46]. A protective coating for marine application should:

- Act as a barrier against seawater and oxygen
- Function in all working environments, regardless of temperature, humidity, service water depth and chemical substances
- Last for many years
- Fit in with other corrosion protection systems such as cathodic protection without causing unfavourable side effects
- Be capable of sacrificial action (metal particles within the coating system are more active electrochemically than the steel to be protected)
- Inhibit corrosion (contain anti-corrosive pigments)
- Be easy to apply with high quality on any substrate, in any environment and by any worker
- Be easy to inspect for failure
- Be easy to repair
- Cost a reasonable amount for production and application and
- Be environmentally friendly to man and nature.

2.1.3. GENERAL FUNCTION OF THE DIFFERENT LAYERS IN A COATING SYSTEM

There are specific functions which each layer of the coating system is designed to fulfil [47, 48]. A primer should have the qualities of

- adhesion to a metal surface
- capacity for sacrificial action when zinc-rich particles are present
- inhibiting corrosion when inhibitive pigments are present.

It is common to apply the top coating in two layers. This method makes it easier to obtain the desired film thickness. The coat applied directly on the primer, the intermediate coat, is supposed to

- give additional thickness for increased mechanical resistance
- give chemical resistance
- supply adhesion between the primer and top coat.

Finally the top coat should have weather and chemical resistance to wear and abrasion. If the coating is to be used in open air, it should also resist change in colour and gloss, as well as UV-radiation.

2.1.4. AGEING PROCESS

Different coatings age in various ways because of a variety of factors including sunlight exposure, migration of compounds out of the polymeric matrix, chemical interaction and elevated temperature. Therefore, coating systems also have different properties which include accounting for ageing.

The ageing effects on the material are related to chemical ageing where the chemical resistance and the resistance to the environment decrease in time. Physical ageing

linked with changes in the mechanical properties of the material, follows chemical ageing. It reduces the flexibility and the toughness of the material, Young's modulus increases and the yield strain as well as the fracture strain decreases [31]. The material gets more brittle, and cracks start to develop in the coating when exposed to high stresses. For coating systems in ballast tanks, ageing is a chemical process where beneficial compounds may migrate out of the material into seawater, thereby resulting in physical ageing.

Usually a high service temperature (T) above the glass transition temperature (T_g) increases the flexibility to a more ductile behaviour for the material. A low service temperature, below T_g, decreases the flexibility and makes the material more brittle [49]. Furthermore, at elevated temperature, the migration-rate of compounds out of the material increases, resulting in chemical ageing of the material. The subsequent degree of physical ageing is determined by temperature range, temperature level and time of exposure. The effect of ageing on mechanical properties of coating materials introduces internal stresses, which usually are tensile. Figure 2.2. illustrates schematically the tensile stresses introduced in coating materials due to ageing with respect to time [50].

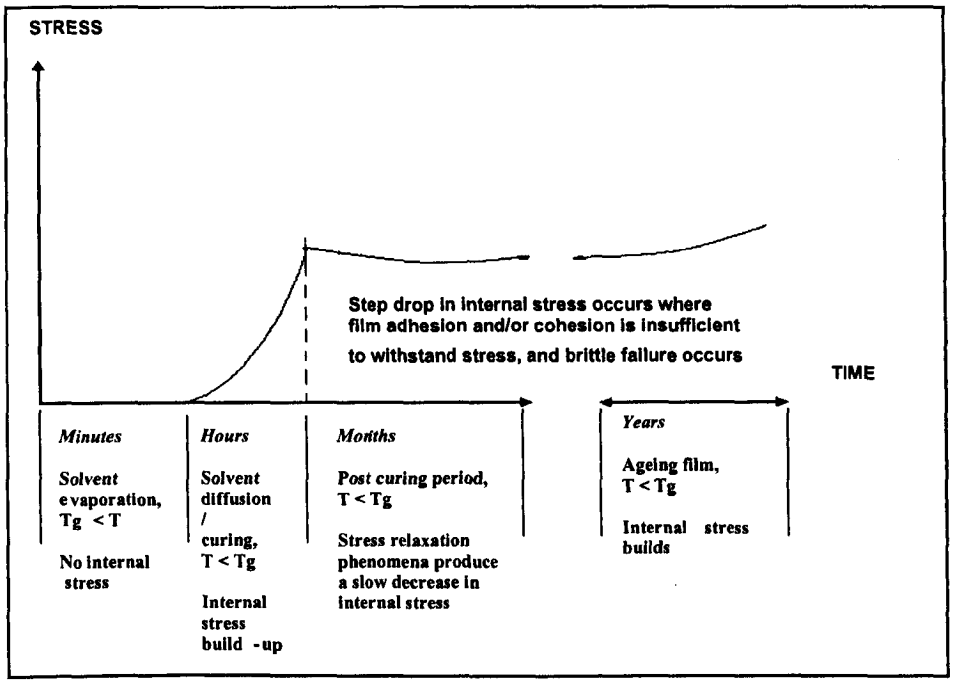

Figure 2.2. Internal tensile stress and the life cycle of the coating film

When polymeric materials are exposed to dynamic loading, internal heat may be generated inside the material. The dynamic loading brings molecular chains in the material matrix into motion [32]. Material properties change rapidly with increased temperature. Extensibility, resistance to environment, and resistance to fatigue, are just a few parameters which are worsened. The threshold of frequency affect on material properties depends on the particular polymer.

Because of their viscoelastic behaviour, polymers generate heat under cyclic deformation which raises the temperature if the rate of heat generation exceeds the heat flow to the surroundings [51]. In view of the characteristically high temperature sensitivity of mechanical polymer properties it is clear that such hysteretic heating can have a major effect on the failure behaviour under cyclic loading. This failure may run the spectrum between excessive softening of the bulk material and ensuing failure by deformation without fracture to the result of localized heating at the tip of a crack accompanied by a redistribution of the stresses and complicated failure characteristics. In the following discussion we shall not address the complications arising from hysteretic heating.

2.2. FAILURE MECHANISMS

The two basic types of failure that occur in coatings are cohesive and adhesive [52]. There can also be a combination of these. The adhesive failures are described as a failure between two interfaces, e.g. between a top layer of a coating and an underlying mid-coat, primer or the steel substrate. Cohesive failure can be vertical or horizontal. The vertical type starts from the coating surface and the cracks grow perpendicular to the coating layer. The horizontal cohesive failure appears as a delamination within a coating layer parallel to the paint film or primer. This type of damage can be difficult to distinguish from adhesion failure when cracks occur very close to a coating interface. However, it is important for product improvement to identify the origin of any failures that appear.

The mechanism by which a coating will fail is governed by a number of parameters. These include not only the properties of the coating, interface, and substrate, but also the distribution of stresses. If the coating is under a residual tensile stress, there are at least three possible mechanisms by which failure can occur [53]. For example, a brittle coating may fracture by the development of cracks through the thickness of the film. Tougher coatings may fail by delamination along the interface or even by the propagation of a crack within the substrate. The failure mechanism associated with a compressive stress in the coating involves simultaneous buckling and delamination.

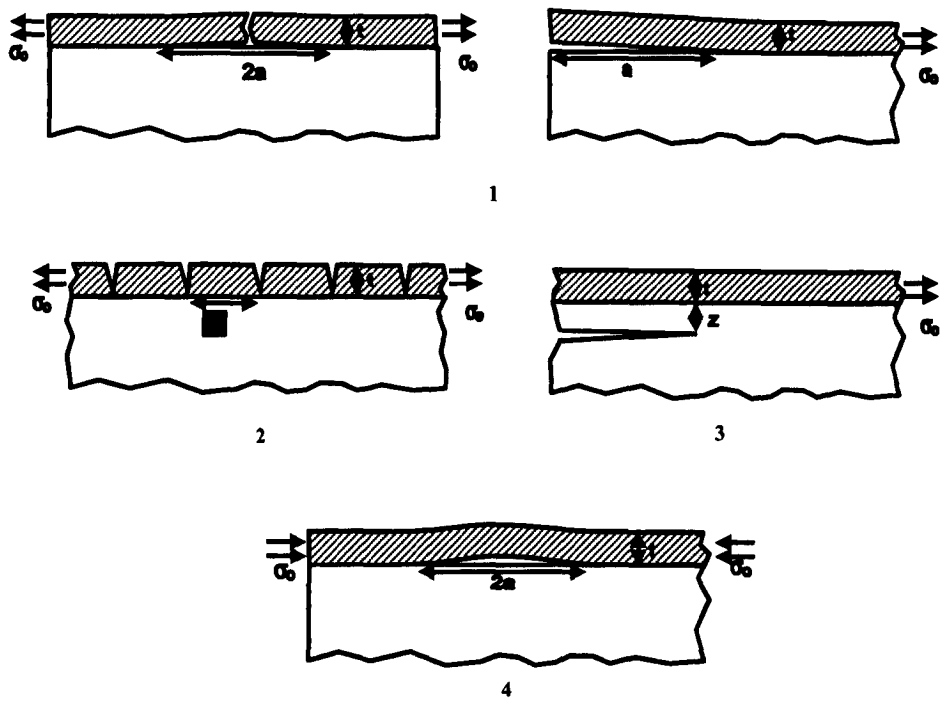

Figure 2.3. Various types of failure occurring in coated systems. (1) Delamination of the interface from a crack in the film and from an edge flaw; (2) Multiple cracking of the film; (3) Substrate cracking and (4) film buckling and associated delamination [53]

2.2.1. THE MECHANISM OF INTERFACE FAILURE

The form of coupling, that is to say the mechanism of interface failure, has been found to depend on the molecular weight of the coupling chains. Short chains can pull out of the bulk material at a force that increases with the length of the pulled-out section. As the length of the chains increases to somewhere between one and four times the length required to an entanglement in the melt, the force required for pullout becomes greater than the force to break chains, so they fail by scission. The scission force is typical of that required to break carbon-carbon bonds, about 2 nN, consistent with both calculations and estimates from flow experiments. The extent of adhesion is strongly affected by the molecular failure mechanism as tough interfaces are normally only

obtained when the failure is by scission. However scission failure does not guarantee a tough interface.

2.2.2. DEFORMATION IN POLYMERS AND EPOXIES

The fracture strengths of most polymeric materials are low compared with those of metals and some other materials. As a general rule, the mode of fracture in polymers is brittle [54]. In simple terms, associated with the fracture process is the formation of cracks at regions where there is localised stress concentration (i.e., scratches, notches and sharp flaws). Factors that influence fracture in polymers are a reduction in temperature, an increase in strain rate, the presence of a sharp notch, increased specimen thickness and/or a modification of polymer structure (chemical, molecular and/or microstructure). One phenomenon that is involved in the fracture of some polymers is crazing. Crazes form at highly stressed regions associated with scratches, flaws, dust particles and molecular inhomogeneities. Unlike cracks, crazes are capable of supporting loads across their faces. The loads supported will be less than in the uncrazed, uncracked materials. If an applied tensile load is sufficient, cracks form along crazes by the breakdown of the structure and expansion of the voids, which is followed by crack tip extension through the craze.

It may be noted that the energy dissipation and failure processes are not as well understood in materials, such as cross-linked polymers, that deform at the crack tip by yield and shear banding, rather than crazing [55, 56]. This lack of understanding is highly relevant in adhesion as the classic structural adhesives, epoxies, are highly cross-linked and do not craze. Instead epoxies deform by the formation of diffuse yield zones. The size of the yield zones, and hence the energy dissipation on crack propagation, can be increased by decreasing the cross-link density of the material. However decreasing the cross-link density inevitably decreases the viscosity and decreases the glass transition temperature of the epoxy, so limiting this approach to increasing the toughness of adhesive joints. The amount of deformation for a given interface stress can also be increased by modifying the epoxy by adding an elastomer or thermoplastic that forms a second phase. Typically an elastomer is dissolved in the

uncured epoxy monomers and a phase separates on curing to form second phase particles, which initiate deformation zones under stress. Because the epoxy forms the continuous phase the elastic modulus and high temperature properties are not profoundly depressed by the elastomer. However the epoxy toughness can increase greatly.

2.2.3. FAILURE ANALYSIS OF SHIP STRUCTURES IN MARINE ENVIRONMENTS

Ship structures while in service are likely to be subject to age related deterioration such as ***corrosion wastage, fatigue cracking or mechanical damage*** (e.g., local denting) which can give rise to significant issues in terms of safety, health, environment and financial expenditures. Indeed, it has reportedly been recognised that such age related deterioration is almost always involved in the catastrophic failures of ship structures including total losses [57-58]. Some researchers studied corrosion of stainless and mild steel in seawater [59]. While such accidents typically cause a great concern to the public, maintenance and repair of aged structures is also very costly and complex. It is thus of great importance to develop advanced technologies which can allow for proper management and control of such age related deterioration.

In the seawater environment, a composite structure is subjected to moisture absorption and fatigue wave loading. Composite materials are known to exhibit some degree of degradation due to moisture absorption [60]. Several studies have examined the fatigue performance of polymeric composites in seawater [61, 62]. By comparing cycles to failure as a function of stress amplitude, some researchers concluded seawater exposure gives degradation in performance, while others observed very little degradation. Few have, however, studied the effect of seawater exposure on damage development and failure mechanisms, which may change, even when there is no significant seawater induced degradation of fatigue strength. Some research has shown that seawater absorption does not significantly reduce the maximum available strain energy release or accelerate the growth of edge cracking in fatigue [62, 63].

When using seawater as a medium, most research tests were performed in natural seawater, collected from the nearest available site or in artificial seawater, made from distilled water and synthetic sea salt or 3 to 3.5% NaCl. The effect of moisture on delamination cracking resistance is critical to the durability of composite materials in seawater environments because delamination crack growth has been identified as one of the dominant failure mechanisms in the fatigue life of composites [57]. A variety of results have been reported on the effect of moisture on delamination cracking resistance of composite materials [63, 64]. Some researchers [62] used the edge delamination test [65] to investigate the effect of seawater exposure on fatigue delamination crack growth.

Corrosion protection of the water ballast tank is achieved by applying coatings to the steel structure. Although the coating is normally very ductile when it is fresh [66], it loses ductility with age [67]. In ageing ships, cracking of the paint is often observed as the primary cause of subsequent, severe corrosion damage to the steel structure. The cracking is typically located in areas of stress concentrations, i.e. fillet welds, transition between structural details, weld toes, etc., where the local stresses are highest [66]. Cracking of the paint due to increasing brittleness or loss of initial flexibility with ageing is often considered to be a primary cause of subsequent, severe corrosion damage to the steel structures in ships' hulls, notably in seawater ballast tanks. There is a recurring state of cyclic loading in ships, due to both temperature variations and movement, which leads to repeated stresses and the presence of relatively large strain magnitudes [52]. According to this reference, very little seems to have been published on the subject of the influence of straining and mechanical fatigue of aged coatings on steel structures for ships. There is an ASTM-standard [68], which describes testing of flexibility properties of polymeric coatings on steel, a bending test done over mandrels of different radii. The tests were performed on specimens according to ASTM-standard E609-92 for uniaxial Low Cycle Fatigue tests [69]. The results from the investigations [52] showed a great spread in the number of cycles to failure of the coating at 0.4% strain, with a variation between 4 and 1,000 cycles. On some of the specimens the cracks appeared on the waist parts of the specimens.

2.2.4. FATIGUE CRACKING

Fatigue crack initiation and fatigue crack growth, are important damage mechanisms in ship structures. An important example of a substrate that is prone to fatigue failure is the large number of longitudinal to web frame connections, which make up an essential part of the production costs of a ship [70]. The slot structures are complicated welded details exposed to dynamic loads during the service of the vessel and, if not adequately designed, significant fatigue cracking may occur causing major costs of repair. For example, this was the case in the early cracking of the second-generation of very large crude oil carriers (VLCCs) [70].

Cracking is a localised problem in ballast tanks and therefore, local detection is needed. As ship structural details are usually similar, there may be repetition of cracking at geometrically similar locations. It is essential to know critical areas prone to cracks for performance of useful surveys [71]. This is easier for standard details, but more difficult in novel designs.

Cracks are most efficiently detected visually as too many locations would need to be monitored by individual sensors. A visual examination should determine the type of crack and assess whether it is likely to propagate. Dye penetrant and magnetic particle tests can also be used after visual inspection, providing approximate measure of surface crack length but not of crack depth. Photographic records of both may be kept. Assessment methods other than visual inspections are generally seldom used for ship structures because a single crack does not impair structural safety due to redundancy. A few researchers compare several methods for fatigue and fracture of ship structures [72-75]. Other, more advanced, techniques include: Acoustic Emission, Infrared Thermography, Laser Shearography, Potential Drop test (ACPD or DCPD), Alternating Current Field Measurement (ACFM), Crack Propagation Gauges, and Automated Ball Indentation. Other methods are commonly used in the offshore field for inspection as well as monitoring. Eddy current, ultrasonics, ACPD, and DCPD are generally able to characterize crack dimensions and location with different degrees of accuracy, and better than visual inspection [76].

Generally, crack detection needs off-service inspections. Ultrasonic surface guided waves were proposed by Vanlanduit [77] for in-service monitoring. One of the advantages of this method is that working stresses do not need to be released and therefore open cracks can be detected, making this method very sensitive. Talei-Faz [78] introduced a novel digital photogrammetric method. The technique allows for real time three-dimensional measurements of local deformations.

Recently a non-contact real-time strain measurement and control system has been established and was successfully utilized in fatigue tests on a epoxy polymer [79]. Uniaxial fatigue tests on a epoxy resin were carried out by this system and quantitative analysis on evolution of various mechanical parameters was conducted [80]. Strain-range-controlled fatigue tests of an epoxy resin with various mean stress/strain levels were also carried out [81].

Kim and Nairn [82] tested a series of coating/substrate systems using four-point bending. The coatings in these specimens usually failed by multiple cracking and they recorded the density of coating cracks as a function of bending strain. These experimental results were fitted to a new fracture mechanics theory of coating failure that predicts the next coating crack forms when the energy released by that fracture event exceeds the toughness of the coating. This fitting procedure led to an experimental result for coating fracture toughness. It was found that coating toughness continually dropped as the coatings were baked for longer times. The toughness of polymeric coatings on steel substrates was more than an order of magnitude lower than the toughness of the same coating on polymeric substrates. The coating toughness was also weakly dependent on coating thickness and it increased as the coating got thicker.

Cyclic fatigue tests on an epoxy polymer were carried out under stress-controlled mode with various combinations of mean stresses and stress amplitudes [83]. The cyclic fatigue tests were carried out with a loading rate of 10MPa/s and at the laboratory ambient temperature. Quantitative results on the evolution of mechanical properties were retrieved from the stress–strain data acquired by a non-contact real-time strain measurement and control system. Analyses of effects of different loading parameters on the evolution of mechanical properties were conducted. Further

investigation by performing additional cyclic tests with multiple resting periods found that strain in the epoxy polymer is mainly recoverable viscoelastic deformation, which will not introduce damage in the material.

Since cracks can conceivably lead to catastrophic failure of a structure, it is essential to properly consider and establish relevant crack tolerant design procedures for structures, in addition to implementation of close-up surveys and maintenance strategies. For reliability assessment of aging structures under extreme loads, it is often necessary to take into account a known (existing or assumed or anticipated) crack for the ultimate limit state analysis as a parameter of influence [84]. To make this possible, it is necessary to develop a time-dependent fatigue crack model which can predict crack damage in location and size as the ship ages.

Fatigue cracks propagate with time progressively in a ductile material. The time-variant cracking damage model is composed of the three separate models, namely: (a) crack initiation assessment or detection, (b) crack growth assessment, (c) failure assessment [85-87].

Crack initiation at a critical structural detail is typically predicted using the S-N curve approach (S = stress range, N = number of cycle until crack occurrence). Cracks at critical joints and details can be detected during inspection when the crack size is large enough, usually about 15 to 30mm. In terms of integrity of aged ship structures, it is assumed that a crack with a certain length at a critical joint or detail initiated some time earlier [88].

Crack growth is assessed by fracture mechanics. In this approach, a major task is to establish the relevant crack growth equations or 'laws' as a function of time (years). The crack growth rate is expressed as a function of the stress intensity factor at the crack tip, based on the assumption that the yielded area around the crack tip is relatively small. The Paris-Erdogan law is often used for this purpose [86, 89].

The duration of each of the stages of fatigue depends on the magnitude of the cyclic stresses or strains at the crack initiation site and along the crack propagation path,

environmental effects, and the resistance of the material to the initiation and propagation of fatigue cracks.

For most engineering materials the failure behaviour is characterized in terms of crack growth per cycle. Initial investigations of polymer fatigue were, therefore, also geared to examinations of crack growth per deformation cycle [90-92]. This behaviour may be appropriate as long as the temperature of the elastomer is well above the glass transition and deformation rates at the crack tip are "somehow small". However, when these rates are comparable to those that give rise to a rate dependent expenditure of fracture energy the question arises whether it is the time spent at elevated stress rather than merely the number of cycles that determine the amount of crack growth. In as much as standard fatigue analysis refers to crack growth as a function of the differential between maximum and minimum stress intensity factor during a cycle one must also ask whether such a characterization is justified for elastomeric solids.

Study has shown [81, 92] that the tear energy could be used, at least approximately, as a correlator for crack growth under both monotonic or static as well as cyclic load histories, although the effect of cycle frequency was considered to be secondary. It was then shown that crack growth in elastomers is essentially governed by the duration of crack tip load rather than merely the number of load cycles [93], although with sufficiently high frequencies the viscoelastically controlled deformations at the crack tip become increasingly important. Figure 2.4. shows crack growth in a polyurethane elastomer under different frequencies, which virtually collapse onto a single curve when plotted against the true rate velocity instead of cyclic growth rate.

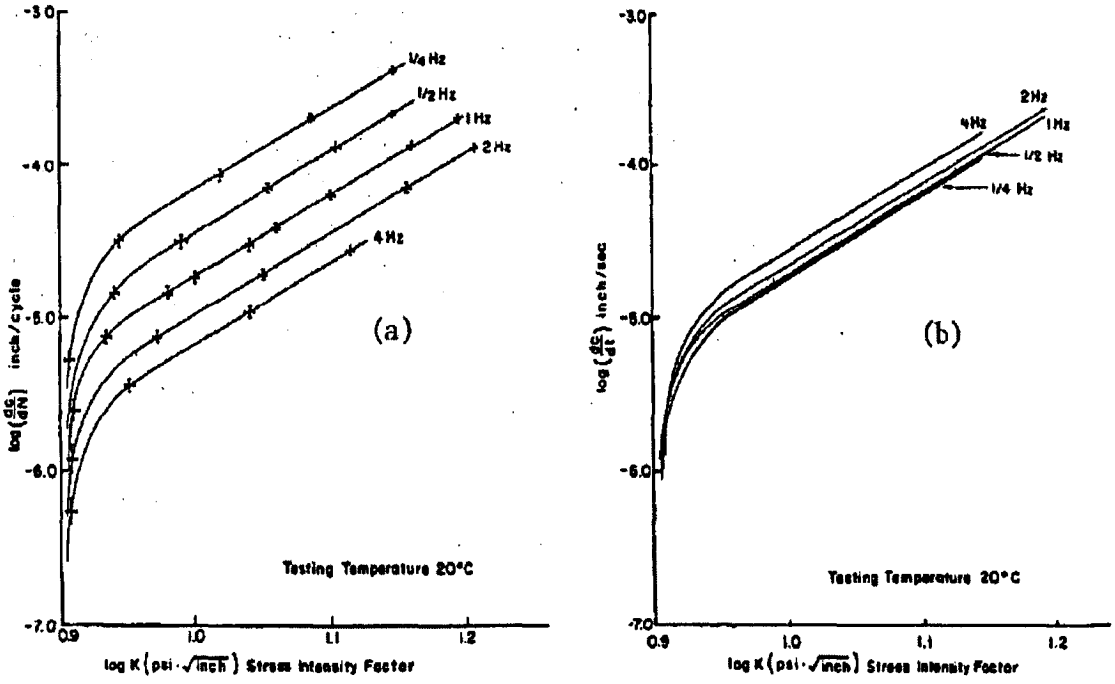

Figure 2.4. Crack growth rate in a polyurethane elastomer; a) cyclic growth rate at different frequencies; b) average velocity $d\bar{a}/dt$ [93]

Similar behaviour is not expected when the material is below its glass transition temperature and when nonlinear material behaviour occurs that is reminiscent of (metal) yield with significant irreversible deformations that influence the stress redistribution during each load cycle. In as much as crosslinking limits the degree of molecular re-arrangement of molecules in the material around the crack tip one would expect that thermosets propagate fatigue cracks more readily than thermoplastics; that this is indeed the case has been demonstrated by Herztberg [40] on the one hand for PMMA crosslinked to differing degrees and by Kim [94] by means of an epoxy crosslinked to different degrees as shown in Figure 2.5. There appears to be no data available that sheds light on the importance of cycle frequency on fatigue crack propagation in thermosets other than the qualitative developments that result from the hysteretic heating mentioned above.

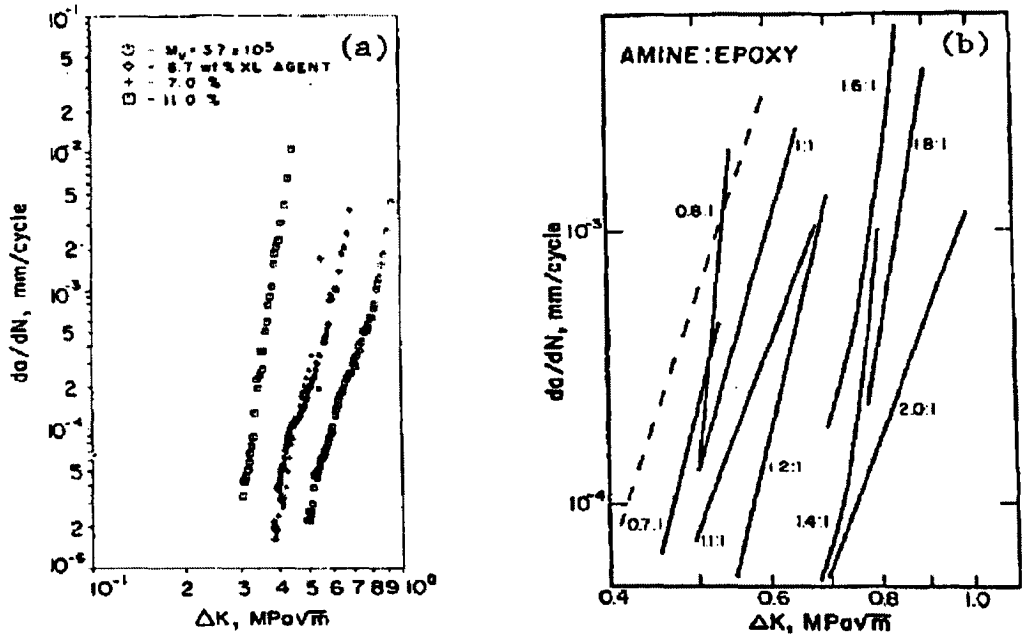

Figure 2.5. Effect of cross-linking on fatigue crack growth; increased cross-linking moves curves to lower ΔK; a) PMMA (Hertzberg, 1980); XL is percentage cross-linking agent; b) Epoxy (Kim, 1978); showing influence of amine-epoxy ratio on ΔK

Estimates of the expected life (durability) of protective (organic) coatings for ships are increasingly desired for the rational management of maintenance practise and the setting of asset policies. The life of coatings also has an influence on the prediction of safe remaining structural life, particularly for ships already subjected to coating deterioration.

Methods for quantitative evaluation of protective coatings are reviewed by Martin [95]. These include direct field and laboratory testing, accelerated laboratory testing and various subjective estimation procedures. Assessment may then be based on subjective interpolation and extrapolation, sometimes with the aid of knowledge-based systems [96]. Field observations have tended to show that percentage coating breakdown as a function of time of exposure can be modelled by a normal distribution, and this has been used by several investigators to propose mathematical models for coating breakdown. Similarly, a few researchers have proposed that coating life could be taken as a normal random variable. However, they did not define what they meant by coating life and it appears to have been assumed as a discrete quantity rather than one of gradual degradation.

More recently, Adamson [97] has used industrial field experience to attempt to correlate field data and opinion for coating degradation with coating characteristics. Degradation was represented in terms of ASTM rust grades and this was found to be a bilinear function of length and severity of exposure.

Another survey was performed by Melchers and Jiang [42] and it was conducted using experts from vessel users, coating contractors and suppliers, and an independent expert. As might be expected, the users tended to be more pessimistic and the contractors/suppliers more optimistic in their estimates compared with those of the independent expert. The collective estimates are reasonably consistent with a normal distribution. It was also found that coating life, described as percentage area breakdown, is approximately normal distributed with both increasing mean deterioration and variance.

Perhaps the most important concept for developing the empirical means of the fatigue process is the S-N diagram (see Chapter 1.3.2). Statistical variability is troublesome in fatigue testing; it is necessary to measure the lifetimes of perhaps twenty specimens at each of ten or so load levels to define the S - N curve with statistical confidence [98]. Obtaining a full S - N curve is a tedious and expensive procedure.

Despite attempts to develop mathematical models of coating deterioration, there is still insufficient unbiased data obtained from actual field experience for sufficiently well-defined vessel areas such as ballast tanks, known to be particularly prone to coating breakdown and poor inspection.

2.3. MECHANICAL PROPERTIES

The mechanical properties of polymers are specified with many of the same parameters that are used for metals, that is, modulus of elasticity, tensile, impact and fatigue strength. For the characterisation of some of the mechanical properties for polymeric materials, simple stress-strain tests can be employed. Polymers are highly sensitive to the rate of deformation (strain rate), the temperature and the chemical nature of the environment.

2.3.1. MECHANICAL PROPERTIES OF THE COATINGS

Mechanical properties such as tensile strength, elongation, and toughness are important characteristics of coatings [99]. Outdoor coatings must withstand the tensile and compressive forces that occur and cause expansion and compression during each day and with the changing seasons, the temperature changes. The changes in the coating occur many times over the course of a number of years. Therefore, the coating–steel composite must have excellent adhesion, strength and toughness to withstand the difficult service conditions.

Polymers behave as both a viscous liquid and a spring-like elastomer. Mechanical properties exhibited by polymer materials are due to such viscoelastic dualism. It is evident [100, 101] that as they are subjected to short-term loads with low deflection and small loads at room temperature, polymers act usually as springs, returning to their previous shape after the load is released. Long-term loads or elevated temperatures make polymers behave in a viscous way. They will deform and flow similarly to viscous liquids, although still solid.

Tensile properties [102, 103] are those characteristics that any material exhibits when a uniaxial force F is applied to a specimen of length L_0 and cross-sectional area A, as depicted in Figure 2.6. Under no-load conditions, the specimen is at rest. When the force is applied, the specimen experiences a tensile stress, that is equal to the applied force per unit area and an elongation to a final length, L, involving a tensile strain,

which is given by change in length per unit length. In the region where stress is directly proportional to strain, a tensile modulus [104], E, can be defined as the slope of the stress–strain relationship as shown in Equations (1) and (2).

$$E = \frac{\text{Tensile stress}}{\text{Tensile strain}} = \frac{\text{Force per unit area}}{\text{Change in length per unit area}} \quad (1)$$

$$E = \frac{F}{A} \div \frac{\Delta L}{L_0} = \frac{\sigma}{\varepsilon} \quad (2)$$

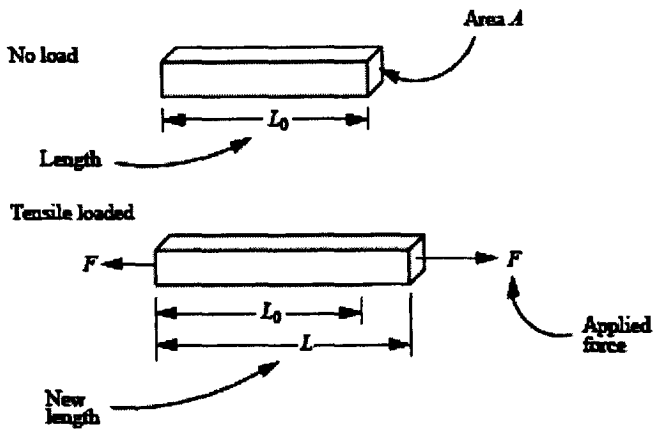

Figure 2.6. A specimen at rest and in a tensile-loaded condition

However, polymers and coatings actually have no measurable region where stress is proportional to strain because polymer molecules can flow under an applied force [105, 106]. That is, polymers are not elastic in nature; rather they are viscoelastic and slowly flow when placed under conditions of loading. The modulus of viscoelastic materials has a storage or completely recoverable elastic component (E') and a viscous or loss component (E'') that is not recoverable and represents the energy which is lost through viscous heating during the stressing process. To circumvent this problem, when measured under static conditions, the value of E is calculated by

measuring the stress at some stated, fixed strain, usually 1% or less, and dividing it by the strain [107, 108].

Dynamic mechanical analysis (DMA) is a technique that enables the two components E' and E'', which together are known as the complex tensile modulus, $E^*, (E^*=E'+iE'')$ to be distinguished and measured [109].

Flexibility is the ability of a coating to be bent or flexed in forming operations without cracking, losing adhesion or failing in some other manner. Flexibility is usually measured by a mandrel bend test [110] or a T-bend test [111].

Toughness is the ability of a coating to withstand large stresses imposed over a short time without cracking, rupturing, shattering or tearing [110]. Toughness can be defined as the ability of a coating to withstand an impact without cracking or breaking. It is dependent on the nature of the polymer or polymers used in the coating and on adhesion. Impact resistance, which is related to formability, can be measured by dropping a weight from various heights through a guide tube onto an indenter that rests on the surface of the coated substrate [111].

The importance of adhesion, the ability of a coating to resist removal from the surface to which is applied, is significant [112]. Such adhesion can be between substrate and coating, between a primer coating and a top coating or between coatings applied to an existing coating. In addition, the coating must adhere under various weathering and cleaning, usually in aqueous conditions. When considering polymer adhesion it is important to recognise that the bulk mechanical properties of the polymer control the type of interfacial forces required for good adhesion. High adhesion can only be obtained if the interface can sustain sufficient stress to induce dissipative forms of deformation, such as flow, yield or crazing, in the polymer. Under most circumstances such deformation modes can only be obtained when the interface is coupled with a sufficient density of covalent bonds, together with perhaps some toughening effects due to surface roughness. However the rubbery but viscous polymer mixtures that make up pressure sensitive adhesives deform and dissipate energy at low stresses and so are capable of giving strong adhesion at an interface coupled just by Van der Waals forces.

Adhesion between a polymer and a substrate often shows a maximum as a function of the number of grafted chains, or alternatively, the density of 'stickers' along a chain. This maximum is believed to have its origin in the requirement that the chains that are attached or tethered to the substrate must also entangle with the bulk material. The entanglement is restricted if the chains are densely end-tethered or, alternatively, have a high density of sticker groups along them.

2.3.2. YOUNG'S MODULUS

The Young's modulus or elastic modulus in tension measures the resistance of a material to elastic deformation. The Young's modulus which was first introduced by Thomas Young, with an investigation of tension and compression of prismatic bars, is measured as the slope of the linear elastic region of the stress-strain curve, when the material is below its elastic limit or yield point.

In this region the material obeys the Hooke's law:

$$\sigma = E\varepsilon$$

Where σ is the stress, ε is the strain and E, the proportionality constant is the Young's modulus. The linear relationship between stress and strain is valid for very low strains for most materials, but beyond that strain some of the materials fracture or plastic deformation appears.

Young's modulus for bulk materials is usually obtained by performing some simple tensile tests. Many techniques are used for the measurement of Young's modulus of thin films like Brillouin scattering [113]; strain gauge measurements [114]; line focus acoustic microscopy [115]; beam-bending tests [116] and nanoindentation [117].

2.3.3. POISSON'S RATIO

When stress is applied to a material, it responds by developing strain. A tensile stress produces the so-called tensile strain. If a cube shaped material of side l is stretched by a length Δl, the nominal tensile strain would be

$$\varepsilon_{nt} = \frac{\Delta l}{l}$$

When it extends in this manner, to conserve volume, the cube gets thinner and the height variation is Δh. Hence the nominal lateral strain is described as

$$\varepsilon_{nl} = \frac{\Delta h}{l}$$

The amount by which it shrinks inwards is described by the Poisson's ratio, ν, which is the negative of the ratio of the lateral strain to the original tensile strain. Hence

$$\nu = -\frac{\varepsilon_{nl}}{\varepsilon_{nt}}$$

It is very difficult to measure the Poisson's ratio of coatings and bulk values are often used in stress calculations. This does not introduce very large errors because most calculations are relatively insensitive to the precise value of ν. One method that can be used to measure ν is to compare the contact modulus, $E_{c,}$ with the Young's modulus, E, measured by a different technique since

$$E_c = \frac{E}{1-\nu^2}$$

2.3.4. HARDNESS

Coating hardness is the ability to resist permanent indentation, scratching, cutting and penetration by a hard object [118]. Hardness is not a fundamental property of a material its values are arbitrary and there are no absolute standards of hardness. Hardness has no quantitative value, except in terms of a given load applied in a specified manner for a specified duration and a specified penetrator shape [119].

The most commonly used hardness measurements are the scratch hardness and static indentation hardness [120]. Scratch hardness depends on the ability of one material to scratch another, or to be scratched by another solid. Solid and thin film surfaces are scratched by a sharp stylus made of a hard material typically diamond, and either the loads required to scratch or fracture the surface, or delaminate the film or the normal/tangential load-scratch size relationships are used as a measure of scratch hardness and/or interfacial adhesion [121, 122].

The methods most widely used in determining the hardness of materials are static indentation methods. In these indentation methods, a spherical, conical, or pyramidal indenter is forced into the surface of the material and forms a permanent indentation in the surface of the material to be examined. Hardness can be measured from the indent in the surface using the formula:

$$H = \frac{P}{A}$$

Where P is the load applied and A is either the area of contact or the projected area of the impression left after the indenter is removed. An equivalent expression for hardness is [120].

$$H = \frac{W}{V}$$

Where W is the work of indentation and V is the plastically deformed volume.

The hardness number [GPa] equivalent to the average pressure under the indenter, is calculated as the applied normal load divided by either the indent surface area (Brinell, Rockwell, and Vickers hardness numbers), or the projected area (Knoop and Berkovich hardness numbers) of the contact between the indenter and the material being tested, under load [123-126]. In a conventional indentation hardness test, the contact area is determined by measuring the indentation size with a microscope after the sample is unloaded.

Hardness testing can be divided into three categories, Macrohardness, Microhardness and Nanohardness. Macrohardness refers to testing with applied loads on the indenter of more than 9.81N. In Microhardness testing, applied loads are 9.81N and below. And Nanohardness is a process where a tip of known geometry is pressed against the material with low loads from a few μN to up to 500 mN.

Though there are many ways of making hardness measurements, like the scratch test with a file to measure the resistance of the material to scratching [127] and a scleroscope test that measures the rebound of a weight that is bounced off the surface of a material [119], in this thesis we will be discussing indentation hardness measurements made at Macro, Micro and Nano levels.

2.3.4.1. Macrohardness

Macrohardness measurements are conducted to assess the bulk hardness. The main equipment used for these measurements are the Brinell for soft materials and Rockwell and Vickers for hard materials hardness testers [124].

2.3.4.1.1. Brinell Test

The first standardized and widely accepted indentation-hardness test was proposed by J.A.Brinell in 1900 [127]. Brinell hardness is determined by forcing a hardened sphere, a 10mm diameter steel ball, under a known load into the surface of a material, and measuring the diameter of the indentation left after the test. The load is maintained for about 30 seconds, and the diameter of indentation at the surface is measured with a low powered light microscope after the ball has been removed. For good results an average of 2 readings of the diameter of the impressions at right angles should be made, also the surface on which the indentation is made should be relatively smooth and free from dirt [35]. The Brinell hardness number (BHN) or simply the Brinell number, is defined in kilograms per square millimeter, as the ratio of the load used to the actual surface area of the indentation, which is, in turn, given in terms of the imposed load W, ball diameter D, and the indentation diameter d or depth of indentation H.

$$BHN = \frac{2W}{\pi D(D - \sqrt{D^2 - d^2})} = \frac{W}{\pi DH}$$

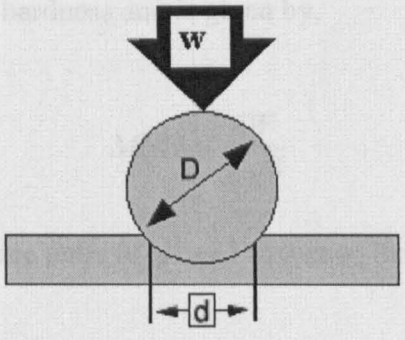

Figure 2.7. Brinell hardness test

Hardened steel balls bearing are usually used up to 450 BHN, but beyond this hardness, specially treated steel or tungsten carbide balls are used to avoid flattening of the indenter. As mentioned earlier the standard size ball is 10 mm diameter and the standard loads are 3000, 1500, and 500 kg, with 250, 125, and 100 kg sometimes used for softer materials. The load and the ball diameter are adjusted to keep the ratio *d/D* within the range of 0.3 to 0.5.

The main advantage of the Brinell test is that one scale covers a large hardness range, although comparable results can only be obtained if the ball size and test force relationship is the same and there are a wide range of test forces and ball sizes to suit most applications. The main drawback of the Brinell test is the need to optically measure the indent size. This requires that the test point be finished well enough to make an accurate measurement. In addition also the test is quite slow, since one indent can take up to 30 seconds not counting the sample preparation time.

Meyer [128] suggested that a more rational definition of hardness than that proposed by Brinell would be one based on the projected area of the impression rather than the surface area. The mean pressure between the surface of the indenter and the indentation is equal to the load divided by the projected area of the indentation.

$$W_m = \frac{W}{\pi . r^2}$$

Meyer proposed that this mean pressure should be taken as the measure of hardness; this is termed as the Meyer hardness and is given by,

$$MHN = \frac{4W}{\pi . d^2}$$

Meyer hardness uses the same units of kg / mm^2 as that of Brinell hardness.

2.3.4.1.2. Rockwell Test

In the Rockwell Hardness test which was invented by Stanley P. Rockwell in 1922, the indenter may be either a steel ball of some specified diameter or a spherical-tipped conical diamond of 120° angle with a 0.2-mm tip radius, called a Brale Indenter as shown in the Figure 2.8. A minor load or preload of 10 kgf is first applied, and this causes an initial penetration that holds the indenter in place and minimises any contact problem caused by surface roughness. At this point, the dial gauge is set to zero, and the major load is applied. Upon removal of the major load, the reading is taken while the minor load is still on. The hardness number may then be read directly from the scale that measures penetration. The Rockwell hardness number is defined by an arbitrary equation of the following form:

$$R = C_1 - C_2 \Delta t$$

Where C_1 and C_2 are constants for a given indenter size, shape, and hardness scale, and $\Delta\ t$ is the penetration depth in millimeters between the major and minor loads. Although Rockwell hardness increases with Brinell hardness, the two are not proportional and the dimensions of the Rockwell hardness are not force per unit area. In fact, the Rockwell hardness number cannot be assigned any dimensions, since it is defined by an arbitrary equation.

A variety of combinations of indenters and major loads are possible; the most commonly used are R_B, which uses 1.59-mm diameter (1/16 inch) ball as the indenter and a major load of 100 kgf; or R_C, which uses a diamond cone as the indenter and a major load of 150 kgf; and R_A, which uses a diamond cone as the indenter and a major load of 60 kgf. Rockwell B is used for soft materials and Rockwell C and A are used for hard materials.

The Rockwell hardness test is very useful and reproducible if the tests are done carefully.

There are two types of Rockwell tests:

Rockwell: The minor load is 10 kgf, the major load is 60, 100, or 150 kgf.
Superficial Rockwell: The minor load is 3 kgf and major loads are 15, 30, or 45 kgf. In both tests, the indenter may be either a diamond cone or steel ball, depending upon the characteristics of the material being tested.

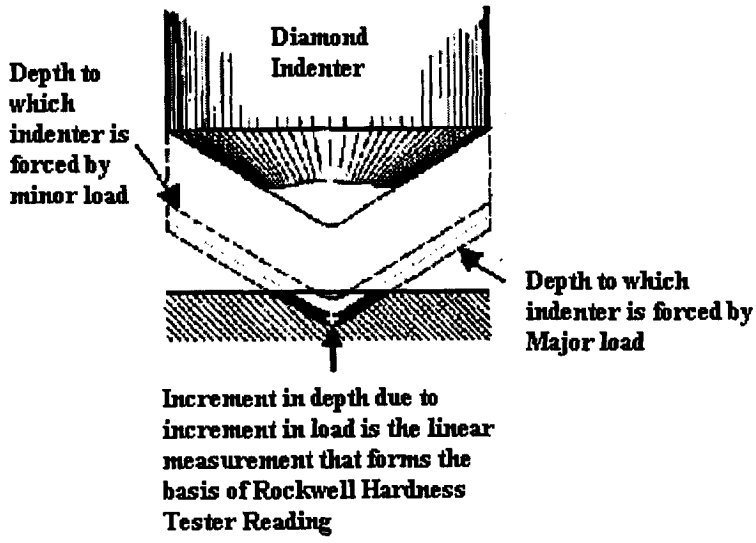

Figure 2.8. Principal of the Rockwell Test

2.3.4.3. Vickers Hardness

The Vickers hardness test method is the most common method for metal and alloys [129] and it consists of indenting the test material with a diamond indenter, in the form of a right pyramid with a square base and an angle of 136 degrees between opposite faces subjected to a load of 0.01 to 100 kgf. The apparatus can be scaled for macro or micro measurements. The full load is normally applied for 10 to 15 seconds. The two diagonals of the indentation left in the surface of the material after removal of the load are measured using a microscope and their average calculated, as shown in Figure 2.9. The area of the sloping surface of the indentation is calculated.

The Vickers hardness number (V or HV), also known as the diamond pyramid hardness (DPH), is given by the load divided by the actual surface area (kg/mm^2). In

practice, this area is calculated from the length of the diagonal of the impression by simple geometry.

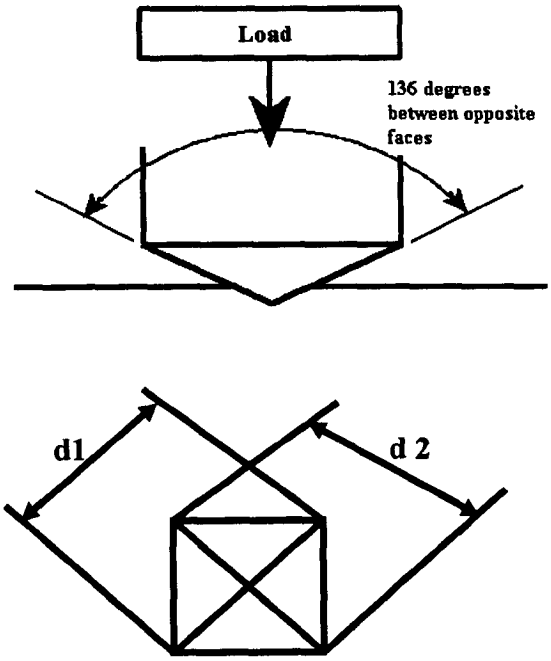

Figure 2.9. Principal of the Vickers Test

$$VHN = \frac{2W\sin(\theta/2)}{d^2} = \frac{1.854W}{d^2}$$

Where, W is the load applied in kg, d is the average length of diagonals in mm, and θ is the angle between opposite faces of diamond which is 136^0.

A perfect indentation made with a perfect diamond-pyramid indenter in a homogeneous material would be a square; however it is always possible to have anomalies as shown in Figure 2.10.(b) and (c) because of the way the indentations are performed hence care has to be taken during the experimental process.

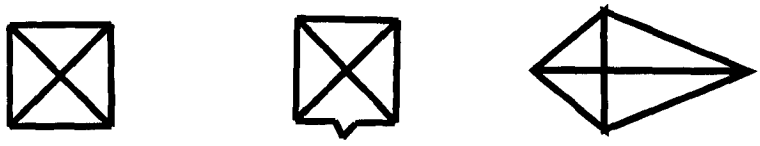

(a) (b) (c)

Figure 2.10. (a) perfect square impression (b) & (c) Abnormal impressions produced by Vickers Indentation. (b) represents a damaged indenter whilst (c) arises due to a non-planar test surface

In the Vickers method to obtain hardness several different loading settings give practically identical hardness numbers on uniform material, which is an advantage when compared with the arbitrary changing of scale with the other hardness testing methods.

Also extremely accurate readings can be taken, and just one type of indenter is used for all types of materials and surface treatments. Although thoroughly adaptable and very precise for testing the softest and hardest of materials, under varying loads, the test area needs to be highly finished to be able to see the indent well enough to make an accurate measurement.

2.3.4.2. Microhardness

Microhardness tests are measurements that allow the indenter penetration to be relatively shallow and of small volume so as to measure the hardness of brittle materials or thin materials or coatings. The apparatus include Vickers and Knoop hardness testers [120] and Berkovich tests. All these tests use highly polished diamond pyramidal indenters.

The Knoop test was introduced in 1939 by the National Bureau of Standards [130]. The principle of this is almost identical to that of the Vickers test, but has an advantage of measuring smaller deforming volumes.

As indentation tests needed smaller and smaller applied loads, the defects within the previously used indentation tests became noticeable as it was extremely difficult to make a perfect point from a square based pyramid because of their chisel edges. Hence new techniques were required. A Berkovich indenter [123] is a three-sided pyramid, and provides a sharply pointed tip compared with the Vickers or Knoop indenters, which are four-sided pyramids and usually have a slight offset.

2.3.4.3. Nanohardness

Nano-indentation is the technique used to measure nanohardness. This has the same basic principle as macro and micro-indentation but working at shallower depths. Its importance comes from the fact it is capable of measuring the mechanical properties of materials at very shallow depths, in the order of nanometres, which is a critical region for the tribological performance of materials.

The basics of the method are simple. A tip of known geometry is pushed against the surface of the material by applying an increasing normal load, while both load and displacement are continuously recorded and the corresponding load-displacement

curve is plotted. The depth resolution is of the order of tenths of nanometers and the load resolution on the order of tenths of a microNewton [131].

For each loading/unloading cycle, the applied load value is plotted with respect to the corresponding position of the indenter. The resulting load/displacement curves provide data specific to the mechanical nature of the material under examination. Established models are used to calculate quantitative hardness and modulus values from such data.

This depends on the area of the indent which is calculated from knowledge of the geometry of the tip of the diamond indenter. The load resolution is about ±75 nN, and position of the indenter can be determined to ±0.1 nm. Mechanical property measurements can be made at a minimum penetration depth of about 20 nm using commercially available indenters.

2.3.4.3.1. Analysis of Indentation Data

An indentation curve is the relationship between load W and displacement h, which is continuously monitored and recorded during indentation. For an elastic solid, the sample deforms elastically according to its Young's modulus, and the deformation is recovered during unloading. As a result, there is no impression of the indentation after unloading. For a rigid-perfectly plastic solid, no deformation occurs until the yield stress is reached, when plastic flow takes place. There is no recovery during unloading, and the impression remains unchanged. In the case of an elastic-plastic solid, it deforms elastically according to its Young's modulus, and then it deforms plastically. The elastic deformation is recovered during unloading. In the case of an elastic-perfectly plastic solid, there is no work hardening.

A schematic of a load displacement curve is shown in Figure 2.11.

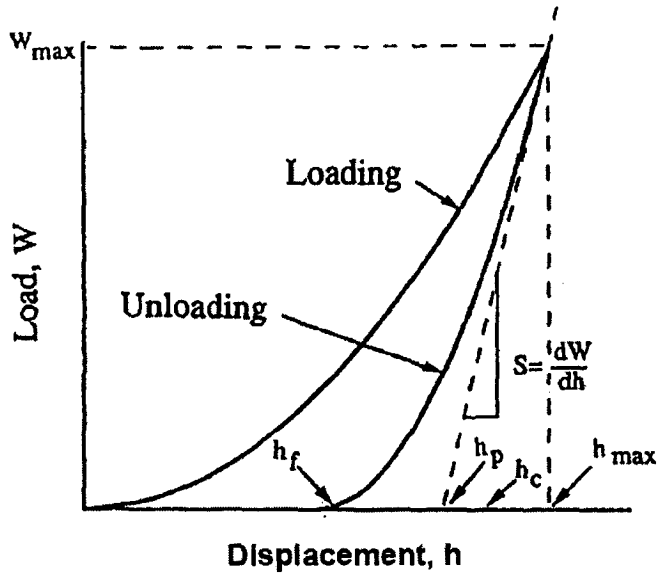

Figure 2.11. Schematic of load-displacement curve.

To predict the deflection of the surface at the contact perimeter for a conical indenter and a paraboloid of revolution, Oliver and Pharr [117] developed an expression for h_c the contact depth, which is required for hardness calculation in terms of h_{max} and other measurable parameters.

$$h_c = h_{max} - \varepsilon W_{max} / S_{max}$$

Where ε =0.72 for the conical indenter, ε = 0.75 for the paraboloid of revolution, and ε =1 for the flat punch, and S_{max} is the stiffness (=1/ compliance), equal to the slope of unloading curve (dW/dh) at the maximum load. Oliver and Pharr [117] assumed that the behaviour of a Berkovich indenter is similar to that of a conical indenter, since the cross-sectional areas of both types of indenters varies as the square of the contact depth, and their geometries are singular at the tip. Therefore, for a Berkovich indenter $\varepsilon \sim 0.72$. Thus h_c is slightly larger than the plastic indentation depth (h_p) which is given by

$$h_c = h_{max} - W_{max} / S_{max}$$

2.3.4.3.2. Determining the Hardness Values

The nanohardness is obtained by using a Berkovich hardness (or *HB*) which is defined as the load divided by the projected area of the indentation. It is the mean pressure which a material will support under load. From the indentation curve, we can obtain hardness at the maximum load as,

$$HB = W_{max} / A$$

Where W_{max} is the maximum indentation load and A is the projected contact area at the peak load i.e. it is assumed that no elastic recovery of the shape of the impression occurs on unloading. This definition was chosen in order that the nanoindentation hardness agreed with conventional hardness test results at comparable loads. For instance, for a Vickers indenter relaxation of the indenter diagonals is minimised on unloading once significant plastic deformation occurs. Thus the indent geometry calculated the indenter diagonal is equivalent to that calculated from the contact depth.

2.3.5. BEND TESTS

The ability of paint to undergo bending (on a suitable substrate) has called for the development of several related bend tests. This type of test is applied to materials that may be expected to undergo bending as a result of the method of fabrication and loading of the articles to which they are applied. Thus the tests find greatest use in connection with industrial finishes.

Most commonly, the paint system to be tested is applied to a suitable panel which can be bent through 180° around a cylindrical mandrel of known diameter. The coating is then examined for cracking or loss of adhesion. Although usually regarded as a test of flexibility, the test is a composite one which encompasses adhesion, flexibility, and extensibility. One form of the test (developed originally as DEF-1053 Method No. 13 and subsequently as BS 3900 Part El) uses a 'hinge' into which the mandrel is incorporated. The hinge consists of two rectangular metal flaps hinged at the extremities of one of their shorter sides with a long pin. The mandrel is fitted around this pin, such that it rotates freely around it. It is so positioned that when the hinge is open there is sufficient clearance to insert the test panel between the mandrel and the flaps. Each mandrel is fitted in its own hinge so that it is necessary to have a complete range of hinges to apply the test in increasing severity as the diameter of the mandrel is reduced. The normal range of mandrels are 3, 5, 6, 9, 12, 18 and 25mm diameter. It is important that the test panel meets certain dimensional requirements. For government specifications 4in x 2in (100 x 50mm^2) aluminium panels conforming to BS 3900: Part A3 are used. In non-specification testing tinplate or aluminium panels may be used, but they should not be thicker than 0.012 in (0.3 mm).

The hinge is used in the following manner: the panel is inserted into the hinge with the coated side outward from the direction of bending. The hinge is closed evenly, without jerking, in not less than one second and not greater than 10 seconds, bending the panel through 180°. The coating is examined immediately after bending and before removing it from the hinge for evidence of cracking or loss of adhesion. The test should be carried out in a constant temperature room (e.g. at 2.5 °C) allowing at least two hours for the panels and hinges to come to temperature. This simple test can be very informative since it may be related to conditions of use of many of the coating

compositions which it may be used to test. It can be developed in different ways to give information of the acceptability or otherwise of materials that may be subject to environmental changes after a coated substrate has been formed. Thus compositions that pass the test at a given mandrel diameter at 2.5°C may crack and lose adhesion when they are heated (subject to a second stoving sequence) or subject to excessive cooling, when the coating becomes glassy.

A variation of the previously described test uses rod mandrels which are supported in a steel cradle. The method is used for test panels which are too thick to fit into the hinges described above. However, the thicker the substrate, the smaller the range of mandrels that can be successfully employed.

An alternative technique for fatigue loading is to use four-point bending. The advantages with this method are that a large part of the specimen is exposed to a uniform stress and that specimen preparation is simple. One disadvantage, however, is that only the outer surface is exposed to the maximum stress.

2.3.4.1. Four-Point Loading

Four-point loading gives a uniform longitudinal tensile stress in the convex surface part of the specimen between the inner supports.

The stress decreases linearly to zero from the inner supports to the outer supports [134, 135]. The relatively large area of uniformly stressed material makes four-point loaded specimens particularly suitable for tests on welded material and for studies of protection by sprayed metal or organic coatings.

The specimen is supported near the ends and bent by forcing the two inner supports against it in the manner as shown in Figure 2.12. The two inner supports must be located symmetrically about the line midway between the outer supports.

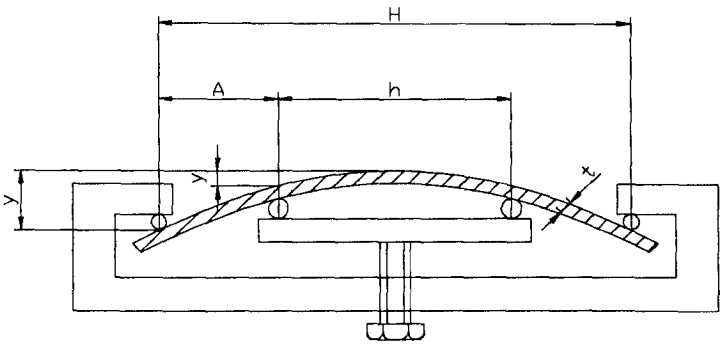

Figure 2.12. Four-point bend loading

Four-point loaded specimens are commonly flat strips 15 mm to 50 mm wide and 110 mm to 250 mm long. The thickness of the specimen is usually dictated by the mechanical properties of the material and the product form available. Specimen dimensions can be modified to suit specific needs but the approximate dimensional proportions should be preserved.

The elastic stress in the convex surface part of the specimen between the inner supports is calculated from the relationship

$$\sigma = \frac{12Ety}{3H^2 - 4A^2}$$

where

σ is the maximum tensile stress in newtons per square metre;

E is the modulus of elasticity in newtons per square metres;

t is the thickness of specimen in metres;

y is the maximum deflection between outer support in metres;

H is the distance between outer support in metres;

A is the distance between inner and outer supports in metres.

The dimensions are often chosen so that $A = \frac{H}{4}$.

An alternative method of calculating the elastic stress between the inner supports is to use the relationship

$$\sigma = \frac{4Ety'}{h^2}$$

where

h is the distance between inner supports in meters;

$y`$ is the deflection between inner supports in metres.

-this equation is a special case of the previous one when A=0.

The above relationships are based on small deflections (y / H or $y` / h < 0.1$). In light gauge specimens the deflections may be larger than this and the relationships are then only approximate. More accurate stress values may be obtained by attaching strain gauges to a specimen of the same material and the same dimensions and stressed in the same way [136].

2.3.6. STRESS IN COATINGS

There is a complex system of forces acting on the cohesion and adhesion of the coating film. When the influencing stresses become too great for the adhesion and cohesive strength of the film, a failure occurs. The forces and stresses that oppose adhesion and cohesion arise from several sources: the service conditions under which the film operates, its chemistry, composition, curing mechanisms, thickness, age and the conditions under which film formation took place [137]. The stresses can be internal, external or hygrothermal. Internal stresses originate from film formation, ageing effects and film thickness effects. The external stresses can include bending, abrasion, impact and solvent absorption. Hygrothermal stresses can be caused by thermal or hygroscopic effects [137]. Tensile stresses develop when the coating contracts during film formation; compressive stresses result from expansion of the film and arise as the film responds to high humidity or elevated temperatures [138]. The only way internal stress can dissipate from a coating applied on a strong substrate is by deformation of the coating film or by brittle failure. Brittle failure means that the coating is released from the substrate or that there is a failure within the film. Tough, elastic films will best resist brittle failure and irreversible deformation. The stresses will accumulate gradually within a film and cause deterioration of its mechanical properties. When film thickness is increased, the impact of its high cohesive strength and greater internal stress, reduces the film's adhesion to the substrate [32].

Desirable adhesion, resulting from strong interaction between paint film and a substrate, increases the amount of stress necessary to produce brittle failure in the system. This is because good adhesion allows a part of the accumulating internal stresses to be transferred to the metal, instead of weakening the coating. The substrate then acts as an energy sink [46].

Although three different types of stresses can be found in polymeric coatings, the internal stress and its development has a significance in this thesis and the following section will give a description of internal stress development and measurement techniques to assess it.

PAGE
MISSING
IN
ORIGINAL

increase or decrease with time, depending on the environmental conditions and the coating chemistry. Conditions of high relative humidity tend to decrease tensile stress and even lead to compressive stresses as moisture is absorbed into a coating.

One of the major factors that influence development of stresses in the coating is temperature. Increasing the temperature, raises the drying and reaction rates, on which stress usually scales. However, for a polymer coating of given solvent content or extent of reaction, stresses relax more quickly as the temperature is raised [152]. Coating stress is also affected by the temperature change itself due to thermal expansion mismatch with the substrate [153, 154].

Internal stresses contribute to adhesion failure which can be immediate or in long-term or may affect mass transport properties such as void growth [155], low temperature recrystallisation [156] or a low strain point temperature in glasses [157].

Stresses are strongly related to the thickness of both the coating and the substrate, since, usually the substrate is much thicker than the coating, the stresses in the substrate are quite low but in the interface region there is a big gradient of stresses and if the forces caused by the difference of stresses are higher than the adhesion forces, delamination occurs. Therefore, for highly stressed films, adhesion has to be extremely good in order for the films to be useful [158].

Other influences that cause stress development of coating are: coating thickness [159, 160], coating pigment [161], solvent and solvent mixtures [162] and any cross-linking effect [163]. Whatever their source, these internal stresses reduce the practical adhesion and may induce cracks in coating materials [164-167] resulting in a drop of the overall performance of coating systems.

2.3.6.2. Internal Stress in Epoxy Marine Coatings

As mentioned before, marine coatings are special paint systems designed for extensive application on ships and static marine structures. A general purpose anticorrosive and antifouling paint might be required to perform equally well on a ship's side or deck or inside ballast tanks. However, one major problem associated with marine coatings is that organic coatings tend to shrink during solvent evaporation or curing period after application. This shrinking results in internal stresses being developed in the coating and tensile forces build up throughout the coating. If these tensile stresses become large enough, cracking or peeling failure may occur in the body of the coating thus exposing the substrate (steel in ballast tanks) to the corrosive environment. Furthermore, the development of tensile stress due to solvent evaporation will occur in the docks before the ship is exposed to water. During the service life, ship's coating experiences both temperature fluctuation and intermittent water cooling/heating. The difference in thermal expansion between paint and metal, results in cyclic compressive and tensile stresses in the coating.

Out at sea, after a period of just a few weeks, the coating is likely to absorb sea water, causing swelling; once the cargo is delivered the ship hull will rise in the water and a margin of surface coating previously exposed to sea water will dry out quickly. There may also be dilatational and shrinkage stresses set up in the coating as water is absorbed or desorbed [168].

Investigations of the magnitude and the mechanism for occurrence of internal stress in solvent based epoxide resin coatings have been performed by some researchers [169-174]. Internal stresses within the rubbery region of the coating systems was not observed in those analyses. Rather, they were generated during cooling from the glass transition temperature T_g of each system to room temperature. The internal stress depends on the strain and the modulus of the coating. Considerable amounts of solvent were retained in the coatings, even after the curing reaction reached an equilibrium state. The magnitude of the internal stress depended on the concentration of the residual solvents, regardless of the variety and the initial solvent content [168].

Perera's group [175] investigated the moisture and temperature induced stresses (Hygrothermal Stresses, S^{HT}) in organic coatings and found that a stress can develop in a coating applied on a substrate as a result of a film formation (Internal Stress, S^F) and of a variation in relative humidity (Hygroscopic Stress, S^H) and/or in temperature (Thermal Stress, S^T). Therefore, total stress (S_{tot}) is:

$$S_{tot} = S^F \pm S^H \pm S^T \qquad \text{Equation 3.}$$

In the above research, the determination of the Hygrothermal Stress dependency on temperature and relative humidity enabled evaluation of the T_g at different relative humidities. When a coating is exposed to wet conditions, a significant compressive stress may be induced as a result of its tendency to expand which is mainly a result of the coating's capacity to relax.

Various marine coatings and the changes of internal stress when coatings are exposed to water and then subsequently dried out were studied by Negele and Funke [176]. They demonstrated that the changes of internal stress were influenced by the relaxation processes at the coating/support interface, which are related to wet adhesion.

Croll [178] defined the initial 'solidified' state in drying polymer solution coatings as the point at which the glass transition temperature of the coating (which is a function of solvent content) is equal to the drying temperature.

2.3.6.2.1. Stress Development

In the simplest case, stress in a marine coating begins to develop when the coating has dried or cured enough so that it has developed elasticity and can support a stress. During the initial stages of drying or curing, the viscous contribution to stress dominates over the elastic, but the viscous stress is small (in comparison with the elastic stresses that develop after the coating solidifies) and is relaxed quickly. For viscoelastic materials, the stress relaxation time scales with the ratio of viscosity to the shear modulus [152]. Early in the drying or curing process, the coating is still a liquid with a low viscosity and the relaxation time is short [179]. However, as drying or curing proceeds, the coating structure changes and the viscosity climbs, resulting in longer and longer relaxation times. As the coating begins to support an elastic stress (i.e. solidifies), there is a competition between stress accumulation driven by the solidification (elastic) and stress relaxation (viscous), with the final state of stress depending on the time scale for the two processes and the evolving material properties.

As stress climbs, it can reach a level sufficient for plastic deformation or yielding. When stress relaxation is fast, increases in stress beyond the yield stress are quickly relaxed and the stress remains at the yield stress. When stress relaxation is slower, the stress in the coatings surpasses the yield stress before relaxing back to a constant value [137].

2.3.6.3. Stress Measurements Techniques

The method used to measure the internal stress depends on the nature and the dimensions of the material to be investigated. However, there are several methods that have been developed to measure internal stresses in organic coatings, each with their own advantages and disadvantages. There are photo-elastic analysis [180, 181], strain gauge method [171], laser inteferometry [182, 183], impulse viscoelasticity and vibration wave [184], X-ray diffraction [185, 186] and also cantilever (beam) methods

[175, 187]. Many of these methods have been based upon plate or beam deflection theory. The deflection in cantilever beam-based method is initially monitored continuously by an optical lever. This type of instrument has been modified to include a video camera for simultaneous video monitoring of the coating's optical characteristics during stress measurements [188, 189]. For simultaneous thickness measurements, similar devices have been equipped with an ellipsometer [190] or a laser interferometer [191]. The beam bending method has also found application in the study of the interaction of polymer coatings with humid or solvent rich atmosphere and water or liquid environments [172, 192-196].

The stress in a coating deforms the underlying substrate, resulting in a curvature of the system (see Figure 2.13.) The most common method to determine coating stress is to measure the curvature or deflection of a coated substrate. The method dates back to 1909, with Stoney's work on electrodeposited coatings [197] and was very useful for analysing the residual stresses of thin coatings where the deflection is small. The main advantage of this process is that there is no need to know the intrinsic properties of the coating,

$$\sigma = \frac{E_{substr} d_{substr}^2}{6(1-\nu_{substr}) d_{coating}} \left(\frac{1}{R} - \frac{1}{R_0} \right) \qquad \text{Equation 4.}$$

where E_{substr} is the Young's modulus and ν_{substr} is the Poisson's ratio for the substrate, $d_{coating}$ is thickness of the coating and R_0 the radius of curvature of the substrate before deposition and R the radius of curvature after deposition.

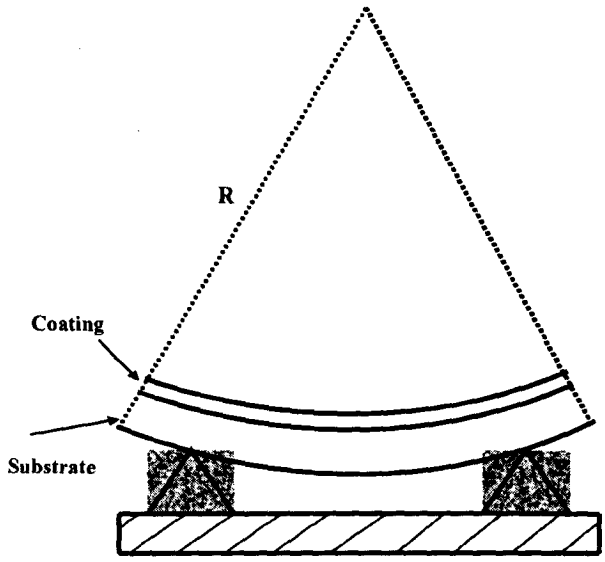

Figure 2.13. The stress in a coating deforms the underlying substrate, resulting in a curvature of the coating-substrate system

However, when the thickness of the coating increases or the Young's modulus of the coating is very high it is necessary to account for the coating properties in order to obtain accurate residual stress results. An improvement of the expression was developed by Senderoff and Brenner in 1949 [198]:

$$\sigma_{res} = \frac{\frac{E_s}{(1-\nu_s)}\left(h_s + \frac{E_c(1-\nu_s)}{E_s(1-\nu_c)}h_c\right)^3}{6Rh_sh_c} \qquad \text{Equation 5.}$$

where σ_{res} is the total residual stress, E_c the Young's modulus of the coating, E_s the Young's modulus of the substrate, ν_s the Poisson's ratio of the substrate, ν_c the Poisson's ratio of the coating, h_s the thickness of the substrate , h_c the thickness of the coating and R the radius of curvature.

The descriptions of the mechanics involved in curvature and deflection-based techniques [199-202] and reviews of stress measurements methods [203, 204] can be found in the literature.

The coating stress (σ) can be determined from the radius of curvature (R), the coating thickness (t_c), the substrate thickness (t_s), the substrate elastic modulus (E_s) and the substrate Poisson's ratio (ν_s):

$$\sigma = \frac{E_s t_s^2}{(1-\nu_s)6Rt_c} \qquad \text{Equation 6.}$$

This expression is derived assuming that the substrate and coating behave elastically with identical elastic moduli, the coating thickness is much less than the substrate thickness and the coating is in a uniform stress state of biaxial stress. This is essentially the same as Stoney's equation (Equation 4.).

Equations 4-6 were all derived using the assumption that the neutral surface of the substrate-coating combination coincides with the neutral surface of the substrate. For thin substrates, as often used to investigate internal stress development in coatings, this approximation breaks down. A full analysis, allowing for the correct location of the neutral surface, gives equation 7.

For a coating with Young's modulus E_c, Poisson's ratio υ_c and thickness a on a substrate with Young's modulus E_s, Poisson's ratio υ_s and thickness b, the relationship between the radius of curvature R and the internal stress in the coating (σ_c) is given by [205]:

$$\sigma_c = \frac{aE_c}{6R(1-\upsilon_c)} \frac{1+4\alpha\beta+6\alpha^2\beta+4\alpha^3\beta+\alpha^4\beta^2}{(1+\alpha)(1+\alpha\beta)}, \qquad \text{Equation 7.}$$

$$\text{where: } \alpha = \frac{b}{a} \text{ and } \beta = \frac{E_s}{E_c}\frac{1-\upsilon_c}{1-\upsilon_s}.$$

This form of the relationship between the residual stress and the curvature takes account of the true position of the neutral surface of the substrate-coating combination, which is displaced slightly from the midplane of the substrate. In a majority of the analyses presented in the literature, the treatment is simplified by taking the neutral surface to be exactly at the mid-plane of the substrate [206]. The approximation incurred by this practice becomes progressively worse as the ratio of coating thickness to substrate thickness increases.

CHAPTER 3.

EXPERIMENTAL PROCEDURES

3.1 TESTING STRATEGY

In view of the wide ranging and interactive nature of the factors which affect the choice of test method for this study, it was not possible to be totally prescriptive about a test regime. Development of an expert system which pursues the various possible paths in a logical way occurred as data was obtained. Nevertheless, the test strategy was focused on development of a laboratory technique for cyclic-loading tests in simulated service conditions.

Failures of ballast tank coatings are recognised by industry and researchers (see section 2.2.4.), but no source of published work has been found to date for precise testing procedures for validation of a fatigue effect on ballast tanks coatings systems or an explanation of whether fatigue was the main cause of coatings breakdown. Fundamental examination of this matter under laboratory conditions started within some research groups (in Sweden and Korea; see references [31, 32, 42]), but the coatings that were used during those tests were laboratory prepared (i.e., epoxy systems were made without all of the additives that commercial marine coatings have) or the testing regimes were extreme in comparison with service conditions. In contrast, the present study gives some indication of the real influence of fatigue on selected marine coatings. Furthermore, the chosen methods cover the determination of the fatigue resistance to cracking of attached epoxy coatings on steel panels and observation and measurements of changes of some properties of the coatings during curing and ageing. It should be emphasised that for most applications these conditions can be considered to be idealised.

In this research, assessment and design of laboratory procedures for fatigue tests were achieved by developing the cyclic-loading tests of the coatings in air at room temperature, artificial seawater at room temperature and at 5°C. Complementary tests were conducted to obtain information to assist the interpretation of the results of the cyclic-loading tests. They were:

- tensile tests;
- hardness tests along with ageing process development and
- internal stress measurements.

This chapter will firstly give a description of coating types used in this research, followed by details of experimental procedures performed in this study.

3.2. MATERIALS AND SPECIMENS

Three experimental epoxy marine coatings used for this project were supplied by 'International Paint Akzo-Nobel' and were coded as:

1. **Coating 'A'**- An aluminium pigmented pure epoxy
2. **Coating 'B'**- An epoxy modified with non-reactive diluents
3. **Coating 'C'**- A coal tar epoxy.

Solvent retention in coatings 'A' and 'B' are given in Table 3.1. and in Table 3.2. values for Young's Modulus for all three coatings measured at 23°C (coatings were cured for 1week at 100°C).

Table 3.1. Solvent retention in coatings; unverified data given by coatings supplier

Coating / Solvent		**Level in wet paint (wt%)**	**1 week ambient cure (wt%)**	**4 weeks in sea water (wt%)**
A	Benzene Cpds.	5.58	2.32	1.7
	Xylene	22.33	4.77	2.9
	Butanol	5.58	1.93	0.7
	Total	*33.49*	*9.02*	*5.3*
B	Xylene	15.22	2.77	2.88
	Butanol	7.82	1.51	0.96
	Total	*23.04*	*4.28*	*3.84*
C	Benzene Cpds.	2.5-10	n/a	n/a
	Xylene	10-25		
	Total	*12.5-35*		

Table 3.2. Young's Modulus for the coatings, unverified data from coating supplier

Coating Type	Young's Modulus [GPa]
A	4.8
B	4.7
C	6.1

Table 3.1. shows that solvent content is high initially but falls to approximately 4%wt upon drying. Table 3.2. indicates that coating 'C' has the highest Young's modulus of the three coatings.

The three types of epoxy coatings were prepared in the laboratory of the supplier industry, where every coating system had its own recommended painting specification, which must be followed strictly to guarantee ultimate coating protection during service life. The application specification describes e.g. temperature range, humidity, drying interval, wet and dry film thickness.

3.3. SPECIMEN TYPES

Three types of specimens were prepared during this research. Each of them was used for a specific test and their description is given below.

3.3.1. PANELS

Panels were prepared as mild steel plates over which the coating system was applied to encapsulate the substrate.

Mild (low carbon) steel has approximately (0.05-0.29)% carbon content [207] and a relatively low tensile strength, but it is cheap and malleable; surface hardness can be increased through carburizing [208]. The density of this metal is 7,860 kg/m^3, the tensile strength is a maximum of 0.5 GPa and it has a Young's modulus of 210 GPa [207, 208].

The three coatings were applied by airless spray to steel-substrates at nominally 3x standard dry film thicknesses in two coats. It was believed that thicker coatings will react earlier to the testing environments then the single dry film thick coat. For that reason, the coatings were sprayed 3 x standards. The standard recommendation for dry film thickness for coatings 'A' and 'B' is 250μm and for the coating 'C' is (250-300)μm. The coating application was carried out over a 5 day period. On the first day the coating was sprayed to 1.5x standard dry film thickness, followed by 2 days of drying of the coating and at the end of the third day, the second coat (which was again 1.5x thicker than the standard) was applied and dried for two days. The panels were cured at 25°C (except coating 'C', cured at 35°C). The specimens were subsequently stored in the laboratory for two weeks (typically conditions 20°C/50%RH) during which the edging was carried out. Steel panels had two strip coats brush applied to the edges. Test panels had the following overall dimensions, including the coating: length 130mm, width 50mm and thickness approximately 5mm (depending on coating thickness). These specimens were used for four-point bend cyclic tests.

After drying, the coating thicknesses on both sides of the samples were measured using a digital coating thickness gauge model Elcometer 300. Panels were labeled with serial numbers and one side was chosen to be the top surface which was the surface that was in tension during bending tests. Typical images of the top surfaces of all three coatings are given in Figure 3.1., showing differences in the inhomogeneous coatings.

Coating 'A'

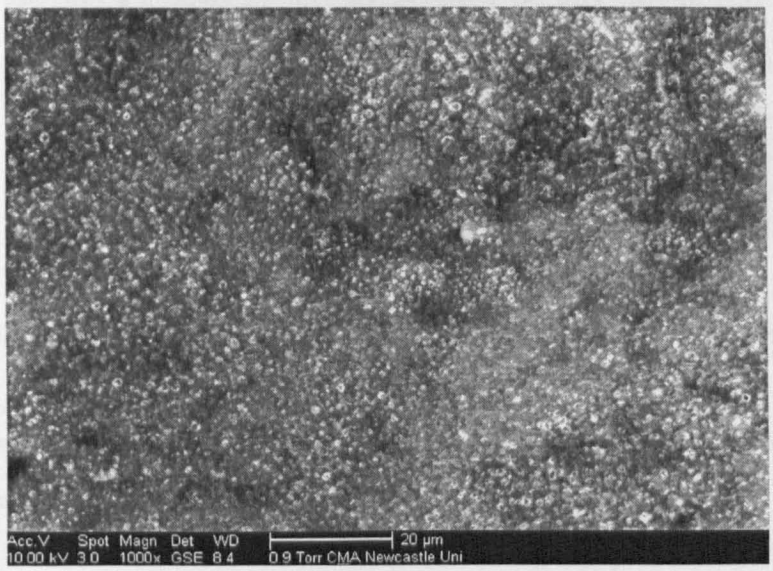

Coating 'B'

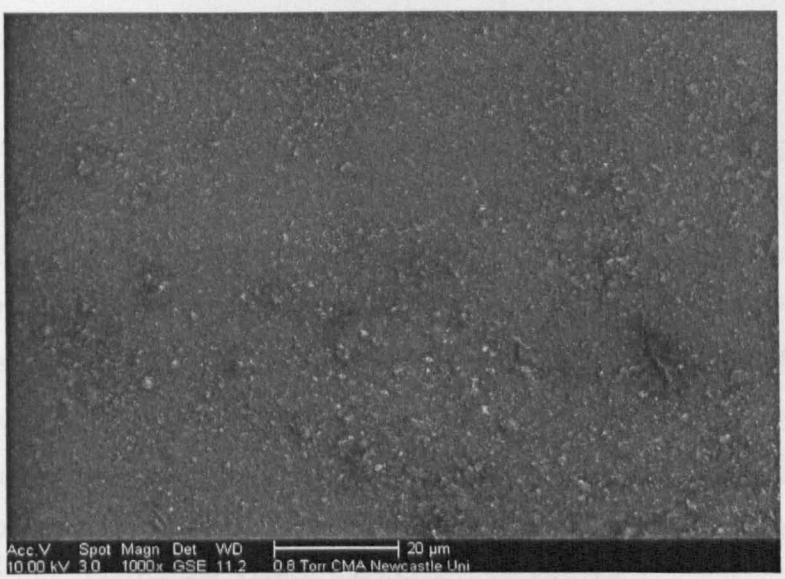

Coating 'C'

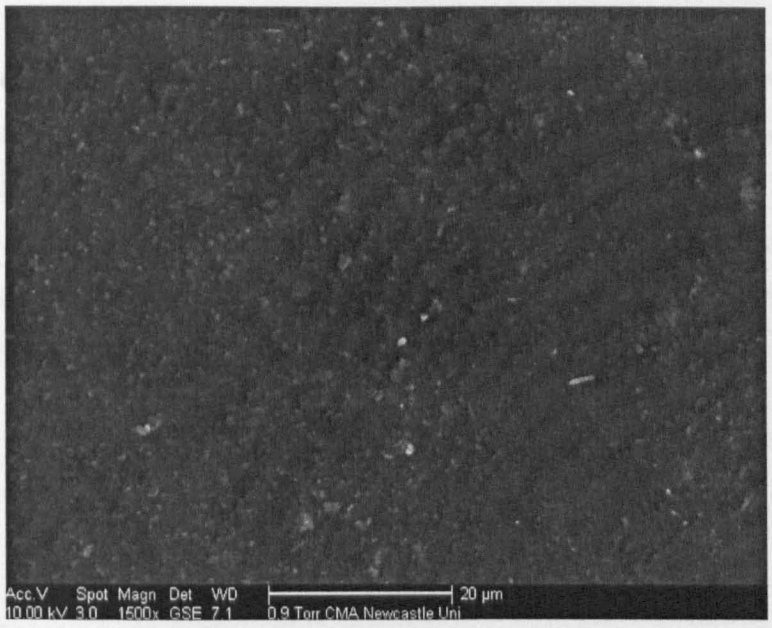

Figure 3.1. ESEM images of surfaces of coatings 'A', 'B' and 'C' before test

The images show that the coatings were all crack-free and that some contained more filler particles that others.

3.3.2. SHIM-COATING SAMPLES

Coatings were applied to stainless steel coupons (shims) of different lengths (150mm and 250mm) and thickness (100µm, 200µm and 300µm). Samples were prepared for all three experimental coatings. Single coating applications were used, but the coupons were coated at ~3x recommended dry film thickness of the coatings. Note some of the stainless steel shims were pre-treated with a polyvinyl butyral (PVB) etch primer (Appendix 3.1.) prior to applying the epoxy coatings. After the coatings were applied, samples were cured at 25ºC ('A' and 'B') or 35ºC ('C') and stored in the laboratory for two weeks. These samples were used for internal stress measurements. Further details of samples preparation are given in section 3.6.1.

3.3.3. FREE FILMS

Tensile properties were obtained using free-films of the coatings which were prepared by spraying the three experimental coatings on to Teflon glass panels to which they did not adhere. After the drying procedure tensile samples (Figure 3.2.) were cut and then peeled off as free-films and used as specimens. Typical cross-sections of fractured coatings 'A', 'B' and 'C' are illustrated in Figure 3.3. and show the filler particulates in the 'A' and 'B' coatings which were obtained by EDX.

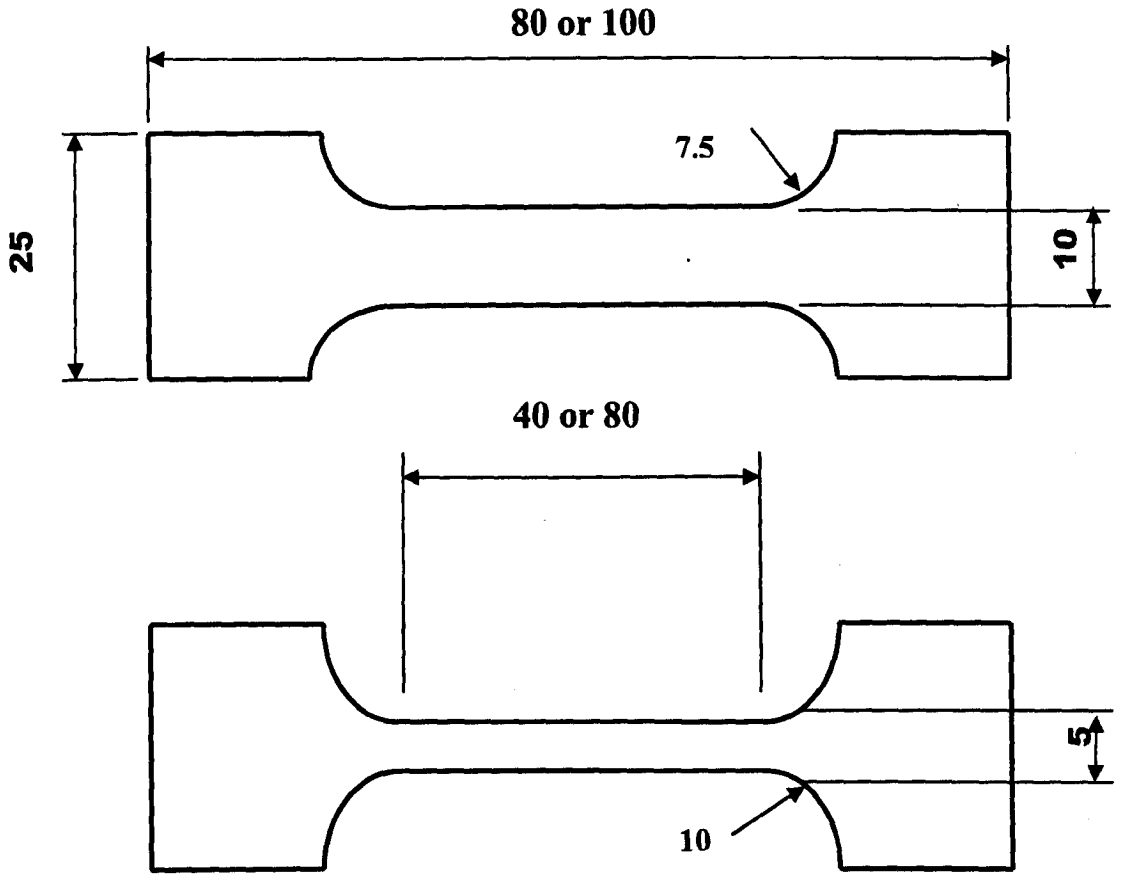

Figure 3.2. Dimensions of tensile samples with 40 and 80mm gauge lengths

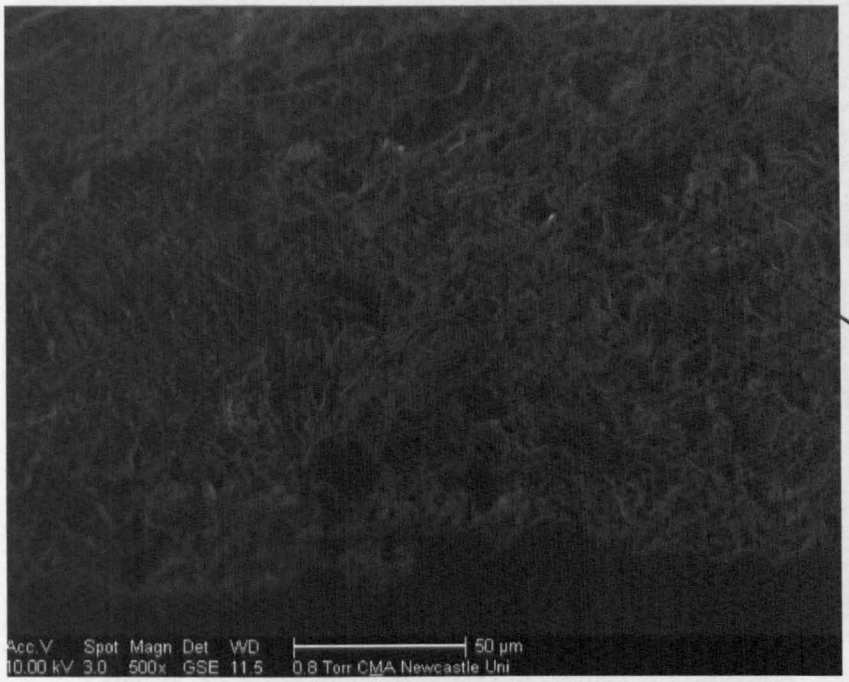

Coating 'A' showing aluminium flake particles

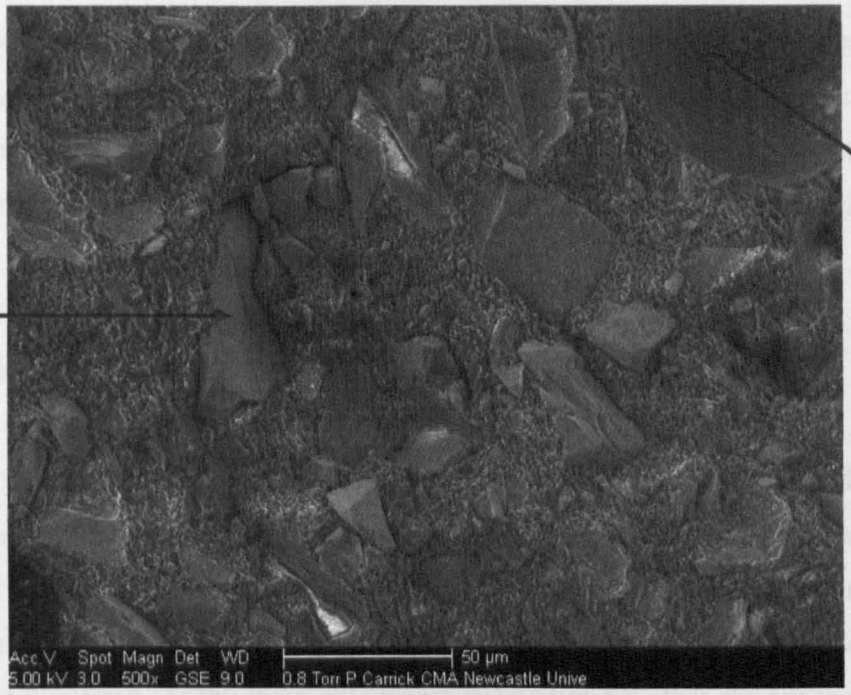

Coating 'B' showing a void and barium sulphate filler particles

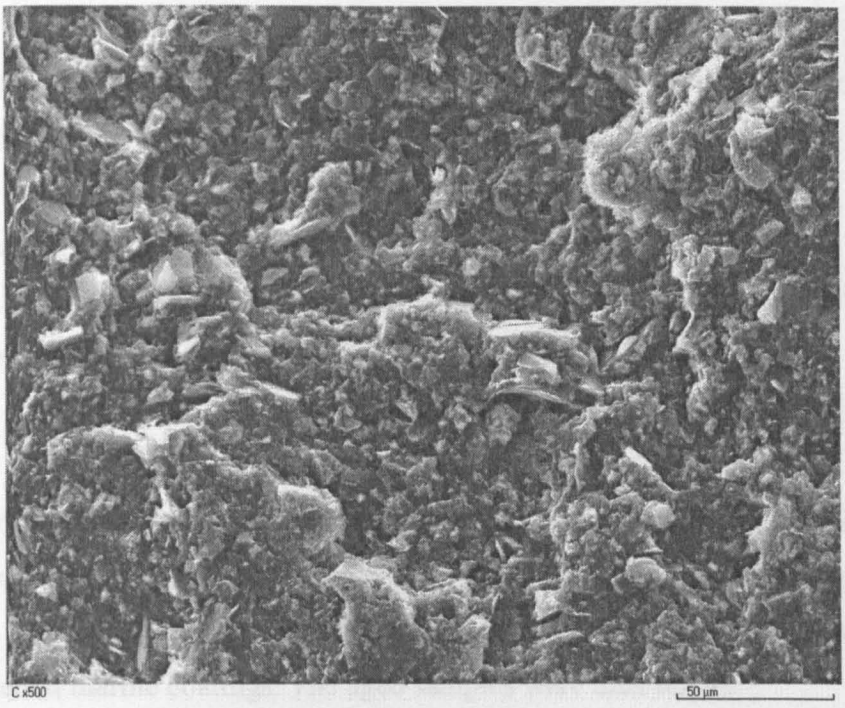

Coating 'C' showing a more homogeneous composition

Figure 3.3. ESEM images of fractured free-films of coatings 'A', 'B' and 'C'

Although, all three coatings were epoxy based, from the presented images in Figure 3.3. it can be seen that EDX method, that was used for particle recognition, showed that coating 'A' consisted of aluminium flake particles, whereas coating 'B' had barium sulphate filler. More constant composition can be observed for coating 'C'.

3.4. AGEING PROCESS

A major consideration in the design of marine structures is the period of time over which the structure is expected to perform its function, the design life. Generally, the design life is at least 20 years, over which time all environmental and mechanical effects on the material and its structural behaviour must be designed for. Contact with water and humidity are the main environmental parameters that govern the behaviour of the material and this can affect the fatigue and long-term performance [10]. However, ageing resistance tends to be considered in material selection rather than during mechanical design. The temperature range is generally relatively small, the sea temperature varying from -2 to 27°C at sea level and becoming almost constant below

300 metres depth at around 4°C. Nevertheless, ballast tank temperature can reach up to 70°C during oil cargo voyage. Therefore, a recommendation for laboratory ageing of marine coatings is given below from Akzo-Nobel:

1) 21 days at 35°C
2) 3 cycles each consisting of 7 days immersion in seawater then 7 days at 23°C in air
3) 10 cycles each of 7 days at 5°C, 7 days at 70°C and 7 days immersion in seawater at 23°C.

This procedure is designed to simulate the changes caused by ageing in service and is used to determine which compositions are likely to behave best under service conditions. The ageing cycle occupies 275 days and was performed on all three types of experimental marine coatings. The aged samples were then tested.

Although the accelerated Akzo-Nobel ageing procedure given above aims to simulate the degradation obtained during a much longer service, it is still much longer than desired. A shorter process has been devised and part of this project was devoted to examining whether this further acceleration can yield meaningful results. The ageing cycle conditions tested were:

1) 7days at 35°C
2) 3 cycles each consisting of 2 days immersion in seawater then 2 days at 23°C in air
3) 10 cycles each of 2 days at 5°C, 2 days at 70°C and 2 days immersion in seawater at 23°C.

The procedure therefore involves reducing the dwell times, but retains the same number of cycles of changes as the Akzo-Nobel procedure. Experience with previous tests on similar materials [139], indicated that 48 hours can be considered adequate to reach equilibrium during the uptake and loss of water from coatings of the thickness applied in this case, therefore it was reasoned that the ageing procedure could be shortened in this way.

3.5. CYCLIC-LOADING TESTS

3.5.1. EQUIPMENT AND DESIGN

Development and design of a test programme started from modifying slow strain rate test rigs for this purpose. As all cyclic-loading (fatigue) tests, regardless of complexity, consist of the same basic elements, the test rigs developed for this project had a load train consisting of a rigid frame, grips, specimen and drive (or loading) system (Figure 3.4.).

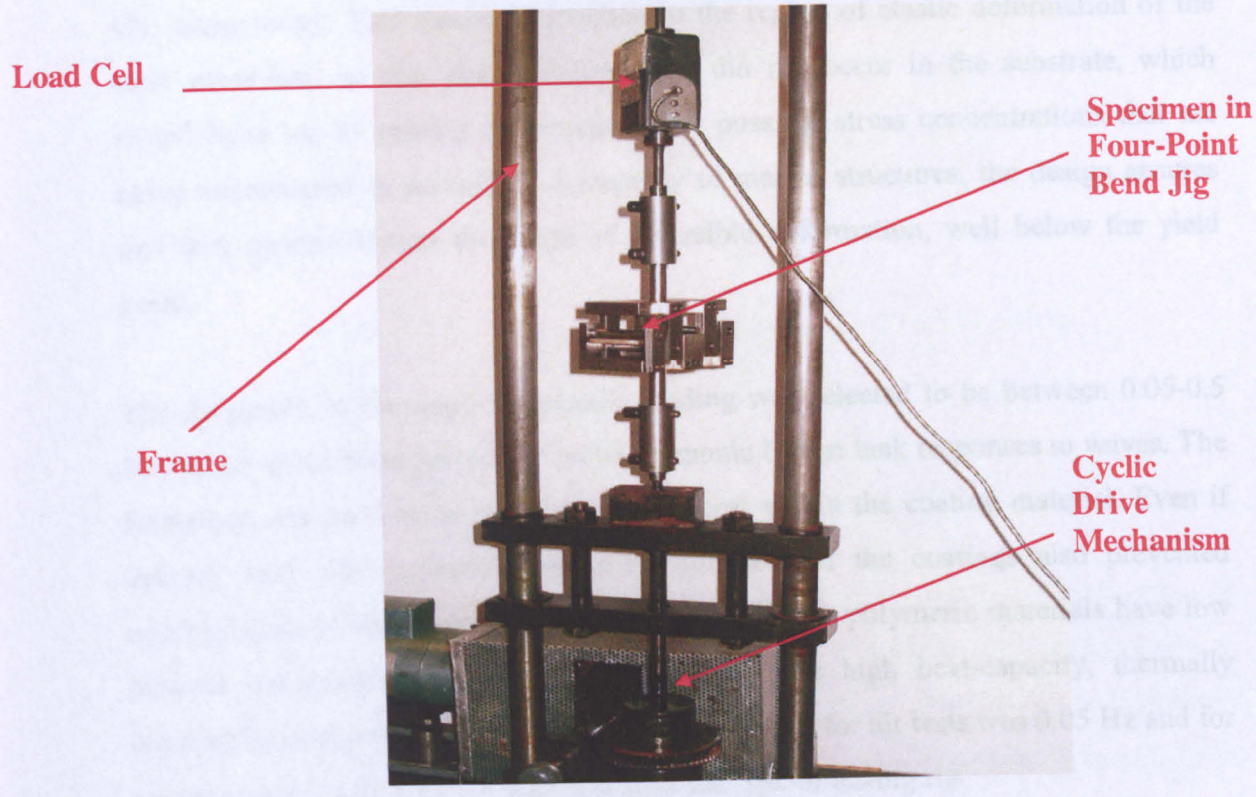

Figure 3.4. Test rig for cyclic-loading, four-point bend experiments in air at room temperature

Five test rigs were constructed in order to conduct the fatigue and corrosion fatigue experiments. Two different types of rigs were used. The difference between them lies in the drive mechanism used. For each test-rig, similar mechanical test settings were arranged.

Before selecting the test conditions for the fatigue tests, a series of preliminary tests were conducted. To select the stress range for the coated panels, which was to correspond to a chosen percentage of the yield strength of the substrate, a slow strain-rate test was performed on uncoated substrate (steel panels) and the load was recorded using a pen chart recorder. The yield strength of the substrate was found to be 2.19 kN. Determination of the substrate yield strength provided the range of loads for steel-coating system which was chosen to be from 15% to 90% of total substrate yield force. Therefore, the load extremes setup for the fatigue test rigs were ~0.3 kN and ~2 kN, respectively. This assured restriction to the region of elastic deformation of the steel substrates, so that plastic deformation did not occur in the substrate, which would have led to coating deformation, and possible stress concentrations that are never encountered in service. In a majority of marine structures, the design ensures that they operate within the range of reversible deformation, well below the yield point.

The frequency of the applied dynamic loading was selected to be between 0.05-0.5 Hz, based on the time-period for cyclic harmonic ballast tank responses to waves. The frequency was too low to produce internal heat within the coating material. Even if internal heat was produced, the small thickness of the coatings also prevented accumulation of heat within the material, even though polymeric materials have low thermal transmission, because of contact with the high heat-capacity, thermally conductive steel-substrate. The frequency maintained for air tests was 0.05 Hz and for seawater test it was 0.33 Hz, depending on the type of testing rig.

All fatigue tests were performed in four-point bending. For that purpose, standard four-point bend jigs were made for every test rig. Figure 3.5. illustrates one of the jigs. The jigs consist of four rollers where the separation between the two (10 mm diameter) outer rollers was 100 mm and between the two (10 mm diameter) inner

rollers was 50 mm. The bend jigs were manufactured from AISI 316 grade stainless steel to be inert in the test environments used.

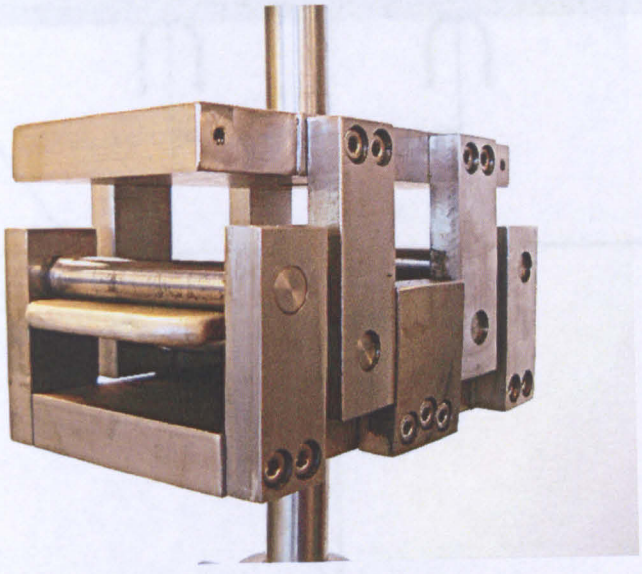

Figure 3.5. Four-point test jig showing 10mm diameter rollers

Four-point loading gives a uniform longidutinal tensile stress in the convex surface of the part of the specimen between the inner supports. The stress decreases linearly to zero from the inner supports to the outer support. Test samples were supported between the outer rollers near the edges and bent by loading the two inner rollers in the opposite directions from the outer ones. The distance between the loading spans was one-half of the support span (Figure 3.6.)

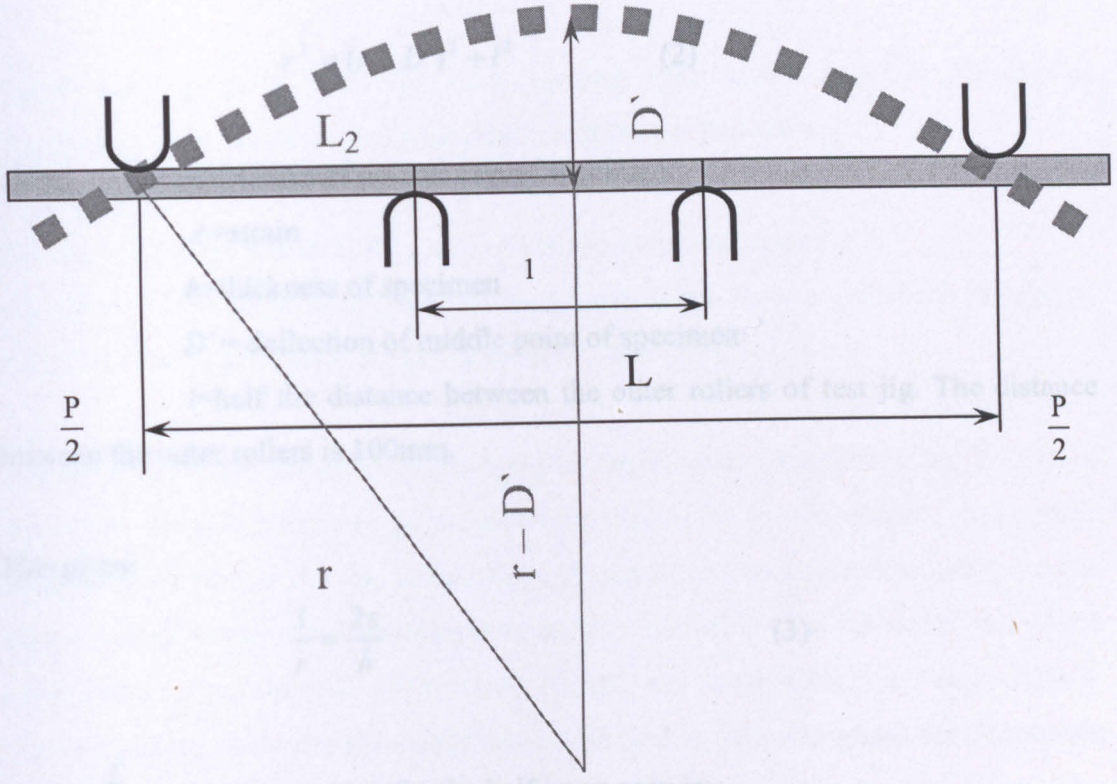

Figure 3.6. Diagram of four-point bend loading

Figure 3.6. illustrates the set-up used in the fatigue loading tests, where loading span is equal to the half of the support span. L_1 is the loading span between the two inner rollers, L_2 is half of support span and L is the support span between two outer rollers, whereas $L_1 = \frac{1}{2}L$.

The strain was determined from displacement measurements of the four-point loading tests. The maximum strain, in the cyclic fatigue tests, was obtained from the following equations:

$$\frac{1}{r} = \frac{1+\varepsilon}{r+\frac{h}{2}} \qquad (1)$$

$$r^2 = (r - D')^2 + l^2 \qquad (2)$$

where: r = radius of neutral axis of specimen

ε =strain

h=thickness of specimen

D' = deflection of middle point of specimen

l=half the distance between the outer rollers of test jig. The distance between the outer rollers is 100mm.

This gives:

$$\frac{1}{r} = \frac{2\varepsilon}{h} \qquad (3)$$

For $l = \frac{L}{4}$, the strain equation for the half inner span is:

$$\varepsilon = \frac{D'h}{3l^2} \qquad (4)$$

This equation was confirmed by standard ISO 8401:1994 [209].

Strain values were obtained for both types of test rigs where different deflections of the middle point of the specimen were obtained. Recorded deflections were 0.55mm and 0.83mm for two types of test rigs. Therefore, strain values on the coating surface during fatigue tests, for a 5mm panel thicknesses and 25mm half inner span, were 0.15% and 0.22%.

In order to investigate the failures in marine coatings under conditions replicating those believed to contribute to failure in coatings in the ballast tanks, the following environments were used for testing:

- air at room temperature,

- artificial seawater at room temperature, where panels were immersed in 3.5% NaCl, which is the approximate salt concentration of seawater [210],
- artificial seawater at 5°C.

Repeat loading-cyclic tests for each coating type were made in all chosen environments. Specimens were tested in three different conditions:
(i) in "as-received" state;
(ii) after curing for 5 days at 80°C (this state was called 'post-cured');
(iii) after a laboratory ageing procedure (Akzo-Nobel recommendation for ageing procedure was used, details of ageing are given in section 3.4.).

The measured strain values in the coatings (at the surface) were 0.15% and 0.22% for the air test rigs and seawater rigs, respectively. Due to the way in which a strain gauge must be attached to a sample, measuring variable strains continuously during the test using a strain gauge was considered to be impractical. It may be noted that if the strain percentages applied were much higher, the steel substrate would deform plastically, an undesirable behaviour that might lead to failure mechanisms that would not happen under service conditions.

Two test rigs were used for fatigue experiments in artificial seawater at room temperature and at 5°C and three test rigs for experiments in air. Loading arrangements for each of the five rigs were similar. One complete strain/release cycle for air tests lasted for 19 s. Artificial seawater environment experiments required further rig development. Firstly, the period was decreased to 3 seconds per cycle, which was achieved.by using a different drive mechanism from the one used for air tests. For room temperature tests, samples mounted in a four-point test jig were placed in a tank which was filled with artificial seawater and cyclic-loading tests were carried out. The test rig for cyclic-loading in artificial seawater at 5°C included in addition a water cooling bath. The samples for this test environment had a water tank around the jig, similar to the one for room temperature seawater tests, but the water was circulated from a controlled temperature water bath so that the medium around samples during investigation had a temperature 5±0.5°C.

During every test, either in air or in seawater, specimens were exposed to loading cycles for a short period of time (after approximately 10,000 cycles) and then testing was stopped, the specimen was inspected visually and using an optical or a scanning electron microscope (SEM). If cracking or any other kind of failure of the coatings was not observed, samples were returned to the test rig for additional loading cycles. Appendix 3.2 describes the procedure used for SEM observation.

3.5.2. SLOT DEFECT - EXPERIMENTAL

After a series of preliminary experiments, in which very little evidence for cracking was found after prolonged cyclic loading, a decision was made that some form of crack initiation was needed. This was achieved by machining slots with carefully controlled dimensions into the coatings. By observing cuts introduced into samples in this way, the monitoring of crack development and growth during and after fatigue tests was facilitated. In service the initial crack may be caused by surface scratches or impact damage. The phase of the research was therefore designed to investigate whether such a flaw would then continue to grow due to the applied cyclic stresses. The experiments indicated that fatigue failures of well-prepared coatings of the types studied are unlikely to occur unless some extraneous damage is suffered to initiate them, but an accidental flaw might nucleate failure and this is the focus of this part of the research. This approach has been developed in the experimental section of this study.

Slots were introduced into each type of coating panel using a rotating slot cutter (Figure 3.7.). The diameter of the cutter was 50 mm and the thickness was 1.59 mm.

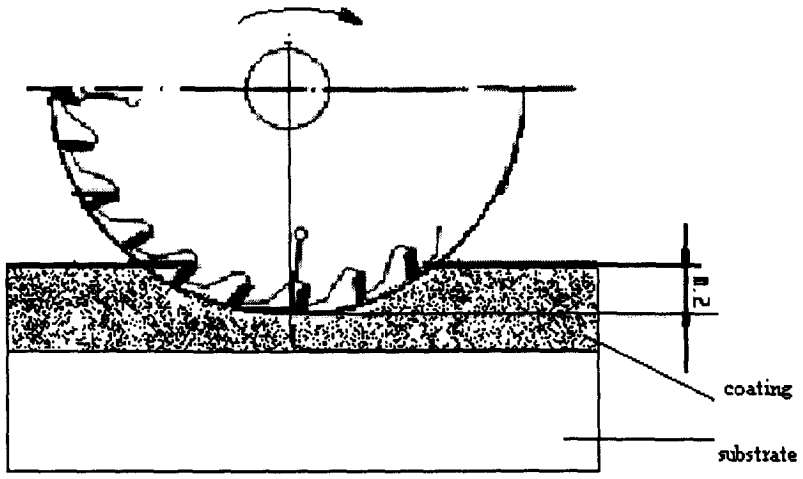

Figure 3.7. Sketch of rotating slot cutter and coated panel [mm]

Slots were made with different lengths and depths and placed in the middle section of the specimens. Figure 3.8. illustrates one pattern of slots that were prepared on test panels. The separation of the slots was 10mm and it was sufficient to prevent them from interacting with one another.

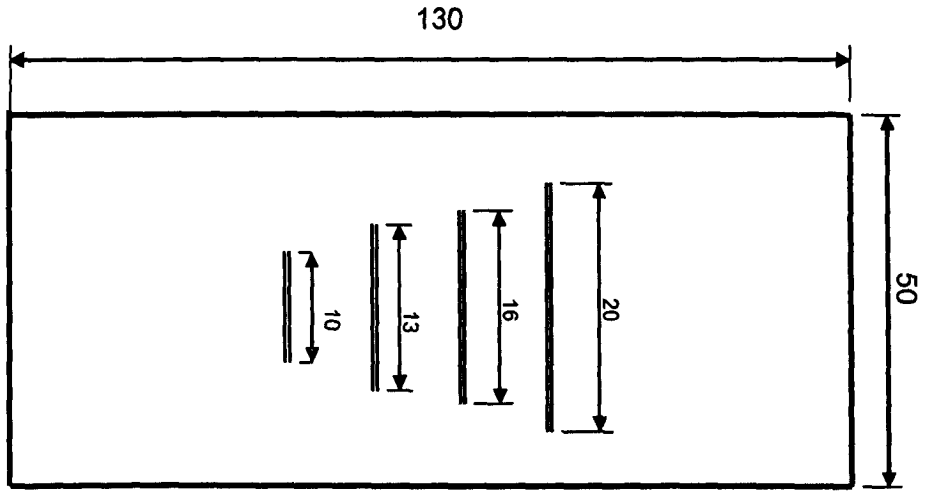

Figure 3.8. Slots with different lengths in mm. Depth of the slots was 0.2 mm

The faster frequency test rigs were used for the tests in air on slotted samples, as frequency is less critical in air tests. The time for one fatigue cycle was 3 seconds per cycle; strain rate was correspondingly higher than that with the rigs operating at a lower frequency.

A second set of the experiments was performed on test panels with three slots with different depths. Figure 3.9. illustrates the positions of the slots with their dimensions.

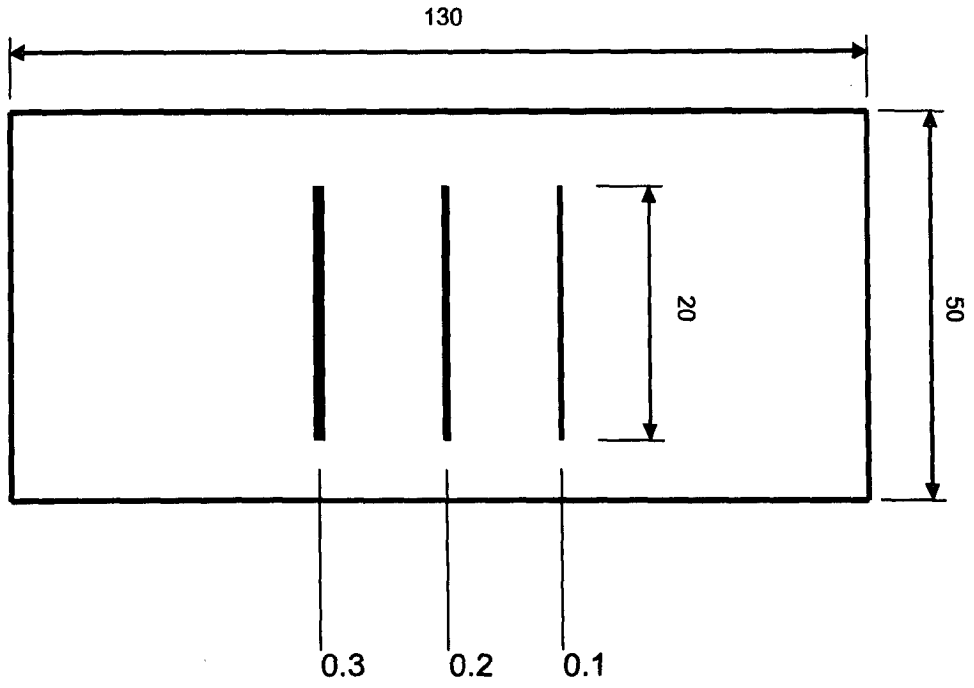

Figure 3.9. Slots with different depths: 0.1; 0.2 and 0.3 mm; distance between slots was 10mm

3.6. TENSILE TESTS

A tensile test is probably the most fundamental type of mechanical test that can be performed on material. By pulling on the material, determination of the material's reaction to the forces being applied is very rapid. Using this kind of test on free-films of the coating materials, their strength was found along with how much they will elongated before failure. The increase in a sample's gauge length measured after rupture divided by the sample's original gauge length is referred to as elongation. The greater the elongation, the higher the ductility of the material. Tensile tests in this study were performed on free-films of the coatings and on the coated steel-substrates.

3.6.1. TENSILE TESTS ON FREE-FILMS

Free-films of the coatings were tested in two conditions: 'as-received' and 'post-cured'. Free-films that were cured for 5 days at 80°C were consider as 'post-cured'. 'As-received' free-films were tested on a Hounsfield testing machine, whereas 'post-cured' samples were tested using the Lloyds tensile testing machine. Due to natural ageing of the coatings and apparatus availability, testing of the 'as-received' free-films on Lloyds tensile machine was impossible.

3.6.1.1. Tensile tests of 'as-received' samples

The set of experiments was carried out on a Hounsfield testing machine, where free-films were strained manually until fracture. A plot of the force versus the extension was obtained using a pen-chart recorder, which was connected to the Hounsfield testing machine. The gauge length as well as the dimensions of the samples was measured before and after the fracture. All three types of the coatings were tested this way with no previous conditioning.

3.6.1.2. Tensile tests of 'post-cured' samples

A Lloyds tensile testing machine was a second type of apparatus used for obtaining tensile strength of the coatings. The drive mechanism was controlled by a computer with a load cell with a maximum 50N capacity. Grip (Figure 3.10.a) selection was very important factor for these tests. The faces of the samples covered a large gripped area so that so called "jaw break" (sample breakage inside the gripped area) could be avoided. A typical graph of applied stress and sample elongation during these tests is shown in Figure 3.10.b.

a) b)

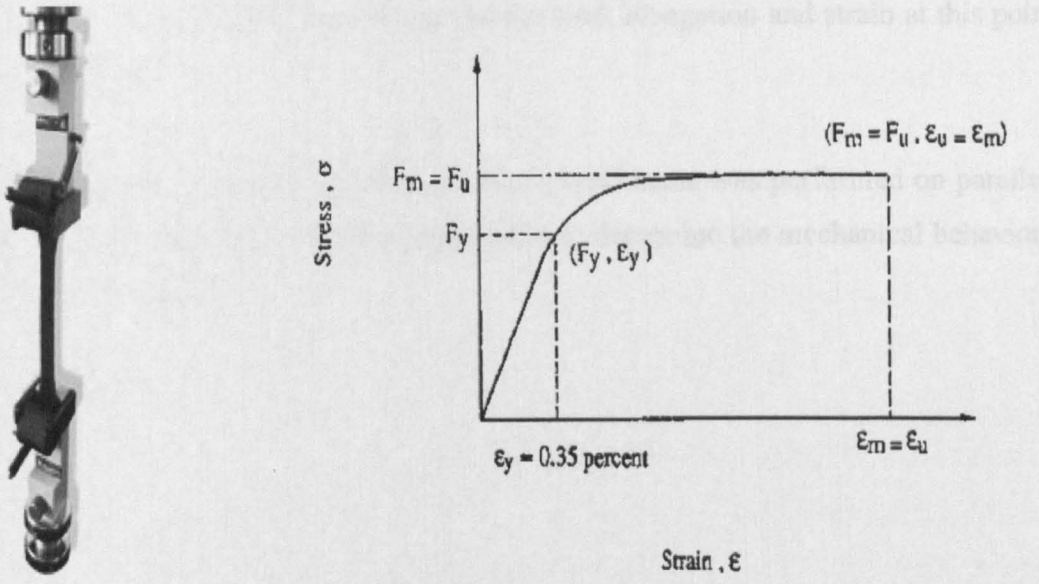

Figure 3.10. a) Gripped sample for tensile tests; b) Typical graph showing an stress-strain curve from a load-controlled tensile test [40]

Another factor that can affect the testing results is the accuracy of the measured elongation of the samples. Even though computer software was used, there is some

changes of samples dimensions. Three experimental marine coatings were tested on this machine after curing for 5 days at 80°C.

3.6.2. TENSILE TESTS ON PANELS

Another type of tensile test was performed using the slow strain rate (SSR) technique. Test specimens of the three coatings on steel substrates were machined into two different shapes, a parallel strip and a notched specimen (Figure 3.11.), each measuring approx 10.5mm across the gauge width. The specimens were then tested in the SSR machine, held in place by a pair of wedge type grips. Specimens were tested dry and after being soaked in de-ionized water for 30 days. The test was stopped when a crack had propagated in the coating and the load, elongation and strain at this point were recorded.

Prior to the tests on coated samples, a set of experiments was performed on parallel, unpolished and uncoated mild steel specimens to determine the mechanical behaviour of the substrate steel.

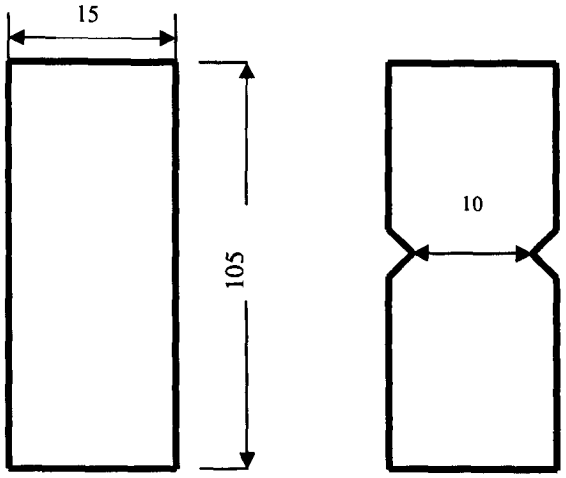

Figure 3.11. Parallel and notched shape of samples used for SSR tests [mm]

All specimens were polished up to 1200grit silicon-carbide to remove any scratches along the edges. The SSR machine was connected to a monitor that gave a printout of load against time, from which the properties of the sample could be calculated. The load cell was set to 1415N/mV output. The coatings were prepared on mild steel substrates measuring ~ 150x75mm. The coating was removed from each end (shoulder) to avoid slippage in the grips.

De-ionized water was used as medium for pre-immersion tests. Unlike the substrate tests, the coatings were tested until a crack propagated on the coating. Crack observation was aided by using a lamp and a magnifying glass. Tests were checked every thirty minutes during straining and the load and elongation at which the crack appeared were recorded.

3.7. HARDNESS TESTS

Indentation methods have been used for almost a century to assess the hardness of materials and to estimate the yield stress. While these conventional hardness measurements are easy to perform, they cannot easily be applied to soft materials.

Hardness testing can be divided intro three categories: macro-; micro- and nano-hardness. In this study measurements were performed on the three chosen epoxy coatings using micro- and nano-hardness tests. Description of equipment and tests details are given in section 2.3.2.

Initial tests were completed on a Vickers machine for samples of all three coating types. Specimens used for these tests were free-films and panels in 'as-received' and 'post-cured' state.

The indenter was pressed into the sample by an accurately controlled test load. The full load was normally applied for 10 to 15 seconds. The two diagonals of the indentation left in the surface of the material after removal of the load were measured using a microscope and their average calculated. The Vickers hardness number was a function of the test force divided by the surface area of the indent. The average of the two diagonals is used in the following formula to calculate the Vickers hardness.

HV = Constant x Test force / Surface area of indentation

The hardness results were obtained from the indentation measurement using conversion tables.

A set of the microhardness measurements were performed on panels sprayed with each type of the experimental coatings before commencing the ageing procedure. The ageing procedure that was used for these tests was the accelerated method developed as part of the research, details of which are given in section 3.4. The measurements were made after every ageing cycle within the 1 hour after the ageing step was

finished. The final cycle was carried out in seawater and measurements were taken immediately after the ageing process and one and two hours afterwards.

Measurements were performed using the Vickers microhardness test. To measure the hardness of a thin film coating (or the surface hardness of a case-hardened part) the microhardness test was the appropriate technique. In the test a very small diamond pyramid is placed on the sample and a small applied load of 10 to 1,000 gf (0.01 to 10 N) is used. This low amount of load creates a small indent that must be measured under a microscope.

When measuring a coated part, the hardness values that are obtained using large loads are very close to the substrate hardness values. As the load is decreased and the depth of penetration of the indenter decreases, the measured hardness value approaches that of the coating. Ideally the depth of the indent can be maintained at about 20% or less of the coating thickness, then the hardness values accurately reflect the coating hardness.

Additional microhardness tests involved investigating the effect of soaking on the hardness of the three marine epoxy coatings. Mild steel substrates coated with each coating system were tested for set periods, ranging from 24 hours up to 1 month and the hardnesses recorded at intervals throughout the soak and dry-out periods.

Firstly, the measurements were made on the panels before immersion into de-ionized water. No pre-treatments were performed prior to these tests. Specimens were placed in the cabinet in the 'as-received' state and naturally aged until tested. Once the soak time of the coating was completed the sample was removed from the de-ionized water and tested. First surface water was removed from the sample so that it did not affect the image under the microscope. The hardness was measured as soon as the sample was removed. Two indents were made and measured to obtain an average. Specimens were immersed in de-ionized water for 3, 7 and 30 days and hardness measurements were made periodically during the dryout period immediately after soaking, up to 24 hours.

A set of hardness tests was carried out using a nanoindentor. While indentation testing is quite simple, requiring only minimal sample preparation, the mechanical interpretation of these tests is not straightforward (see section 2.3.2.3.). There is still no widely accepted method available which permits determination of both elastic and plastic properties of a material from nanoindentation tests. Nano-indentation is a process where the maximum displacement (area of observation=indentation depth) is around 1μm. Thus the presented data is more sensitive to local material heterogeneities than other mechanical measurements. Nano indentation of polymeric materials can be difficult. The aim of these measurements was to check hardness values of the coatings prior to any conditioning. Therefore, samples used for those measurements were in the 'as-received' state. Since this method was automatic under the control of computer-software, the placement of the indents was not selected individually – a row of indents was made, with pre-determined spacing, and if a surface irregularly was present it would not necessarily be avoided. From the unloading curve the values for Young's modulus and hardness were obtained.

3.8. INTERNAL STRESS MEASUREMENTS

3.8.1. SAMPLE PREPARATION

To assess the stresses inside the coatings thin standard shim steel was chosen as a suitable substrate. The coating was applied to one surface of the substrate and if the coating shrank or expanded the coating-substrate combination bent, the curvature depending on the internal stress in the coating. The present investigation used several different measuring methods for radius of the curvature, on shims with different lengths (150mm and 250mm), steel thicknesses (0.1mm, 0.2mm and 0.3mm) and types of coatings (coating A, coating B and coating C). Experiments were conducted using stainless steel shims provided by three different manufacturers.

Substrates were cut into coupons measuring 150x20mm and 250x20mm. All dirt, grease, rust, etc. were removed by using silicon-carbide emery paper #120 and #500 grit. The stainless steel coupons were pre-treated with a poly(vinyl-butyral) (PVB) based etch primer prior to applying the epoxy coatings. PVB primer was applied by brush. Some characteristics of PVB primer are given in Appendix 3.1. The substrates were laid down on a board and placed in a fume cupboard where coating application was performed. Ideally, coatings should be applied on the substrate with a fine spray in order to obtain a fine, evenly distributed surface. However, coatings application was performed under industrial conditions, using a hand brush, as smoothly and as evenly distributed as possible.

3.8.2. METHOD OF INTERNAL STRESS MEASUREMENTS

As the most common method used to determine coating stress is measuring the curvature of a coated substrate, that technique was applied in this investigation. The stainless steel shims were normally curved somewhat in the 'as-received' state and the initial curvatures were measured prior to the spraying. The initial radius was called the 'zero radius' and was the reference state. The curvature (=1/radius) for this reference state was subtracted from the curvature of the coating-substrate combination

to determine the effect of the stressed coating. After coatings applications, shims were air dried for 2 days at 25°C for coatings "A" and "B" and at 35°C for coating "C", replicating a standard procedure used in industry. Samples were transferred to the test laboratory 48 hours after application. Brief inspection of the specimens was carried out, and there was no visible stress developments (i.e. the contour of the shims was no different from the one they had before the coatings were applied). Further curing of the samples in fan oven at 80°C for 5 days was performed. During this drying cycle the samples were free to bend (the samples were not restrained in any way). The samples were placed on the oven tray with the uncoated steel facing down. After 5 days, the specimens were taken out of the oven and allowed to cool to room temperature (about 22±2°C) followed by radius measurements. The radius measurements on cured samples were performed by matching the shim radius to a set of circular curves already drawn on a transparency and was calculated geometrically. Geometrical calculations were carried out with the following procedure: samples were clamped lightly in one location so that they were free to bend with the width direction vertical, and held above a piece of white paper. The contour of the curved surface was copied onto the paper and the curvature determined using standard geometric measurements. With this arrangement, there was no gravitational contribution to bending. The reproducibility of the curvature measurements was good and comparison of two used methods for obtaining radius of shims curvature gave a standard error $<0.003\ m^{-1}$.

Equation 7. from the section 2.3.6.3. was used for calculations. For a coating with Young's modulus E_c, Poisson's ratio υ_c and thickness a on a substrate with Young's modulus E_s, Poisson's ratio υ_s and thickness b, the relationship between the radius of curvature R and the internal stress in the coating (σ_c) is given by [205]:

$$\sigma_c = \frac{aE_c}{6R(1-\upsilon_c)} \frac{1+4\alpha\beta+6\alpha^2\beta+4\alpha^3\beta+\alpha^4\beta^2}{(1+\alpha)(1+\alpha\beta)}, \qquad \text{Equation 7.}$$

where: $\alpha = \frac{b}{a}$ and $\beta = \frac{E_s}{E_c}\frac{1-\upsilon_c}{1-\upsilon_s}$.

3.9. CHAPTER SUMMARY

The Experimental chapter of this thesis provides details of three types of coatings that were used in this study, coded as coatings 'A', 'B' and 'C'. Types of samples are categorised (panels, shims-coatings samples and free-films) and their preparation is described. Specimen conditioning is given. Samples can be found in three different states:

- in 'as-received' state (samples were supplied manufactured in that condition)
- in 'post-cured' state (in a laboratory conditions, samples were post-cured for 5 days at 80°C)
- after ageing procedure (note: Two ageing processes were performed; the first one was an industrial procedure lasting 275 days. The second was developed during this research, a shorter version of the industry scheme. Specimens that were aged according to the first ageing procedure were used for cyclic-loading tests and samples prepared using the second ageing process were used to follow the hardness values of the tested coatings.)

Experiments were divided into five different sections:

(i) Cyclic-loading using panels in three different conditions. Tests were performed in three different environments: air at room temperature, artificial seawater at room temperature and at 5°C.

(ii) Cyclic-loading of the panels with introduced slot defects. Tests were performed in air at room temperature, on panels with 4 slots of different lengths and on panels with 3 slots of different depths.

(iii) Tensile testing of epoxy coatings.

(iv) Microhardness measurements were made using 'as-received' and 'post-cured' free-films of all three coatings. The Vickers hardness method was carried out for those measurements. The same type of tests was used for assessing the hardness values of epoxy systems during ageing. Nanoindentation was performed on coated panels in the 'as-received' state.

(v) Internal stress measurements were performed on shims after curing at 80°C for 5 days on all three coating systems.

The next chapter gives the results for each experimental method performed for all four testing types and some additional tests that were developed during this project.

PAGE
MISSING
IN
ORIGINAL

CHAPTER 4.

RESULTS

4.1. CYCLIC-LOADING TESTS

Cyclic-loading tests for each coating type were performed using 'as-received', 'post-cured' and aged panels in the various environments described earlier (Section 3.5.1.). All three types of coatings were tested in those three conditions using the experimental set up described in Chapter 3.5.1.

The measured strain amplitude values in the coatings (at the surface) were 0.15% and 0.22% for the air tests and seawater tests, respectively. Strain calculations are given in chapter 3. Due to the way in which a strain gauge has to be attached to a sample, because of the low natural frequency of the rig system, measuring variable strains continuously during the test using a strain gauge was considered to be impractical. It may be noted that if the applied maximum strain were higher, the steel substrate would deform plastically, an undesirable behaviour that might lead to failure mechanisms that would not happen under service conditions. After tests, the panels were inspected visually using optical and scanning electron microscopy. Tests were initially stopped for surface inspection after approximately 10,000 cycles. Samples that went on beyond 100k cycles were examined at interval of approximately 50k cycles. Panels for all three types of the coatings were tested with an additional number of loading cycles to take them all to approximately 500,000 cycles.

The following sections will give details of the achieved results for each coating type separately.

4.1.1. 'AS-RECEIVED' SAMPLES

Prior to the investigations, samples were not additionally conditioned, just air dried after coating application. That state of the samples was called 'as-received'. Experiments were performed in three test environments: air; simulated seawater at room temperature; and simulated seawater at 5°C. 3.5% NaCl was used for seawater investigations. The tests were observed visually and the total number of test cycles was recorded. Results for cyclic-loading tests for each coating type are presented below.

4.1.1.1. Coating 'A'

Performance of the coating 'A' panels were investigated under cyclic-loading for various test environments. Each sample was consisted of mild steel substrate and applied coating system, as was described earlier in section 3.3.1. The side of the specimens which was put into tension during cyclic-loading was inspected prior the testing and images of the coating surfaces were taken. Panels were tested as described in section 3.5.1. Observations of the cyclic-loading tests for 'as-received' coating 'A' are given in table 4.1.

Table 4.1. Cyclic-loading test results for 'as-received' coating 'A'

TEST ENVIRONMENTS	'AS RECEIVED' Panels, Coating 'A'		
	Panel Number	Total Number of Test Cycles	Visual Observation
Air at Room Temperature	A1	502,024	Tensile Surface Changed
	A2	20,000	No Changes
Simulated Seawater (3.5% NaCl) at Room Temperature	A40	512,508	No Changes
	A41	94,081	No Changes
Simulated Seawater (3.5%NaCl) at 5°C	A101	524,637	No Changes

Generally, coating 'A', when tested in 'as-received' condition, showed high resistance during the tests. No evidence of cracking was observed when samples were tested for 500k cycles. Indication of the changing of coating surface was recorded in air cycling-loading tests. Sample which was tested for 20,000 cycles did not show changes on the tensile coating surface, but the observed changes were recorded for the sample which was tested for just over 500k test cycles. Inspection of the sample did not indicated changes of the surface after 450k test cycles. Prolonged testing produced changes as shown in Figure 4.1.

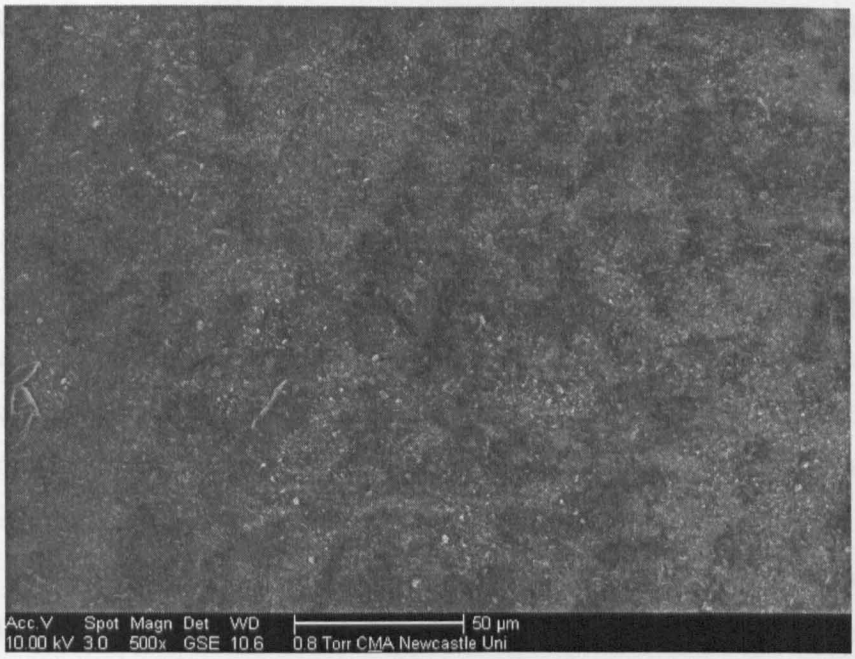

a) before cyclic test

b) after just over 500k test cycles; panel tested in air; tension side

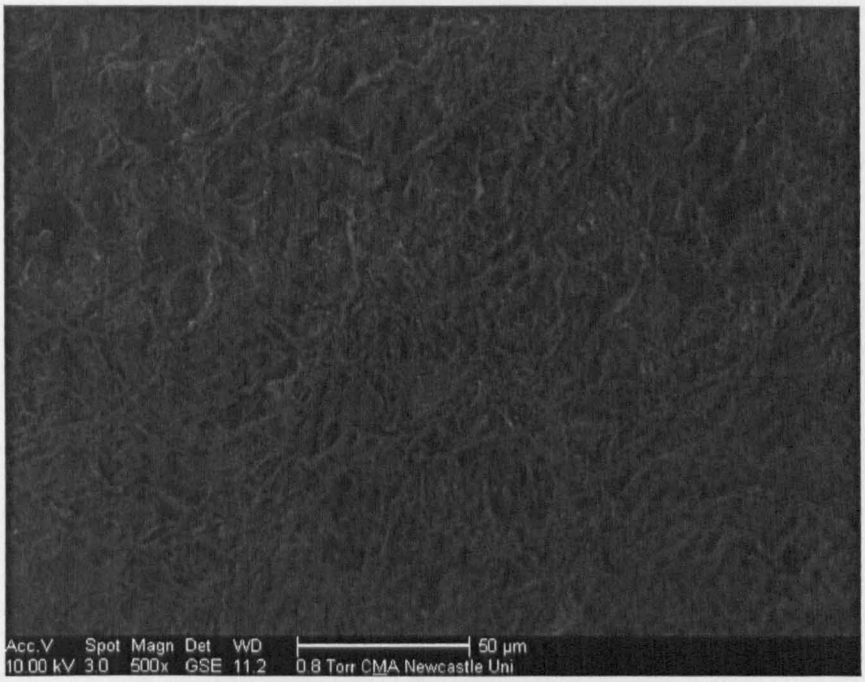

Figure 4.1. Typical surface of a panel coated with a coating 'A', sample A1

Figure 4.1. shows surface ripples, dimples and increased topographic features due to a combination of solvent loss (causing shrinkage), the cyclic deformation and the test environment. According to the number of cycles needed to produce the coating changes (500k), solvent evaporation was progressed after longer testing and effect of solvent evaporation on coating surface was distinguished. Since the coating was not preconditioned, solvent was still trapped within coating system. No visible changes of the coating 'A' tensile surface were obtained in seawater environment at different temperatures, when tested under chosen cyclic-loading in 'as-received' state after 500,000 cycles. Explanation as to why seawater environment did not produce any changes of the tensile surface of the coating could be two-fold. Either tests in air allowed solvent loss more effectively then the seawater or that seawater plasticise the polymer matrix (second hypothesis was obtained by other researchers [211]). Nevertheless, possible combination of the both ways could be the main reason why 'as-received' coating 'A' showed surface changes only when fatigue tested in air at ambient temperature.

4.1.1.2. Coating 'B'

'As-received' Coating 'B' panels were tested under cyclic-loading in air, simulated seawater at room temperature and at 5°C. Test procedure is described in 3.5.1. Surface of the coated samples were investigated before testing and inspection of the specimens were performed visually after approximately 10k test cycles. Only the tensile surface of the specimens were observed. Obtained results are presented in table 4.2.

Table 4.2. Cyclic-loading test results for 'as-received' coating 'B'

TEST ENVIRONMENTS	'AS RECEIVED' Panels, Coating 'B'		
	Panel Number	Total Number of Test Cycles	Visual Observation
Air at Room Temperature	B12	493,102	Tensile Surface Changed
	B29	95,494	Tensile Surface Changed
Simulated Seawater (3.5% NaCl) at Room Temperature	B28	194,400	Tensile Surface Changed
	B34	561,079	Tensile Surface Changed
Simulated Seawater (3.5%NaCl) at 5°C	B101	578,541	No Changes

Cyclic-loading tests of coating 'B' in 'as-received' conditions showed no indication of cracks when samples were loaded for about 500,000 test cycles. Visual investigations of the specimen surfaces indicated that the coating surface was changed after some test procedures. For air tests, coating 'B' showed surface changes after 95,000 test cycles. Prolonged testing for nearly 500k cycles for the sample B12 in air at room temperature still showed surface changes, but no additional coating defect was observed. Surface appearance changed for the samples of coating 'B' when tested in simulated seawater at room temperature, but changes took longer to develop than in air. Figure 4.2. shows the coating surface before and after testing. Over 550k test cycles of coating 'B' in seawater at 5°C did not give any coating visual defect.

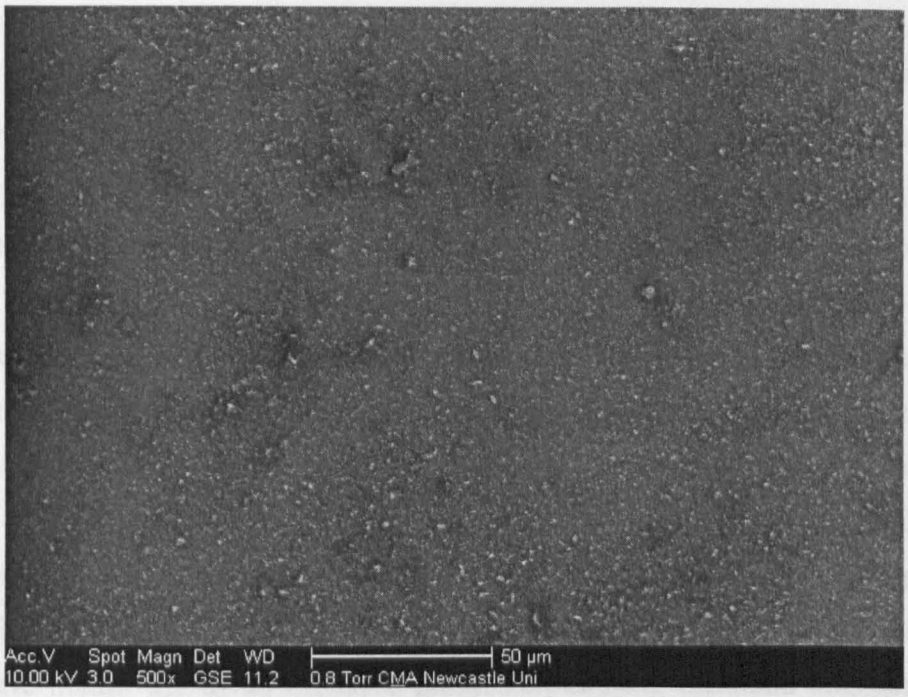

a) before test

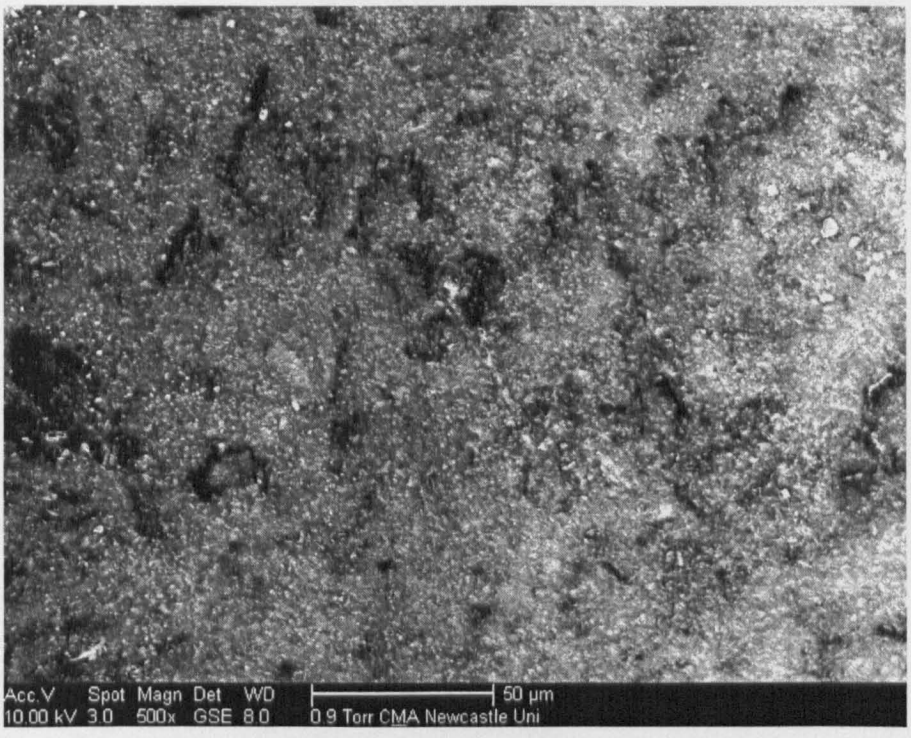

b) after 560k test cycles in simulated seawater at room temperature; tension side

Figure 4.2. Typical coating 'B', 'as-received', sample B34

Presented images in figure 4.2. shows surface before and topographic changes of the surface after cyclic-loading tests where coating 'B' showed visible changes after tests in seawater when tested in the 'as-received' state at room temperature. This could be due to polymer plasticization by seawater. In the presence of water, a polymer may become swollen, exhibiting major changes in mechanical and chemical properties [201]. Water can plasticise the polymer matrix or form stable bridges through hydrogen bonding, resulting in a plasticizing effect. The behaviour of water can be transformed in the presence of a polymer, depending on the degree of chemical or physical association between the water and polymer phases. Plasticization occurs when a small molecule blended with a polymer results in a decrease of the T_g of the polymer and its elastic modulus. Such plasticization normally increases polymer flexibility or mobility. It has been reported that water molecules absorbed into a polymeric matrix act as an effective plasticizer, causing profound changes in the physicochemical properties of solid [213].

4.1.1.3. Coating 'C'

'As-received' coating 'C' panels were tested using four-point bend loading tests in different environments. Test procedure was matching the tests that were performed for other two experimental coatings. The surfaces of the tested samples were visually inspected before testing procedure. Observations that were obtained during these tests are given in Table 4.3.

Table 4.3. Cyclic-loading test results for 'as-received' coating 'C'

TEST ENVIRONMENTS	'AS RECEIVED' Panels, Coating 'C'		
	Panel Number	Total Number of Test Cycles	Visual Observation
Air at Room Temperature (0.15% strain)	C	478,334	No Changes
	C1	112,145	Tensile Surface Changed
Simulated Seawater (3.5% NaCl) at Room Temperature (0.22% strain)	C102	492,997	No Changes
Simulated Seawater (3.5%NaCl) at 5°C (0.15% strain)	C101	496,334	No Changes

The total number of test cycles for each test environment was nearly 500,000 cycles. Cracking behaviour was not obtained for that number of test cycles. One of two samples that were tested in air at room temperature showed tensile surface changes after over 100k cycles, as shown in Figure 4.3. C102 specimen was tested in simulated seawater at room temperature for 492,997 cycles and no evidence of coating defects was apparent. Nearly 500k cycles for coating 'C' sample in 'as-received' state in simulated seawater at 5°C showed high coating resistance under those test conditions.

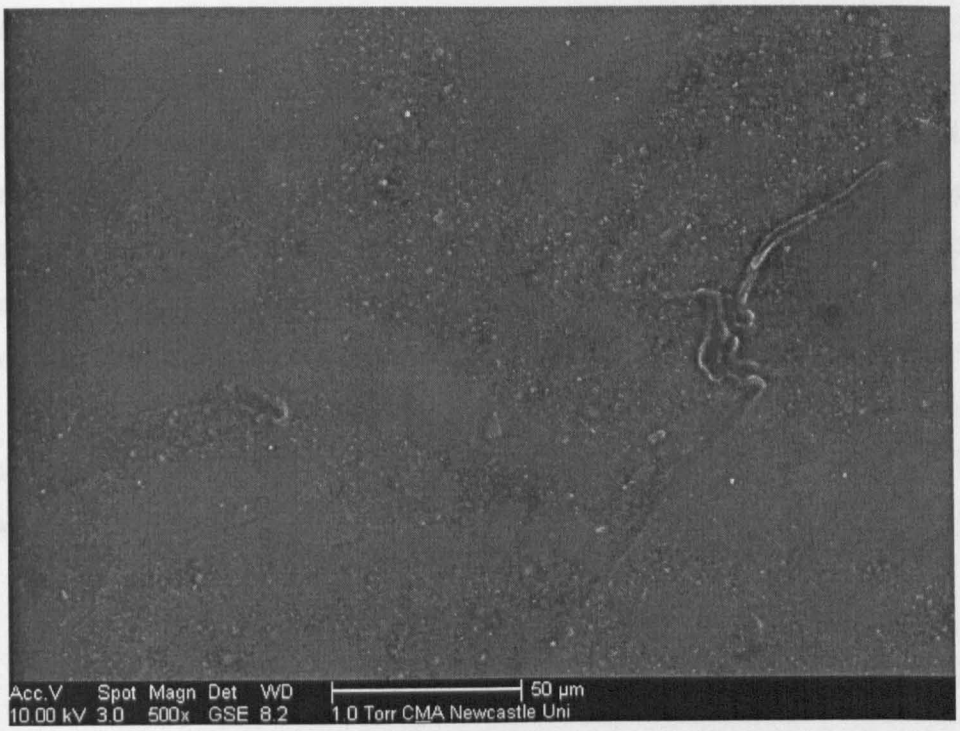

a) before test

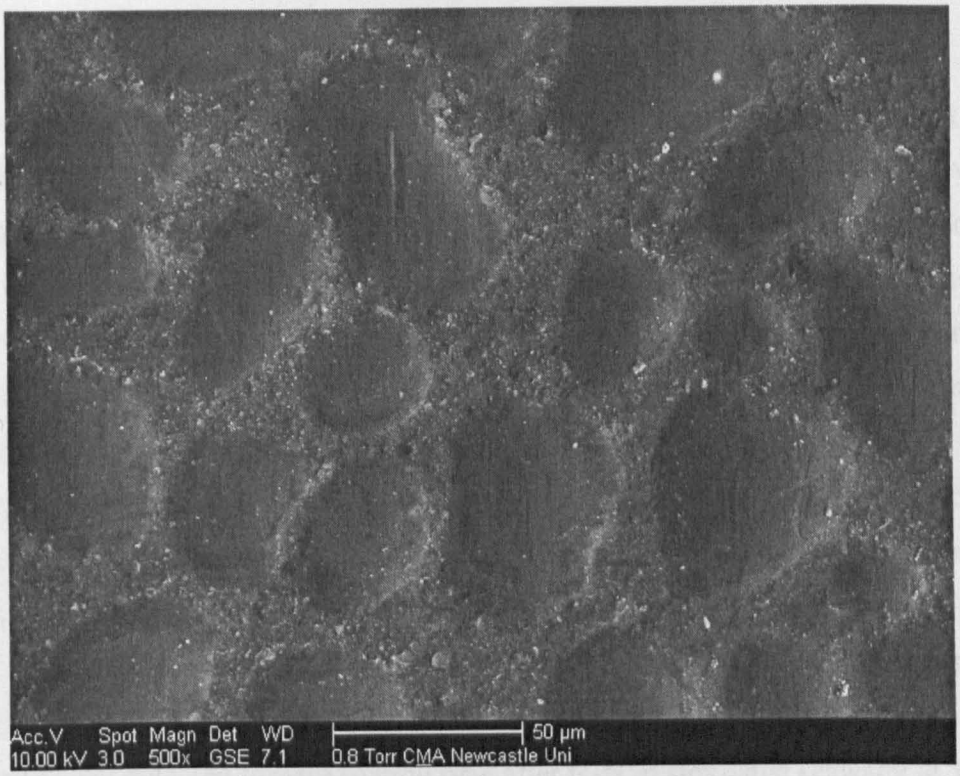

c) after 110,000 cycles in air; tension side

Figure 4.3. Typical coating 'C', 'as-received', sample C1

Curiously, although one sample tested in air (C1) showed surface changes after just over 100k cycles, a similar sample (C) showed no visible changes within ~480,000 cycles under similar conditions. The panels were not sprayed at the same time and the difference in their performance under the same test conditions could be due to different storage/drying periods. After spraying panel C was stored in air for a considerable time prior to the cyclic tests and the extended drying period of this panel may have caused the top layer of the coating resin to become harder. Panel C1 was fatigue tested soon after the coating application (5 days upon receiving the sample from the manufacturer, panel C1 was tested). The changes may be considered to be a degradation of the coating.

4.1.1.4. Summary of the cyclic-loading tests for 'as-received' samples

The experiments indicated that 'as-received' coated panels did not show cracking on the tensile side of the specimens at the fairly low strain levels applied. However, visible surface modifications were detected after the tests in some cases. Each epoxy coating showed changes on the surface when tested in air. The investigations presented in Tables 4.1. - 4.3. indicate that surface changes of the coatings occurred only after long duration cyclic fatigue tests (approximately 500,000 cycles). All three types of coating showed changes on the surface after a significant number of test cycles (the average number of test cycles needed for visible surface changes to occur was ~100,000) when tested in air. Simulated seawater environment showed visible changes only for coating 'B' when tested at room temperature. The reason for this may be caused by the different solvent mixture than for the other two coatings (see Table 3.1.) where solvent content effectively changes coating performance. However, no changes were detected for any coating type after tests in simulated seawater at 5°C.

4.1.2. 'POST-CURED' SAMPLES

Investigations were performed on samples that were transferred from "as-received" to "post-cured" state by temperature conditioning for 5 days at 80°C. Testing procedure was matching 'as-received' tests (for testing procedure see section 3.5.1.). All three coating systems were investigated in three different test environments. Inspection of the samples surfaces were performed at approximately 10,000 test cycles and after 100k cycles samples were monitored after every 50k cycles. The inspection period of 50,000 cycles was selected according to the resistance period of the uncured ('as-received') samples observed earlier (see section 4.1.1.). The following sections give observation of these experiments for each coating individually.

4.1.2.1. Coating 'A'

Post-cured samples of coating 'A' were four-point bend cyclic-loading tested in air at room temperature, simulated seawater at room temperature and simulated seawater at 5°C. The tests performed are summarised in Table 4.4.

Table 4.4. Cyclic-loading results for 'post-cured' panels of the coating 'A'

TEST ENVIRONMENTS	'POST-CURED' Panels, COATING 'A'		
	Panel Number	Total Number of Test Cycles	Visual Observation
Air at Room Temperature	A12	68,210	No Changes
	A15	503,441	No Changes
Simulated Seawater (3.5% NaCl) at Room Temperature	A601	495,303	Under-Roller Cracks
Simulated Seawater (3.5%NaCl) at 5°C	A13	403,300	No Changes

Air tests at room temperature showed no indication of changes of coating 'A' in post-cured condition after 503,441 cycles. A12 sample was tested for just over 68k cycles and prolonged tests for over 500k cycles of A15 sample did not affect coating appearance. Cracks were observed on a panel coated with coating 'A' type after being

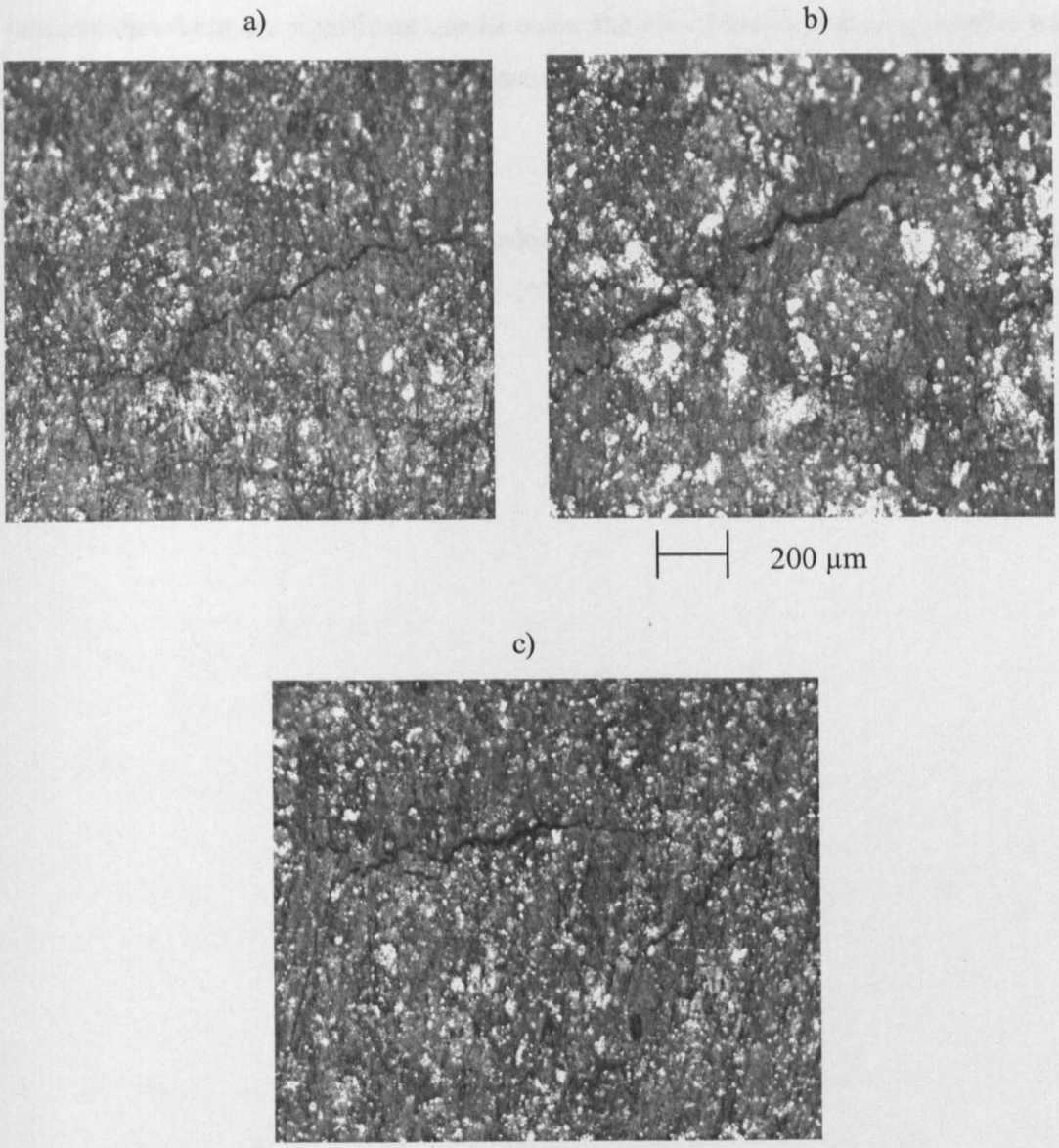

Figure 4.4. a,b,c) Showing cracks formed under the roller, panel-A601 after 195,000 cycles tested in simulated seawater at room temperature; optical micrographs; the images are oriented so that the roller axis is horizontal

tested in simulated seawater at room temperature (sample A601). During the inspection of that sample after just over 195,000 cycles, cracks were visible under the jig-roller and further testing of the sample to 495,303 cycles did not cause any further cracks to appear. After additional test cycles on the panel, the cracks on the one roller-mark were still visible and no changes in their length were detected and no new cracks were observed. Figure 4.4. shows images obtained from the inspection. The figures indicate that there are significant cracks under the pin of the jig, running parallel with it. No cracks were observed in the central area of the specimen, distant from the loading postions.

Cracks were not detected after cyclic-loading tests of the post-cured coating 'A' sample (A13) in simulated seawater at 5°C and no indication of coating degradation was apparent after 403,300 test cycles.

4.1.2.2. Coating 'B'

Coating 'B' panels were tested under cyclic-loading after post-curing and showed very little uniformity. Three different test environments were used during those experiments and observations are presented in Table 4.5.

Table 4.5. Cyclic-loading test results for coating 'B' 'post-cured' panels

TEST ENVIRONMENTS	'POST-CURED' Panels, Coating 'B'		
	Panel Number	**Total Number of Test Cycles**	**Visual Observation**
Air at Room Temperature	B38	486,631	Sample Bent due to Overload* Coating Cracked
	B1	195,500	No Changes
	B4	427,500	Fatigue Cracks
	B39	192,500	Under-Roller Cracks
	B46	577,600	No Changes
Simulated Seawater (3.5% NaCl) at Room Temperature	B2	704,492	Under-Roller Cracks
Simulated Seawater (3.5%NaCl) at 5°C	B35	497,073	Under-Roller Cracks

* Note: Due to an unexpected electrical fault, load values during the test were extreme. Calculated strain on the coating surface after this test was 1.8%. Therefore, the substrate was into the plastic zone and the coating showed cracking under these extreme conditions.

The samples of coating 'B' that were post cured for 5 days at 80°C prior to the experiments showed significant variation when tested in air at room temperature. B38 sample was tested for over 485k cycles, but due to unexpected electrical fault, load values during the tests were extreme (see *Note). Under the same testing circumstances, two samples, B1 and B39 showed different development. No changes were obtained for the B1 specimen after 195,500 test cycles whereas the B39 sample showed under-roller cracks after 192,500 cycles with no indication of cracking over the rest of the coating surface. Cracks appeared under the rollers (under two of four,

both on the tension side of the specimen) after the first 150k cycles. Their lengths were greater after accelerated testing (total number of test cycles was 192,500k) but the coating still showed resistance to fatigue (e.g. no cracks were observed in the central area). Figure 4.5. shows images of the cracks that were observed under two jig-rollers of that specimen.

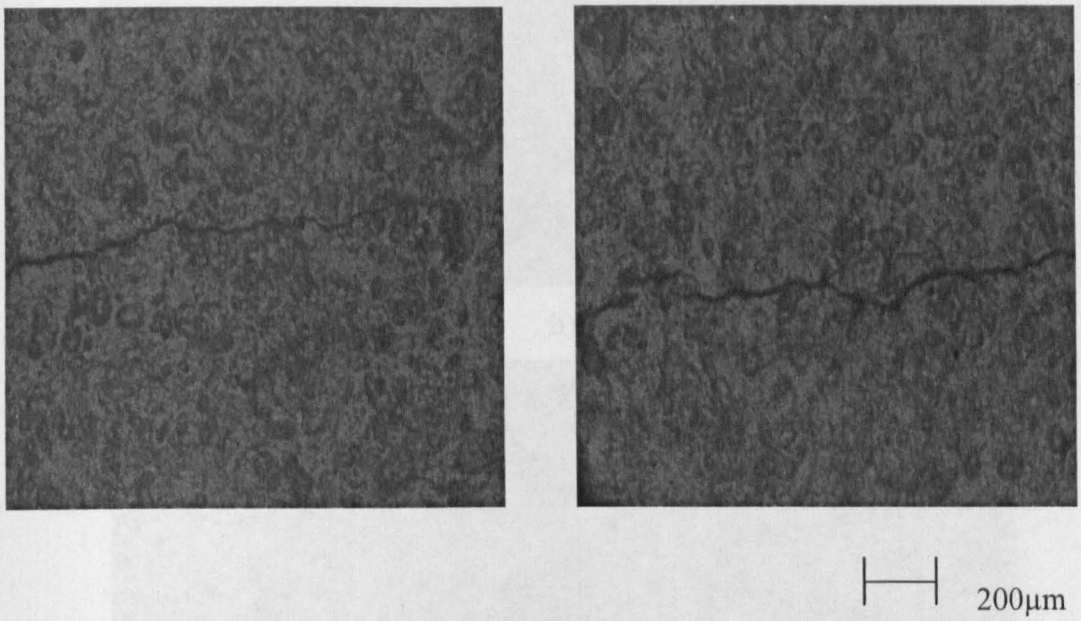

Figure 4.5. Panel B39 after fatigue tests in air, 190,000 cycles; optical microscopy; ~60x, showing cracks formed under the rollers; roller orientation was horizontal

Quite different behaviour was observed with panel B4, tested in air at room temperature. Fatigue cracks were apparent after over 400,000 cycles (Table 4.5.). Images at low magnification are given in Figure 4.6. where the position of the cracks on the sample can be observed. The tension side of the panel is shown in each figure. The cracks were formed at positions well away from the loading rollers. Interestingly, there was no evidence of cracks under the rollers.

a)

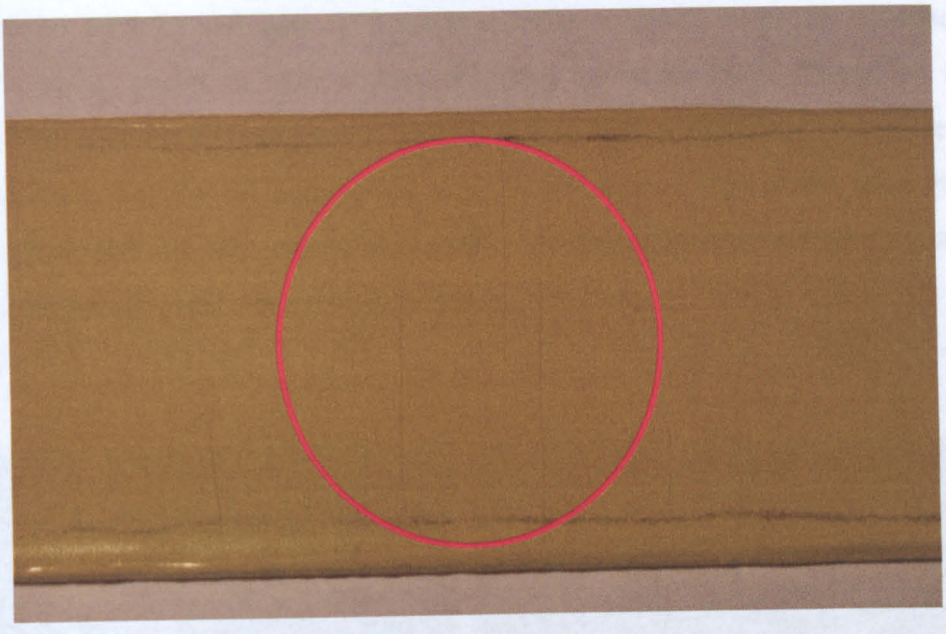

b)

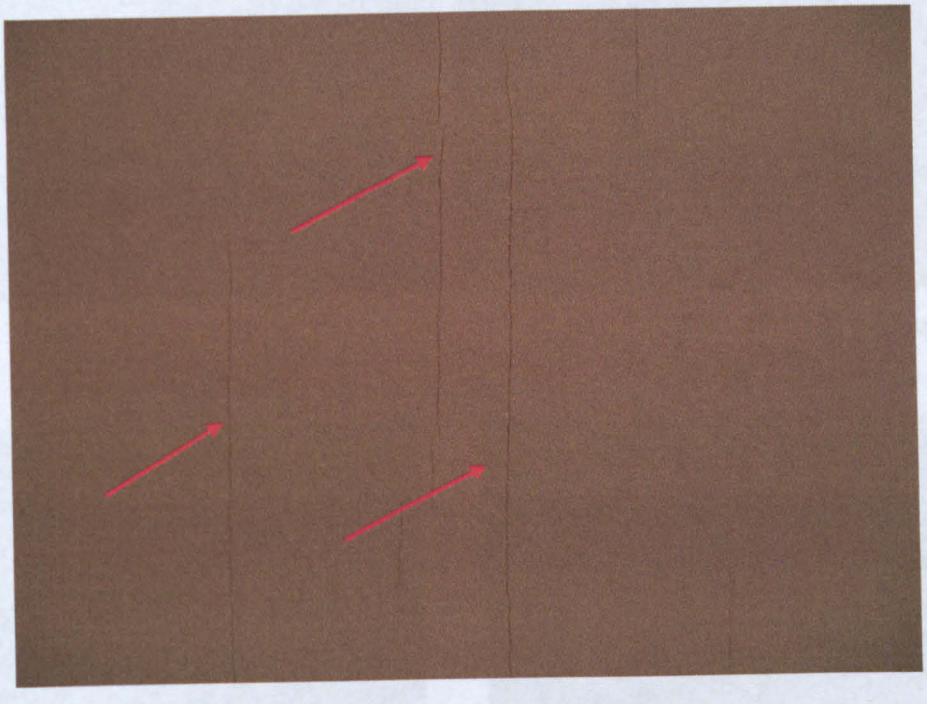

Figure 4.6. Panel B4 tested in air after 400,000 cycles; a, b) optical images, showing multiple fatigue cracks. Note in a) the hand finished edge to the coating

The panel coated with coating 'B' was examined earlier in the 'as received' state in air (section 4.1.1.2.) and apart of the surface change, cracks were not detected after nearly 100,000 cycles or after prolonged testing for nearly 500k. Therefore, it was expected that post cured sample of the same coating type would show resistance in the first instance. For the B4 panel there was no evidence of any cracks after 300,000 cycles. Between 300,000 and 400,000 cycles the first cracking occurred. Figure 4.7. shows images of cracks observed at this stage of the test.

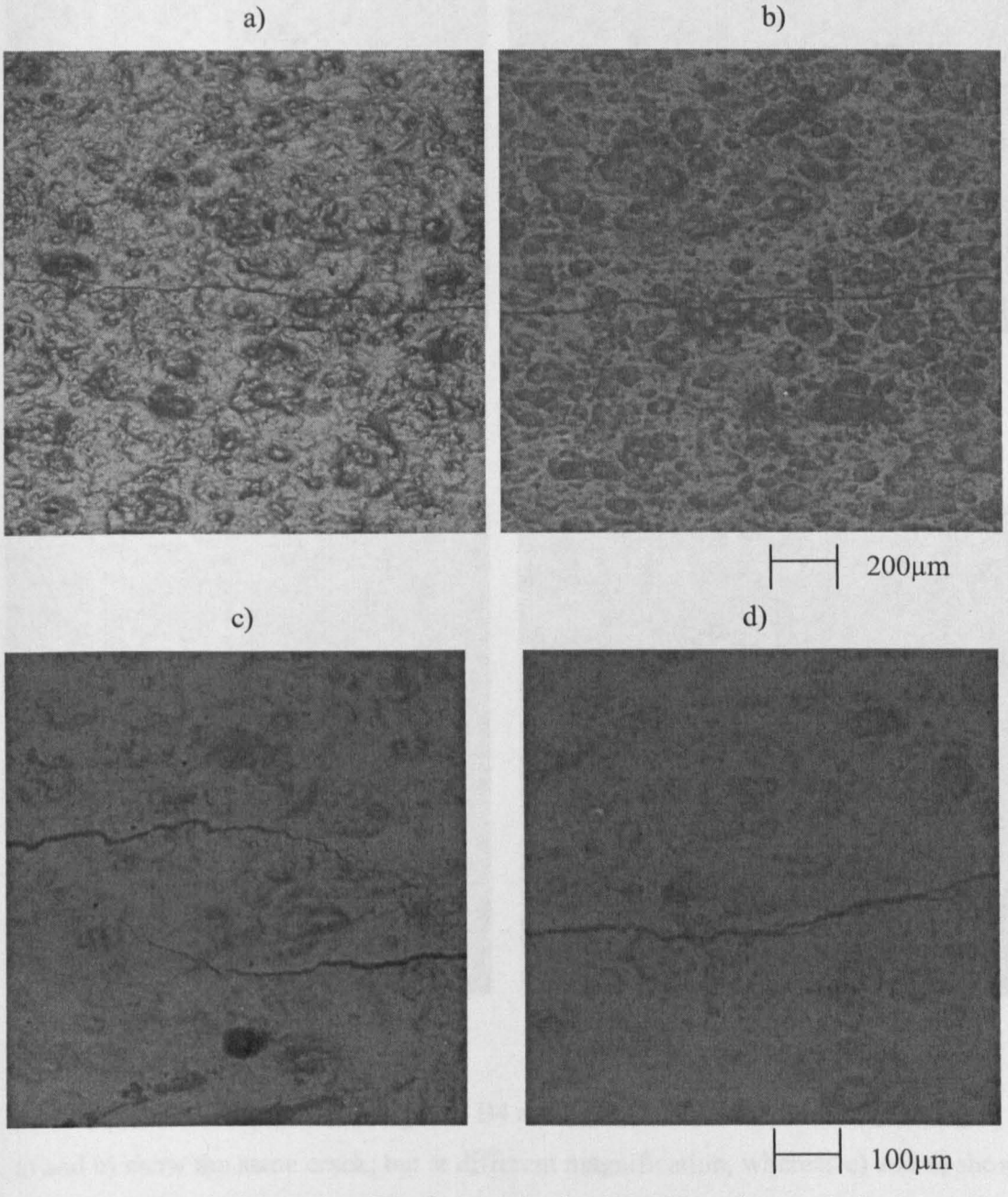

Figure 4.7. Cracks in coating 'B' after test in air; 400,000 cycles; optical microscopy a, b) ~60x, c, d) ~120x, showing fatigue cracks and crack coalescence

Further investigation of the B4 sample was obtained using an environmental scanning electron microscopy (ESEM) and images are given as Figure 4.8.

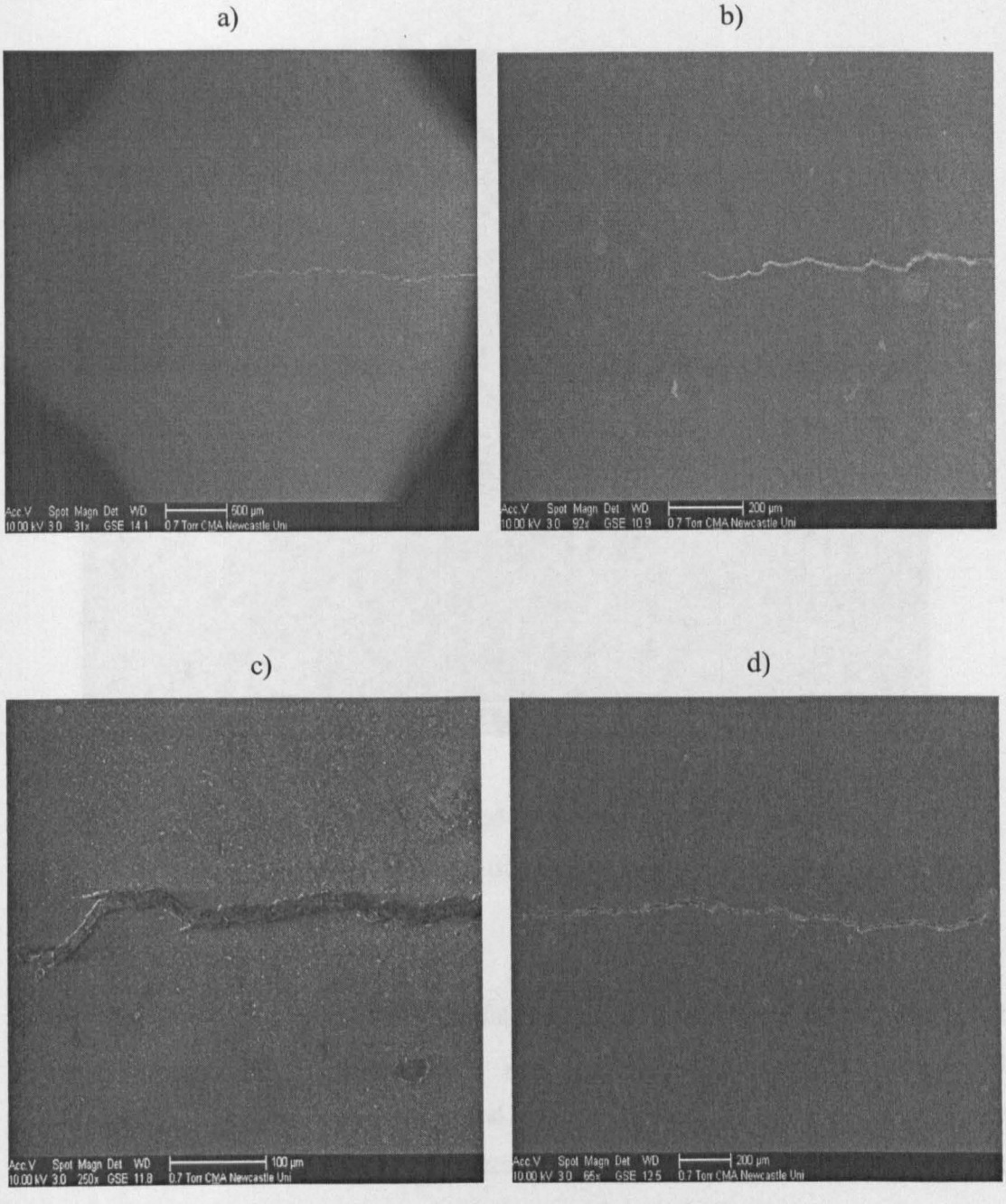

Figure 4.8. ESEM images of panel B4 after 400,000 cycles of air fatigue test; a) and b) show the same crack, but at different magnification, whereas c) and d) show cracking development at other places of the sample

Another typical crack on panel B4 is illustrated as Figure 4.9. where it can be seen that cracks did not develop in a straight line and that there is indication of crack coalescence.

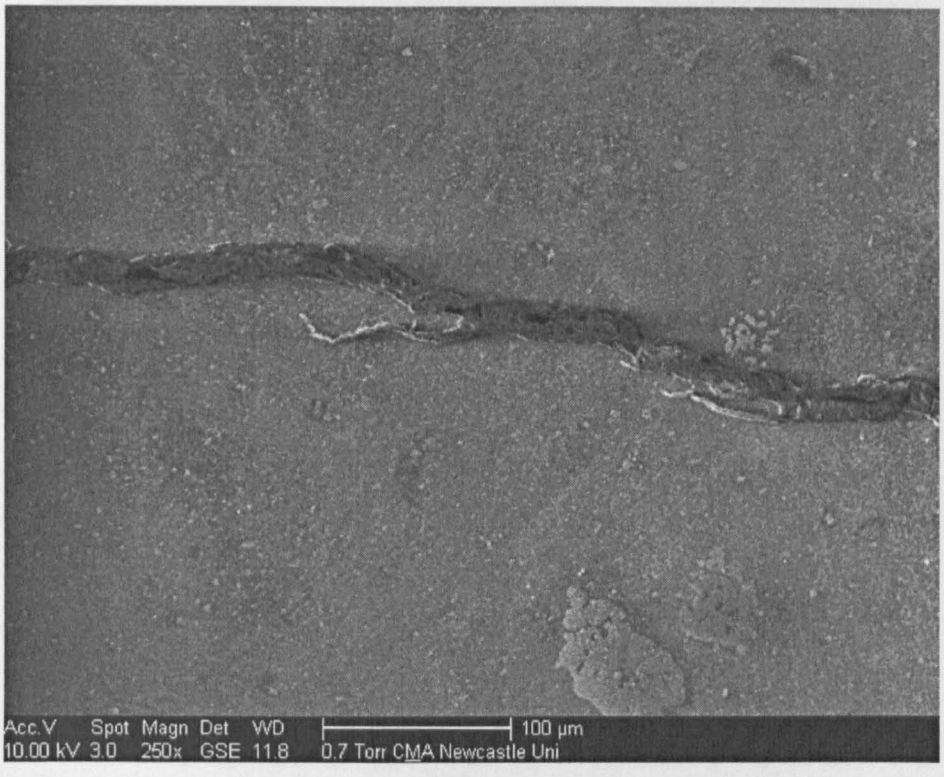

Figure 4.9. Panel B4 tested in air after 400,000 cycles;
ESEM image of a fatigue crack

In the observations of the surface of the fatigue tested B4 specimen evidence of crack coalescence was apparent. This usually took the form of two slightly misaligned cracks growing so that their tips passed one another for a small distance before turning and growing towards one another, as is apparent from Figure 4.10. Crack coalescence is a phenomenon commonly observed in metal alloys.

a)


Acc.V Spot Magn Det WD 50 µm
10.00 kV 3.0 350x GSE 11.7 0.7 Torr CMA Newcastle Uni

b)


Acc.V Spot Magn Det WD 20 µm
10.00 kV 3.0 1000x GSE 11.8 0.7 Torr CMA Newcastle Uni

c)

Figure 4.10. Crack coalescence, panel B4, ESEM image, showing same cracks under different magnifications, a) low, b) medium, c) high

Such coalescence was observed with cracks all over the sample. As the probability of two cracks being close enough to interact increases with increase in crack density and crack length, the frequency of occurrence of coalescence increases with time [9].

Air fatigue tests for the panel coated with the coating 'B' in the "post-cured" condition were performed for a second time, panel B46 (see Table 4.5.). No evidence of fatigue cracking was observed with this sample. Faster frequency rigs (0.3Hz rather than 0.05Hz) were used during the experiment and therefore the test conditions were not identical with those used for panel B4 which showed fatigue cracking. Samples B4 and B46 were from different spraying batches and due to natural ageing of the panel B46 the performances of panels were not the same.

4.1.2.2.1. Seawater Tests

Seawater cyclic-loading tests showed that coating B panels in post-cured condition developed under-roller cracks (Table 4.5.). B2 sample was tested for over 700k cycles and cracks were observed under three rollers (of four) during the whole testing period. Figure 4.11. shows significant cracking under the pins of the jig running parallel with it due to the triaxial loading.

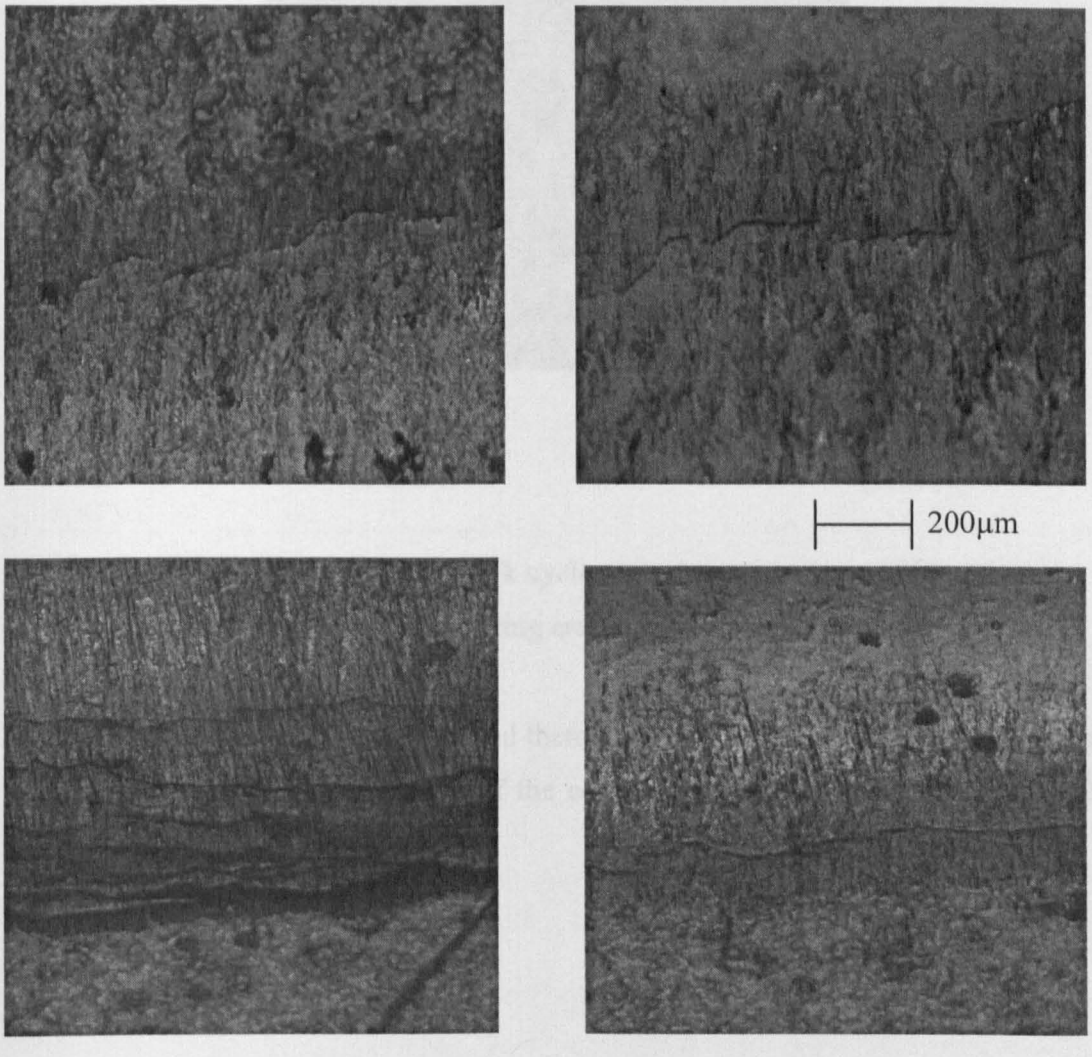

Figure 4.11. Panel B2 after over 700,000 cycles in seawater at room temperature; showing cracks formed under the rollers (rollers orientation was horizontal)

Under-roller cracks were also obtained in sample B35 tested in seawater at 5°C for 497,073 cycles. Observation of detected coating behaviour is given as Figure 4.12. showing cracks that were distinguished under jig-roller (one of four).

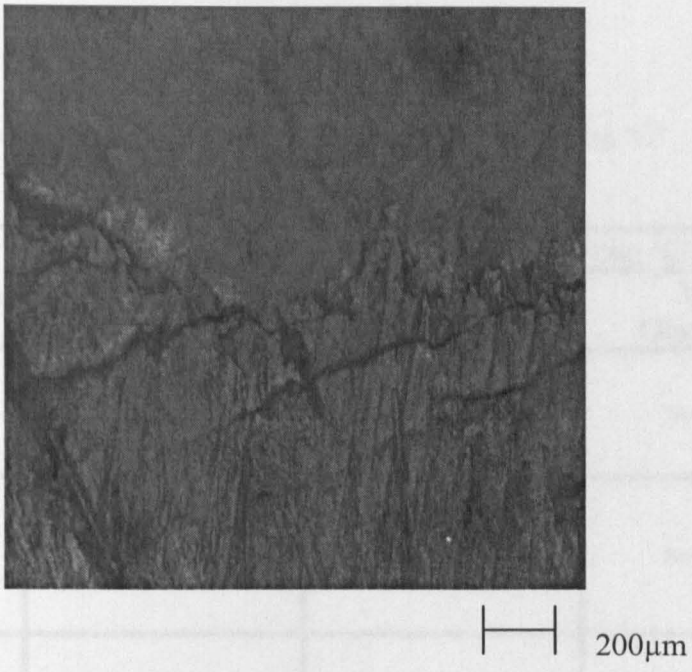

Figure 4.12. Panel B35 after 497k cycles tested in seawater at 5°C; optical microscopy ~ 60 x, showing cracks formed under the roller

The high stress under the rollers caused them to sink into the coatings to some extent, and the corresponding deformation of the coating probably contributed to the crack development.

4.1.2.3. Coating 'C'

Post-cured samples of the coating 'C' type were investigated under cyclic-loading conditions. Experiments were performed in three different environments and observations were presented in Table 4.6.

Table 4.6. Fatigue test results for 'post-cured' coating 'C'

TEST ENVIRONMENTS	'POST-CURED' Panels, Coating 'C'		
	Panel Number	**Total Number of Test Cycles**	**Visual Observation**
Air at Room Temperature	C11	531,007	No Changes
Simulated Seawater (3.5% NaCl) at Room Temperature	C18	598,334	No Changes
Simulated Seawater (3.5%NaCl) at 5°C	C19	501,040	No Changes

Test in air at room temperature was performed on C11 sample for over 500k cycles and no indications of cracks were obtained. Simulated seawater test at room temperature and in simulated seawater at 5°C for C18 and C19 panel were performed for nearly 600k and just over 500k cycles, respectively. High resistance to cracking of the coating 'C' was maintained during this investigation when coating 'C' samples were post-cured for 5 days at 80°C. This high performance of the coating system indicated that the combination of the relatively low loads and chosen environment that were experienced during the tests, were not high enough for developments of any defects for this coating.

4.1.2.4. Summary of the cyclic-loading tests for 'post-cured' coatings

During some of the cyclic-loading tests on samples in 'post-cured' condition, cracks formed under the rollers of the test jig. Two of the three coating systems exhibited this behaviour. Coating 'B' was the only one that showed under-roller cracks when tested in all three test environments (air, seawater at room temperature and 5°C). Coating 'A' developed cracks after testing in seawater at room temperature. Only coating 'B' produced fatigue cracks after 300k test cycles. Coating 'C' confirmed high resistance when tested under these conditions.

4.1.3. AGED SAMPLES

Further investigations involved tests on samples artificially aged according to the Akzo-Nobel recommended procedure (see section 3.4.). All tests were conducted in air, artificial seawater at room temperature and artificial seawater at 5°C.

Table 4.7. Fatigue test results for the panels aged by Akzo-Nobel recommended procedure

TEST ENVIRONMENTS	IP AGED panels		
	Coating Type and Panel Number	Total Number of Test Cycles	Visual Observation
Air at Room Temperature	A21	579,866	No changes
	A4	468,510	No changes
	B17	459,548	No changes
	C9	495,717	No changes
Simulated Seawater (3.5% NaCl) at Room Temperature	B3	453,182	No changes
	B10	512,079	No changes
	A8	522,124	No changes
Simulated Seawater (3.5% NaCl) at 5°C	C8	498,615	No changes
	A27	503,806	No changes

All three coating types showed high fatigue resistance after they had been subjected to the ageing procedure. No evidence of any surface changes was spotted during the subsequent cyclic-loading tests. Even when samples were tested in seawater environments, cracks under the jig-rollers were not observed.

*Test Note: The ageing procedure (prior to cyclic-loading) did not cause any changes in appearance of the coating surfaces.

4.1.4. SUMMARY OF CYCLIC-LOADING TESTS

The results show that the fatigue resistance of the experimental ballast tank coatings 'A', 'B' and 'C' is high after ageing and that the coatings do not show fatigue failure within approximately 500,000 cycles. The investigations indicate that different conditioning of the samples prior to testing provided different types of changes. While for the 'as-received' state of the coated panels the appearance changed after fatigue tests, for the 'post-cured' samples, cracks under-loading points were observed. The only sample in which fatigue cracks in the region of uniform strain (away from loading rollers) were observed was a panel coated with coating 'B'. The panels after the ageing procedure showed high fatigue resistance during the tests. Coating 'C' was the only coating that did not show any cracks under any combination of conditioning and test environemt.

It has been reported that some polymers appear to possess a fatigue limit (i.e. a stress below which fracture by fatigue does not occur even after an unlimited number of cycles). Although there may or may not be an initial induction period during which fatigue cracks are initiated under cyclic deformation, fatigue fracture eventually occurs by the increased growth of cracks. The cracks may grow each cycle but only by a small amount insufficient to cause macroscopic failure of the material [7].

In metals this stability is the result of plastic flow, the fatigue crack being supposed to originate and grow by the movement of dislocations to the tip. In polymers the stability factors may depend upon the loading rate and might contribute significantly to the number of cycles required to cause fatigue fracture [8].

4.2. STRAIN TO CRACK INITIATION BY MONOTONIC FOUR-POINT BEND LOADING

Coatings applied to mild-steel substrates showed high coating fatigue resistance. This testing phase started with the idea that limitation of substrate flexibility could affect overall coating performance and the next step in this investigation involved coating thinner stainless steel substrates. Stainless-steel coupons 150mm length were coated on one side with each experimental coating system. To observe the influence of the substrate on coating resistance, three different substrate thicknesses were prepared for this research, 100μm, 200μm and 300μm. Following the standard recommended drying procedure for each coating type and with additional curing of 5 days at 80°C, samples were tested by four-point bend loading, where load was applied manually by forcing the outer spans against inner ones. The lengths of the inner and outer spans were 100mm and 50mm, respectively. Initially, four-point bend tensile loading was applied on uncoated substrates to check their response to the tests. No defects were obtained on substrates when tested in the test-jig. The coated samples were tested such that coated surface was in tension. The investigation was performed in air at room temperature. In-situ observations were carried out visually and then with optical microscope. Samples were tested until the coatings cracked and strain levels at breaking points were calculated. Table 4.8. shows the results obtained.

Table 4.8. Strain to crack initiation for 150mm length shims, by four-point bend tensile loading

Coating/ substrate thickness	**'A'**	**'B'**	**'C'**
	Strain to coating cracking [%]		
100μm	0.47	0.09	0.31
200μm	0.36	0.19	0.34
300μm	0.35	0.11	0.28
average	***0.39***	***0.13***	***0.31***

Results showed that the highest loading strain was needed to crack coating 'A' in comparison with other two coatings. Coating 'B' showed least capability (average of 0.13%) to withstand loading when tested on all three substrate thicknesses. Coating 'C' demonstrated average of 0.31% strain that was required for this coating to crack. It can be noted that each coating type cracked at approximately the same strain level when coated on different substrate thicknesses, which indicates that the thickness of the stainless steel substrates did not affect the coating failure.

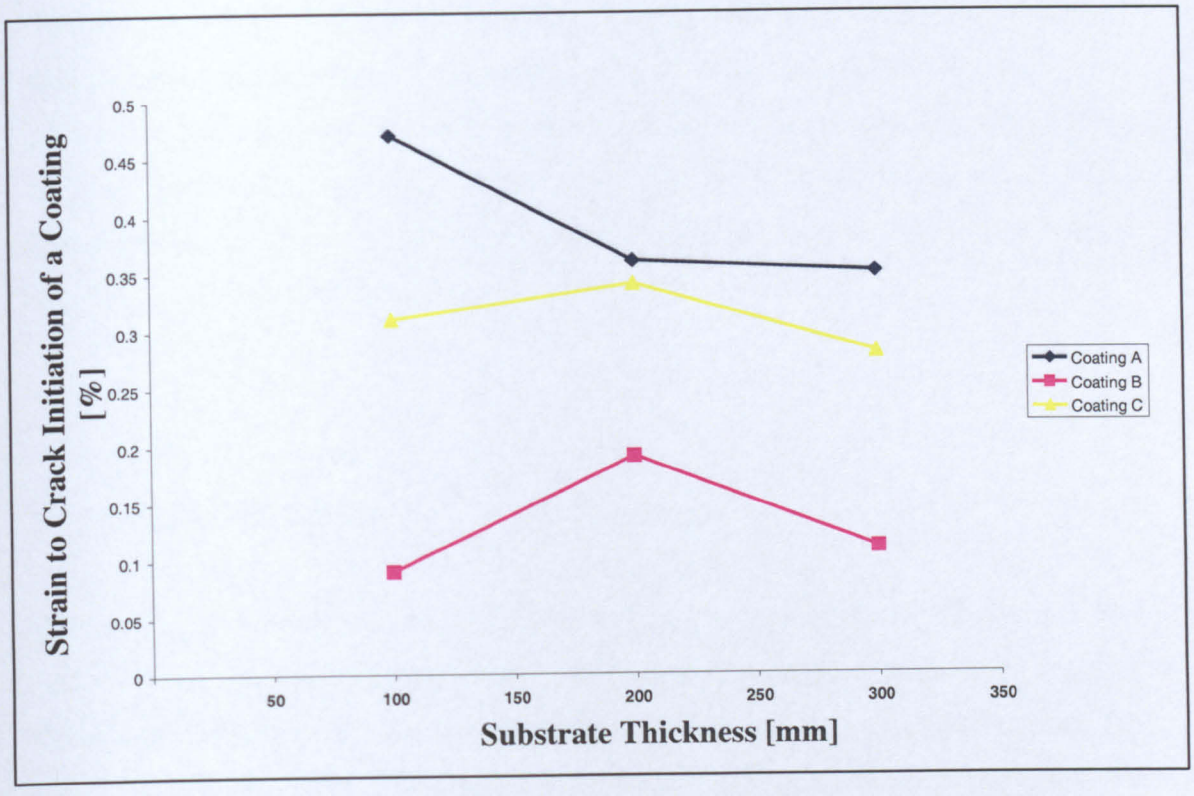

Figure 4.13. Strain to crack initiation by four-point bend tensile loading

As expected, the tensile loading tests illustrated in Figure 4.13., show that strains higher than those used in the cyclic-loading tests are required to cause coating failure in monotonic loading. The effect of cyclic-loading is to decrease the strain required to cause crack initiation and propagation.

Since the thickness of the coated substrate was eliminated as a main influence for fatigue tests, the next set of experiments were carried out in order to examine coatings applied on more flexible substrates.

4.3. FATIGUE TESTS ON COATINGS ON PLASTIC SUBSTRATES

As stated before, from the fatigue tests performed on coated mild-steel substrates, coatings showed high resistance when tested under laboratory conditions. The main issue during those experiments was substrate yield strain limitation, where testing conditions were setup so that the substrate did not fail before the coating. Additional cyclic-loading tests were performed on coated plastic substrates to increase the allowable strain range.

Coated 'Perspex' substrates were tested in 'as-received' state. The same method of applying the coatings systems and drying as used for steel substrates was performed prior to the tests. Experiments were carried out in air at room temperature for all three coatings. The set up of the rigs was the same as for the steel substrates, except that a higher strain was used. The plastic substrates allowed more deformation and a strain of 1.33% was chosen for the tests.

4.3.1. COATING 'A'

The coating 'A' sample showed immediate failure of the substrate. During the first and only test cycle that was performed in this test, the specimen cracked all the way throughout substrate and the coating. The coating did not delaminate from the substrate. The immediate cracking of the sample coated with coating 'A' led to the conclusion that the coating solvent content made 'Perspex' brittle (one of the disadvantages of the plastic used) and/or that the solvent used was more aggressive towards Perspex and the whole sample was thus weakened. Environmental stress cracking of polymers is a common phenomenon and 'Perspex' has a reputation of vulnerability when in contact with various solvents. From Table 3.1. in chapter 3, it can be seen that the solvent percentage in coating 'A' was higher than for the coating 'B'. Therefore, further tests for this coating on this substrate were impractical.

4.3.2. COATING 'B'

Cracking of a coating 'B' was observed during this experiment and an example is given as Figure 4.14., showing multiple cracking. The number of test cycles needed for coating cracking was small (just 2,000 test cycles made coating to fail). For that reason, defining the exact moment of the first crack that appeared on the coating surface was difficult.

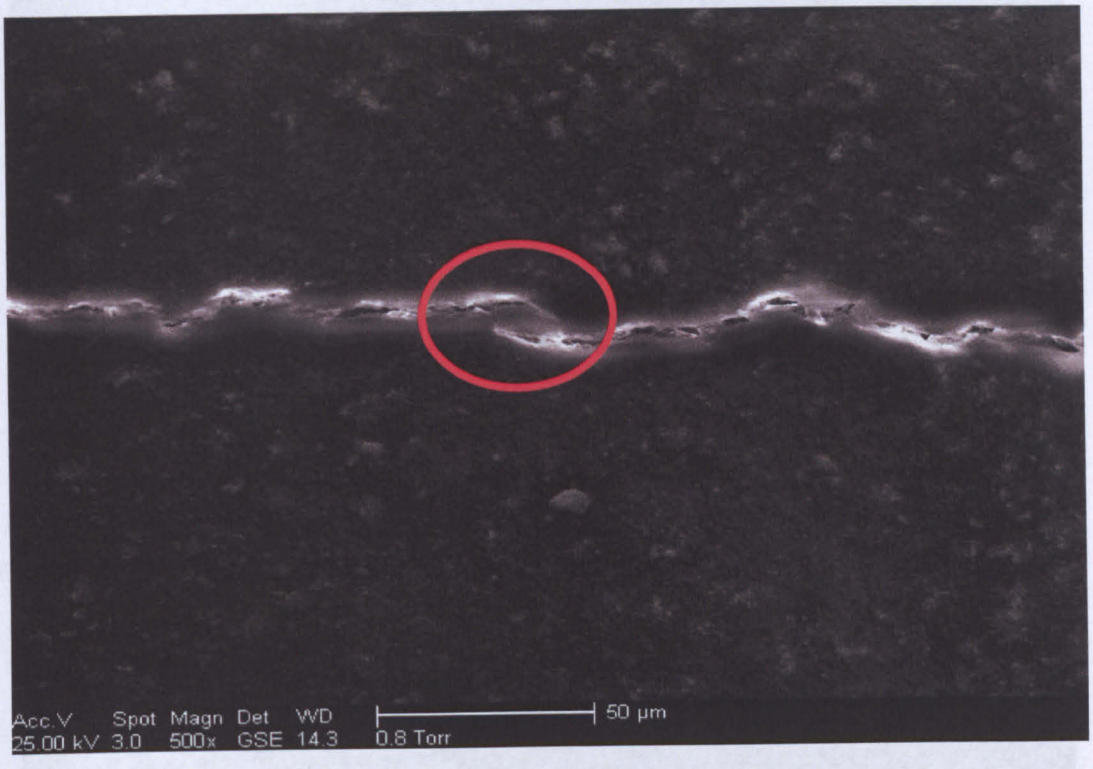

Figure 4.14. Coating 'B' applied on the Perspex substrate after 2,000 test cycles

From the image above it can be observed that cracks were formed on the coating surface. The red ring on the image (Figure 4.14.) indicates the start and the end of two cracks, showing that crack coalescence was detected similar to that observed with the same coating composition in fatigue tests on steel substrates (see Figure 4.10). That a similar mechanism is observed indicates that using deformable substrates to increase the strain amplitude may be a suitable method for accelerating cyclic-loading tests for this type of coating.

4.3.3. COATING 'C'

For a coating 'C' cracking was observed on the edge of the sample as a single small crack. No evidence of cracking was spotted anywhere else throughout the specimen. ESEM images of the coating 'C' sample are presented as Figure 4.15.

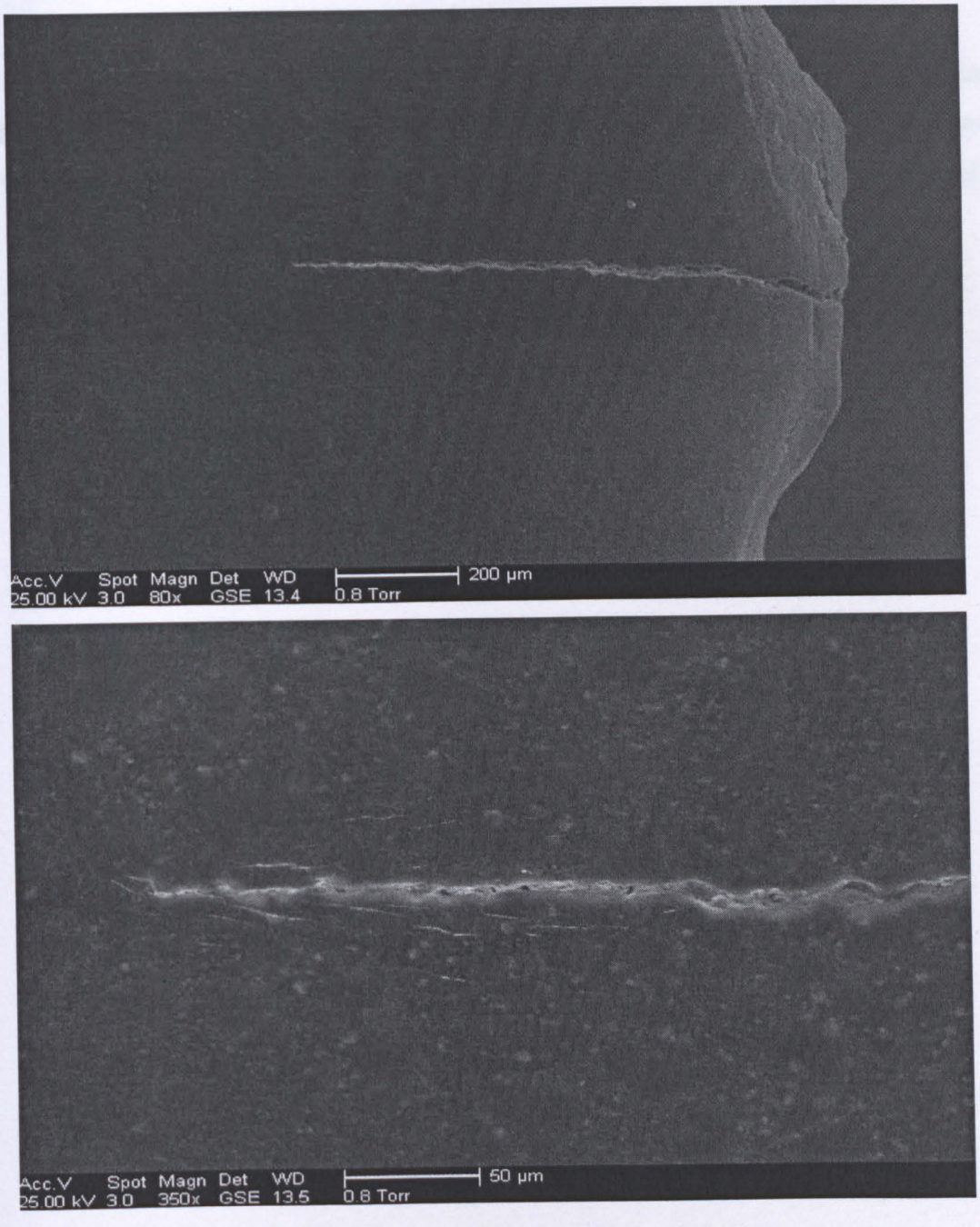

Figure 4.15. Coating 'C' on a Perspex substrate after 15,000 test cycles, showing the same crack at different magnifications

Coating 'C' showed only one small crack near the edge (figure 4.15) of the sample after 15,000 test cycles and prolonged cyclic tests did not show any other coating failure or any new crack initiation. Interestingly, additional cyclic-loading testing did not extend the length of the already initiated crack. Therefore, it is speculated that the reason why only one crack commenced during the tests on one specific place on the sample could be that some sort of a flaw was initiated during coating application.

Test Note: The tests on Perspex substrates were conducted to permit testing of the chosen epoxy coatings at higher strain levels than those possible on steel substrates. There was no thought of investigation of 'Perspex' as a possible replacement for steel.

4.3.4. SUMMARY OF FATIGUE TESTS ON COATINGS ON PLASTIC SUBSTRATES

Different coating compositions presented different results. Immediate failure of the substrate was observed for coating 'A', probably due to solvent attack of the 'Perspex' causing embrittlement. This may be because the solvent content in coating 'A' was higher than for the other two coating systems.

Multiple cracking was observed on the surface of a coating 'B' sample, after a fairly modest number of test cycles.

The coating 'C' showed only one small crack near the edge of the sample after 15,000 test cycles and prolonged cyclic tests did not show any other coating failure. Additional cyclic-loading did not extend the length of the already initiated crack. This suggests that the crack may be related to a flaw in the coating rather that to general fatigue failure of the whole coating system.

4.4. SLOT DEFECTS

The results from cyclic-loading tests on panels after different conditioning procedures were fairly consistent, but fatigue cracks did not form easily. To investigate the effect of the presence of flaws, slot-defects were machined into the coatings. This was intended to simulate damage that might occur due to accidental collision with hard objects (for example, a hand tool dropped in the ballast tank during inspection).

Slot defect tests performed in this research was divided into two types: firstly samples were made with four slots of different length; and secondly samples were made with three slots of different depth. For more details of how the slots were introduced see section 3.5.2. 'As-received' panels were machined with slots and then fatigue tested. Observations that were obtained for each epoxy coating system are given in the following sections.

4.4.1. FOUR SLOTS OF DIFFERENT LENGTH

Four slots of different length were machined into the panels of the three experimental coatings 'A', 'B' and 'C', where the lengths of the slots were as follows: 20mm, 16mm, 13mm and 10mm (see Figure 3.9.). The depth of each slot was 0.2mm. A reminder of how the slots were inserted into the coating surfaces is illustrated on Figure 4.16.

The panels were in the "as received" state. After slot inspection and verification that the slot cutter did not cause any crack initiation, the test rig was set up with the strain level maximum of 0.22% at the surface of the coating for testing in air.

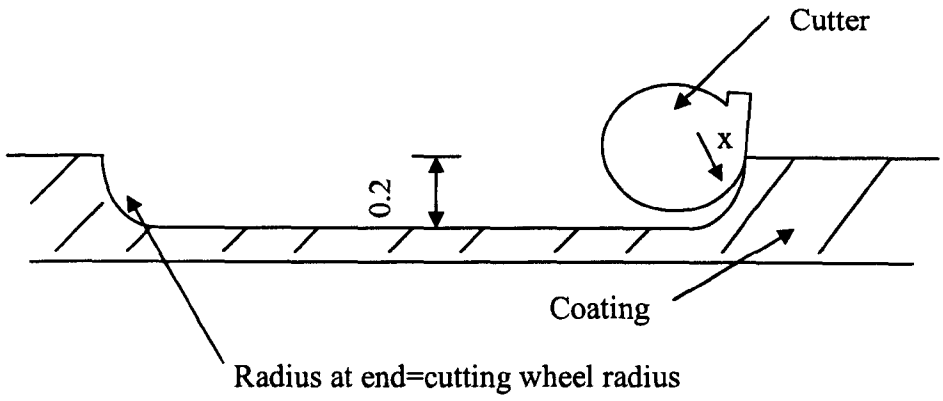

Figure 4.16. Slot formation on the coating surface, cutter has 100 mm radius

Each slot was measured and special attention was given to the ends and roots of the slots. Specimens prepared in this way were then fatigue tested. The slot side of the panels were put in tension during the cyclic-loading tests. The experiment set-up was matching testing procedure performed earlier (see chapter 4.2.). Inspection of the samples was performed visually using an optical microscope after every 50k cycles approximately.

The next sections will give results of the slot defect tests for each coating type.

4.4.1.1. Coating 'A'

The cyclic-loading tests were performed on a substrate coated with coating 'A' with four inserted slots. The depth of all four slots was 0.2mm and the width was 1.59 mm. The end of each slot was a radius related to the cutting wheel diameter.

Each slot was examined prior to the tests and the images presented as Figure 4.17. show both ends of one slot before cyclic-loading.

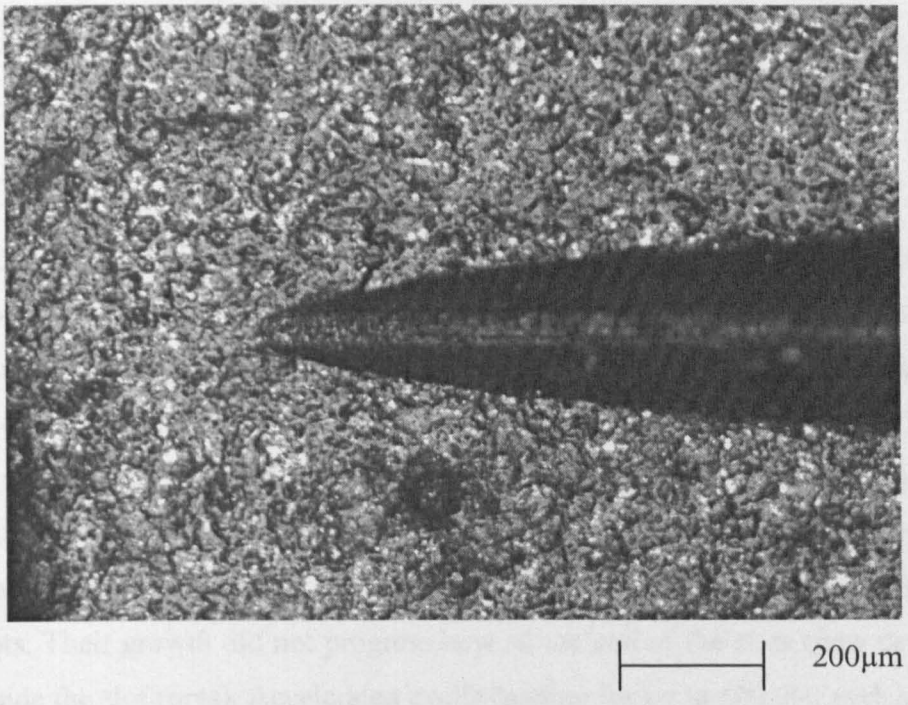

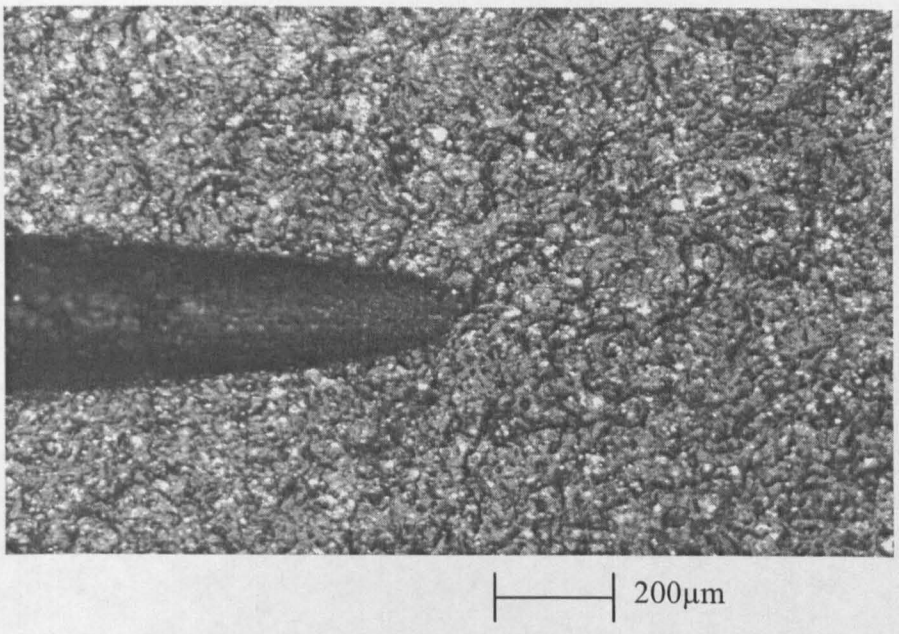

Figure 4.17. Typical ends of a slot cut in coating 'A', before tests, X60

After 30,000 cycles the loading phase was stopped and the specimen was taken out of the test-jig for examination. At this stage no crack development could be observed either on the edge of the slots or inside them. The sample was returned to the rig for further cyclic loading under the same conditions as initially set up. After 150,000 cycles (5 days of testing) cracks started to grow inside the slots. Significant observation of crack development in the root of a slot is presented as Figure 4.18. where a single crack initiation is evident. Cracks were developed inside each of the four slots. Their growth did not progress beyond the end of the slots (they developed only inside the slot roots). Accelerated cyclic-loading for up to 500,000 cycles did not develop further growth of any of the four cracks in the introduced slots. The rest of the coating surface had no evidence of any cracking behaviour. The cyclic-loading was stopped after approximately 500k test cycles (18days of testing).

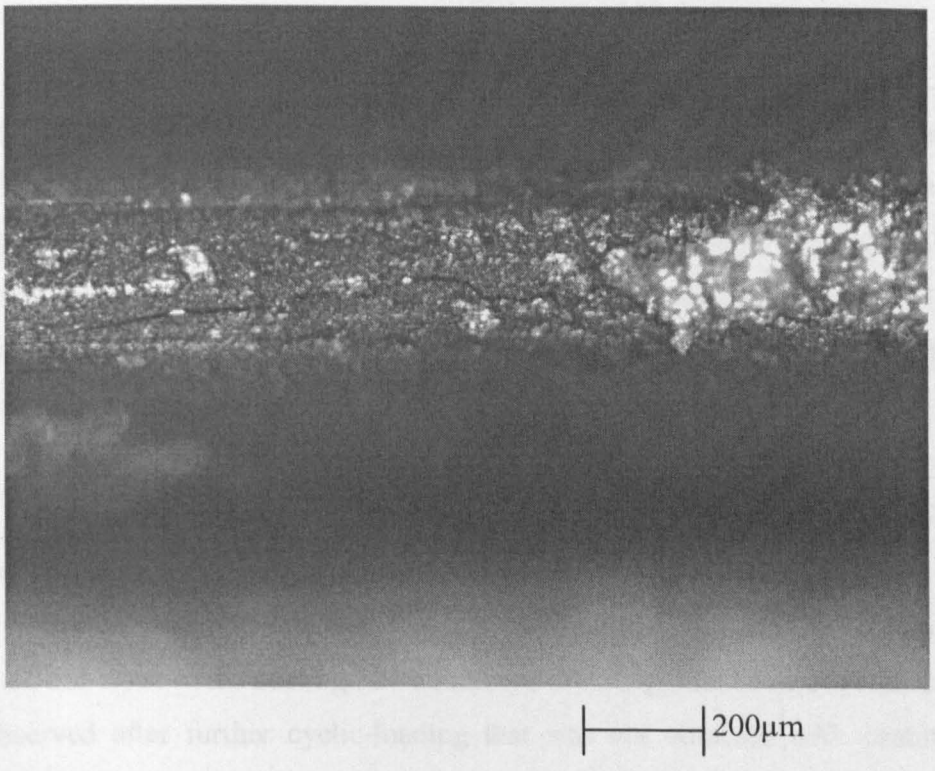

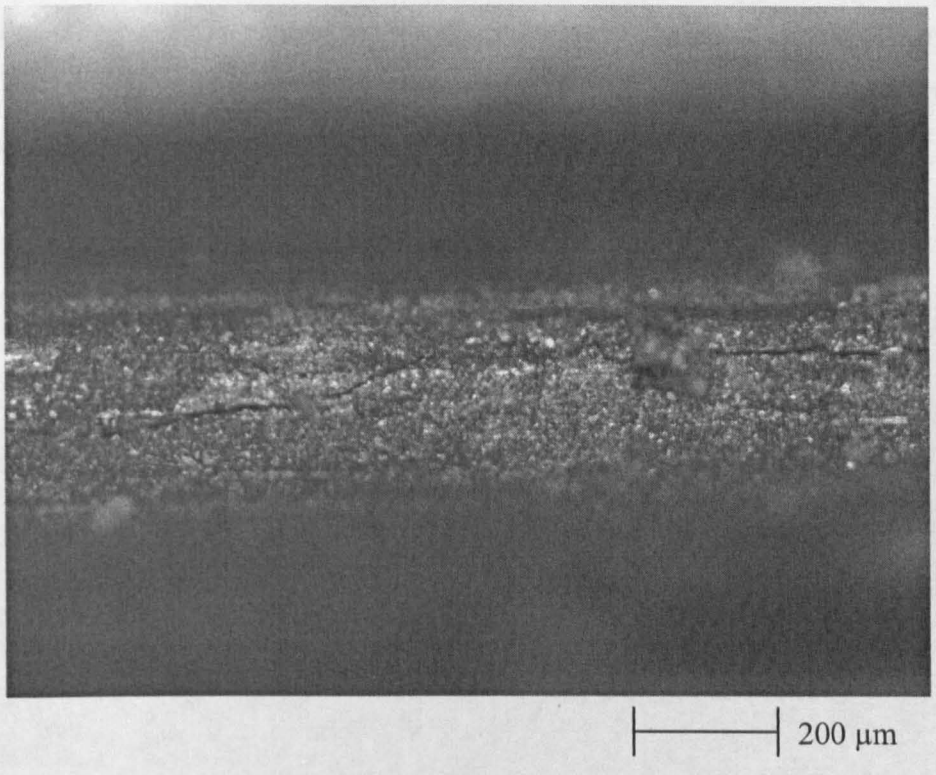

Figure 4.18. Typical initiation of cracks inside the slots in coating 'A' after 150,000 cycles, X120

4.4.1.2. Coating 'B'

Whereas using slots in coating 'A' did not show any significant crack growth after 500,000 cycles, apart from cracks developed inside the slots, a panel coated with coating 'B' was prepared in the same way and tested in the same environment. Four slots with different lengths and the same depths were inserted into the panel. Tests were performed in air with the period of 3 seconds per cycle. Inspection of the slots was made prior to the tests.

After 30,000 cycles the same findings were observed as for the coating 'A' panel. First cracks initiated inside the slots, regardless of the slot length. Extension of the cracks inside the slots was fast and after 150,000 cycles, cracks increased to equal the length of the slots. With coating 'B' additional cracking extension beyond the slots was observed after further cyclic-loading that was not obtained with coating 'A'. Figure 4.19.a) gives a typical segment along an initiated crack. Initiation of cracks at the slot root occurred over the entire length of the inserted slots. Figure 4.19. (b and c) shows the beginning of crack development from the ends of the slots into the material adjacent to the slot ends.

a)

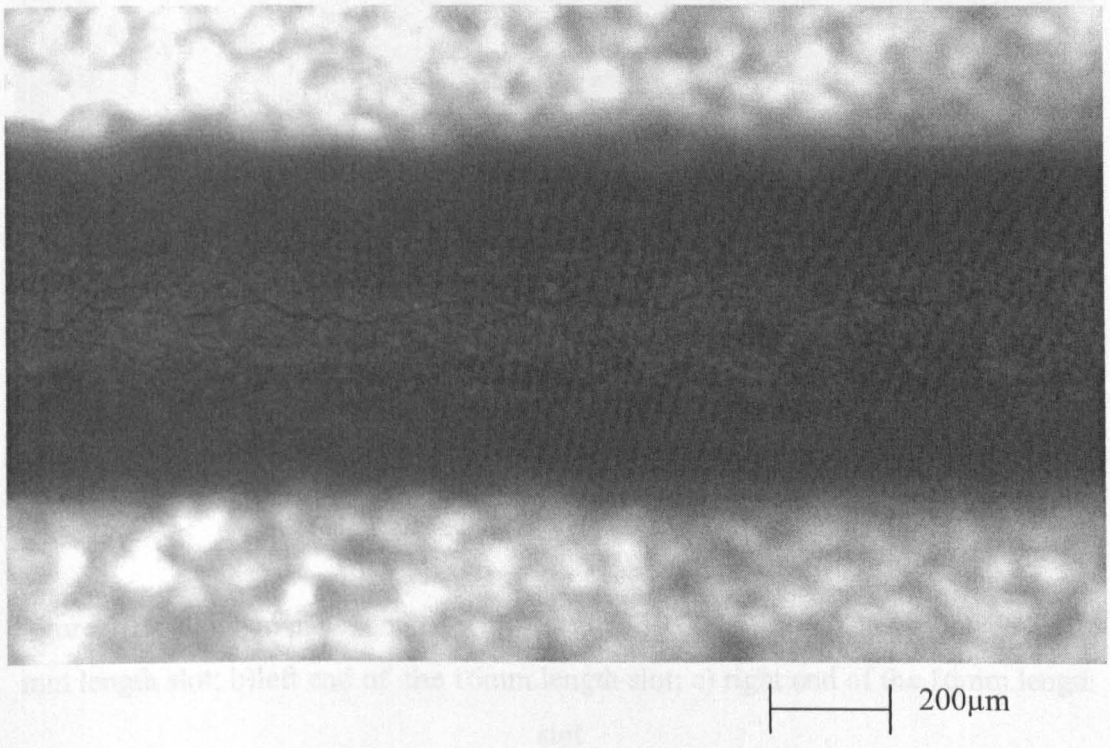

b)

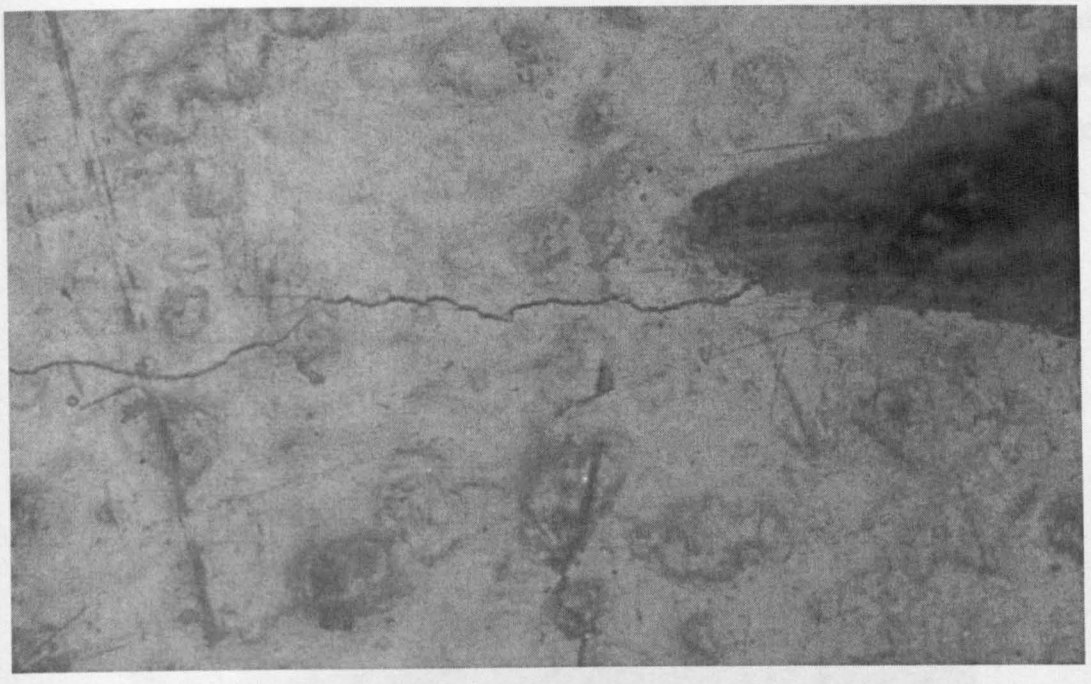

c)

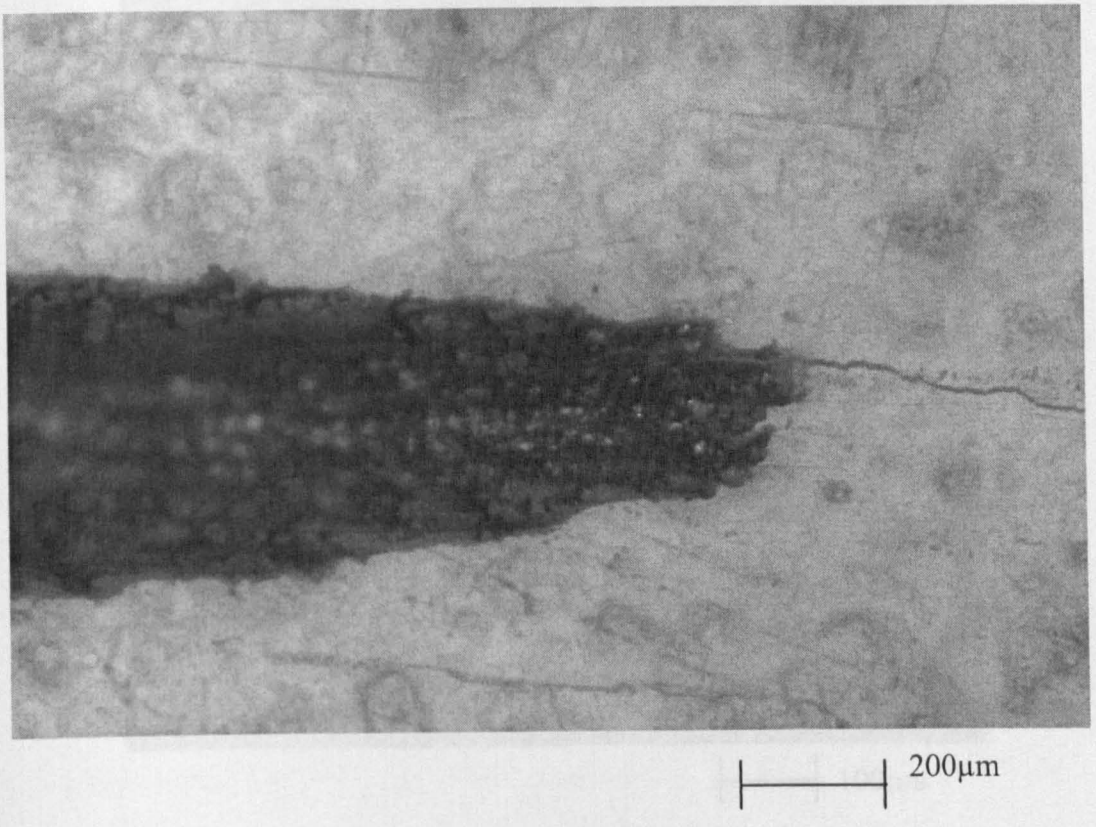

Figure 4.19. Slots on panel coated with 'B' after 50,000 cycles; X120 a) inside the 16 mm length slot; b)left end of the 16mm length slot; c) right end of the 16mm length slot

As with coating 'A', the slot length did not affect crack initiation or growth. With increased test time the cracks developed further and the tests were interrupted periodically, so that the crack extension could be recorded. The appearance of the cracks and their additional development are presented in Figure 4.20. and a schematic diagram of the crack propagation on the sample due to fatigue is given as Figure 4.21.

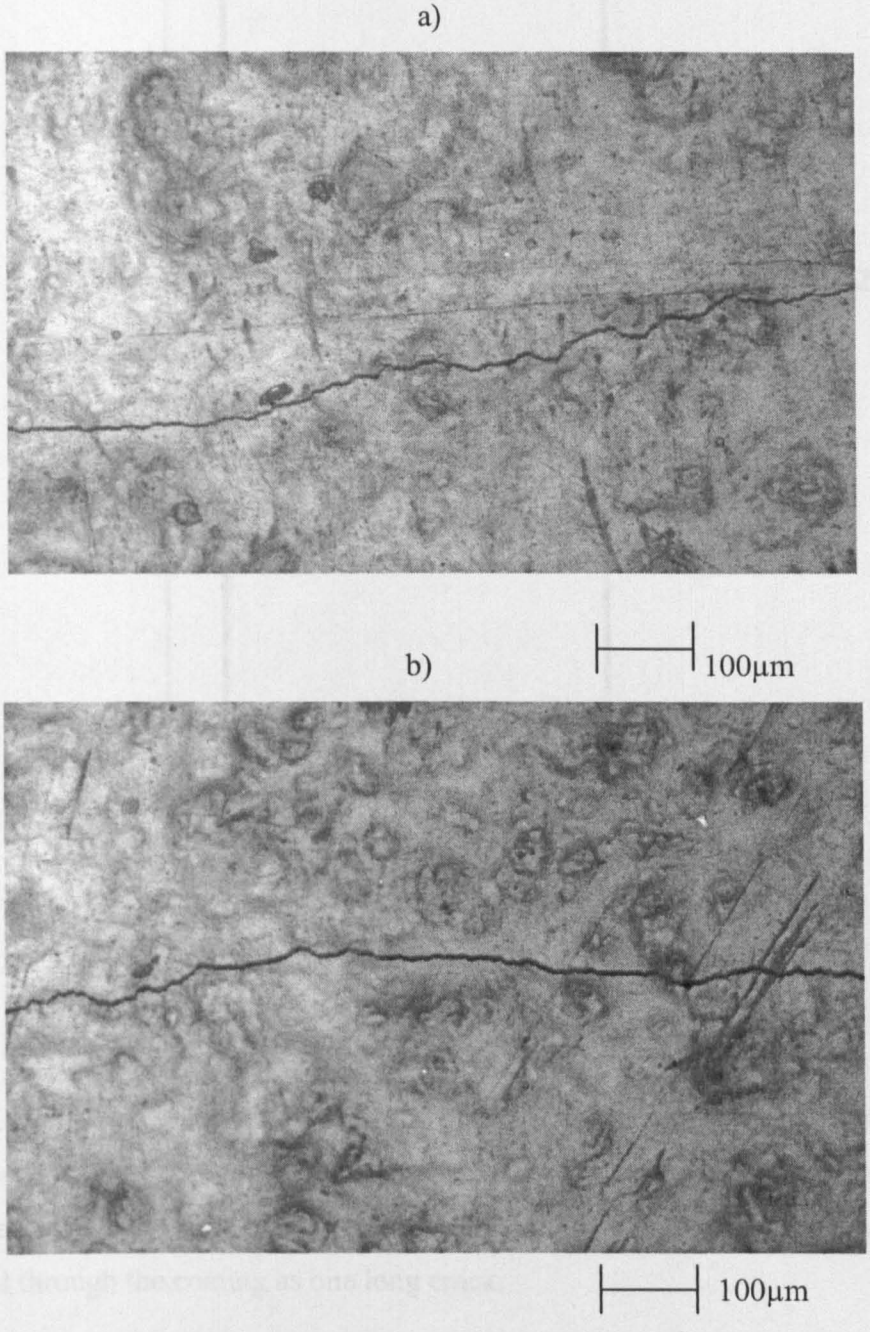

Figure 4.20. Further crack development, coating 'B' with four slots, images of the 16 mm length slot after 250,000 cycles, a) and b) X120

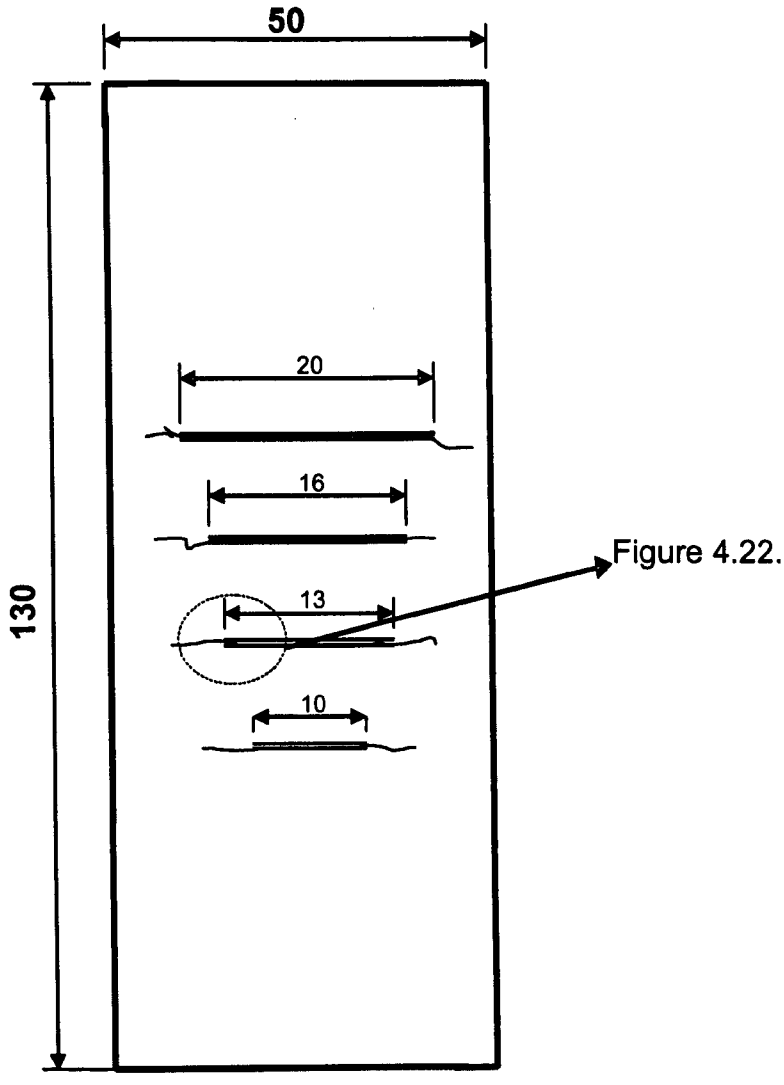

Figure 4.21. Schematic diagram of crack propagation in coating 'B' due to fatigue loading [mm]

Figure 4.22. shows a crack that has grown along the coating. Even after 250,000 cycles there was no evidence for the existence of any new cracks either inside the slots or elsewhere on the sample. Inside each slot the crack initiation occurred and continued through the coating as one long crack.

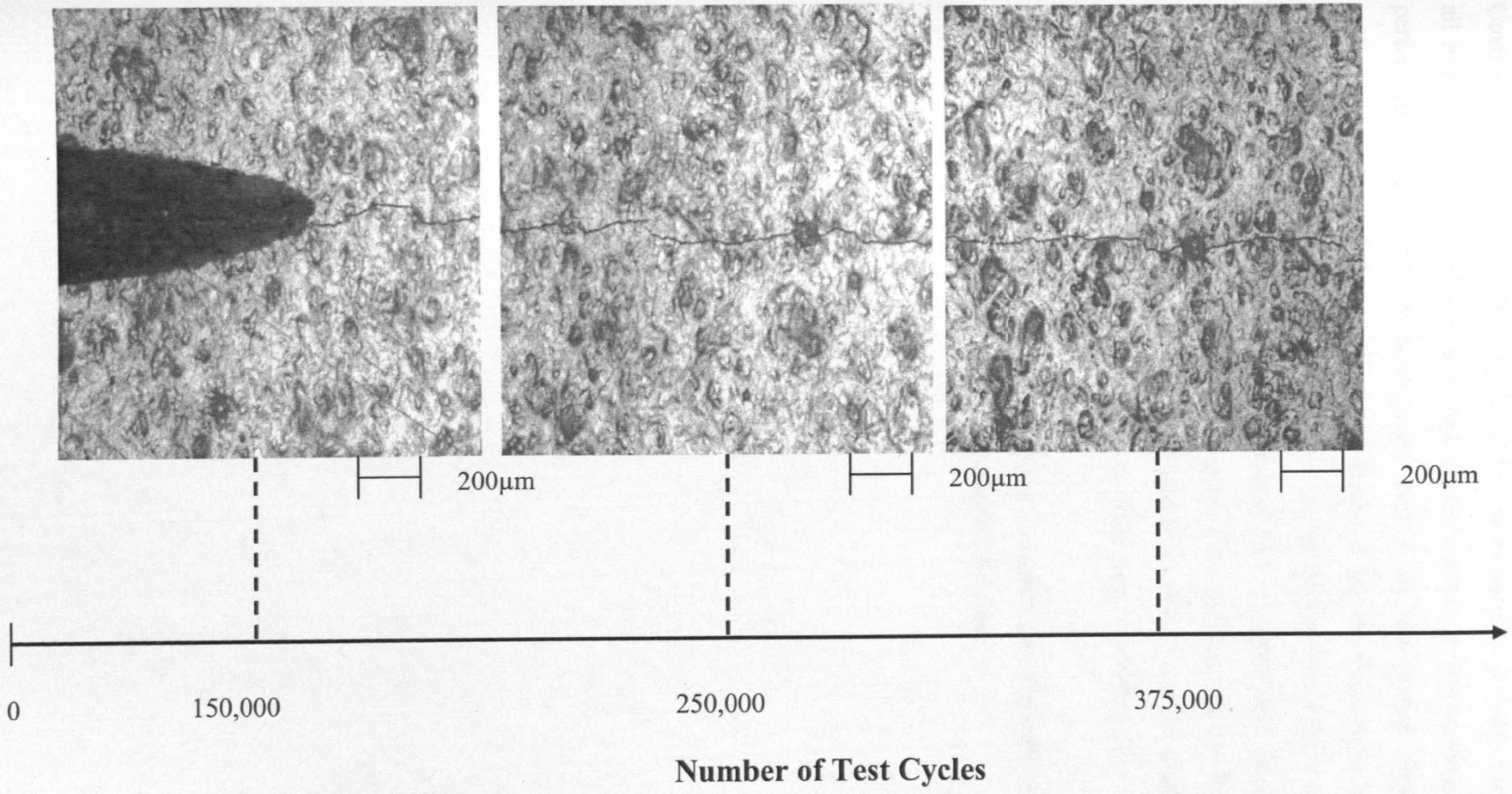

Figure 4.22. Typical crack development for the 13mm length slot, between 150,000 and 375,000 cycles, coating 'B'

Coating 'B' tested for 375,000 cycles (13 days of testing) showed crack initiation in all four slots where cracks were spread all the way across the coating. Observations performed using an optical microscope during the test period illustrate that the initiation patterns of the cracks were identical for all four slots lengths. Crack propagation did not depend on slot length. The graph given as Figure 4.23. illustrates the results of crack extension measurements and indicates that all four slots had comparable crack progressions. The hand finished coating edge is thicker than the centre area of the coating and this will have an effect on the crack propagation through this region. Crack growth rate in the edge region is likely to be slower.

Within the experimental error due to coating variation, the crack growth rate appears to be independent of slot length in the range of slots tested.

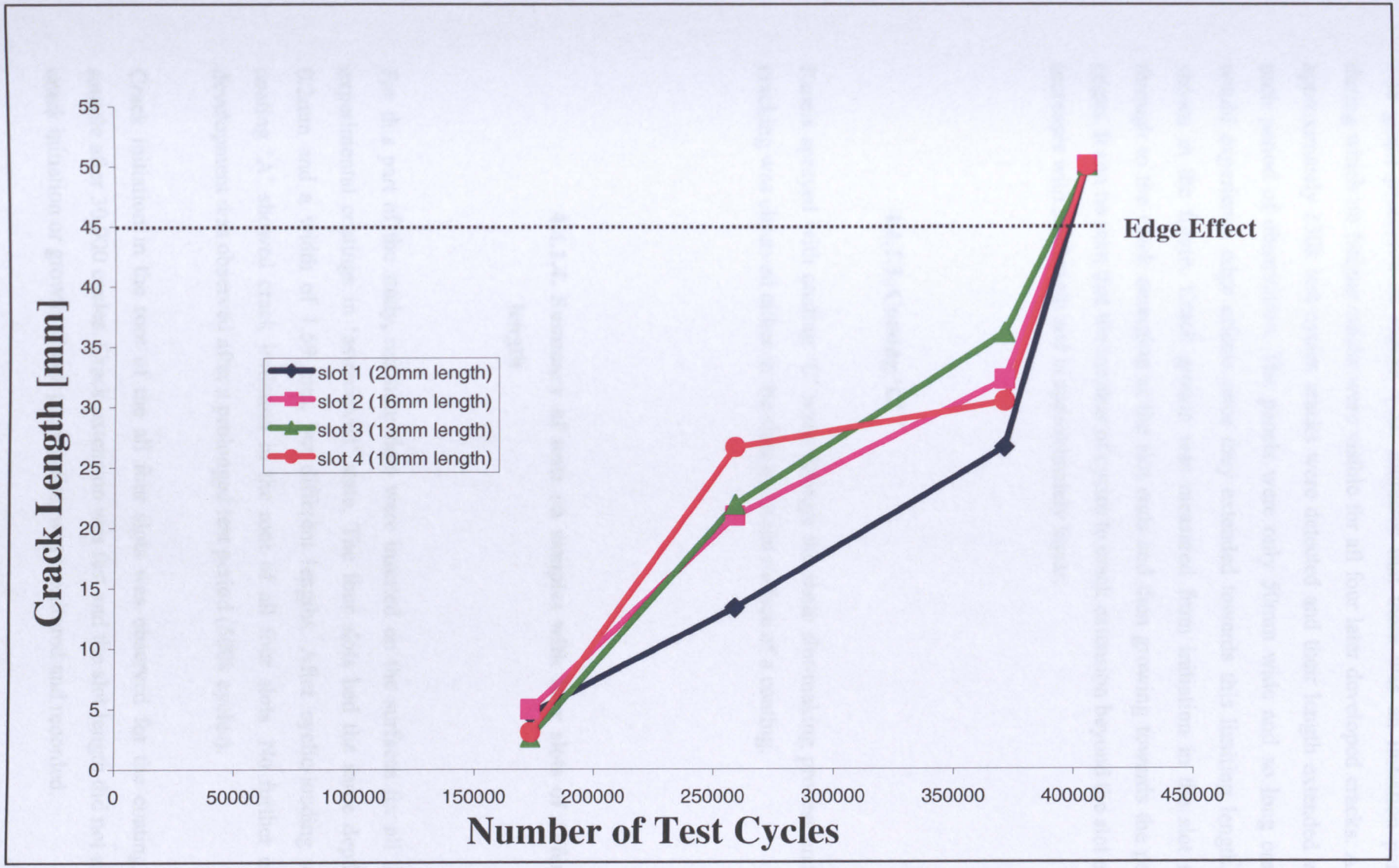

Figure 4.23. Total crack length development on coating 'B' slotted-panel during fatigue tests

The graph presented as Figure 4.23. indicates that there was an initiation period during which no fatigue cracks were visible for all four later developed cracks. After approximately 130k test cycles cracks were detected and their length extended with each period of observation. The panels were only 50mm wide and so long cracks would experience edge effects once they extended towards this limiting length, as shown in the figure. Crack growth was measured from initiation in the slot root through to the crack emerging at the slot ends and then growing towards the panel edges. It can be seen that the number of cycles to crack extension beyond the slot ends increases with slot length and is approximately linear.

4.4.1.3. Coating 'C'

Panels sprayed with coating 'C' went through the same slot-making process and no cracking was observed either in the slots or on the surface of a coating.

4.4.1.4. Summary of tests on samples with four slots of different length

For this part of the study, machine slots were inserted on the surfaces for all three experimental coatings in 'as-received' state. The four slots had the same depth of 0.2mm and a width of 1.59 mm, but different lengths. After cyclic-loading tests, coating 'A' showed crack initiation in the root of all four slots. No further crack development was observed after a prolonged test period (500k cycles).

Crack initiation in the root of the all four slots was observed for the coating 'B' sample after 30,000 cycles. Crack extension was fast and the slot length did not affect crack initiation or growth. Crack propagation was monitored and recorded.

Throughout this test, coating 'C' maintained high resistance. Cracking was not observed for this coating type.

This test showed different performance of the different coatings under the same testing conditions. Coating 'C' proved to be the most fatigue resistant coating system. Cracks inside the slots of the coating 'A' showed that this coating system can produce cracking when slots were initiated. Coating 'B' showed constant cracking performance, regardless of slot length.

4.4.2. SLOTS OF DIFFERENT DEPTH

A second set of the experiments was performed on test panels with three slots with different depths. The reason for this study was to explore if there was any variation in performance of the coating during fatigue tests if slots were cut into the sample with various depths because this will affect the stress concentration also, and because the coating was known to have some layered structure (each sample was coated with two coats of experimental coating, see section of panels preparation in chapter 3.3.1). Figure 3.10. illustrates the positions of the slots with their dimensions. Coatings were tested in the as-received condition, with no further conditioning treatment apart from the cutting of the slots. The same testing regimes, e.g. load levels, strain and cycle period, were used as for the previous investigation.

4.4.2.1. Coating 'A'

Coating 'A' showed the same performance as when four slots of different lengths were induced. Crack initiation started in all three slot roots after 130,000 test cycles and further testing up to 500k cycles did not produce crack growth beyond the limits of the slots.

Typical images of the observed results are presented in Figure 4.24. The end of one slot is illustrated in Figure 4.24.a) and b). and both images show the same slot at different magnifications, where a single crack development is evident in the root of the slot, but the crack did not extend any further.

(a)

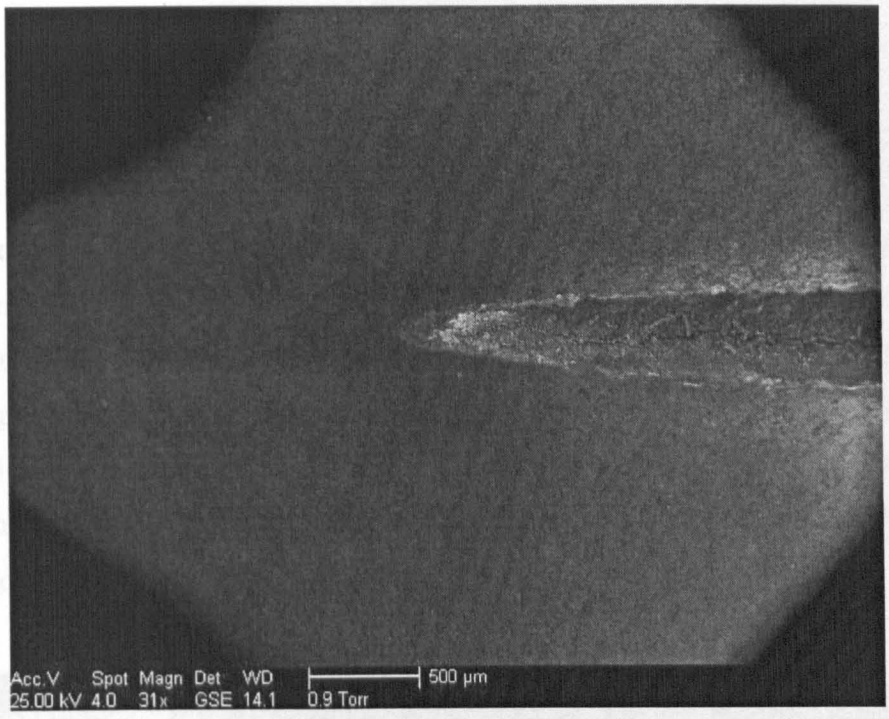

(b)

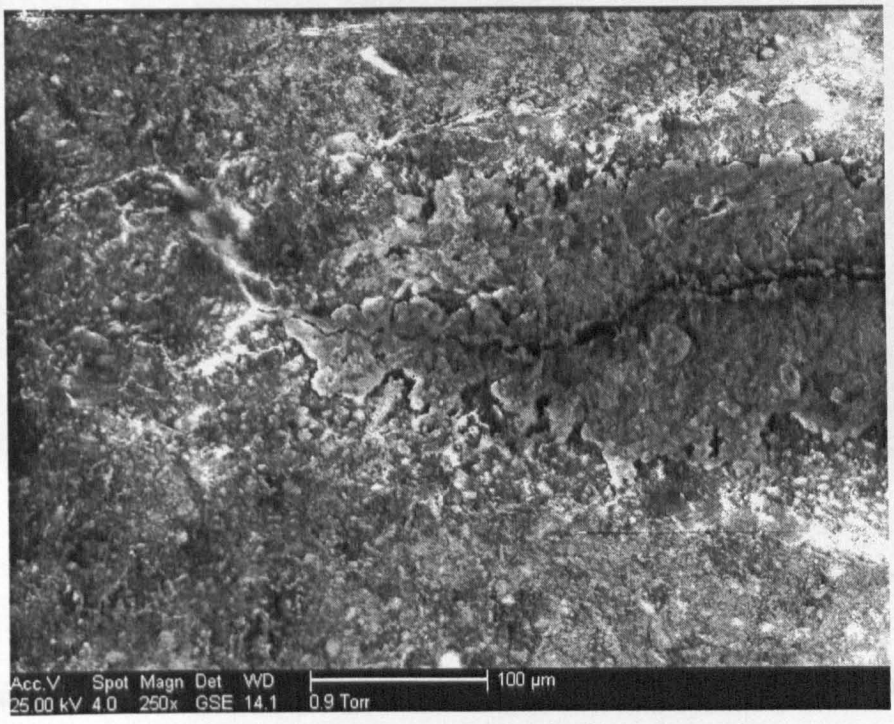

Figure 4.24. Typical crack development in the root of the slot, coating 'A' after 500k cycles; a) and b) ESEM images of different magnification

4.4.2.2. Coating 'B'

A panel coated with coating 'B' was tested under the same settings. Before the fatigue tests the sample was examined thoroughly. Early observation verified that during the slot making procedure no crack or any other significant damage was introduced. After approximately 30,000 cycles, a similarity to the previous test with four slots of different length was observed. Inside all three slots cracks were present. Yet again cracking commenced at an early stage of the fatigue cycles and initiated irrespective of the slot depths. The first cracks detected were in the roots of the slots and Figure 4.25. shows an image of the root of the 0.3mm depth slot when cracking was observed.

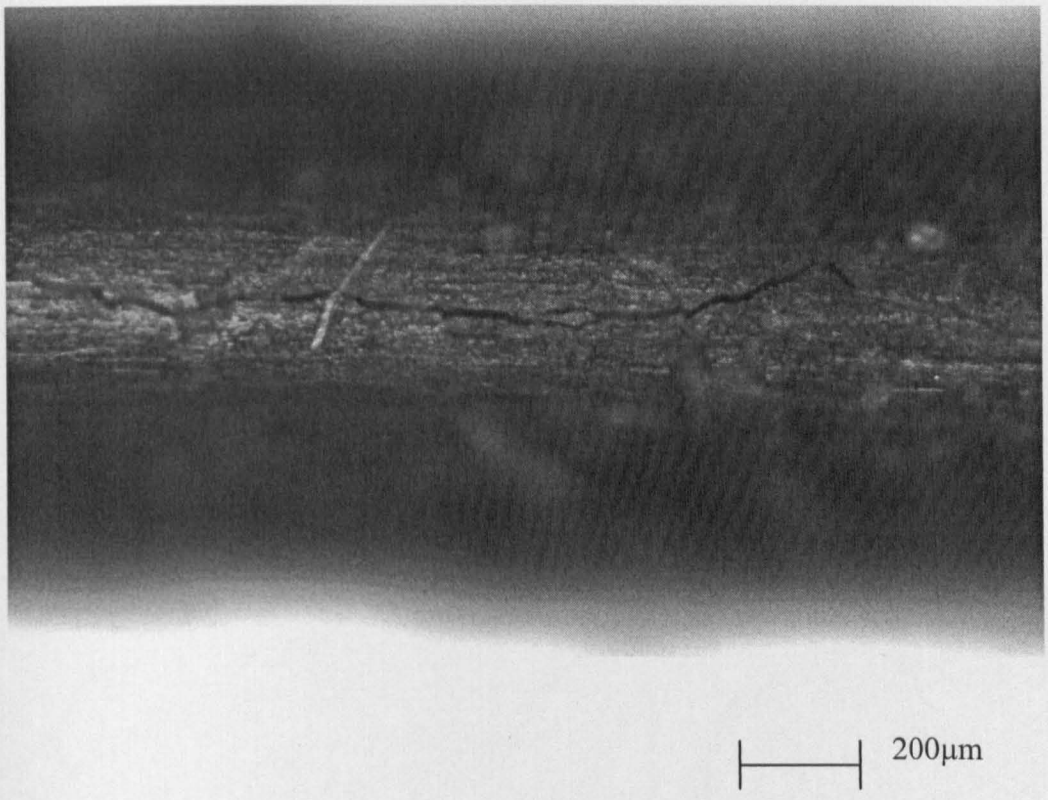

Figure 4.25. Typical inside-slot cracking, panel 'B', after 30,000 cycles, X120

With an increased number of test cycles, cracks propagated further from the ends of the slot to the edge of the specimen at right angles to the loading direction. After 300,000 cycles the cracks reached the panel edge.

Following crack initiation, development of cracks in coating 'B', is shown in Figure 4.26. The figure shows crack extension during the whole fatigue period for one of the three slots.

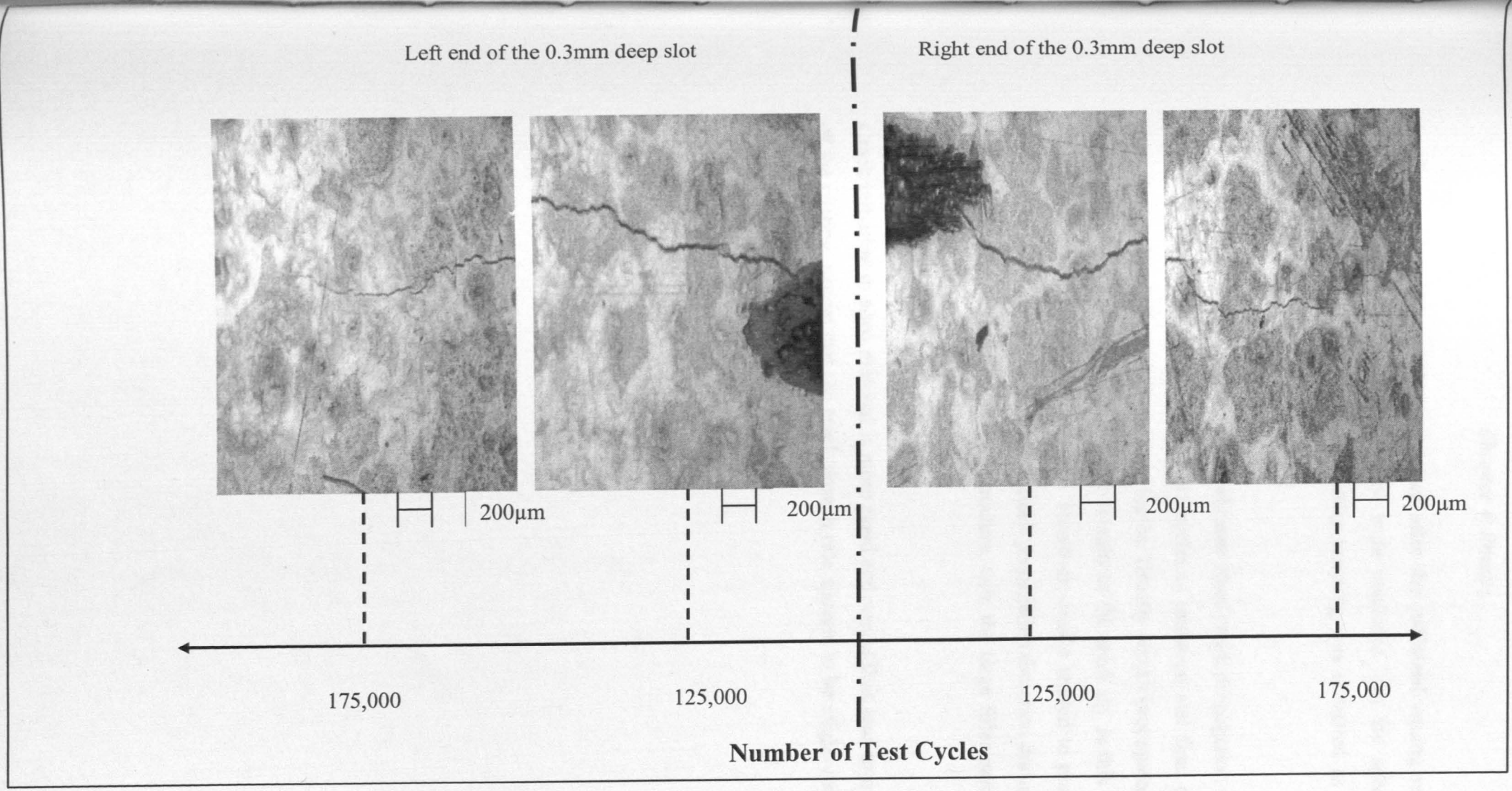

Figure 4.26. Typical crack propagation, panel 'B', up to 175k cycles

Another coating 'B' sample was tested after the industrial ageing recommended process. Three slots of different depths were machined into the aged 'B' panel. Fatigue testing was performed and similar cracking was observed as for the 'as-received' sample.

The crack length graph (Figure 4.27.) indicates when crack propagation started and it can be reported that the number of load cycles to initiation and final crack lengths were similar for all three different slot depths. Usually cracks propagated in different ways depending on the stress state in the vicinity of the crack tip. In this study, cracks extended linearly due to the symmetry. However, cracks tended to propagate in an individual manner, with changes in the crack propagation direction during the loading period probably due to coating microstructure, with the large filler particles causing crack deflection.

Crack initiation in aged material is more rapid and would thus lead to quicker failure of the coating, except that the crack growth rate appears to be slightly slower than in the 'as-received' material.

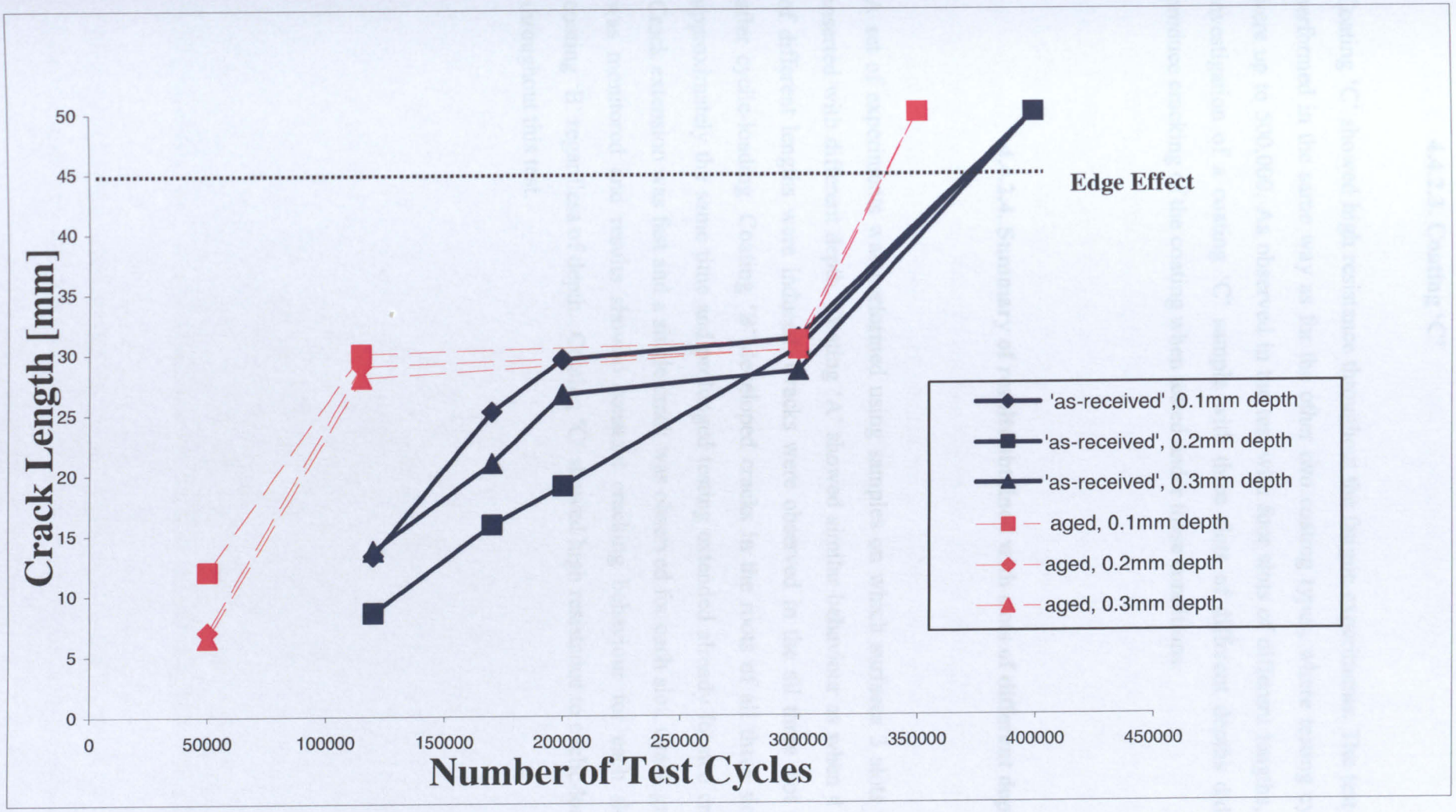

Figure 4.27. Total crack length versus number of test cycles, coating 'B', three slots of 20mm in length and of different depths

4.4.2.3. Coating 'C'

Coating 'C' showed high resistance throughout the fatigue experiments. The test was performed in the same way as for the other two coating types, where testing cycles were up to 500,000. As observed in the test with four slots of different lengths, this investigation of a coating 'C' sample with three slots of different depths did not produce cracking of the coating when tested under these conditions.

4.4.2.4. Summary of results obtained with slots of different depth

A set of experiments was performed using samples on which surfaces 3 slots were inserted with different depth. Coating 'A' showed similar behaviour as when 4 slots of different lengths were induced. Cracks were observed in the all three slot roots after cyclic-loading. Coating 'B' developed cracks in the roots of all three slots at approximately the same time and prolonged testing extended already formed cracks. Crack extension was fast and a single crack was observed for each slot. Crack growth was monitored and results showed constant cracking behaviour for each slot of coating 'B' regardless of depth. Coating 'C' showed high resistance to cyclic-loading throughout this test.

4.4.3. OBSERVATION OF SUBSTRATE CORROSION

During the cycling-loading tests on panels with introduced slots, evidence of the crack development was observed (section 4.4.2. and 4.4.3.). Coatings 'A' and 'B' formed cracks for each introduced slot. After fatigue tests the samples of coatings 'A' and 'B' were soaked in 3.5% NaCl solution at room temperature for 1 month. Chosen samples were coating 'A' panel with inserted 4 slots of different length and coating 'B' panel with 3 slots of the different depth. In tests on panels with no cracking it was found that this soaking procedure did not produce any visible corrosion of the substrate. Therefore, it was evident that diffusion of the corrosive environment through the coatings was not sufficient to cause corrosion. Hence, the observation in cracked samples can be taken to indicate that the cracks penetrated through to the substrate, providing a path for the aggressive environment. Evidence that cracks reached the substrate i.e. cracks penetrated all the way through the coating thickness is presented in Figures 4.28. and 4.29. for coatings 'A' and 'B', respectively.

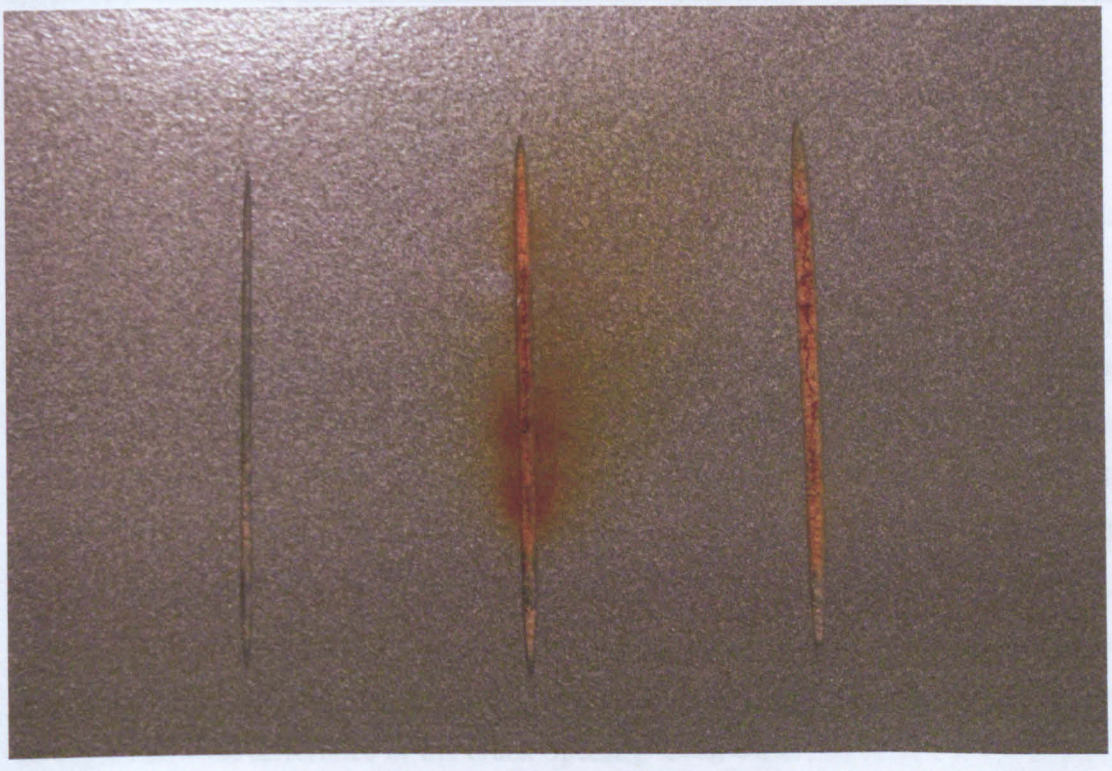

Figure 4.28. Corrosion test on coating 'A' slotted panel, showing corrosion products from the steel substrate indicating that the fatigue cracks in the coating reached the substrate

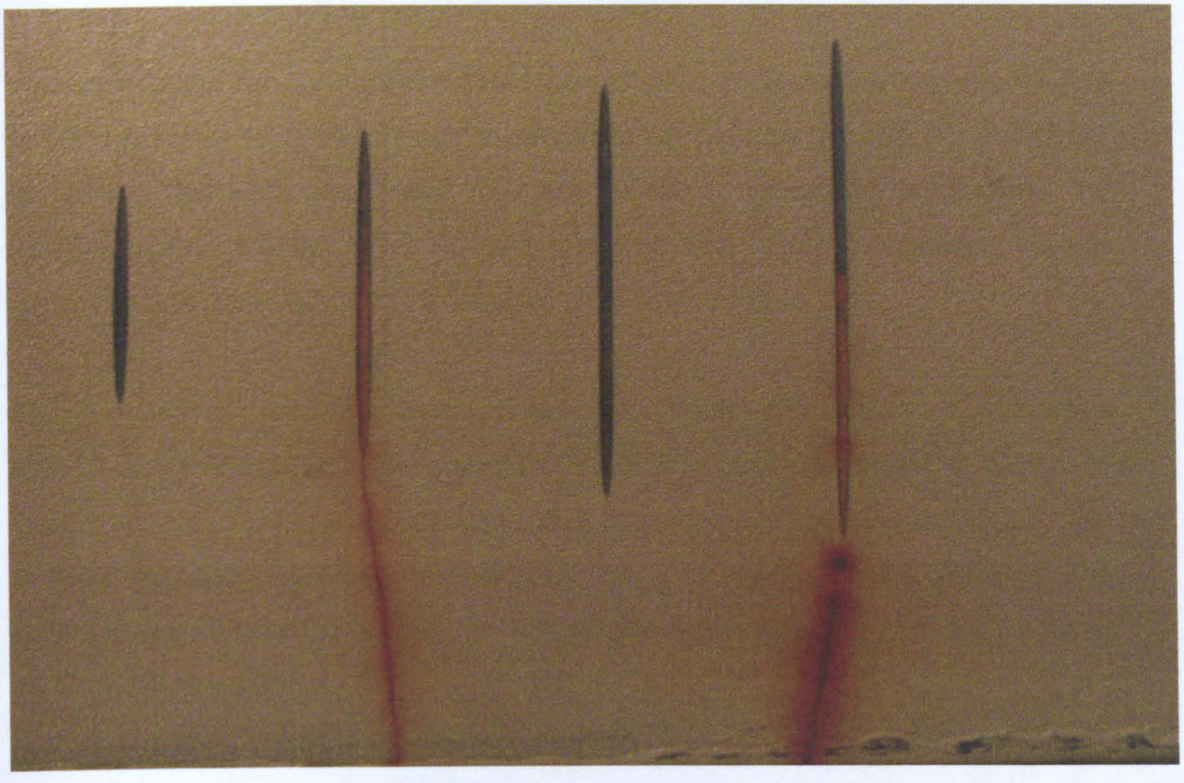

Figure 4.29. Corrosion test on coating 'B', showing corrosion that suggests that cracks reached the substrate

Knowing that in any environment the basic mechanism of corrosion is in principle an electrochemical action, this investigation was made by soaking the specimens in the artificial seawater. For corrosion to occur there must be a source of oxygen and a flow of electricity between certain areas of a metallic surface through a solution capable of conducting the electric current. The cracks developed in the coatings reached the mild steel substrate and artificial seawater migrated towards the coating/substrate interface. From the images presented above, it is indicated that the cracks had different depths within the same coating type therefore the corrosion rate was not identical. This can be explained with difference of the crack opening level, which varied from slot to slot, possibly depending on the local coating composition (e.g. particles of these inhomogeneous coatings could deflect or even arrest cracks formed during the cyclic-loading tests).

4.5. CRACK DEVELOPMENT DURING SLOW STRAIN RATE TESTS

The experiments on slotted coated panels, which were performed at a cyclic-loading rate of 19s per cycle, showed crack development for coatings 'A' and 'B'. Following the thought that slots were 'base' for crack formation throughout the coatings, the next stage of the research involved slow strain rate tests of the experimental coating systems at an extension rate of 10^{-5}mm/sec in uniaxial tension.

The 'as-received' coatings were prepared on mild steel substrates measuring approximately 150mm x 75mm (see section 3.6.). Two types of samples were used for these tests for each coating: parallel-sided and edge-notched (Figure 3.12.). The samples were first machined to a suitable size to fit into the testing machine. The coatings were removed from each end (shoulder) to prevent them from slippering in the grips (Figure 4.30.).

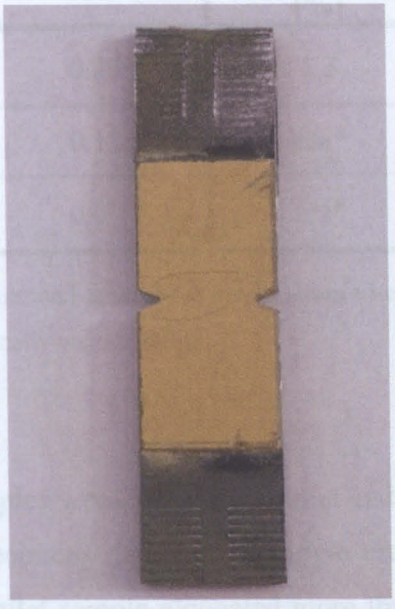

Figure 4.30. Coated notched specimen for slow strain rate test, showing uncoated shoulders for gripping

Specimens were tested in the dry condition for parallel samples and after soaking for one month in de-ionized water for both parallel and notched samples. The specimen surface was carefully observed to determine when cracks developed in the coatings (see section 3.6. for experimental procedure).

4.5.1. COATING 'A'

Parallel and notched samples of coating 'A' were tested under slow strain rate tests. Elongation of the specimens during the tests, as well as strain to crack observation was monitored. Table 4.9. shows the results obtained from these experiments.

Table 4.9. Slow strain rate results for parallel and notched samples for coating 'A'

Sample	Elongation [mm]	Strain to Crack Observation [%]	Comments
Parallel	0.26	1.3	Single Crack
Notched	0.12	n/a*	Single Crack
Notched Soaked	0.07	n/a*	Single Crack

*Note: Because of stress concentrated around the notch, strain to crack observation was recorded as significantly higher than realistically were possible.

Although coating 'A' samples were tested as parallel and notched samples (in dry and soaked condition), all specimens developed a single crack along the coating. Table 4.9. indicates that the parallel sample elongated more than the notched samples prior to cracking, 0.26mm compared to 0.12mm (dry) and 0.07mm (soaked), but that lower strain was needed for crack initiation.

Visual differences between the cracks that occurred on the surfaces of the tested coatings were observed. A single crack on the surface of the parallel, notched dry and notched soaked specimens of the coating 'A' are illustrated on Figures 4.31.-4.33., respectively.

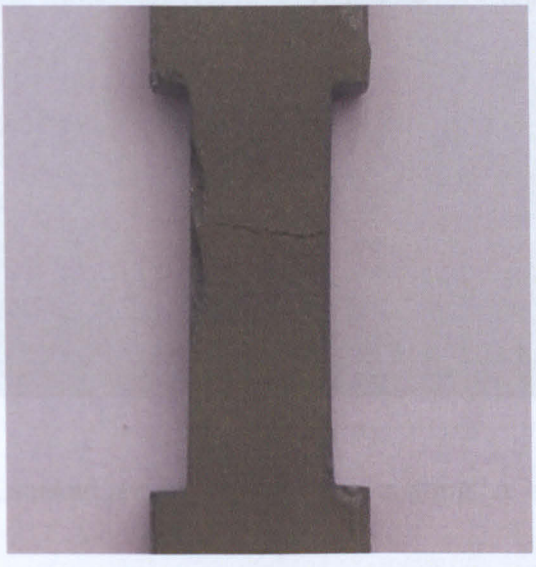

Figure 4.31. Cracked, parallel specimen of coating 'A', showing a single crack. The damage on the left was created during sample preparation

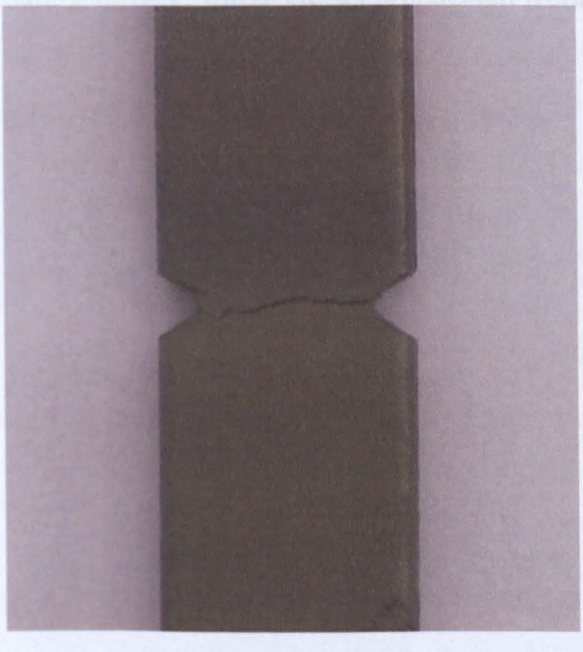

Figure 4.32. Cracked, dry notched specimen of coating 'A' showing a single crack

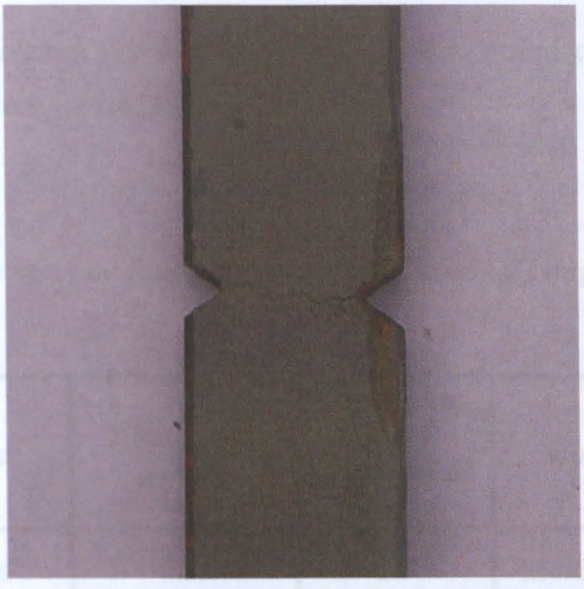

Figure 4.33. Cracked, soaked notched specimen of coating 'A' showing a single crack

Both notched samples of the coating 'A' regardless of their conditioning, produced a single crack on the coating surface, where cracks propagated from only one notch.

4.5.2. COATING 'B'

Both parallel and notched samples of coating 'B' were examined under slow strain rate tests. Observed results are given in Table 4.10.

Table 4.10. Slow strain rate results for parallel and notched samples for coating 'B'

Sample	Elongation [mm]	Strain to Crack Observation [%]	Comments
Parallel	0.35	1.7	Multiple Cracks
Notched	0.03	n/a	Double Crack
Notched Soaked	0.02	n/a	Double Crack

Table 4.5.5. shows that parallel sample of the coating 'B' produced multiple cracking and higher elongation than notched samples (Figure 4.34.). Double cracking was observed for both dry and soaked notched samples. Images from obtained results are illustrated in Figures 4.34.-4.36.

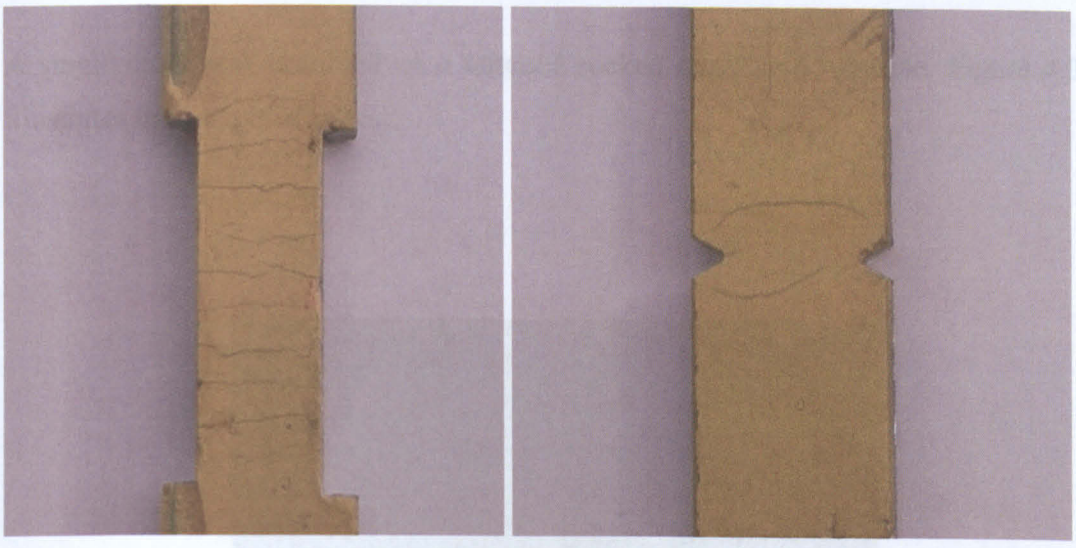

a) b)

Figure 4.34. a) Cracked, parallel specimen of coating 'B' showing multiple cracks; b) Cracked, dry notched specimen of coating 'B' showing a double crack

Figure 4.34. a) shows multiple cracks appearing on the surface of the coating 'B' parallel dry specimen. On the notched dry sample (Figure 4.34. b)), a double crack had appeared but unusually, neither crack started from the notch tip, but displaced from it. A reason for this could be that the cracks could have initiated beneath the surface; further investigation would be needed to determine the cause of this. However the result is consistent with the observation of multiple cracks in this coating after fatigue testing.

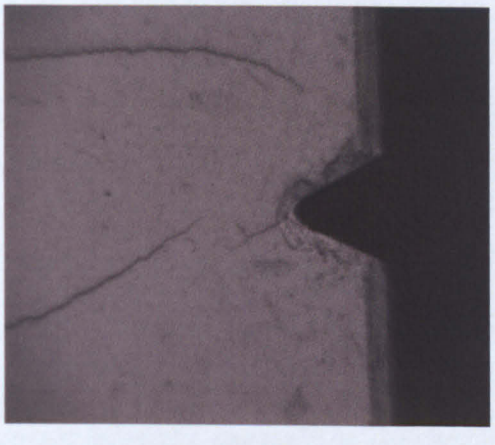

Figure 4.35. Magnified image of the cracked notched dry specimen of coating 'B', showing coating damage around the machined notch

A single crack was observed on a notched soaked coating 'B' sample. Figure 4.36. illustrates the sample after test.

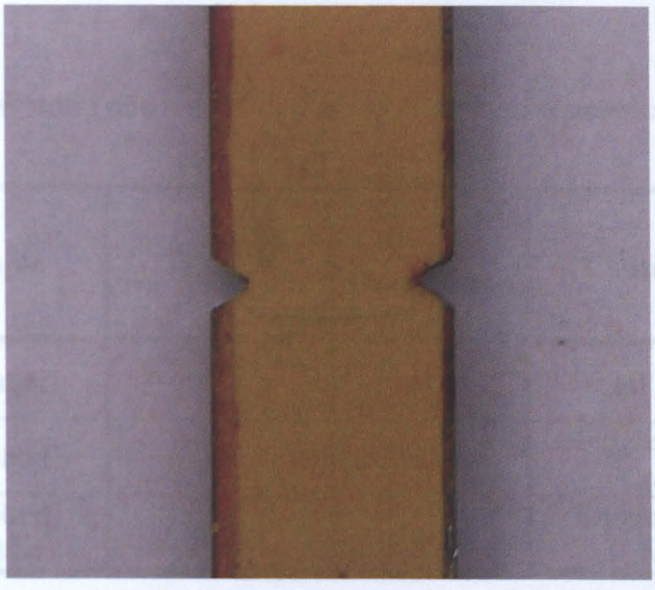

Figure 4.36. Cracked, soaked notched specimen of coating B showing a single crack

4.5.3. COATING 'C'

Obtained results for the coating 'C' samples under slow strain rate tests are presented in Table 4.11.

Table 4.11. Slow strain rate results for parallel and notched samples for coating 'C'

Sample	Elongation [mm]	Strain to Crack Observation [%]	Comments
Parallel	4.7	23.0	Small Cracks
Notched	0.11	n/a	Single Small Crack
Notched Soaked	0.08	n/a	Single Small Crack

Table 4.11. reports that coating 'C' samples developed small cracks after test procedures. The parallel sample had elongation of 4.7mm before a crack appeared, whereas the notched dry and notched soaked samples elongated 0.11mm and 0.08mm, respectively before cracking was visible.

Parallel dry coating 'C' specimen showed small cracks appearing at the edge. The cracks observed for this coating type were very small and did not propagate across the whole sample. A typical image of the observed cracking of coating 'C' is given in Figure 4.37. and shows a small crack that was developed in notched coating 'C' sample. It is noted that a very large strain was applied before cracking commenced, approximately two orders of magnitude higher than the design stress for steel and therefore, very far removed from the limiting service conditions. Hence, although cracking was provoked in coating 'C' in this test, it is not indicative of possible failure under service conditions.

Figure 4.37. Magnified image of the cracked, notched specimen of coating 'C'

4.5.4. SUMMARY OF SLOW STRAIN RATE TESTS

Slow strain rate tests showed that all three coatings failed after the yield strength of the steel (measured to be ~250MPa [214]) was exceeded. Consistency in a single crack performance was characteristic for the coating 'A'. Coating 'B' showed most cracks in comparison with the other two coating types (multiple and double cracks). Small cracks were obtained on the surface of the coating 'C' when tested under slow strain rate, but only after a very high strain. Soaking the specimens in de-ionised water did not drastically affect the cracking. The specimens were soaked for one month and this prolonged exposure did not significantly change the ductility of the substrate-coating combination. All coatings exhibited excellent adhesion and cracked rather than delaminated from the steel substrate.

4.6. TENSILE TESTS ON FREE-FILMS

4.6.1. TENSILE TEST ON 'AS-RECEIVED' FREE-FILMS

A set of tensile experiments were performed on the coatings as free-films, i.e. without a substrate. Samples were tested in 'as-received' state, within 48 hours after the spraying was performed. Hounsfield tensile tests are made by gripping the ends of a suitably prepared standardised test piece in a tensile test machine and then applying manually a continually increasing load until failure occurs. Tensile specimens are standardised in order that results are reproducible and comparable.

Free-film specimens had *gauge length*, L_0, approximately 40mm, and the total length of tensile specimens was approximately 100mm (Chapter 3.6.). Samples were prepared with 5 and 10 mm widths. The charts below show the results of the tensile tests.

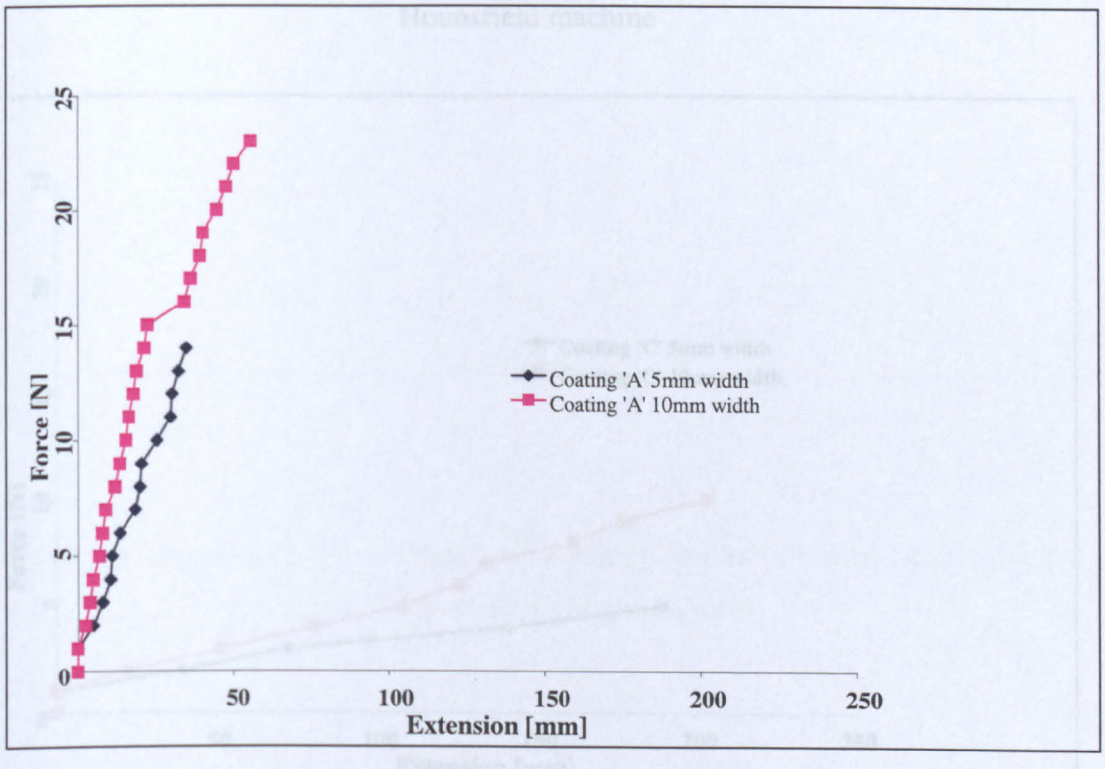

Figure 4.38. Tensile test, 'as-received' free-films of different widths, coating 'A', Hounsfield machine

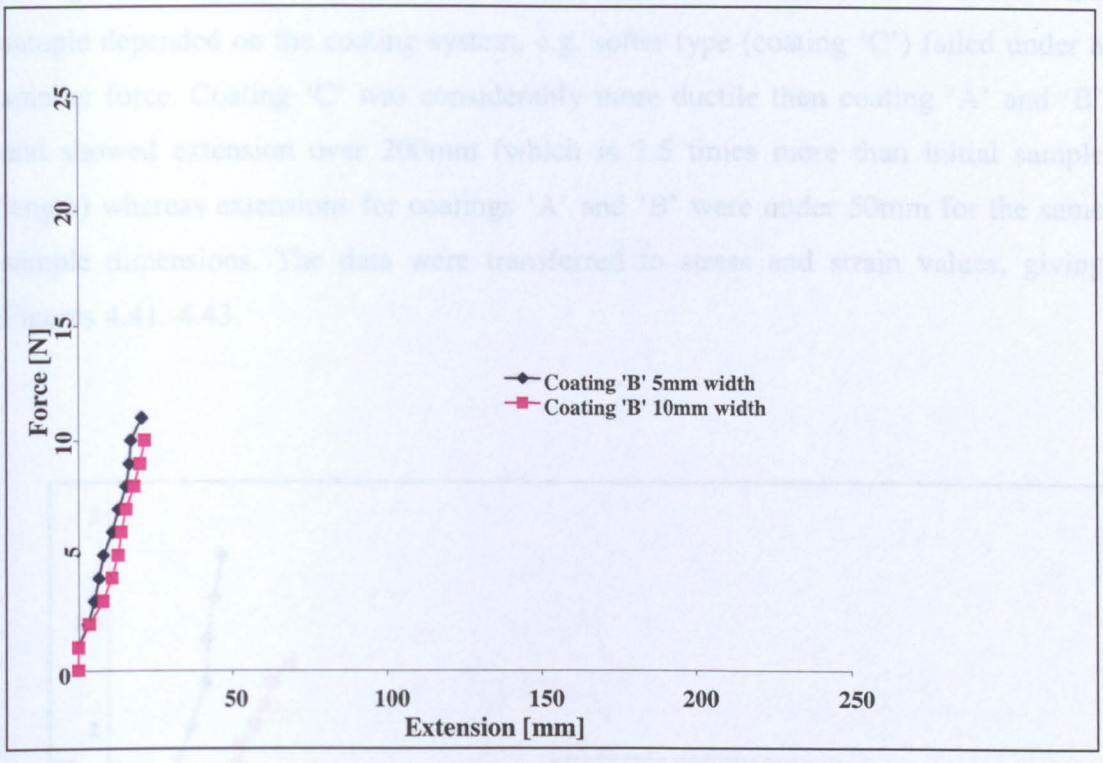

Figure 4.39. Tensile test, 'as-received' free-films of different widths, coating 'B', Hounsfield machine

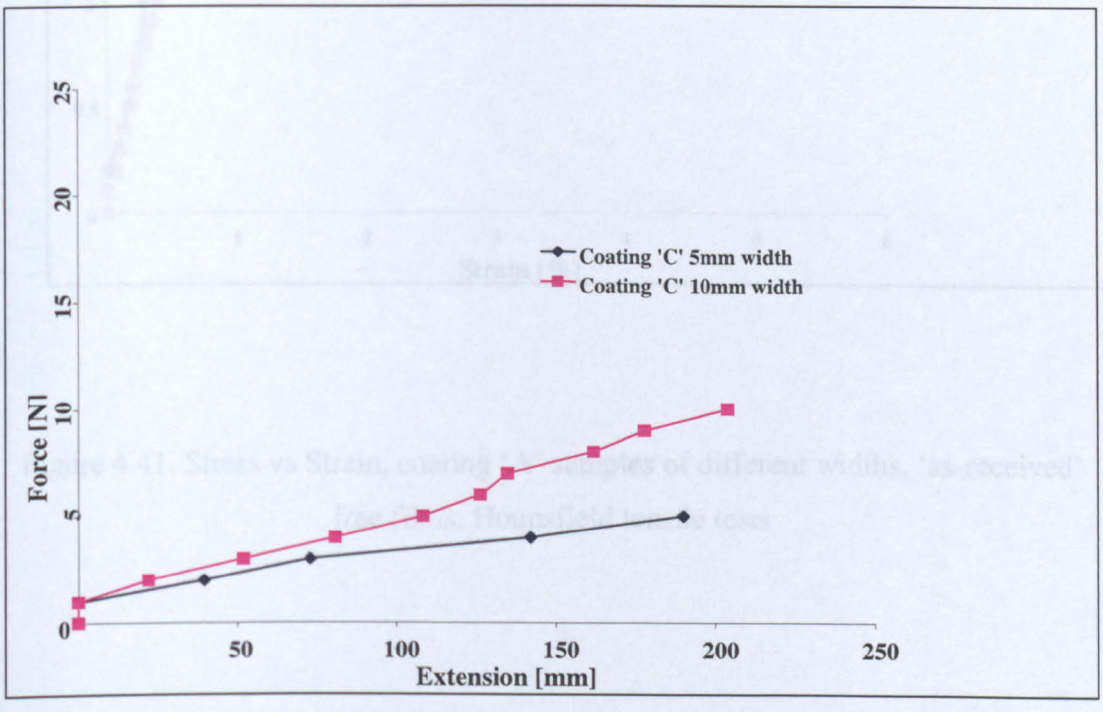

Figure 4.40. Tensile test, 'as-received' free-films of different widths, coating 'C', Hounsfield machine

In Figures 4.38.-4.40. it is shown that the amount of force needed to fracture the sample depended on the coating system, e.g. softer type (coating 'C') failed under a smaller force. Coating 'C' was considerably more ductile then coating 'A' and 'B' and showed extension over 200mm (which is 2.5 times more than initial sample length) whereas extensions for coatings 'A' and 'B' were under 50mm for the same sample dimensions. The data were transferred to stress and strain values, giving Figures 4.41.-4.43.

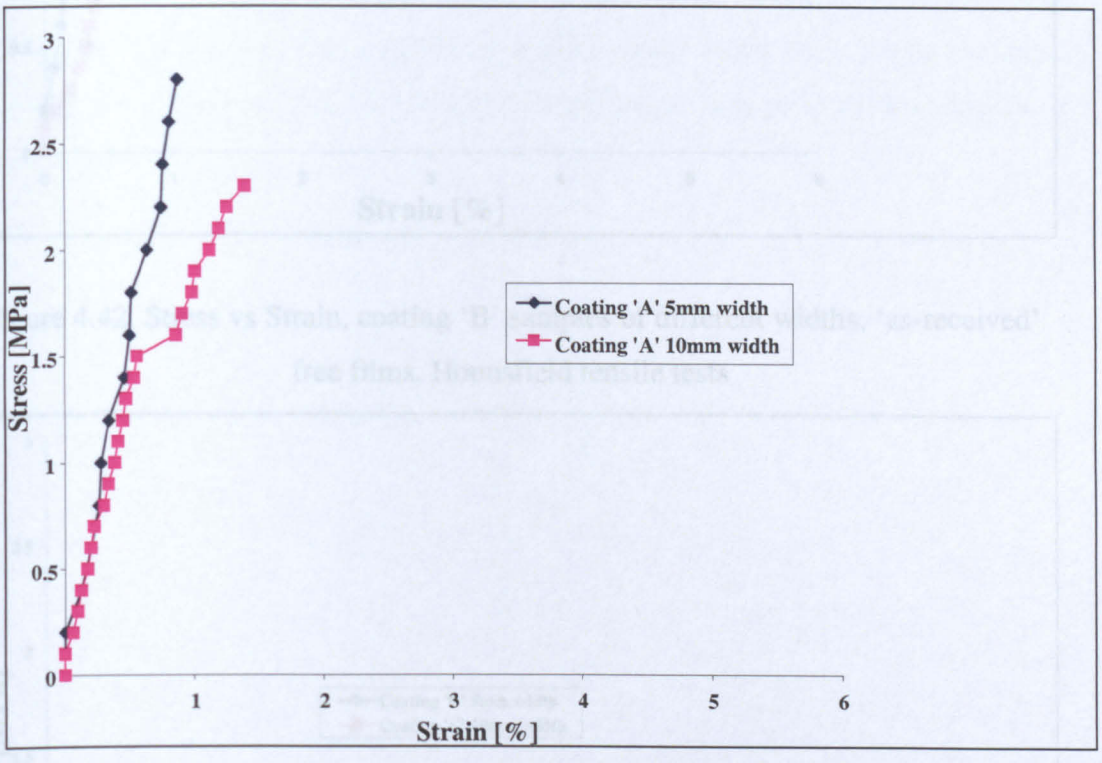

Figure 4.41. Stress vs Strain, coating 'A' samples of different widths, 'as-received' free films, Hounsfield tensile tests

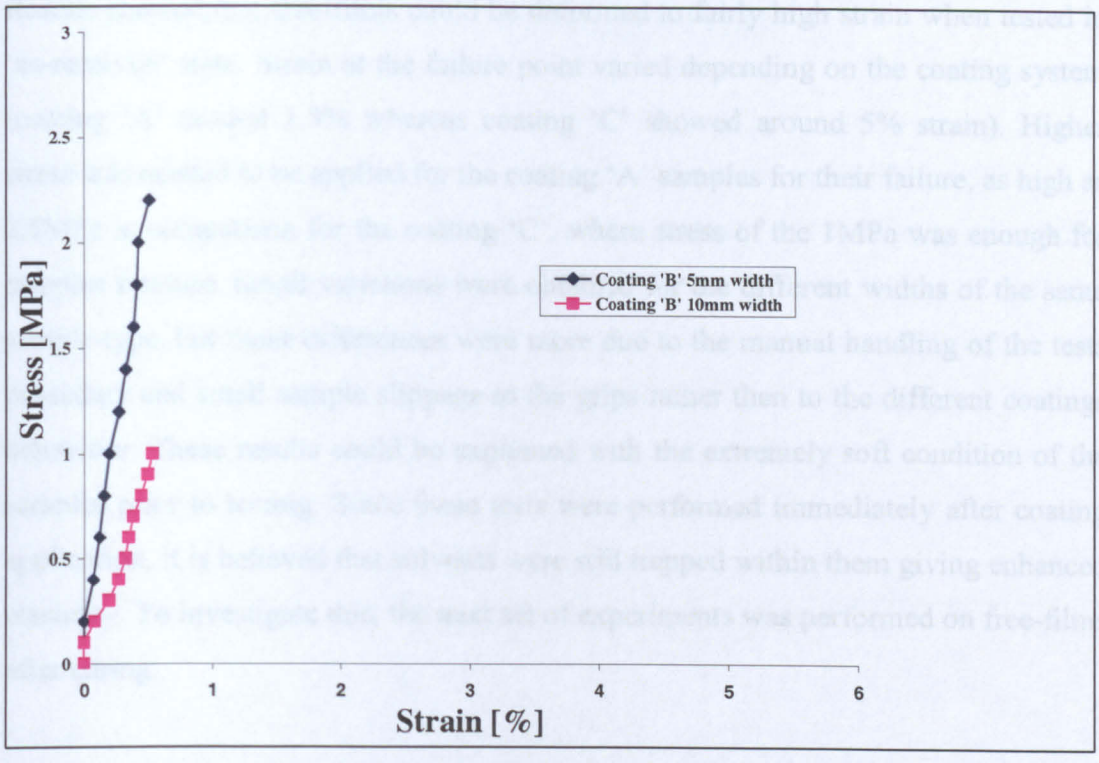

Figure 4.42. Stress vs Strain, coating 'B' samples of different widths, 'as-received' free films, Hounsfield tensile tests

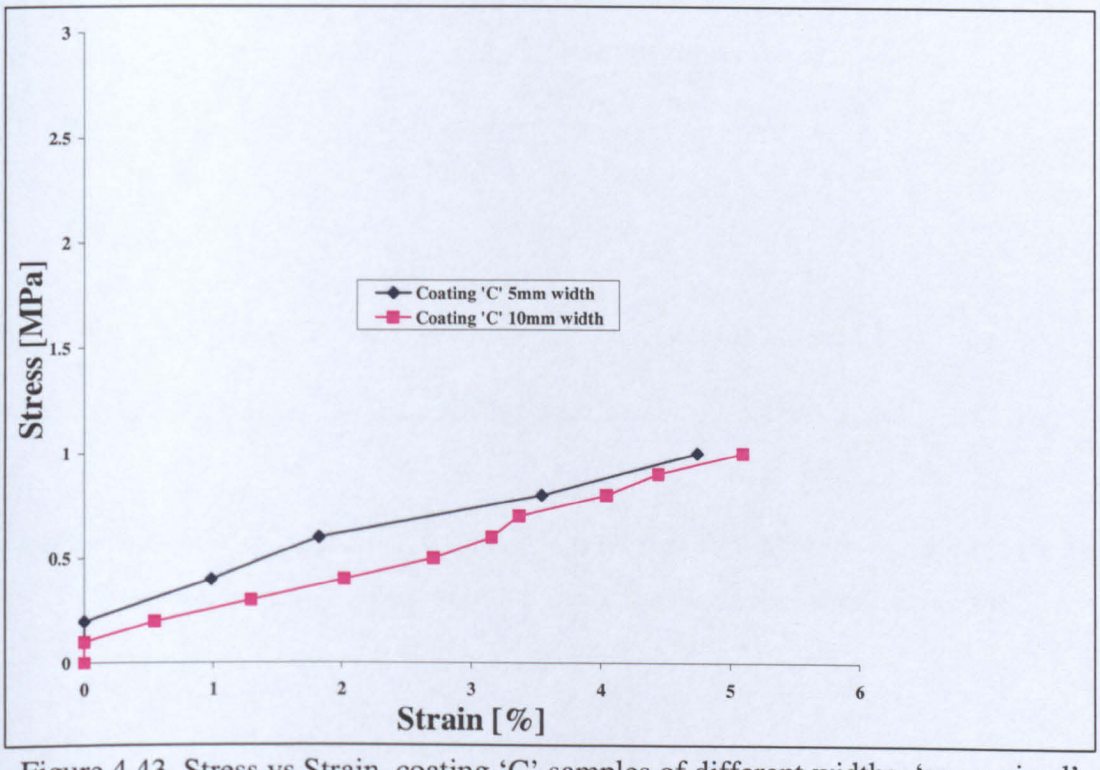

Figure 4.43. Stress vs Strain, coating 'C' samples of different widths, 'as-received' free films, Hounsfield tensile tests

Results showed that free-films could be deformed to fairly high strain when tested in 'as-received' state. Strain at the failure point varied depending on the coating system (coating 'A' around 1.5% whereas coating 'C' showed around 5% strain). Higher stress was needed to be applied for the coating 'A' samples for their failure, as high as 2.8MPa in comparison for the coating 'C', where stress of the 1MPa was enough for samples fracture. Small variations were obtained for the different widths of the same sample type, but those differences were more due to the manual handling of the tests procedure and small sample slippage in the grips rather then to the different coatings behaviour. These results could be explained with the extremely soft condition of the samples prior to testing. Since these tests were performed immediately after coating application, it is believed that solvents were still trapped within them giving enhanced elasticity. To investigate this, the next set of experiments was performed on free-films after curing.

4.6.2. TENSILE TEST ON CURED FREE-FILMS

Free-film samples of each coating type were tested on a Lloyd tensile machine set to provide a constant strain rate. Two of the four samples within the same coating system had 10mm gauge width and two had 5mm width. Prior to testing, samples were post-cured for 5 days at 80°C. The stresses needed to fracture the samples were recorded and Figures 4.44.-4.46. show the results. The crosshead speed was 5.0 mm/min.

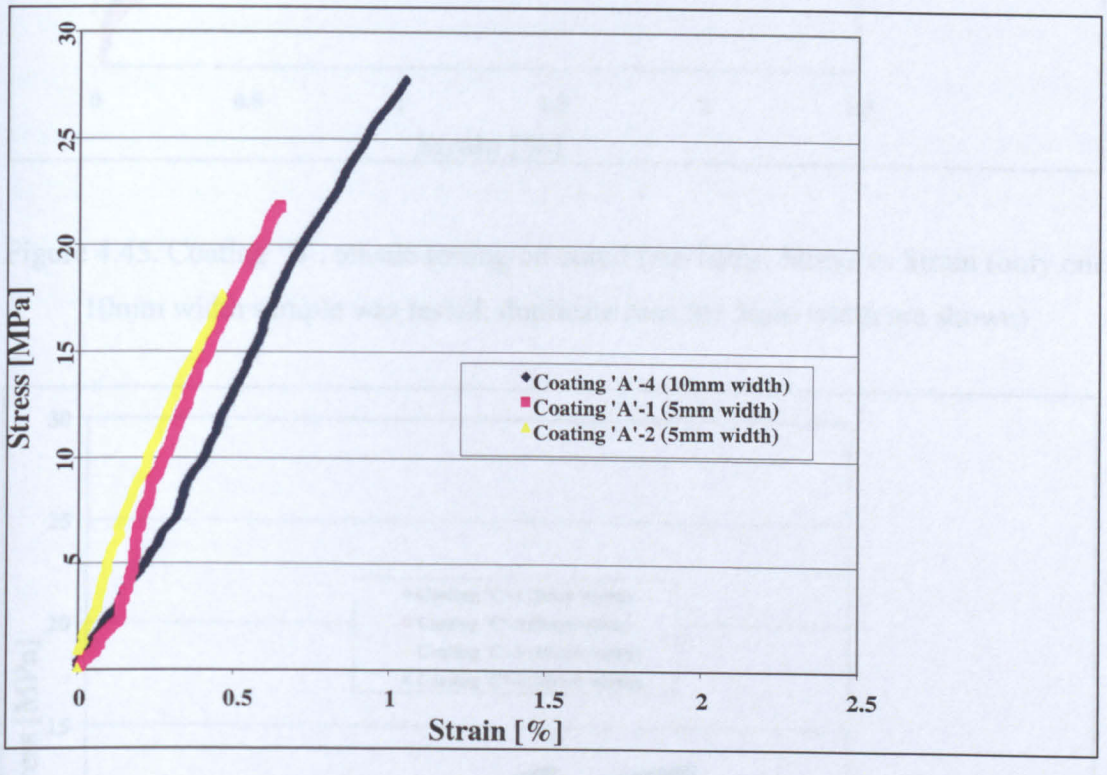

Figure 4.44. Coating 'A', tensile testing on cured free-films; Stress vs Strain (only one 10mm width sample was tested; duplicate runs for 5mm width are shown)

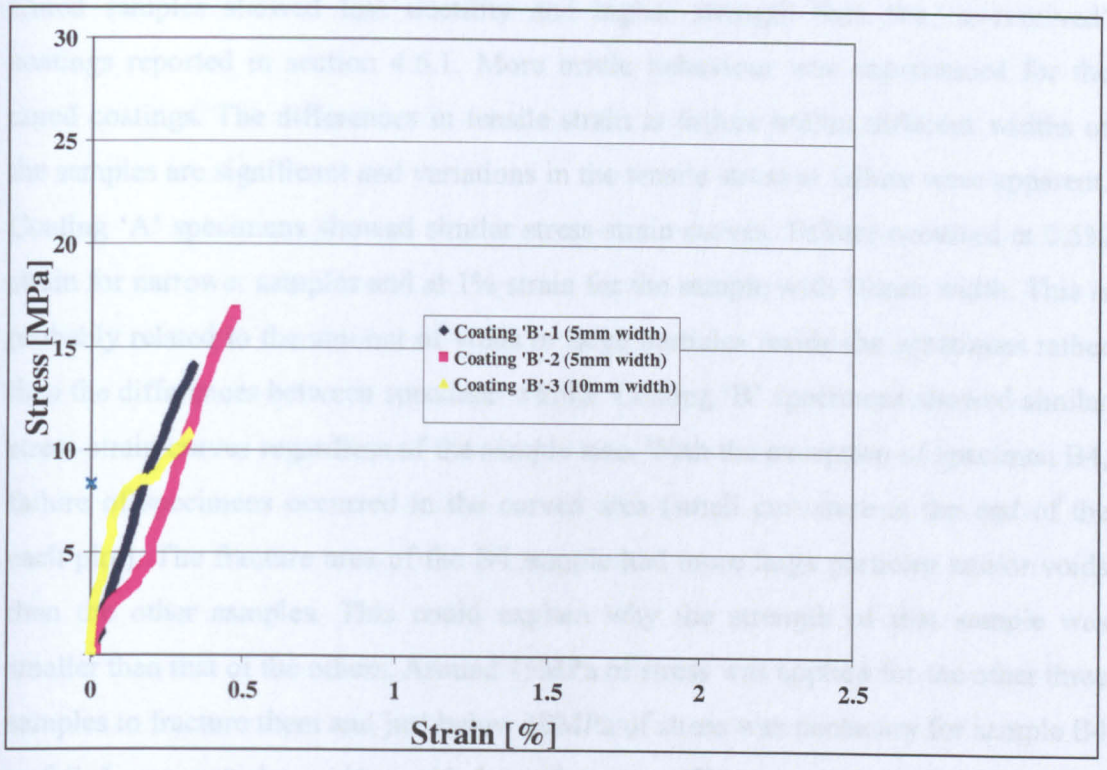

Figure 4.45. Coating 'B', tensile testing on cured free-films; Stress vs Strain (only one 10mm width sample was tested; duplicate runs for 5mm width are shown)

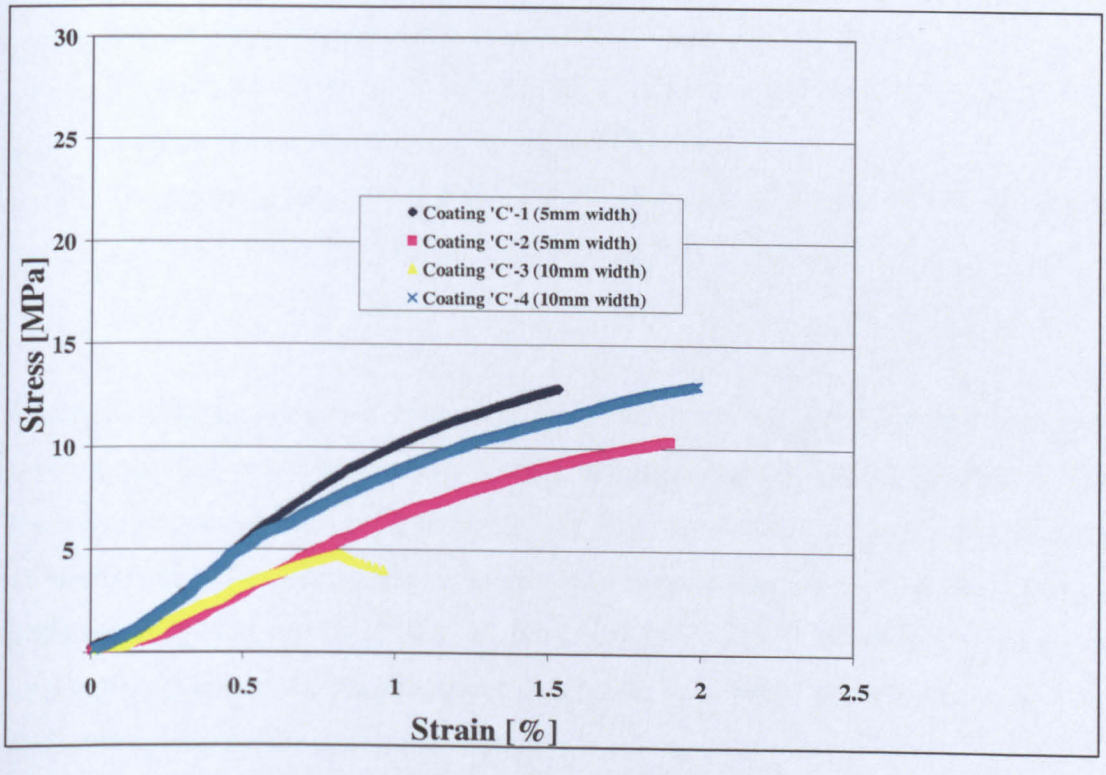

Figure 4.46. Coating 'C', tensile testing on cured free-films; Stress vs Strain; duplicate runs for 10mm and 5mm widths are shown

Cured samples showed less ductility and higher strength than the 'as-received' coatings reported in section 4.6.1. More brittle behaviour was experienced for the cured coatings. The differences in tensile strain at failure within different widths of the samples are significant and variations in the tensile stress at failure were apparent. Coating 'A' specimens showed similar stress-strain curves. Failure occurred at 0.5% strain for narrower samples and at 1% strain for the sample with 10mm width. This is probably related to the amount of voids or large particles inside the specimens rather then the differences between specimen widths. Coating 'B' specimens showed similar stress-strain curves regardless of the sample size. With the exception of specimen B4, failure of specimens occurred in the curved area (small curvature at the end of the each plot). The fracture area of the B4 sample had more large particles and/or voids then the other samples. This could explain why the strength of that sample was smaller than that of the others. Around 15MPa of stress was applied for the other three samples to fracture them and just below 10MPa of stress was necessary for sample B4 to fail. Large particles and/or voids have the same effect as micro-cracks, producing stress concentration and cause fracture to happen. More ductile behaviour was observed for coating 'C' samples where strain levels reached 2%.

4.7. HARDNESS AND YOUNG MODULUS

4.7.1. MICRO-HARDNESS MEASUREMENTS DURING AGEING

Given that the main goal of this investigation was to understand fatigue failure under service conditions, one of the main requirements throughout the tests was that plastic deformation of the substrate should not occur during cyclic loading. Changes in the coatings produced by cyclic loading and other conditions (temperature change or immersion in water) can be followed through hardness measurements, as hardness is an ability of a material to resist plastic deformation. When a substrate made from a material similar to that used for ballast tanks is coated with epoxy coatings and cycled through constant- or varying-loading amplitude, large changes could occur in the coating hardness or softness [8]. During the ageing process that has been performed in our laboratory, attention was given to monitoring hardness values of the coatings on panels that were exposed to ageing at various stages of the ageing process. The laboratory ageing process, based on the recommended industrial procedure, consisted of the following cycles:

1. First ageing stage consisted of :1 cycle of 7 days at 35°C in air;
2. Second ageing stage consisted of: 3 cycles each consisting of 2 days immersion in seawater then 2 days at 23°C in air;
3. Third ageing stage consisted of: 10 cycles each of 2 days at 5°C, 2 days at 70°C and 2 days immersion in seawater at 23°C.

Multiple micro-hardness measurements were performed on panels sprayed with each type of the experimental coatings before commencing the ageing procedure. The measurements were made after every ageing stage on all three coatings (after all three of them). The hardness measurements of the final stage that was carried out (firstly on different temperatures and then in seawater) were taken immediately after the concluding stage of ageing process and one and two hours afterwards. Table 4.12. gives the results of those measurements.

Table 4.12. Average micro-hardness on coatings during the ageing process

Coating Type	Hardness [MPa]					
	STEP 1	**STEP 2**	**STEP 3**	**STEP4**	**STEP 5**	**STEP 6**
	Before Ageing process	After 1st ageing stage (35°C)	After 2nd ageing stage (23°C)	After 3rd ageing stage (5°C/70°C/23°)		
				After 1hour	After 2 hours	After 3 hours
A	39	324	137	294	216	223
B	43	196	196	330	356	252
C	10	20	20	16	24	10

The scatter on repeat measurements was approximately ±2MPa. The hardness values obtained depended on coating composition, e.g. epoxy resins/hardener ratio, and the difference between the three types of coatings was established. All three epoxy coatings showed very low hardness values prior to any conditioning (Table 4.11.). This might explain why coatings had a high fatigue resistance in the "as received" state. According to these measurements, coatings were much softer in 'as-received' condition then after 'post-curing' and therefore, more ductile, so during the fatigue tests they showed more elastic behaviour which did not produced cracking. However, all three coatings demonstrated surface changes in the 'as-received' stage and that observation was not seen for the post-cured coatings.

The hardness measurements are presented graphically given as Figure 4.47.

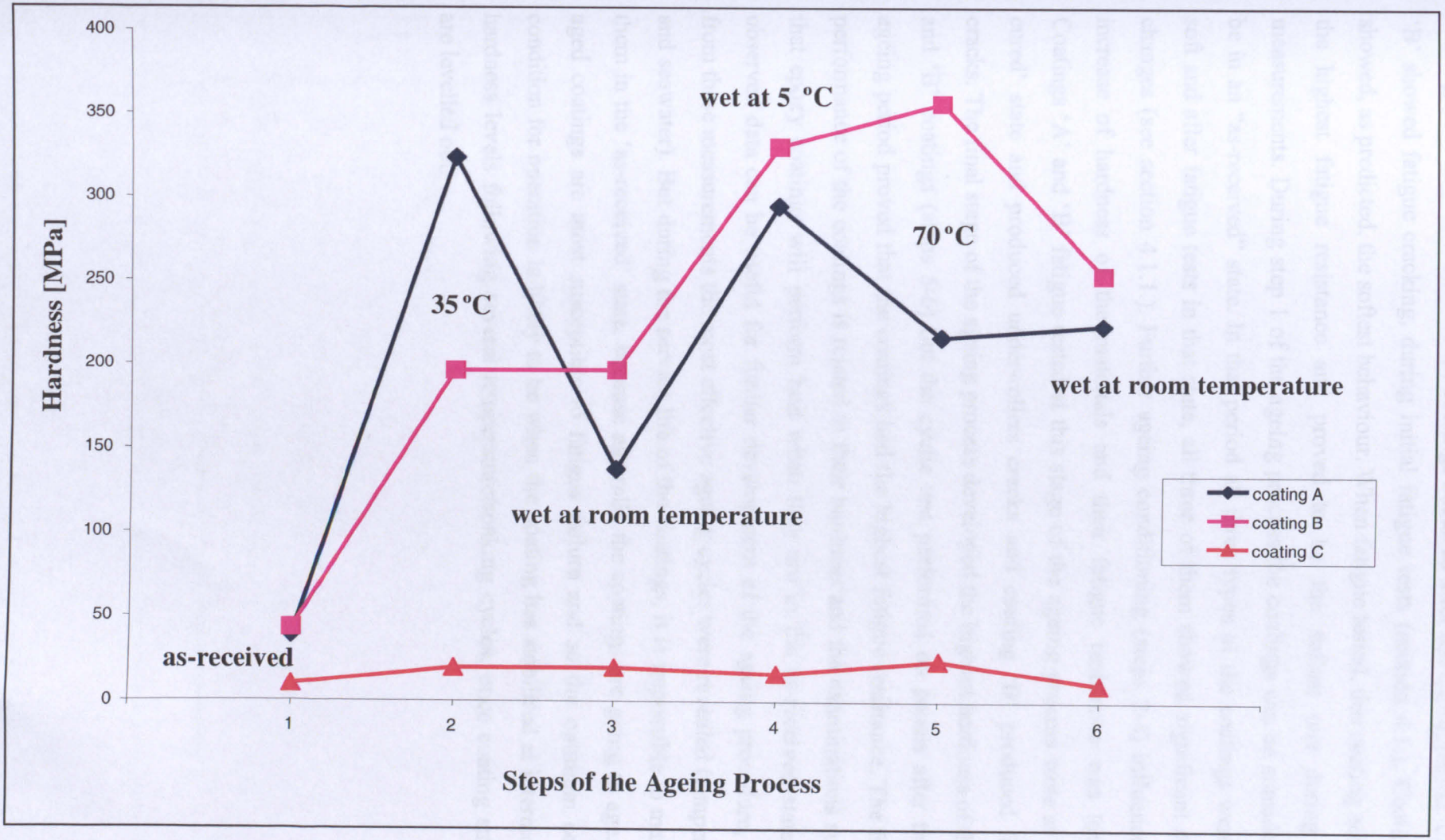

Figure 4.47. Average hardness measurements during the ageing process

The highest hardness values for the coatings occurred after the curing period. Coating 'B' showed fatigue cracking, during initial fatigue tests (section 4.1.). Coating 'C' showed, as predicted, the softest behaviour. When fatigue tested, this coating achieved the highest fatigue resistance and proved to be the softest one during these measurements. During step 1 of the ageing process the coatings can be considered to be in an "as-received" state. In that period all three types of the coatings were very soft and after fatigue tests in that state, all three of them showed significant surface changes (see section 4.1.1.). Further ageing conditioning (steps 2-4) influenced the increase of hardness of the materials and their fatigue resistance was lowered. Coatings 'A' and 'B' fatigue tested at this stage of the ageing process were at 'post-cured' state and produced under-rollers cracks and coating 'B' produced fatigue cracks. The final stage of the ageing process developed the highest hardness of the 'A' and 'B' coatings (steps 5-6) but the cyclic test performed on panels after the full ageing period proved that the coatings had the highest fatigue resistance. The fatigue performance of the coatings is related to their hardness and the examinations suggest that epoxy coatings will perform best when they are in the as-received state. The observed data can be useful for further development of the ageing procedure, since from these measurements the most effective ageing cycles were revealed (temperature and seawater). But during the service life of the coatings, it is impossible to maintain them in the 'as-received' state, because naturally the coatings are going to age. Dry, aged coatings are most susceptible to fatigue failure and so the optimum coating condition for operation is likely to be when the coating has stabilised at intermediate hardness levels following several temperature/soaking cycles, once coating stresses are levelled out.

4.7.2. THE EFFECT OF DE-IONIZED WATER ON THE HARDNESS OF EXPERIMENTAL COATINGS

Each coating sample (panels) was soaked for set periods and the micro-hardness tests were performed throughout the soak and drying-out period after the coating was removed from the water.

4.7.2.1. Soaking Period

Samples of the coatings were soaked in de-ionized water for various times up to 24hours after storage at room temperature and humidity for 12 months. Micro-hardness measurements were obtained during those periods and Figure 4.48. shows hardness values for each coating type obtained from those measurements.

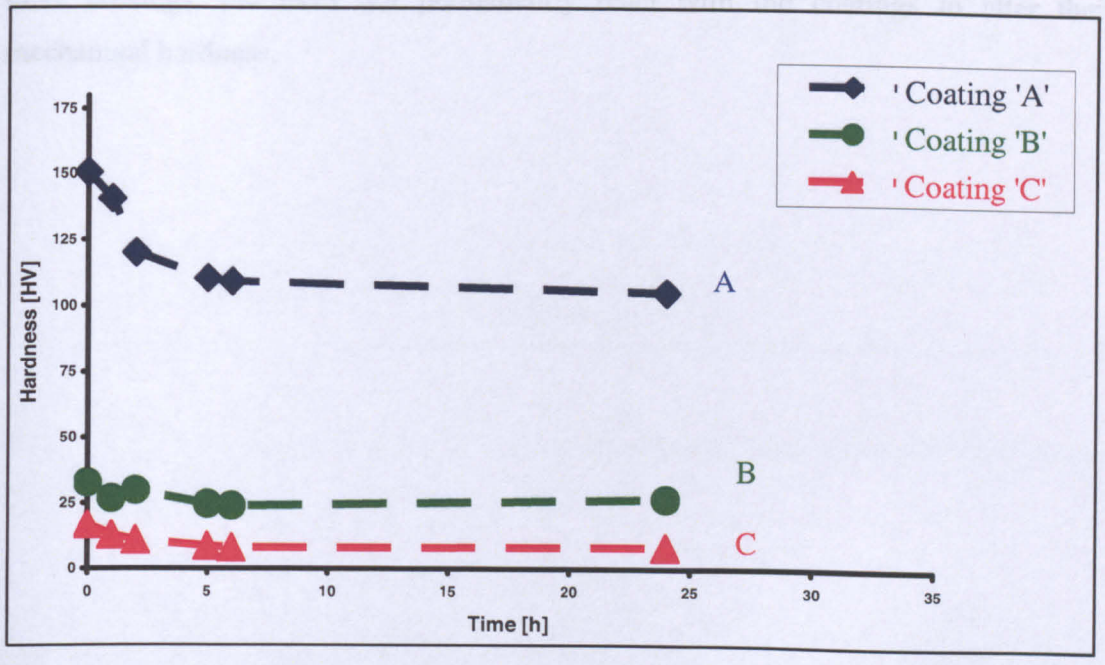

Figure 4.48. Hardness of the coatings during soaking in de-ionized water

Initial hardness measurements on the experimental epoxy coatings showed that the hardest coating was coating 'A' with 150.8HV. Values of 32.4HV and 8.04HV were obtained as starting measurements for coatings 'B' and 'C', respectively. Appendix 4.1. tabulates the obtained data. When submerged in de-ionized water environment, the hardness of the coatings changed. A rapid decrease of the hardness was observed during the first 5 hours of soaking. Within the first immersion hour, the largest decrease of the hardness was observed with coating 'C', 23.4%. The decrease for coating 'A' was 6.5% and for coating 'B' was 15.4% in the first hour. After 5 hours of soaking coating 'C' showed again the highest hardness reduction, of nearly 50% of the original value. Decrease of around 25% was obtained for both 'A' and 'B' coatings. Further immersion for up to 19 hours generated more stable hardness for each coating type. This can be expected as coatings consist of the polymer matrix and hard filler particles which do not absorb the water in the same manner. Once the particles attracted water and gain the balance of the amount of water that can be absorbed, further hardness changes were hardly measurable. As a softest coating 'C' experienced largest changes in hardness during soaking, therefore, particles of coating 'C' proved to be less absorbable. Primarily, water plasticises the resin matrix of all three coatings, but does not permanently react with the coatings to alter their mechanical hardness.

4.7.2.2. Drying-out Period

Another set of the experiments were performed during a drying out period after a range of soaking intervals (1day, 3days, 1week and 1month). Hardness measurements obtained during soaking and drying out for all three coatings are presented below.

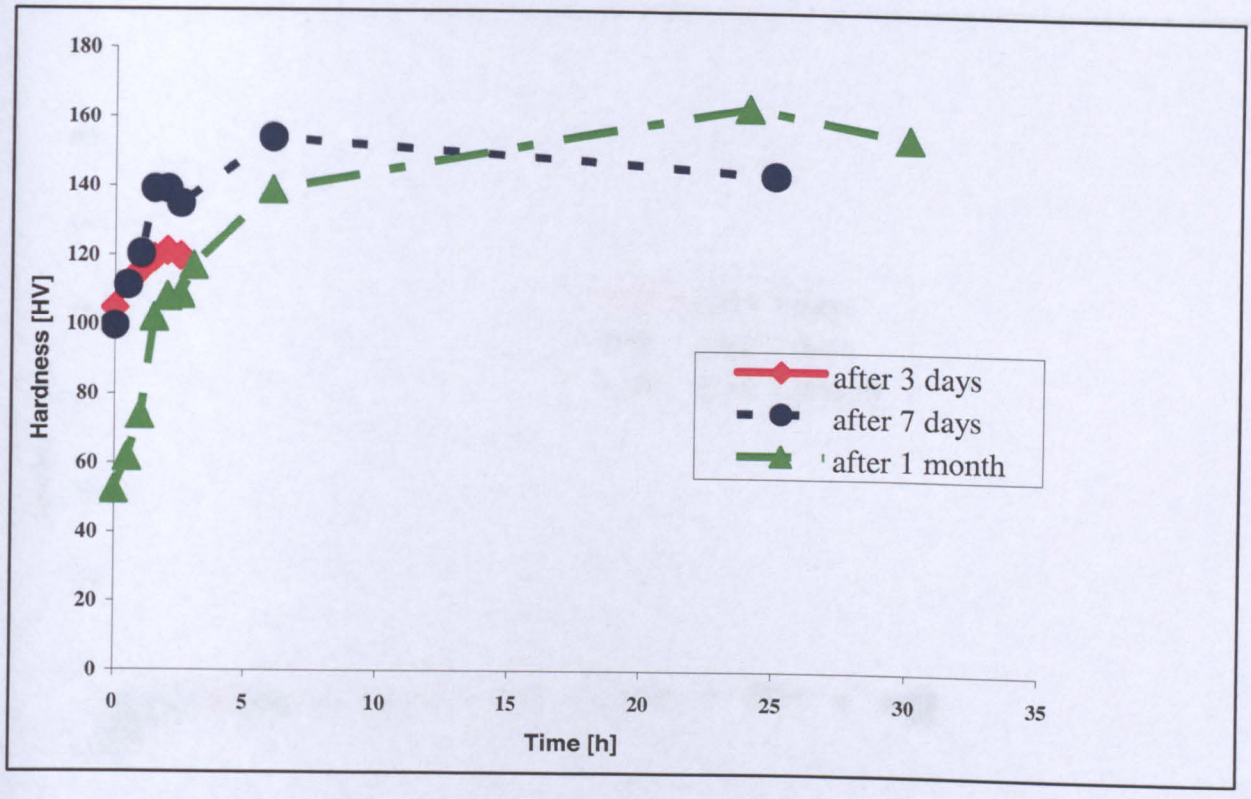

Figure 4.49. Hardness of coating 'A' during drying-out period selected soaking times

Subsequent to prolonged immersion periods of 3 days, 1 week and 1 month, micro-hardness values on the surface of all three coatings were measured during drying-out for a period for up to 30 hours. The biggest changes were observed within the first hours of drying where most of the coatings experienced increase of the hardness.

When coating 'A' was removed from water after it had been soaked for 1 month, hardness was found to have reduced from 150.8HV to 52.3HV, a reduction of around 65%. Increase of the hardness then commenced and was monitored for coating 'A' in the first 4 hours of drying after each soaking cycle. Then a small hardness drop was observed followed by further increase in hardness after further drying. Drying-out period of around 30 hours after soaking for 1 week and 1 month, provided starting hardness value of 150HV for coating 'A' that was measured at the beginning of soaking period (see Figure 4.48.).

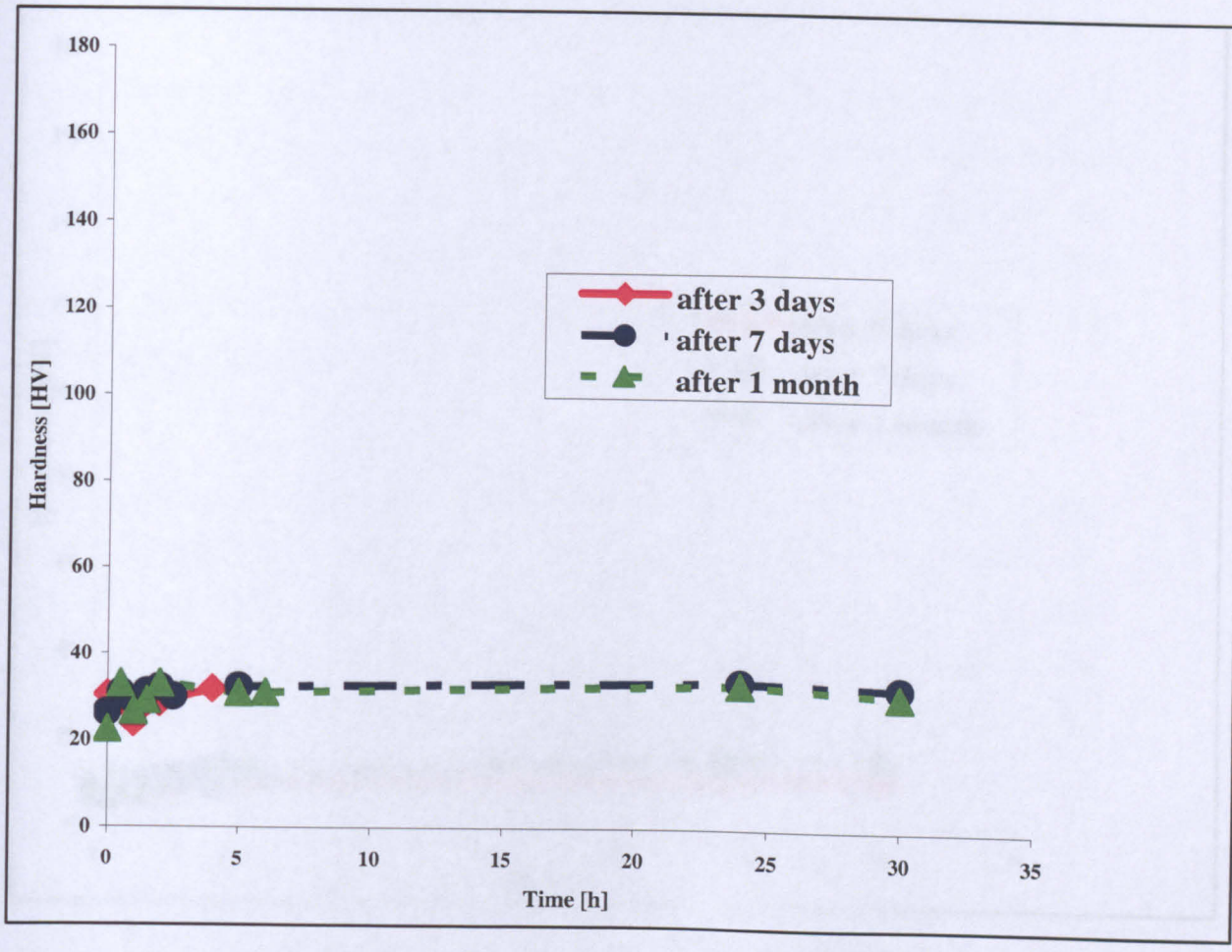

Figure 4.50. Hardness of coating 'B' during drying-out period after selected soaking times

Coatings 'A' and 'B' were exposed to water for 1 month, they became progressively softer. Immersion periods of 3 and 7 days did not produce significantly different results within the same coating type. The drying out of coating 'B' was high in the first few hours. Hardness decreased within the first hour of drying after each immersion stage. The level of absorption was high for this specimen giving the lowest hardness measurements for the coating, but within a few hours of commencing drying, the coating produced a higher, stable hardness and reached its original value of around 32HV.

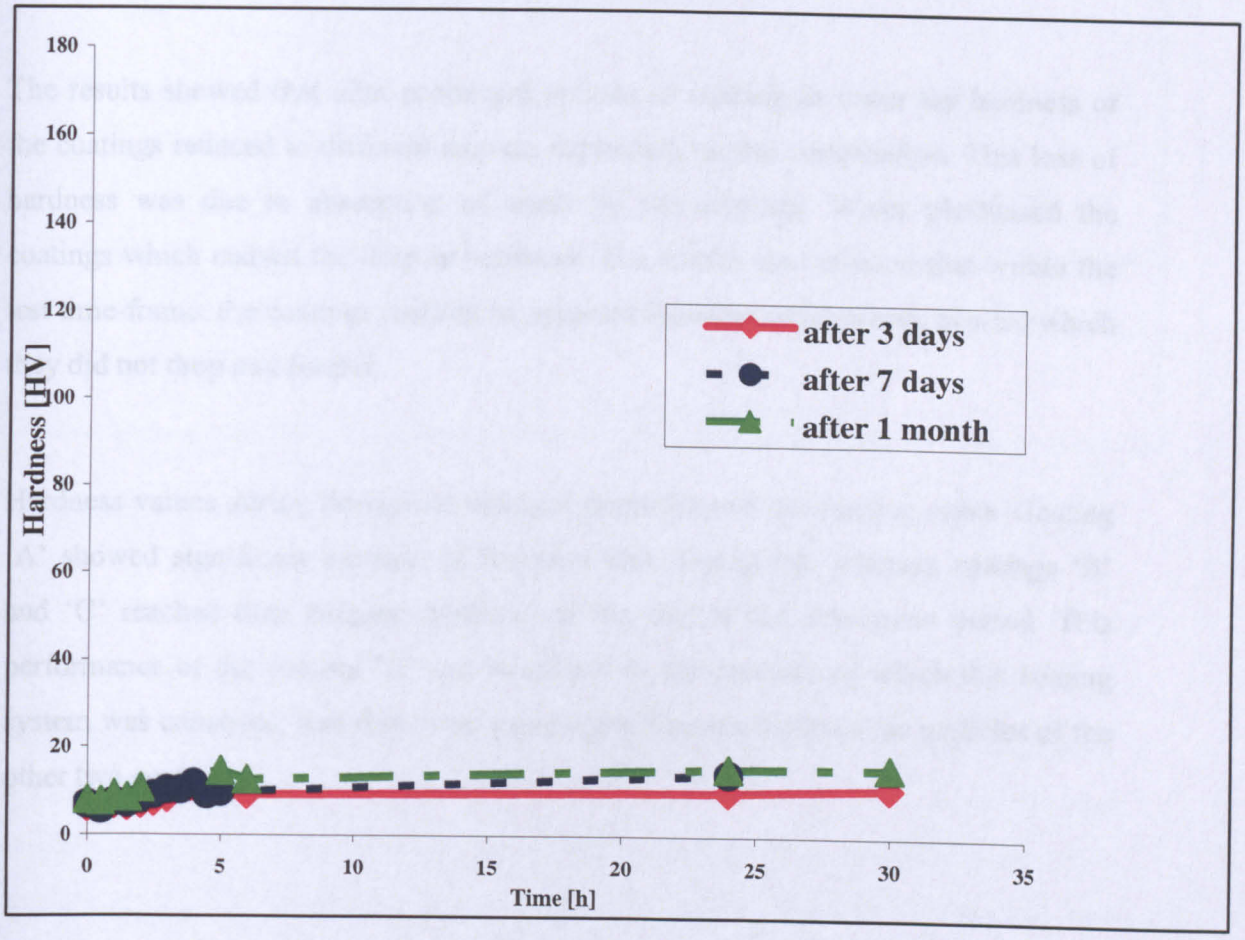

Figure 4.51. Hardness of coating 'C' during drying-out period after selected soaking times

Coating 'C' showed a much different dry-out pattern that of the other two coatings. More consistent hardness was obtained for this coating system. Figure 4.51. shows that when the hardness was tested after 3 different soaking periods, the trends were similar, a steeper gradient to begin then slowing to an increase in hardness. When the coating was soaked for shorter periods, the time required to return the more steady hardness level was shorter.

4.7.2.2. Summary of the effect of the de-ionized water on hardness of experimental coatings

The results showed that after prolonged periods of soaking in water the hardness of the coatings reduced to different degrees depending on the composition. This loss of hardness was due to absorption of water by the coatings. Water plasticised the coatings which caused the drop in hardness. The results also showed that within the test time-frame, the coatings reached an apparent hardness equilibrium, beyond which they did not drop any further.

Hardness values during drying-out changed depending on the coating types. Coating 'A' showed significant increase of hardness after drying-out, whereas coatings 'B' and 'C' reached their original hardness, at the end of the drying-out period. This performance of the coating 'A' can be related to the particles of which this coating system was consisted, that they were more water-absorptable than the particles of the other two coatings.

PAGE
MISSING
IN
ORIGINAL

Table 4.13. shows that the hardest coating was coating 'A', whereas coating 'C' was the softest one. The maximum load that was achieved was the highest for coating 'A', 786.1μN. These measurements confirmed differences in mechanical properties between the three types of coating and it is schematically presented in Figure 4.52.

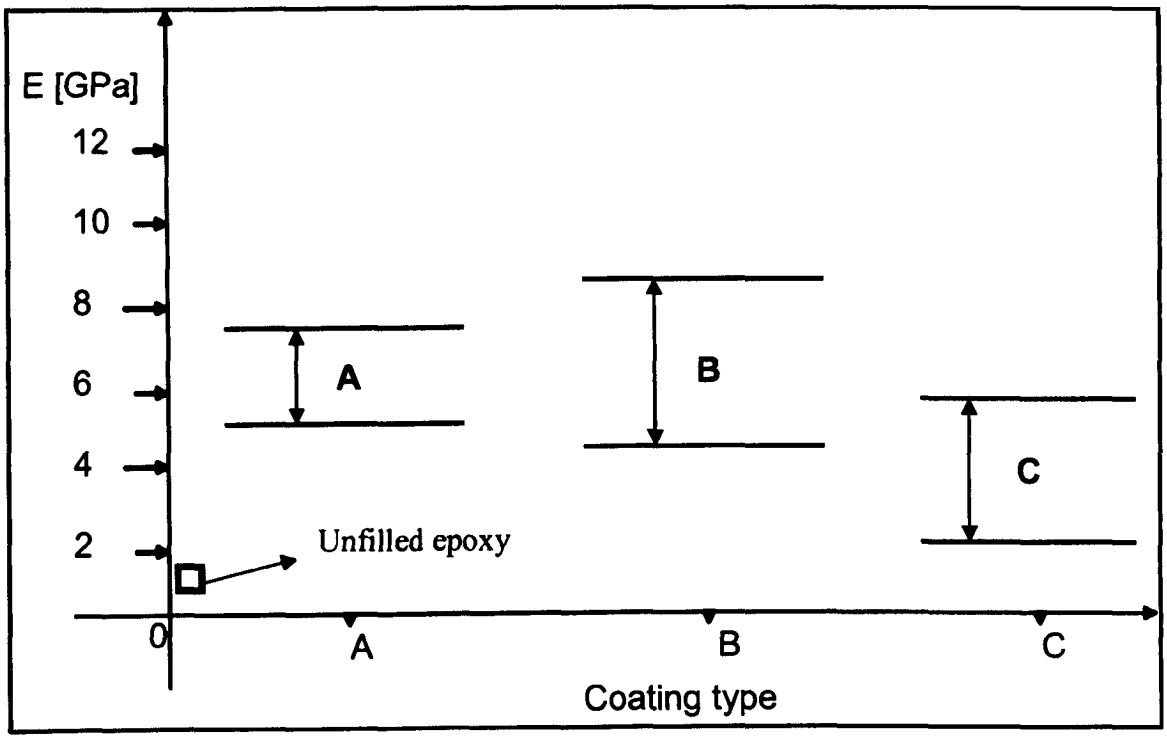

Figure 4.52. Minimum and maximum values for Young's modulus obtained from nanointendation; Unfilled epoxy data is literature value [40]

From the Figure 4.52. it can be seen that unfilled epoxy had Young's modulus about 0.9GPa whereas the experimental coating systems possessed average values of about 5-6GPa. Coating 'A' was established to be the hardest coating and showed most uniform values for elastic modulus, average about 6GPa. On the other hand, the softest coating 'C', exhibited the lowest level of elasticity when subjected to nanoindentation. Depending on the coating composition, Young's modulus varied even within the same coating type. Knowing that a small indentation area of 1μm will generate some variation in data values for this kind of heterogeneous coatings, these measurements were performed in order to illustrate the difference between each type and to show different performance of the chosen systems.

4.8. INTERNAL STRESS MEASUREMENTS

These measurements were made using coating deposition onto thin shims, on one side only. Film thickness meaurements were performed within 24 hours after air drying. The dry film thickness of each shim was calculated from the difference of the average sample thickness and the uncoated steel thickness. Those measurements are tabulated in Appendix 4.2.

Samples of all three coatings were cured for 5 days at 80°C and internal stresses were determined following the procedure described in Chapter 3.8. and using Equation 8 (see section 3.8.2.). Young's modulus values were provided by the coating manufacturer and those figures were obtained from free-films of coatings after curing for 1 week at 100°C. Appendix 4.3. shows values for Young's modulus and Poisson's ratio of the different coating types and the substrate. Although, the Young's moduli were measured by nanoindentation in this study, the obtained values were for the 'as-received' coatings. Taken that internal stresses were determined after curing, provided data from the manufacturer were obtained for the coating at 100°C and those values were chosen to be more suitable for calculations.

The most common statistical parameters were calculated in this study and they are: standard deviation, coefficient of variation and standard error.

Different lengths of the samples were used for these measurements as well as different thicknesses of the substrates. Results obtained from these experiments are given in the following sections.

4.8.1. 150mm LONG SAMPLES

The internal stress measurements were obtained for shims 150 mm length sprayed on one side with all three types of coating on different steel thicknesses 0.1mm, 0.2mm and 0.3mm. Each type of the epoxy coatings had three samples within one thickness range with the exception of coating 'A' type, where two shims were available with 0.1mm steel thickness and four for 0.2mm steel thickness. Coating thickness obtained for all substrate-coating combinations, radius and internal stresses, as well as standard deviations of the obtained values, were achieved. The results are summarised below. Tables with individual sample values for each coating and standard deviations are listed in Appendix 4.4.

Table 4.14. Internal stress in three different epoxy coatings obtained from shims 150mm length, after curing for 5 days at 80°C

Coating Type	**Internal Stress in the Coating, σ_c [MPa]**		
	Nominal Steel-Substrate Thickness [mm]		
	0.1	**0.2**	**0.3**
A	4.8	17.0	13.2
B	5.6	16.8	12.8
C	2.6	3.8	1.8

The assessment of the internal stresses within three different types of marine coatings for three different substrate thicknesses is summarised in Figure 4.53. It can be noted that all three coatings showed the lowest stress when applied to the thinnest substrate. Coating 'C' constantly displayed the smallest stress, regardless of steel thickness and this can be related to its greater relaxation. All three coating types demonstrated the highest internal stress when applied on medium thick substrate (0.2mm), but this may be a measurement error related to twisting of the 0.1mm substrate which was observed to occur and which probably decreased the radius of curvature recorded for

them. Remarkable agreement was observed between measurements made for coatings 'A' and 'B'.

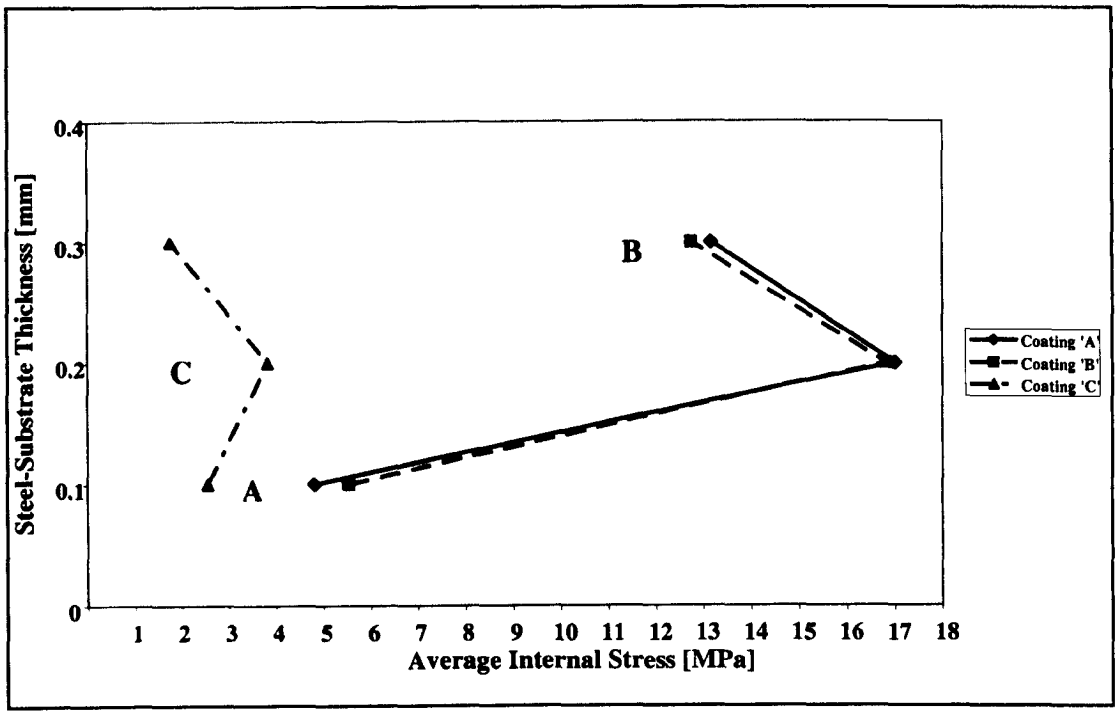

Figure 4.53. Average internal stress values for all three coatings, 150mm length shims; three different steel substrate thicknesses

There is significant influence of substrate thickness on internal stress development for these epoxy coatings and it is believed that 0.2mm substrate values are the most reliable because of the problem with the 0.1mm substrate twisting and because the thicker the substrate the less curvature is achievable making measurement less accurate. The highest stress results were observed for coating 'A'. Subsequent changes in stress within a coating were small (Appendix 4.4.). Coatings 'A' and 'B' achieved a very similar stress level for each substrate thickness and significantly higher than coating 'C'.

4.8.2. 250mm LONG SAMPLES

An identical temperature curing as for 150mm long samples was performed on a series of coatings deposited on shims 250mm length. Six samples were prepared for each coating. This time, the steel-substrate thickness was 0.3mm for every specimen. Standard application procedures were applied to all shims. Steel-substrates were cut into coupons 250x20mm and curvature measurements made on the finished samples were recorded.

After pre-treatment with PVB primer, coatings were applied on one side and cured for 2 days at 25°C (35°C for coal-tar epoxy, coating 'C'). Temperature curing was continued in a fan-oven for 5 days at 80°C. Radii of curvature of free to bend samples were measured within 24hours after temperature cycle and internal stress measurements were obtained. Data tables of coating thicknesses for each shim are given in Appendix 4.5. Internal stress calculations were carried out using Equation 8 and the values obtained are presented in Table 4.15.

As can be seen from table 4.15, coating 'C' showed the lowest average internal stress. However, standard deviation and errors (Appendix 4.5.) for coating 'C' shims were high due to the rather "twisted" than "curled" state of the samples after curing. As occurred for the 150mm shim length samples, coating 'A' displayed the highest stress throughout the examination.

Table 4.15. Internal stress in coatings A, B and C measured on shims 250 mm length and 0.3 mm steel thickness

Type of Coating	Shim Number	Internal Stress in the Coating σ_c [MPa]
Coating A	1	18.7
	2	21.6
	3	21.4
	4	25.2
	5	19.8
	6	16.4
	Average	***20.5***
Coating B	7	16.2
	8	17.5
	9	15.5
	10	17.2
	11	12.2
	12	17.2
	Average	***16.0***
Coating C	13	1.2
	14	1.0
	15	0
	16	2.6
	17	0
	18	2.3
	Average	***1.2***

Plotted results can be found in Figure 4.54. It can be noted that the primer has high cohesive strength, as well as the coatings, along with good adhesion to the steel. The permanent stress, in the coating and on the bond to the substrate, occurs due to those high cohesive strengths. Internal stress in the coating resulted from the restraint provided by the substrate, preventing shrinkage.

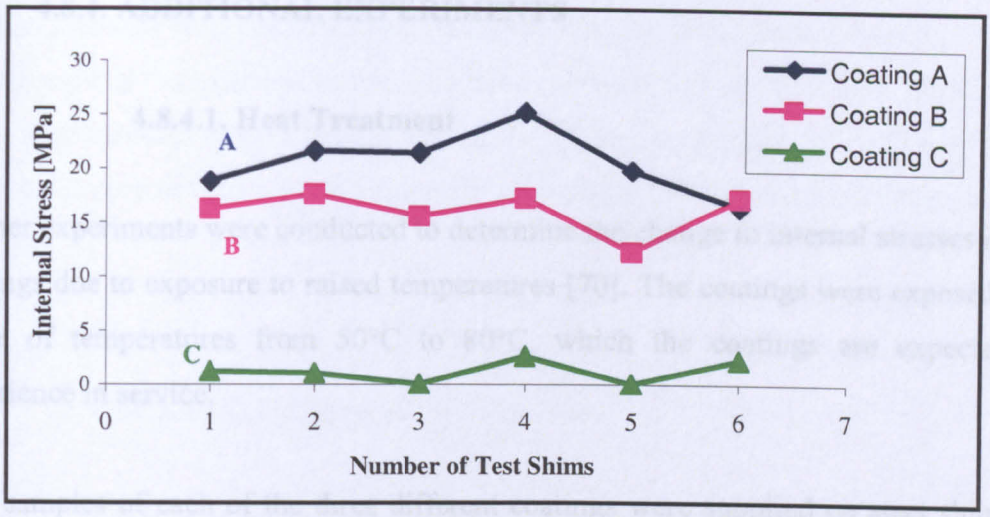

Figure 4.54. Internal stresses for 6 shims for each coating, 250mm length, 0.3mm steel thickness

Figure 4.54. shows that different coating compositions introduced different internal stresses. Coating 'A' showed highest internal stress of over 20MPa and coating 'C' provided the lowest internal stress of all three coatings. The values of the internal stress varied within the same coating type. The data for standard deviation can be found in Appendix 4.5.

4.8.3. SUMMARY OF THE INTERNAL STRESS MEASUREMENTS

Internal stress measurements obtained with different substrate thicknesses and lengths were significantly different. Thinner and longer shims gave results that reflect the coating properties more accurately and it can be suggest that the higher internal stress values are probably the most correct for each coating. Regardless of the substrate dimensions, coating 'A' showed the highest internal stress in every combination and coating 'C' always observed lowest. Coating 'B' gave slightly lower stress than coating 'A', but still relatively high range (up to 17MPa) than coating 'C' (up to 2.6MPa).

4.8.4. ADDITIONAL EXPERIMENTS

4.8.4.1. Heat Treatment

Further experiments were conducted to determine the change in internal stresses in the coatings due to exposure to raised temperatures [70]. The coatings were exposed to a range of temperatures from 50°C to 80°C, which the coatings are expected to experience in service.

Five samples of each of the three different coatings were supplied on steel shims of dimensions 250x20x0.3mm. The standard procedure for shim preparation and application of coatings was performed, as described earlier in section 3.8.

Coatings were applied on substrates 60 days prior to these experiments and were dried for 2 days at 25°C (35°C for coating 'C'). After initial drying, they were placed in a laboratory cupboard, where the coatings experienced natural drying for 58 days. The curvature of the samples was evident and radii were recorded. The measured radii of curvature of the specimens at this state are referred to as the 'zero radiuses'. This was the reference state for the sample and changes in curvature from this state were used to determine the changes in internal stress caused by bent treatment. Prior to any temperature treatment, samples were placed into a rack, which was composed of two aluminium blocks with grooves of 10mm width and 200mm depth cut into them, held together by two steel shafts. This holder was designed to minimise the effect of gravity so that bending was truly due to changes in the coating caused by temperature conditioning. The samples were placed in the oven sideways on.

The samples were treated at temperatures 50°C, 60°C, 70°C and 80°C. One sample of each coating was tested at all of these temperatures in step-wise series (reference sample) and the other four samples of each of these coatings were tested at only one temperature.

Internal stress measurements were obtained from measuring the curvature of the samples after each temperature cycle. One of each coating was left at 50°C for a period of 1hour and then only one shim of each coating was removed, cooled for 15

minutes and curvature was measured. Then the samples were placed back in the oven. This procedure was carried out at one hour intervals for the first four hours, once again after 24 hours at elevated temperature and then finally again after 72 hours. The full procedure was then repeated for each temperature, with 4 days intervals between the tests.

4.8.4.1.1. Coating 'A'

Figure 4.55. shows how the internal stress changed with time for coating 'A'. The results were obtained by subtracting the initial stress, calculated using the 'zero radius', prior to the heat treatment, from the value calculated directly from the curvature measured after heat treatment. The graph illustrates a general change in the internal stresses towards the tensile domain during heating.

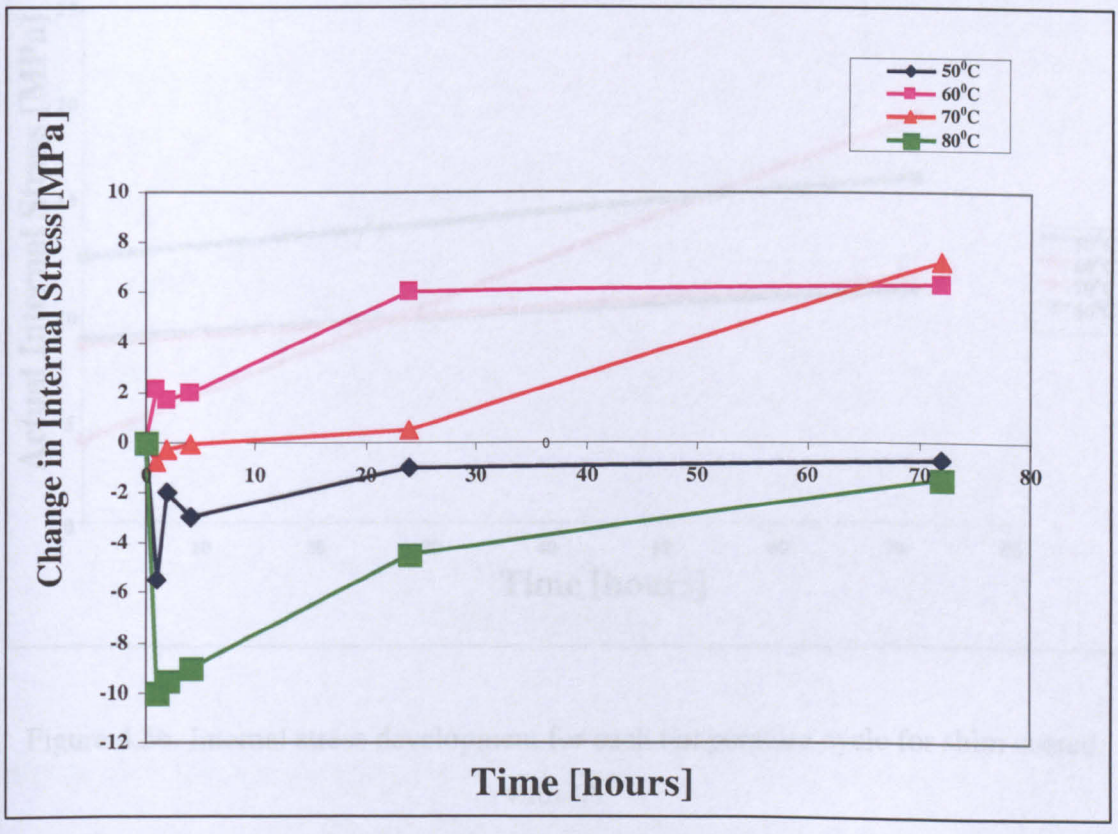

Figure 4.55. Changes of internal stress (measured at room temperature) after exposure at different temperatures for coating 'A' shims

The 'zero radius' measurements indicated that the coatings showed a wide range of internal stresses prior to heating. Although it was expected that the stresses in that initial state should be tensile, some samples had compressive stresses (the coating had apparently expanded as opposed to shrinking as expected). The samples were kept in a laboratory cupboard for 58 days prior to the temperature treatment and natural ageing of the coatings could be related to the presented compressive stresses. Another explanations for the compressive stresses obtained could be that after application of the coatings moisture from the atmosphere was absorbed during storage period.

Actual changes of internal stresses for reference samples, which were tested repeatedly at different temperatures (4 days interval between two temperature tests), are given below.

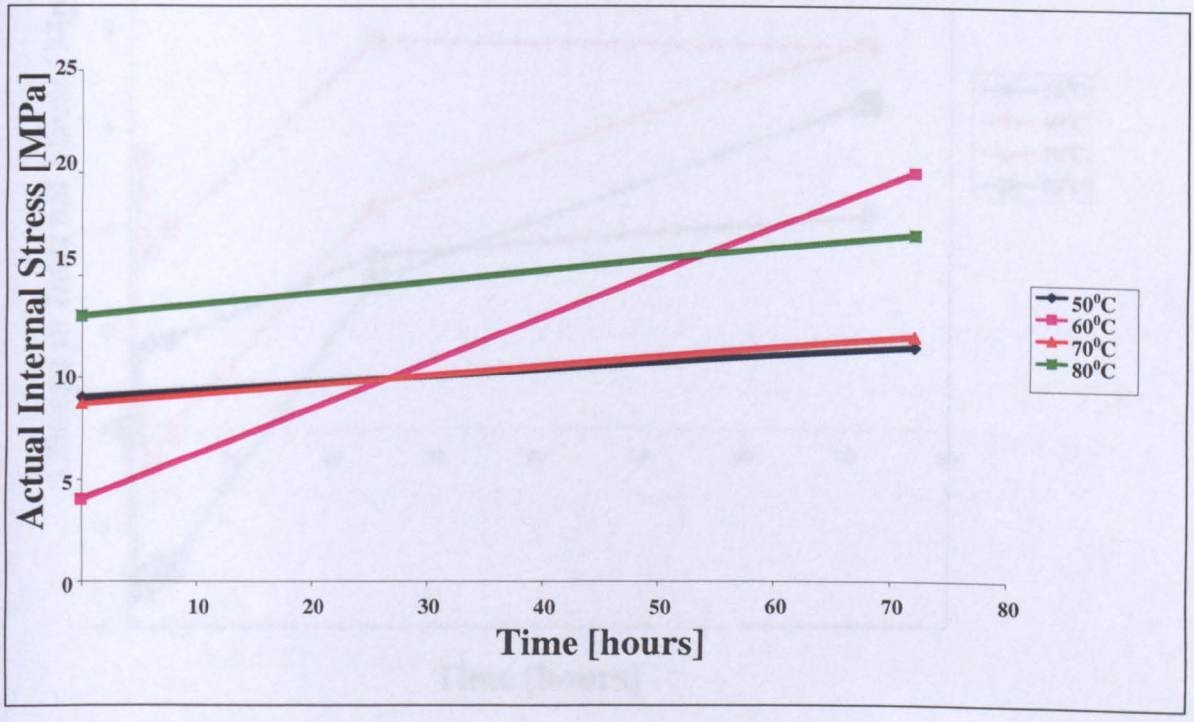

Figure 4.56. Internal stress development for each temperature cycle for shim coated with 'A'

Figure 4.56. indicates that changes in internal stress of the coating 'A' depended on the temperature. The thermal conditioning of the coating on every chosen temperature increased coating's internal stress. Highest temperature did not produce the highest internal stress in the coating.

4.8.4.1.2. Coating 'B'

The internal stress changes for coating 'B' with the respect to time are given in Figure 4.57., which shows that internal stress changes were towards the tensile domain.

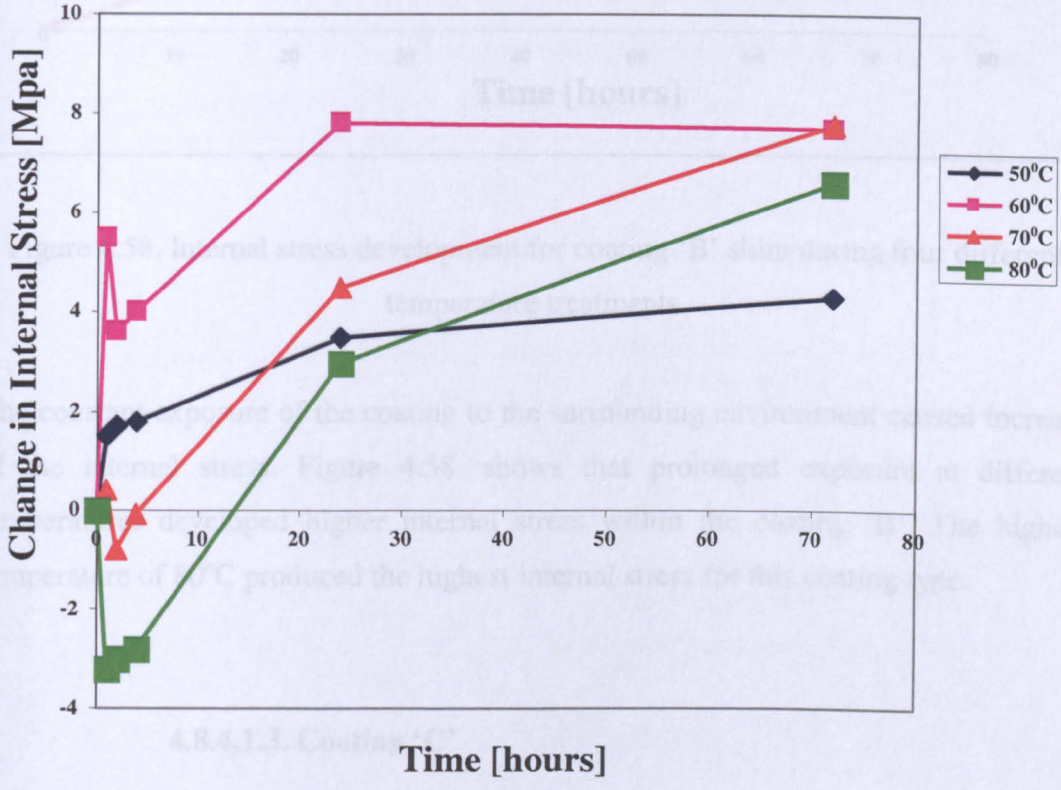

Figure 4.57. Changes of internal stress (measured at room temperature) after exposure at different temperature for coating 'B' shims

Actual changes of the reference sample for coating 'B' are presented in Figure 4.58.

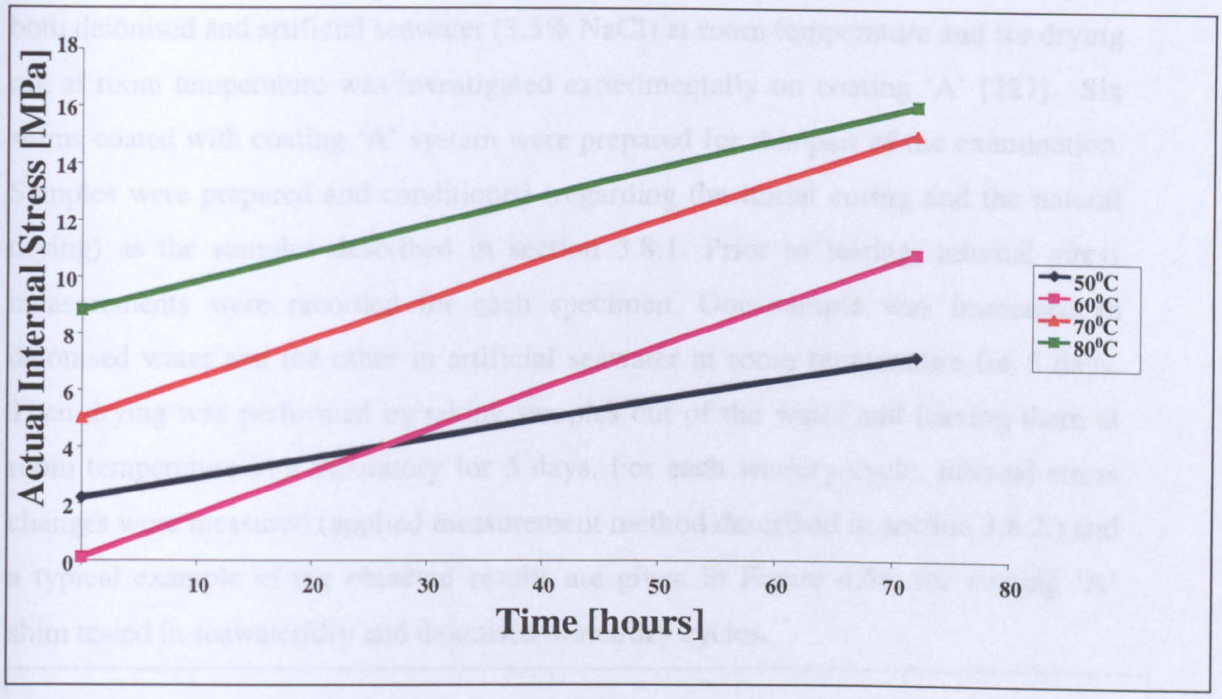

Figure 4.58. Internal stress development for coating 'B' shim during four different temperature treatments

The constant exposure of the coating to the surrounding environment caused increase of the internal stress. Figure 4.58. shows that prolonged exposure at different temperatures developed higher internal stress within the coating 'B'. The highest temperature of 80°C produced the highest internal stress for this coating type.

4.8.4.1.3. Coating 'C'

Changes measured for coating 'C' samples were very insignificant (in some cases any change was too small to be measured) and a full set of results could not be obtained.

4.8.3.2. Wet/dry treatment

The development of internal stress as a function of time during immersion in water, both deionised and artificial seawater (3.5% NaCl) at room temperature and for drying out at room temperature was investigated experimentally on coating 'A' [227]. Six shims coated with coating 'A' system were prepared for this part of the examination. Samples were prepared and conditioned (regarding the initial curing and the natural drying) as the samples described in section 3.8.1. Prior to testing, internal stress measurements were recorded for each specimen. One sample was immersed in deionised water and the other in artificial seawater at room temperature for 5 days. Then drying was performed by taking samples out of the water and leaving them at room temperature in a laboratory for 5 days. For each wet/dry cycle, internal stress changes were measured (applied measurement method described in section 3.8.2.) and a typical example of the obtained results are given in Figure 4.59. for coating 'A' shim tested in seawater/dry and deionised-water/dry cycles.

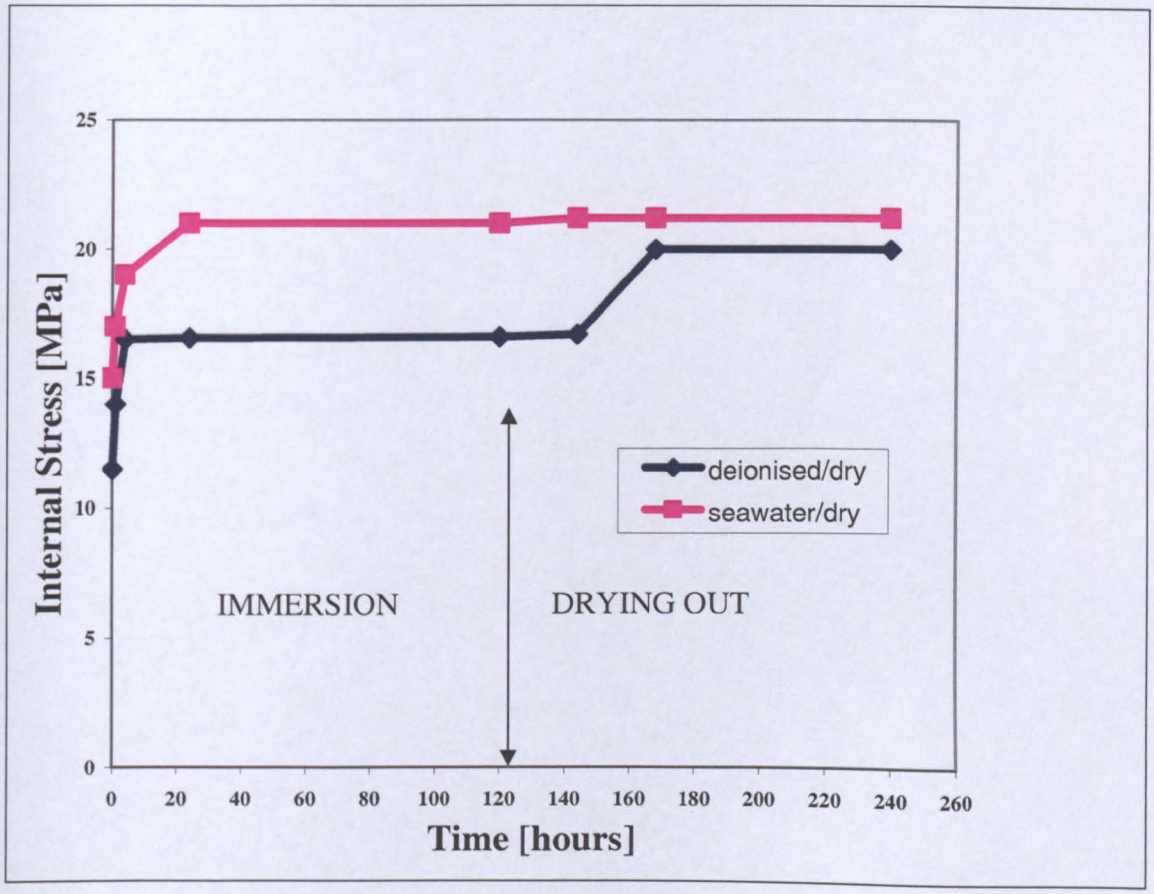

Figure 4.59. Internal stress development during one wet/dry cycle, coating 'A'

The presented Figure 4.59. shows that when coating 'A' was immersed in water additional tensile internal stress developed quite rapidly in the first few hours and then reached a stable state. At the beginning of the drying part of the cycle, the coating stress increased. Seawater soaking introduced significantly larger internal stress compared with the deionised water.

Measurements of internal stresses in three epoxy coatings performed in this study, have led to a greater understanding of the difference of each coating system. While the evolution of a coating from an as-applied liquid to a final solid is complex, the principle that stress in coatings is the consequence of the strain due to constrained shrinkage after solidification, has been indicated here.

*Tests Note: During each internal stress investigations, no evidence of cracking or delamination of the coatings was observed.

CHAPTER 5.

DISCUSSION

Up to now, limited research has been done on the fatigue behaviour of polymeric coatings. No data was found in the literature comparing a range of the marine coatings under fatigue loading. The approach that was taken in this study was to concentrate on coating performance in terms of the response to mechanical stress and environmental attack. Although the mechanical performance of a coating is rarely the sole criterion for an application, it is one of a group of properties which must be achieved and maintained at an acceptable level. The importance of mechanical properties may vary from being a key factor to being one of secondary consideration. Nevertheless, failure to resist some form of physical or mechanical abuse, which results in cracking or other coating damage and any subsequent loss of coating must always be regarded as a limiting performance parameter.

5.1. CYCLIC-LOADING TESTS

Cyclic-loading test rigs were designed and built to allow the various environmental experiments to be achieved. Cyclic-loading tests were performed in order to simulate the service conditions of marine coatings. The constant-amplitude stress-time pattern for this investigation was released tension. The fatigue testing of epoxy coatings, which was the main objective, revealed similarities between the fatigue response of the polymers and metals. Generally, fatigue failure in metals is a process of crack initiation, propagation and failure. Also, fatigue damage in metals is cumulative and cycle dependant, but remains essentially independent of test frequency. Unlike that of many metals, the fatigue behaviour of polymers is also influenced by viscoelastic effects [215].

Test frequency was one of the factors that could influence coatings performance. If the test frequency is high, softening and melting of the polymer could occur and fatigue failure would then depend largely upon frequency. At lower frequency, fatigue failure becomes less sensitive to test frequency and results from crack initiation and propagation. Knowing that, the test frequency for the performed cyclic-loading tests was chosen to be low (0.05-0.5Hz), similar to the average sea-wave frequency under service conditions for ballast tanks (see section 3.5.1.). The importance of the test frequency was extinguished given that the cracking polymer characteristic arises from

the production of hysteresis energy during cycling-loading procedures. A portion of this energy is released as heat, some of which is dissipated, but most is absorbed in the substrate, because of the small thickness of the coatings relative to the substrate thickness. If the temperature did rise in the coating, it would have led to degradation of the material and a shorter fatigue life.

When 'as-received' samples were subjected to fatigue tests, the changes that were observed on all three coating types were some form of surface degradation. Solvent evaporation at this stage of the coating life probably caused those changes. Visible appearance of fatigue damage was observed when marine coatings were tested after 'post-curing'. Cracks were recorded firstly under the rollers of the test jig and then coating 'B' showed cracks on the surface after just over 300k cycles when tested at room temperature.

From the results of the cyclic-loading analysis, it is noticeable that the degree of ageing of coating materials strongly influences the fatigue performance of the coating systems. Due to the large extensibility of the unaged coatings compared with the steel-substrate, the coatings did not accumulate plastic strain on the surface during the cyclic-loading. Surface modifications of the coatings were observed, but the experimental marine coatings were resistant to fatigue failure when tested in the 'as-received' condition. However, the fatigue resistance of cured samples showed an increase in cracking behaviour when tested under the same conditions as unaged samples. Ageing of coatings has been shown to be a strong contributing source of embrittlement of coatings, resulting in failure of ballast tank coatings before the expected service life is reached, mainly in stress-concentration locations. Some researchers showed that the failure characteristics of ballast tank coatings depended on the degree of ageing [52]. In their study it was shown that a high degree of ageing was more detrimental than a low degree of ageing. The investigations presented in this thesis demonstrated that a low degree of coating ageing (e.g. 'post-curing') produced more cracking, whereas high ageing cycles made coatings more resistant to fatigue. Under the conditions applied in the tests described above, which included a combination of low frequency and relatively low strain levels (the strain had to be low to prevent the substrate yielding) and using flat/smooth mild-steel substrates that did not provide stress concentrations, fatigue cracking resistance was very good. This was

true for all of the test environments and with coatings typically three times thicker than standard, which is expected to heighten vulnerability to cracking. Therefore, the coatings appeared to have good fatigue resistance. The cyclic-loading experiments presented here used tests with low strain-rate. In service conditions, the strain-rate might be locally higher. Raised strain-rate or cyclic-loading is expected to affect the material characteristics in the same way as ageing does, i.e. decreased fracture strain, increased stiffness, brittle material failure [32, 52]. However, the results obtained in a form of cracking for coatings 'A' and 'B', lower the ability of the coatings to be resistant to fracture from harsher environments. In service, damage may therefore be more significant.

Experiments carried out in this study showed that there was no significant change when testing at a lower test temperature, 5°C, even though an influence on the epoxies failure performance due to temperature changes has been observed by some researchers [216-218]. As a result, these authors concluded that longer exposure of the samples to higher temperatures caused ductile breaks in epoxy composites. In their study, it was observed that seawater temperature had a significant effect on the performance of epoxy coatings. If the higher temperature caused ductile breaks on epoxy composites then higher sea water temperature proved to cause more coating deformation. For epoxy marine coatings monitored throughout this investigation, sea-water exposure during cyclic-loading proved to provide more changes of the samples at room temperature (coatings 'A' and 'B' formed under-rollers cracks for 'post-cured' samples). In the 'post-cured' condition only coating 'B' sample developed cracks under the rollers when tested in seawater at 5°C. None of the 'as-received' coatings produced tensile surface changes after tests in seawater at the lower temperature. For epoxy coatings in laboratory test conditions, exposure to seawater will have decreased solvent loss and improved heat dissipation. It may be noted that coating 'A' has approximately 10% more solvent than coating 'B' when applied (see Table 3.1.) and is likely to retain more solvent and hence be more ductile. The decreased solvent loss during seawater tests is contrary to hypothesis that was given by some authors [211].

The coating thickness is an important parameter when a coating is exposed to seawater. Very thin coal tar epoxy coatings (below 40 μm) in seawater, according to

Rowlands and Chuter [226] showed a high capacitance and low electrical resistance after only a few days immersion, whilst coating layers 200-300 μm thick kept a high electrical resistance even after one year's exposure. Therefore, it would be reasonable to expect that if a thicker coating is applied on the substrate, the coating will provide a high resistance to the testing environment. This can be explained by the inhomogeneous nature of polymer films and the effect on ionic resistance. Marine coatings investigated in this research had thicknesses 3x that of the standard recommendation, so that total coating thickness was approximately 800μm (varies for different coating types; see section 3.3.1.) and they indeed showed high performance when fatigue tested in seawater. In service, thinner layers will be more susceptible to deterioration.

5.2. SLOT DEFECTS

Dealing with the fatigue of polymers, some researchers [219] obtained fracture behaviour in unnotched specimens. Usually fatigue crack growth has been studied using a fracture mechanics approach. From the micro-mechanics point of view, the fatigue failure of polymeric coatings results from development of initial defects such as micro-voids and/or micro-cracks [219]. In this study, a similar approach was used. Unnotched and notched samples were tested. Only coating 'B' showed fatigue cracks when unnotched coatings were examined. As notch defects are one of the commonly used tools for describing the effects of stress level and flaw size on the fatigue crack propagation behaviour of materials, the new tool was used in this research. This is based on the stress intensity factor as the crack driving force. However, there exists difficulty in using this fracture mechanics criterion for studying the fatigue crack propagation behaviour of most polymeric materials due to their viscoelasticity and in our case, because of the substrate presence. Various models have been proposed to describe the fatigue crack propagation of materials under cyclic-loading [220]. These models have employed mechanistic approaches which are based on the concept of fracture mechanics. The stress or strain of the crack was considered and in some cases, the failure criteria were also included. The effect of machined slots on the coating surfaces was investigated in this research. Coating 'B' proved to be most prone to cracking during these experiments. The results lead to the conclusion that the

crack initiation and growth were not dependent on the length or depth of the inserted slots. From an inspection perspective, the conditions that led to initiation of a crack were important. Unnotched coatings showed high resistance to fatigue and if crack initiation does not occur when a potentially damaging event occurs (e.g. impact of a hard object on the coating), it is unlikely to form later in service. The analysis of coating 'B' showed the failure (cracking) had three distinct phases:

- initiation,
- stable growth and
- edge effect (slower growth).

Initiation refers to the formation of a crack in response to the mechanical damage process. Stable phase refers to the transition of a crack running inside the slot to emerge as a horizontal crack beyond the slot and its continued growth through the coating.

The microstructure of the coating plays a dominant role in many aspects of crack growth as the coating is inhomogeneous, distorting the stress field so cracks are not perfectly linear. The cracks grow in each test cycle and the stress field around the slot ends generate only one crack for each slot end.

The results obtained during cyclic-loading tests showed that coating 'C' had the highest resistance to cyclic-loading, whereas coating 'B' showed the most cracking. It may be noted that the experimental approach enabled a relative ranking of the coatings to be made. The higher ductility of the coal tar epoxy material and the absence of fillers that might act as stress raisers are believed to be responsible for these observations.

5.3. MECHANICAL PROPERTIES

5.3.1. TESTS ON FREE-FILMS

Throughout this research effort was put into determining more fundamental material properties of the coatings. This required the preparation of 'free-films' of the coatings. 'Free-films' were prepared by an applying the coating systems to a low energy surface (in this case, glass) to prevent solvent, water or any other volatile products forming voids in the coatings. Once the difficulties of specimen preparation were overcome, a range of material property measurements and characterisation techniques were applied. The experiments performed on 'free-films' (see section 4.6) measured the strain-to-failure of the free-film to investigate whether the coatings on a substrate will fail when the surface strain reaches the critical film strain.

Samples of each coating were tested in two conditions, 'as-received' and 'post-cured' state. While higher failure stresses were obtained for 'post-cured' coatings, it was noticeable that strain-to-failure for all three coating types was considerably smaller than when the coatings were tested in the initial condition. After the curing procedure the coatings were solvent-free and it was noticeable that coatings became less flexible in this stage. Again, as for the cyclic-loading tests, 'B' showed the least strain-to-failure, 0.5%, after post-curing. Investigations were also made regarding the effect of sample size during these tensile tests, for both conditions of the prepared samples. It was confirmed that the performance of the coatings was not significantly affected by changes of the specimen widths.

5.3.2. TESTS ON PANELS

Knowing that the 'free-film' experiments do not account for substrate effects on the coating, such as adhesion effects or internal stresses, this research obtained measurements for some properties of steel-coated samples. Stress-strain properties were measured by deformation of the samples at constant strain rate and the resultant stress was measured by load cell. Since the strain rate and temperature were constant and similar for all coating types, the dependence of the formed cracking behaviour was highly influenced by the structure of coatings. The strain to crack observation for coating 'A' was 1.3%, and was 1.7% and 23% for coatings 'B' and 'C', respectively. Coating 'C' showed the highest resistance during these tests, whereas coating 'B' with multiple cracks showed the smallest resistance. The difference between the coating materials agrees with the generally more brittle nature of coating 'B' and arises from the difference in coating internal stress in comparison with that found for the other coatings. Exposure to de-ionised water did not affect the cracking behaviour of the coating systems.

One of the important mechanical properties of the marine coatings is to withstand applied stresses during service and to fulfil that they must be designed to ensure that only elastic deformation will result when a stress is applied. It is therefore desirable to know the stress level at which plastic deformation begins, or when the phenomenon of yielding occurs. For better recognition of the results, it is important to distinguish between the nominal stress, which is the load at any time during deformation divided by the initial cross-sectional area, and the true stress, which is the load divided by the actual cross-section at any time. The cross-section of the sample decreases with increased extension, so the true stress may be increasing when the apparent stress remains constant. This has been discussed thoroughly by Nadai [221].

For the tensile tests that were performed in this study, presented stress levels in Chapter 4 were nominal stresses and as such will be lower than the true stresses.

Yield stress may be defined most simply as the minimum stress at which permanent strain is produced in the material after the stress is removed. This deformation (which

defines elastic recoverable definition and plastic irrecoverable deformation) has a clear definition for metals. That distinction is not so straightforward for polymers. Orientation of the polymer molecules during tensile testing significantly alters the polymer mechanical behaviour as the test proceeds. As the coating elongates, the polymer molecules orient and the coating becomes stronger and more rigid. The tensile stress will begin to rise with further extension and may exceed the yield stress. While all three epoxy coatings 'yield', they may not exhibit the classical 'yield point' (the point at which there is a zero slope). They exhibit 'pseudo-yield', that is, they deviate significantly from linear behaviour, but their stress continues to rise with increased strain.

5.4. INTERNAL STRESS MEASUREMENTS

Measurements of internal stresses in the three epoxy coatings were performed in this study. While the evolution of a coating from an as-applied liquid to a final solid is complex, the principle that stress in coatings is the consequence of the strain due to constrained shrinkage after solidification, has proven here a solid concept for cured coatings.

During the formation of the coating its volume decreases due to curing and solvent evaporation. Subsequent to curing, the length of the covalent bonds being formed is less than the distance between the neighbouring molecules prior to their reaction. In the early stages of solvent evaporation and/or cross-linking, the coating is above its T_g, and the polymer chains have sufficient mobility to allow for shrinkage. However, as film formation via solvent evaporation or continual cross-linking proceeds, the T_g continues to rise, the polymer chains have reduced mobility and internal stress results from the coating's inability to undergo further shrinkage. When the coating shrinks, this is actually a form of stress relaxation, and the stress or internal energy has been dissipated. Because the formation of adhesive bonds occurs more rapidly than solvent evaporation and curing, internal stress develops in the coating. As seen from the curing tests at 80°C (see sections 4.8.1. and 4.8.2.), when samples were analysed right after coatings application, internal stress development bends the steel substrate in the direction of the coating.

Another possible response to internal stress occurs if the substrate is another coating, such as a primer. Although a range of different zero radius in both directions were observed, after coating application (with primer) and curing process, the radius of all shims were more or less uniform for each type of coating. It may be noted that the primer and coatings have high cohesive strength, along with good adhesion to the steel. The permanent stress, in the coating and on the bond to the substrate, occurs due to the high cohesive strengths.

The influence of different dimensions of the substrates on the internal stresses was monitored. When the coating was applied on a thinner substrate, tensile stresses in all coatings were smaller than when applied on a thicker steel substrate. The final stresses developed in the coating systems on different substrate thicknesses and lengths, always showed coating 'C' with the smallest internal stress. Coatings 'A' and 'B' were similar to one another and gave much higher stresses then coating 'C'. From these results it can be deduced that when these three marine epoxy coatings are in service, no matter what the substrate thicknesses, coating 'C' would be expected to produce the smallest internal stresses, while the stresses in 'A' and 'B' are likely to be of the order of 5x larger than for coating 'C'.

While cured at different temperatures (50°C to 80°C), some samples demonstrated stress changes towards the compressive domain, which could be the result of relaxation of stress within the coating and although it moves in the compressive direction, the mean stress remains tensile. The heating process appeared to cause internal stresses in the coatings, to converge towards an increased tensile value after prolonged exposure. Actual stress development started only from shrinkage after solidification and increased due to further curing. Little stress developed in the early stages of drying (50°C) because the coatings were not yet solidified; the modulus was low and stress relaxation was relatively fast. With further drying, the coating solidified and the measured stress climbed as more solvent was lost (strain increased). In addition, the modulus of the coating grew. The stress rate fell (60°C) as the solvent became depleted and the process became limited by diffusion of solvent through the coating. Even after the stress had fallen off significantly, it continued to accumulate in the coating, because even a tiny amount of shrinkage leads to strain. Due to the

relatively high modulus of the coating at the end of heat treatment (70°C and 80°C), the small strain results in a noticeable increase in stress.

The variation of the internal stress was observed as a function of time during immersion in water (deionised and artificial seawater). Tensile stresses developed quite rapidly when coatings were immersed in water and then reached a stable stage. It is interesting that the increase of the internal stress stops after a short time of exposure to water. Swelling by water causes an expansive internal stress, until the equilibrium state is reached. On subsequent drying, internal stress develops again, which was higher than the initial stress. The increasing of internal stress may be explained by the extraction of water-soluble coating material which causes an additional shrinkage of the system. There was a significant change in the coatings performance when immersed in deionised or artificial seawater. Water may plasticize the coating, assisting this process and also assisting the escape of any residual solvent. Another possible explanation is that plasticization by water accelerates physical aging, giving a volumetric reduction (and tensile stress when constrained by the substrate) and an increase in Young's modulus.

It is desirable that the level of internal stresses can be predicted for a coating system during a service period. To achieve that it will be necessary to know the detailed service dynamic that can influence the development of internal stresses in the coatings as well as the relaxation behaviour of the coatings. Most of the components in ballast tank coatings are chosen for reasons unconnected to the development of internal stress and it is therefore of significant importance that the internal stress was found to be sensitive to the combination of the substrate dimensions, surrounding environment and coating composition.

5.5. SUMMARY

Contrary to Nielsen [222] and Sauer and Richardson [223] who mentioned that monitoring of the mechanical properties during fatigue does not appear to be a promising method for filled polymers, this research gives hope that, for some filled epoxies, i.e. marine coatings, it could nevertheless be possible.

Comparison of some measured mechanical properties for marine coatings can be useful for identification of the best coating system. The data presented in Tables 5.1. and 5.2. provide information of the summarised results for each coating when observed for different coating conditions. As ranking of the three epoxy coatings was one of the aims in this research, it should be recognised that the concept presented here, can provide relative ranking of the ballast tanks coatings.

Table 5.1. Summary of measured mechanical properties of the 'as-received' coatings

Coating Type	**Fracture Stress, tensile tests, [MPa]**	**Young's Modulus [GPa]**	**Hardness [MPa]**	**Fracture Tensile Strain [%]**	**Fracture Strain of Notched Samples [%]**
A	~2.5	6.7	39.2	1.5	1.3
B	~1.5	7.1	43.1	<1	1.7
C	~1	3.9	9.81	5	23

Table 5.2. Summary of measured mechanical properties of 'post-cured' coatings

Coating Type	Fracture Stress, tensile tests, [MPa]	Young's Modulus [GPa] *	Hardness [MPa]	Fracture Tensile Strain [%]	Internal Stress [MPa]	Fracture Strain of Shim-Coating [%]
A	25	4.8	323.6	0.7	25	1
B	25	4.7	196.3	0.4	15	0.5
C	23	6.1	19.61	1.5	13	2

* Data from coating supplier

Tables 5.1. and 5.2. show that all three coatings are significantly harder after curing and that coating 'C' retains the most ductility. The results from the range of test methods applied are complementary. Considering the tensile strains at fracture and fracture strain values, coating 'B' was the least ductile material after curing and this correlates with fatigue data reported earlier describing multiple fatigue crack development.

The composition and mechanical properties of the investigated inhomogeneous coatings had a big impact on their performance during cyclic-loading. This research showed that it is possible to measure more properties of the coating via nanoindentation than just hardness. Young's modulus, for instance, was obtained from those measurements. Young's modulus varies from point to point, when achieved during this test on polymer coatings (see Appendix 4.6.). Some researchers indicated that the inhomogeneities of the coatings are more important in the 'growing' direction (from substrate to the coating surface). As such, Young's modulus should be almost constant for each indent if the measurements can be obtained at the cross-section. In order to avoid any deviant point during measurements on the coating surface, average values should be considered as the most adequate. Figure 4.52. showed minimum and maximum values for Young's modulus which were obtained over the whole loading curve during nanoindentation. The first 50nm measurements were not taken into

consideration to avoid artefacts linked to surface detection. Average Young's modulus for coating 'A' was 6.7GPa, for coating 'B', 7.1GPa and 3.9GPa for coating 'C' (Appendix 4.10.; obtained data for 'as-received' coatings).

It is easy to calculate the ratio H/E from the hardness (H) and Young's modulus (E). This quantity can be used to assess the wear resistance of coatings. This can be an important factor for the prediction of coating life, along with the use of hardness alone. Its advantage is that it takes into consideration Young's modulus' independence to hardness that appears for example in some composite materials. When materials having similar hardness, as with 'as-received' coatings 'A' and 'B', the best wear resistance should be observed when Young's modulus is lower and thus when the H/E ratio was higher [224, 225]. H/E for coating 'A' in 'as-received' condition is 0.0058 and 0.006 for the coating 'B'. The small difference between H/E ratios did not produce different performance between these two coating types when fatigue tested in this condition. Both coatings experienced surface changes and cracking was not observed. As can be seen in Table 5.2, Young's modulus for each coating was significantly lower after heat treatment (e.g. 'post-curing'). The H/E ratio changes, 0.07 for coating 'A' and 0.04 for coating 'B'. This lower H/E ratio, e.g. wear resistance, for coating 'B', complements the observed fatigue data, where this coating showed cracking. Lower H/E for coating 'C' (0.0025 for 'as-received' and 0.0032 for 'post-cured' condition), in comparison with the other coating systems, corresponded to the coating 'C' high fatigue resistance.

From the results presented in Tables 5.1. and 5.2., it is reported that the degree of ageing of the coating strongly influences fatigue response. Due to the relatively large fracture stresses for the 'post-cured' coatings compared with the 'as-received' fracture stresses, the coatings exhibited more cracking. An interesting finding for polymeric coatings is that, depending on the structure of the polymer and the mechanism of deformation, there are two distinct responses to an increase in stress. Some polymers exhibit an increase in crack propagation rate, while others show a decrease in crack growth rate. A literature value for fracture stress for ballast tank coating is 7.68 MPa for unaged and 18.03MPa for the aged coating [32], which agrees with the data obtained in this research, where fracture stresses were significantly lower that the ones

observed after the curing procedure. In the present study, fairly small stresses were needed for the coatings the fracture in the unaged condition and showed that after fatigue tests, the top layer of the coating surfaces were changed by some form of degradation.

The results from the 'post-cured' coatings showed a remarkable decrease in fracture strain, more than for the 'as-received' coatings. It can be assured that ageing of the coatings was a source of weakening of the coatings behaviour during the fatigue test, resulting in failure of ballast tank coatings before reaching the expected service life.

The overall results indicated that the coating identified as 'C' in the test programme exhibited the best and coating 'B' the worst behaviour in terms of fatigue resistance under laboratory conditions. Consequently, the ranking list, as deduced from the data, is as follows:

BEST.....WORST

'C'.....'A'.....'B'

(Coal-tar) (Al filler) (Barytes filler)

Although, this research investigated three quite different coatings, the range of manufactured epoxies is large. The data produced demonstrates that a relative ranking of coatings can be achieved regardless of their composition, using an accelerated test method.

CHAPTER 6.

CONCLUSIONS AND RECOMMENDATIONS FOR FUTURE WORK

6.1. CONCLUSIONS

The outcome of the study shows that the resistance to failure of epoxy ballast tank coatings before reached expected service life in strained and stress-concentrated locations can be determined. Exposure of three different epoxy coatings to fatigue test accelerates comparable, but different, failure. Tests were carried out in air, seawater at room temperature and seawater at 5°C. The investigations of the 'as-received' samples indicated that surface changes of the coatings occur during fatigue tests. All three types of coating showed changes on the surface after significant number of test cycles (average number of the test cycles needed for surface changes was 100,000). Main characteristics of the fatigue test for 'post-cured' samples was development of fatigue cracks for coating 'B' and detection of the under-loading points cracks for coatings 'A' and 'B'. The fatigue resistance of the experimental marine coating type 'C' was high. After the ageing procedure the panels showed high fatigue resistance during the tests.

A test procedure was developed that ranked coatings according to their resistance to cyclic-loading. Insights into coating failure mechanisms and the influence of artefacts such as slots were proved to be suitable for the evaluation of the fatigue behaviour of marine coatings. A method for initiation of cracks and monitoring of fatigue crack growth was developed that helped the comparison of the coating types. Machined-in slots were found to initiate fatigue cracking and for coating 'A', slots of different lengths and depths showed similar behaviour under cyclic-loading. Crack initiation was recorded in the root of each slot, but crack growth was not observed beyond the end of the slots. Coating 'B' showed crack growth beyond the machined slots.

Under these low strain, high cycle, fatigue conditions crack initiation is a considerable portion of the coating life time. The behaviour is similar to that observed for metals and other materials.

Furthermore, an accelerated ageing procedure has been developed along with methods of monitoring the mechanical properties of coatings. Micro-hardness measurements made during the ageing process showed that fatigue behaviour correlated with the

coating hardness. The coating with the lowest Young's modulus and lowest hardness had the greatest fatigue resistance.

Tensile tests on free-films indicated that the coating most resistant to fatigue showed the lowest tensile strength and the highest strain to failure.

Internal stress measurements showed the coating which was most resistant to fatigue (coating 'C') had the lowest internal stress. It is possible that comparing the internal stress of different coatings, could provide a relative ranking of them, but more substrate-coating combinations need to be tested before this can be established as a general rule.

This investigation brings about some novelty to the method of comparison of the coating performances as it has been the first attempt to evaluate and rank the performance of ballast tank coatings under cyclic-loading conditions. Accelerated laboratory tests incorporating the impact of cyclic stress on coating life will certainly be valuable in terms of comparison of marine coatings.

In this Chapter the key findings which may be drawn as a result of the current investigation have been pointed out. In addition, the next section of the Chapter is dedicated to potential followers and contains recommendations for future work.

6.2. RECOMMENDATIONS FOR FUTURE WORK

Three experimental epoxy marine coatings, sprayed in 3x standard thickness over mild-steel substrates, were fatigue tested in this research. Extended monitoring of the coating-layers performance and coating-substrate interface would help to achieve better understanding of coating behaviour during fatigue. Also, testing of a single layer coating during fatigue would bring some new observations.

Introduction of alternative substrates (in addition to mild steel or Perspex) would be useful to consider. More flexible substrates would allow testing of the coatings at the higher strain levels.

The present work developed test procedures to determine the relative ranking of marine coatings of different compositions in three chosen marine environments. As a step towards understanding coating behaviour in different environments, experiments could be arranged to investigate the effect of combinations of testing environments, e.g. the same sample to be tested in air and then in simulated seawater.

It is likely that filler particles influence the coating performance and it would be informative to prepare two batches of an epoxy, with and without filler, to assess the filler effect.

A method of slot introduction was tried in this study, further development of that procedure could be achievable (for example, observing how slots position effect on cracking).

The estimation of life-time prediction of the selected coatings and mathematical modelling of crack growth after fatigue tests could be considered as a future task.

Fatigue tests of welded and corner substrates with applied coatings would be beneficial for better understanding of ballast tank structure and service behaviour.

The developed ageing procedure gives a good platform for the determination and monitoring of mechanical properties. Information of any changes of the coating mechanical properties during ageing would be considered useful.

References

[1] G D Mills and J Eliasson, *Future Cargo and Ballast Tank Lining for Ship Tanks-Forward Looking Technology,* SSPC, New Orleans, USA, 2005.

[2] J Azevado, *A new approach for steel structures protection using UHP hydroblasting and a solvent-free and humidity tolerant epoxy system with edge-retentive properties*, EUROCORR 2005 The European Federation of Corrosion Conference, Lisbon, Portugal, September 2005.

[3] E D Thomas, A A Webb, *World Class Tank Coating Materials, Practices, Procedures*, in: SSPC2000 Industrial Protective Coatings Seminar, Nashville, Tennessee, USA, November 2000.

[4] J P Quintela, A T M Silva and P B Leite, *Ecological Paint Systems – The Petrobras View*, Corrosao e Proteccao de Materiais, Vol. 21 (3), Jul/Aug/Sept 2002.

[5] A A Webb and B Brinckerhoff, *Reducing Navy Fleet Maintenance Costs with High Solids Coating and Plural Component Spray Equipment,* The Journal of Protective Coatings and Linings, March 2003.

[6] A Lodhi, *Double Hull Tankers Ballast Tank Maintenance – Experience Feed-Back*, The 22nd DNV Technical Committee Meeting, Dubai, report, 7th December 2005.

[7] P Le Calve, P Meunier, J M Lacam, *Evaluation of Reference Paint Systems after UHP Water Jetting*, Protective Coatings Europe, Vol.8, Number 1, January 2003.

[8] J Eliasson, *Coating Ballast and Cargo Tanks on Ships: a Status Report,* Journal of Protective Coatings and Linings, July 2005.

[9] P Meunier, *The Experience of SNCF in Preparing Previously Painted Metal Surfaces by UHP Water Jetting*, Protective Coatings Europe, Vol.3, Number 9, September 1998.

[10] INTERTANKO, *Crude Oil Tanker Cargo Tank Corrosion – Update*, report, Cardiff, UK, 24th October 2002.

[11] H Petershagen, *Fatigue Problems in Ship Structures,* Advances in Marine Structures, Elsevier Applied Science, pp 281-304, London, UK, 1986.

[12] A Malakhoff, W T Packard, A H Engle and R A Sielski, *Towards Rational Surface Ship Structural Design Criteria,* Advances in Marine Structures-2, Elsevier Applied Science, pp 495-528, London, UK, 1991.

[13] S C Hollister, J Garcia and T R Cuykendall, *Fatigue Tests of Ship Welds,* SSC-7, Ship Structure Committee, Washington D.C., USA, 1946.

[14] S C Hollister, J Garcia and T R Cuykendall, *Final Report on Fatigue Tests of Ship Welds,* SCC-14, Ship Structure Committee, Washington D.C., USA, 1948.

[15] J W Fisher, K H Frank, M A Hirt and B M McNamee, *Effect of Weldemnts on the Fatigue Strength of Steel Beams,* National Cooperative Highway Research Program (NCHRP) Report 102, Highway Research Board, Washington D.C., 1970.

[16] J W Fisher, P A Albrecht, B T Yen, D J Klingerman and B M McNamee, *Fatigue Strength of Steel Beams with Welded Stiffeners and Attachments,* National Cooperative Highway Research Program (NCHRP) Report 147, Transportation Research Board, Washington D.C., USA, 1974.

[17] E Signes, R G Baker, J D Harrison and F M Burdokin, *Factors Affecting the Fatigue Strength of Welded High Strength Steels,* Report M/11/66 of the British Welding Research Association, British Welding Journal, pp 108-116, March 1967.

[18] T R Gurney and S J Maddox, *A Re-Analysis of Fatigue Data for Welded Joints in Steel,* Welding Research Institute, Abington Hall, Abington, Cambridge, UK, 1971.

[19] S J Maddox, *Some Aspects of the Influence of Residual Stresses on the Fatigue Behaviour of Fillet Welded Joints in Steel,* Report 123/1980, The Welding Institute, Abington Hall, Abington, Cambridge, UK, 1980.

[20] AASHTO, *Standard Specification for Highway Bridges, 14th ed.*, The American Association of State Highway Transportation Officials, Washington D.C., 1989.

[21] British Standard Institute, BS5400, *Steel, Concrete and Composite Bridges, Part 10, Code of Practise for Fatigue*, 1980.

[22] American Welding Society, *Structural Welding Code, Steel, ANSI/AWS D1.1-92*, AWS, Miami, USA, 1992.

[23] American Institute of Steel Construction, Manual of Steel Construction, Load and Resistance Factor Design, First Edition, AISC, Chicago, USA, 1986.

[24] European Convention for Constructional Steelwork, Recommendation for the Fatigue Design of Steel Structures, Publication No 43, ECCS, Brussels, Belgium, 1985.

[25] T Handyside, *Marine Paint Technology and Practices,* International Paint, Marine Coatings, internal script, 1985.

[26] H Peters, *The Maritime Transport Crisis*, The World Bank, Washington, D.C., USA, 1993.

[27] G M Hallegraeff and C.J. Bolch, *Transport of diatom and dinoflagellate resting spores in ships' ballast water: Implications for plankton biogeography and aquaculture*, Journal of Plankton Research, vol. 14, pp 1067–1084, 1992.

[28] National Research Council (U.S.), *Double-hull Tanker Legislation: An Assessment of the Oil Pollution Act of 1990,* National Academies Press, USA, 1998.

[29] W Schütz, *A history of fatigue,* Engineering Fracture Mechanics vol. 54(2), pp 263-300, 1996.

[30] R A Higgins, *Properties of Engineering Materials,* Hodder and Stoughton Ltd., Suffolk, UK, 1997.

[31] L Carlsson and M Palm, *Fatigue resistance of aged ballast tank coatings,* Report on Mechanical Fatigue Testing of Aged Tank Coatings, NORDTSET-Project, Swedish National Testing and Research Institute, 2001.

[32] J W Ringsberg, *On Mechanical Interaction Between Steel and Coating in Welded Structures,* thesis, Chalmers University of Technology, Gothenburg, Sweden, 1997.

[33] R L Carlson and G A Kardomateas, *An Introduction to Fatigue in Metals and Composites,* Hartnolls Limited, Cornwall, UK, 1996.

[34] *Materials engineering-web site (www.materialsengineer.com)*

[35] G E Dieter, *Mechanical Metallurgy, chapter 12, Fatigue of metals,* pp 375-431, London, UK, 1988.

[36] R W Hertzberg, *Deformation and Fracture of Engineering Materials,* 3rd edition, Wiley, New York, USA, 1989.

[37] P Beardmore and S Rabinowitz, *Treatise on Material Science and Technology,* Academic Press, Vol 6, p. 267, 1975.

[38] S Suresh, *Fatigue of Materials,* Cambridge University Press, UK, 1991.

[39] G J Sansilands, *Internal Stresses and Fatigue Fracture in a Methyl Pentene Polymer,* Thesis, Department of Metallurgy and Engineering Metals, University of Newcastle upon Tyne, UK, February, 1983.

[40] R W Hertzberg and J A Manson, *Fatigue of Engineering Plastics,* Academic Press, New York, USA, 1980.

[41] R W Hertzberg and J A Manson, *Fatigue-Encyclopedia of Polymer Science and Engineering, vol. 7,* Wiley, New York, USA, 1986.

[42] R E Melchers and X Jiang, *Estimation of models for durbability of epoxy coatings in water ballast tanks*, Ships and Offshore Structures, Vol.1, No.1, pp.61-70. 2006.

[43] B Ellis, *Chemistry and Technology of Epoxy Resins,* Blackie Academic & Professional, Glasgow, UK, 1993.

[44] D Stoye and W Freitag, *Paints, Coatings and Solvents,* Cambridge Press, UK, 1998.

[45] A E Batog, I P Pet'ko, and P Penczek, *Aliphatic-Cycloaliphatic Epoxy Compounds and Polymers*, Advances in Polymer Science, Vol. 144, 1999.

[46] L S Salem, *Epoxies for Steel*, Journal of Protective Coatings and Linings, Vol. 8, pp 65-75, 1996.

[47] R F Gibson, *Principles of Composite Material Mechanics*, McGraw-Hill, Singapore, 1994.

[48] R S Bauer, S Corley, *Reference Book for Composites Technology*, (Ed) S M Lee, Technomic Publishing Co, Lancaster, UK, 1989.

[49] R F Bunshah, *Deposition Technologies for Films and Coatings,* Noyes Publications, New Jersey, USA, 1982.

[50] W L Bradley, *Thermoplastic Composite Materials,* Carlsson, Los Angeles, USA, 1989.

[51] W G Knauss, *Time Dependent Fracture of Polymers,* In: Advances in Fracture Research - Proceedings of the 7th International Conference on Fracture (ICF-7), pp. 2683-2711, Houston, Texas, USA, 20-24 March 1989.

[52] M Molin, *Strain Capacity of Aged Polymeric Coating on Ship Structures*, Thesis, Department of Naval Architecture and Ocean Engineering, Chalmers University of Technology, Gothenburg, Sweden, 1999.

[53] M D Thouless, *Cracking and Delamination of Coatings*, Journal of Vacuum Science & Technology a-Vacuum Surfaces and Films, Volume 9, pp 2510, 1991.

[54] W D Callister, Jr., *Materials Science and Enginnering – An Introduction*, John Wiley & Sons, USA, 1994.

[55] G P A Turner, *Introduction to Paint Chemistry and Principles of Paint Technology*, Chapman and Hall, London, UK, 1988.

[56] A Adomenas, K Curran and M Falconer-Flint, Epoxy resins and curing agents, (Surface coatings-raw materials and their usage), volume 1, Chapman & Hall, London, UK, 1993.

[57] B Z Jang, *Advanced Polymer Composites: Principles and Applications*, ASM International, Materials Park, Ohayo, USA, 1994.

[58] MARSTRUCT (2005), *In service monitoring of structural strength, class requirements for hull monitoring notations*, Report Task 2.7, European Network of Excellence, Project No. FP6-PLT-506141, Contract No. TNE3-CT-2003-506141, http://mar.ist.utl.pt/marstruct/

[59] T Hodgkiess, N Eid and W T Hanbury, *Corrosion of welds in seawater*, Desalination, vol 27, pp 129-136, 1978.

[60] G S Springer, *Environmental Effects on Composite Materials*, *Vol 1*, Technomic Publishing Co., Westport CT., 1981.

[61] G Marom, *Application of Fracture Mechanics to Composite Materials,* Elsever, Amsterdam, Holland, 1989.

[62] A Kootsookos and A P Mouritz, *Sewater Durability of glass- and carbon-polymer composites.*Composites Science and Technology, Vol. 64, issue 10-11, pp. 1503-1511, 2003.

[63] P A Schweitzer, *Mechanical and Corrosion-Resistant Properties of Plastics and Elastomers,* Dekker, New York, USA, 2000.

[64] P Chiou and W L Bradley, *Effects of seawater absorption on fatigue crack development in carbon/epoxy EDT specimens,* Composites vol. 26, pp 869-876, 1995.

[65] T K O'Brien, *Damage in Composite Materials,* ASTM STP 775, ASTM, Philadelphia, USA, pp 140-1677, 1982.

[66] *Tanker Structure Cooperative Forum. Guidelines for Ballast Tank Coating Systems and Surface Preparation*, 3rd draft, London, 1999.

[67] F Maurer, *Viscoelastic Behaviour of Polymers, Part 5*, Department of Polymer Technology, Chalmers University of Technology, Gothenburg, Sweden, 1993.

[68] Standard test methods for mandrel bend test of attached organic coatings, American Society for Testing and Materials, ASTM Standard D522-93a, 1995.

[69] Standard practice for strain-controlled fatigue testing, American Society for Testing and Materials, ASTM Standard D2370-92, 1995.

[70] D Brock, *The Practical Use of Fracture Mechanics,* Kluwer Academic Publisher, Dordrecht/ Boston/ London, 1989.

[71] P Grundy, *Bulk carriers – editorial*, Marine Structures, Vol.16, pp 545 –546, 2003.

[72] L N Pussegoda, L Malik and W R Tyson, *Effects of plastic deformation on fracture toughness of ship plate steels,* Canadian Metallurgical Quarterly, Vol. 36, Issue 1, pp 39-47, 1997.

[73] J D G Sumpter and J S Kent, *Prediction of ship brittle fracture casualty rates by a probabilistic method.* Marine Structures, Vol. 17, Issue 8, pp 575-589, 2004.

[74] A Müller, J Wenck, S Goswami, J Lindemann, J Hohe and W Becker, *The boundary finite element method for prediction directions of cracks emerging from notches at biomaterial junctions,* Engineering Fracture Mechanics, Vol. 72, Issue 3, pp 373-386, 2005.

[75] J D G Sumpter and J S Kent, *Probability of cleavage fracture for a crack propagation by fatigue.* Engineering Fracture Mechanics, Vol. 73, Issue 10, pp 1414-1425, 2006.

[76] R J Ditchburn, S K Burke and C M Scala, *NDT of welds: state of the art,* NDT&E International, Vol. 29, No. 2, pp 11-117, 1996.

[77] S Vanlanduit, P Guillaume and G Van der Linden, *On-line monitoring of fatigue cracks using ultrasonic surface waves,* NDT and E International, Vol. 36, No 8, pp 601-607, 2003.

[78] B Talei-Faz, F P Brennan and W D Dover, *Residual static strength of high strength steel cracked tubular joints,* Marine Structures, Vol. 17, pp 291-309, 2004.

[79] G Tao and Z Xia, *A non-contact real-time strain measurement and control system for multiaxial cyclic-fatigue tests of polymer materials by digital image correlation method.* Polymer Testing, Vol.24, issue 7, pp 844-855, 2005.

[80] G Tao and Z Xia, *An experimental study of uniaxial fatigue behaviour of an epoxy resin by a new non-contact real-time strain measurement and control system,* Polymer Engineering Science, in press, doi:10.1002/pen.20754, 2007.

[81] G Tao and Z Xia, *Mean stress/strain effect on fatigue behaviour of an epoxy resin,* International Journal of Fatigue, in press, doi:10.1016/j.ijfatigue.2006.12.009, 2007.

[82] S R Kim and J A Nairn, *Fracture Mechanics Analysis of Coating/Substrate Systems: I. Analysis of Tensile and Bending Experiments,* Engineering Fracture Mechanics, Vol.65, Issue 5, pp 573-593, 2000.

[83] G Tao and Z Xia, *Ratcheting behaviour of an epoxy polymer and its effect on fatigue life,* Polymer Testing, Vol.26, Issue 4, pp 451-460, 2007.

[84] J K Paik, A K Thayamballi, Y I Park and J S Hwang, *A time-dependent corrosion wastage model for bulk carrier structures,* International Journal of Maritime Engineering, Vol. 145, Part A2, pp 61-87, 2003.

[85] S Farfan, C Rubio-Gonzalez, T Cervates-Hernandez and G Mesmacque, *High cycle fatigue, low cycle fatigue and failure modes of a carburized steer,* International Journal of Fatigue, Vol. 26, Issue 6, pp 673-678, 2004.

[86] W C Cui, *A feasible study of fatigue life prediction for marine structures based on crack propagation analysis,* Journal of Engineering for the Maritime Environment, Vol. 217, No M1, pp 11-23, 2003.

[87] H Emi, M Yuasa, A Kumano, H Kumamoto, N Yamamoto and M Matsunaga, *A study on fatigue strength and inspection of hull structures for planning a long life service,* ClassNK Teshnical Bulletin, pp 25-51, 1993.

[88] U O Akpan, T S koko, B Ayyub and T E Dunbar, *Risk assessment of ageing ship hull structures in the presence of corrosion and fatigue,* Marine Structures, Vol. 15, pp 211-231, 2002.

[89] J K Paik and A KA Thayamballi, *Ultimate limit state design of steel-plated structures,* John Wiley & Sons, Chichester, UK, 2003.

[90] W G Knauss, *Time Dependent Fracture of Polymers,* In: Advances in Fracture Research - Proceedings of the 7th International Conference on Fracture (ICF-7), pp. 2683-2711, Houston, Texas, USA, 20-24 March 1989.

[91] A G Thomas, *Rupture of Rubber-V, Cut Growth in Natural Rubber Vulcanizates,* Journal of Polymer Science, Vol. 31, pp 467, 1958.

[92] A N Gent, P B Lindley and A G Thomas, *Cut Growth and Fatigue of Rubbers I, The Relationship between Cut Growth and Fatigue,* Journal of Applied Polymer Science, Vol. 8, pp 455, 1964.

[93] J K Y Chang, *Crack Propagation in Viscoelastic Materials under Transient Loading with Application to Adhesively Bonded Structures,* Thesis, Aeronautical Engineering, California Institute of Technology, Pasadena, USA, 1983.

[94] S L Kim, M D Skibo, J A Manson, R W Hertzberg and J Jenisewski, *Tensile, Impact and Fatigue Behaviour of an Amine-Cured Epoxy Resin,* Polymer Engineering Science, Vol.18, pp 1093, 1978.

[95] J W Martin, S C Saunders and F L Floyd, *Methodologies for Predicting the Service Lives of Coating Systems,* Federation of Societies for Coatings Technology, Blue Bell, Pennsylvania, USA, 1996.

[96] H Emi, M Matoba and T Arima, *Corrosion Protection System for Long Ships' Water Ballast Tanks,* in Proceedings of the International Conference on Marine Corrosion Prevention, paper 15, London, UK, 11-12 October, 1994.

[97] N Adamson, *Performance of Coating Systems – Numerical Life Prediction,* in Proceedings of the Australian Corrosion Congress, paper 39, Sydney, Australia, November 1999.

[98] A Guide for Fatigue Testing and the Statistical Analysis of Fatigue Data, ASTM STP-91-A, 1963.

[99] L W Hill, *Mechanical Properties of Coatings,* Federation of Societies of Coatings Technology, Philadelphia, USA, 1987.

[100] P A Schweitzer, *Mechanical and Corrosion-Resistant Properties of Plastics and Elastomers,* Dekker, New York, USA, 2000.

[101] K P Menard, *Dynamic Mechanical Analysis: A Practical Introduction,* CRC Press, New York, 1999.

[102] ASTM D 4885, *Initial/Offset/Secant Modulus – Geomembranes by Wide Strip Tensile Method*, in Annual Book of ASTM Standards, V 04.08, ASTM, West Conshohocken, PA, USA

[103] L W Hill, *Dynamic Mechanical and Tensile Proprieties*, in Paint and Coating Testing Manual, 14th edition, ed. J V Koleske, Chapter 46, ASTM, Philadelphia, PA, 1995.

[104] C H Hare, More about modulus, time and temperature, Journal of Protective Coatings and Linings, 4(13), pp 73-84, 1996.

[105] G S Springer(ed), *Environmental Effects on Composite Materials*, Vol. 1, Technomic Publishing Co, Westport, USA, 1981.

[106] J R Moraes Delelmeida, G Wagner de Menezes, S Neves Monteiro, *Ageing of the DGEBA/TETA epoxy system with off-stoichiometric compositions*, Material Research, Vol. 6, 2003.

[107] G Odian, *Principles of Polymerization, 3rd ed.*, J. Wiley, New York, USA, 1991.

[108] B Z Jang, *Advanced Polymer Composites: Principles and Applications*, ASM International, Materials Park, Ohayo, USA, 1994.

[109] L E Nielsen, *Mechanical Properties of Polymers,* Reinhold', New York, USA, 1962.

[110] M P Morse, *Flexibility and Toughness,* in *Paint and Coatings Testing Manual,* 14th edition, ed. J V Koleske, Chapter 47, ASTM, Philadelphia, USA, 1995.

[111] ASTM D 2794, *Resistance of Organic Coatings to the Effects of Rapid Deformation (Impact),* in *Annual Book of ASTM Standards,* V 06.01, ASTM, Philadelphia, USA, 1995.

[112] R E Melchers, *Effect of nutrient-based water pollution on the corrosion of mild steel in marine immersion conditions*, Corrosion (NACE), Vol.61, No.3, pp.237-245, 2005.

[113] X Jiang, *Elastic-Constants and Hardness of Ion-Beam-Sputtered TINx Films Measured by Brillouin-Scattering and Depth-Sensing Indentation,* Journal of Applied Physics, Vol.69, pp 3053, 1991.

[114] C C Chiu and E D Case, *Elastic-Modulus Determination of Coating Layers as Applied to Layered Ceramic Composites,* Materials Science and Engineerins-a Structural Materials Properties Microstructure and Processing, vol.132, pp 39, 1991.

[115] J O Kim, *Elastic-Constants of Single-Crystal Transition-Metal Nitride Films Measured by Line-Focus Acoustic Microscopy,* Journal of Applied Physics, Vol.72, pp1805, 1992.

[116] Y Tsukamoto, H Yamaguchi and M Yanagisawa, *Mechanical-Properties of Thin-Films-Measurements of Ultramicroindentation Hardness, Young Modulus and Internal-Stress,* Thin Sold Films, VOl.154, pp171, 1987.

[117] W C Oliver and G M Pharr, *An Improved Technique for Determining hardness and Elastic Modulus Using Load and Displacement Sensing Indentation Experiments,* J. Mater. Res., Vol.7, pp 1564, 1992.

[118] P R Guevin, Jr, *Hardness,* in *Paint and Coatings Testing Manual,* 14th edition, ed. J V Koleske, Chapter 48, ASTM, Philadelphia, USA, 1995.

[119] H R Wilde and A Wehrstedt, *Martens Hardness HM- and International Accepted Designation for Hardness under Test Force, Materialwissenschaft und Werkstofftechnik,* Vol.31, Issue 10, pp 937, 2000.

[120] D Tabor, *The Hardness of Metals,* Clerendon Press, Oxford, UK, 1951.

[121] P Benjamin and C Weaver, *Measurement of Adhesion of Thin Films,* Proceedings of the Royal Society of London, Series A, Mathematical and Physical Sciences, Vol. 254, Issue 1277, pp. 163-176, 1960.

[122] J Ahn, K L Mittal and R H Macqueen, *Hardness and Adhesion of Filmed Structures as Determined by the Scratch Technique,* in *Adhesion Measurement of Thin Films, Thick Films, and Bulk Coatings,* (K. L. Mittal, ed.), STP 640, pp. 134–157, ASTM, Philadelphia, USA, 1978.

[123] E S Berkovich, *Three-Faceted Diamond Pyramid for Micro-Hardess Testing,* Industrial Diamond Review, Vol.11, pp 129, 1951.

[124] B Bhushan and B K Gupta, *Handbook of Tribology: Materials, Coatings and Surface Treatments,* McGraw Hill, New York, USA, 1991.

[125] P J Blau and B R Lawn, *Microindentation Techniques in Materials Science and Engineering,* STP 880, ASTM, Philadelphia, USA, 1986.

[126] K L Johnson, *Contact Mechanics,* Cambridge University Press, Cambridge, UK, 1985.

[127] A J Wahlberg, Iron and Steel Institute, Vol.59, p 243, 1901.

[128] E Meyer, *Z. ver. Deut. Ing,* Vol. 52, p 645, 1908.

[129] R L Smith and G E Sandland, *Some Notes on the Use of a Diamond Pyramid for Hardness Testing,* Journal of Iron and Steel Institute CXI:285, 1925.

[130] F Knoop and C G Peters, *A Sensitive Pyramidal-Diamond Tool for Indentation Measurements,* J. Res. Nat. Bur. Stand.23: 39, 1939.

[131] M F Doerner and W D Nix, *A Method for Interpreting the Data from Depth-Sensing Indentation Instruments,* Journal of Materials Research, Vol.1, pp 601, 1986.

[134] *Corrosion of Metals and Alloys-Stress Corrosion Testing Part 2: Preparation and Use of Bent-Beam Specimens,* British Standard BS EN ISO 7539-2, 1995.

[135] *Standard test methods for mandrel bend test of attached organic coatings,* ASTM D522-93a, 1995.

[136] *Standard practise for strain-controlled fatigue testing,* ASTM D2370-92, 1995.

[137] L A Francis, A V McCormick and D M Vaessen, *Development and measurements of stress in polymer coatings,* Journal of Material Science, Vol. 37, pp 4717-4731, 2002.

[138] C H Hare, *Internal stress:Part 1,* Journal of Protective Coatings and Linings, Vol.8(13), pp 65-75,1996.

[139] G Yan and J R White, *Residual stresses in marine coatings under simulated service conditions,* Polymer Engineering and Science, Vol. 39, pp 1866-1879, 1999.

[140] E D Cohen, E J Lightfoot and E B Gutoff, *A primer on forming coatings,* Chemical Engineering Progress, Vol. 30, pp 30-36, 1990.

[141] E D Cohen, *Modern Coating and Drying Technology,* edited by E D Cohen and E B Gutoff, VCH Publishers, New York, USA, 1992.

[142] K Sato, *The Internal Stress of Coating Films,* Progress in Organic Coatings, Volume 8, issue 2, pp 143-160, 1980.

[143] A G Evans, M D Drory and M S Hu, *The Cracking and Decohesion of Thin Films,* Journal of Material Research, Vol. 3, pp 1043, 1988.

[144] M D Thouless, *Cracking and Delamination of Coatings,* Journal of Vacuum Science and Technology A, Vol. A9,issue 4, pp. 2510-2515, 1991.

[145] H Lei, L F Francis, W W Gerberich and L E Scriven, Multiscale Modeling of Materials, Materials Research Society, Pittsburgh, USA, 2000.

[146] H Lei, PhD thesis, University of Minnesota, USA, 1999.

[147] K N Christodoulou, E J Lightfoot and R W Powell, *Model of Stress-Induced Defect Formation in Drying Polymer Films,* AlChE Journal, Vol. 44, issue 7, pp. 1484-1498,1998.

[148] S G Croll and A D Skaja, *Quantitative Spectroscopy to Determine the Effects of Photodegradation on a Model Polyester-Urethane Coating,* Journal of Coatings Technology, Vol. 75, pp. 945, 2003.

[149] R W Hoffman, *Stress Distributions and Thin Film Mechanical Properties,* Surface and Interface Analysis, Vol. 3, issue 1, pp. 62-66, 1981.

[150] M D Thouless, *Decohesion of Films with Axisymmetric Geometries,* Acta Metallurgica, Vol. 36, issue 12, pp. 3131-3135, 1988.

[151] D Y Perera, *Plastic and Coatings Durability, Stabilization, Testing,* Hanser Gardner Publication, Cincinnati, Ohayo, USA, 2001.

[152] L H Sperling, *Introduction to Physical Polymer Science,* John Wiley, New York, USA, 1992.

[153] D S Campbell, *Handbook of Thin Film Technology,* McGraw-Hill, New York, USA, 1969.

[154] R W Hoffman, *Physics of Non-Metallic Thin Films,* Plenum, New York, USA, 1976.

[155] C Y Li, R D Black and W R LaFontaine , *Analysis of thermal stress-induced grain boundary cavitation and notching in narrow Al-Si metallizations*, Appl. Phys. Lett.,Vol. 53, 1988.

[156] J W Patten, E D McClanahan and J W Johnson, *Room-Temperature Recrystalization in Thick Bias-Sputtered Copper Deposits,* J. Appl. Phys., Vol. 42, 1971.

[157] D M Mattox and G J Kominiak, *Structure Modification by Ion Bombardment During Deposition,* J. Vac. Sci. Technol., Vol. 9, p 528, 1972.

[158] S J Bull, *tribology of Carbon Coatings-DLC, Diamond and Beyond,* Diamond and Related Materials, Vol. 4, 1995.

[159] S G Croll, *Internal Stress in a Solvent-Cast Thermoplastic Coating,* Journal of Coatings Technology, Vol. 50, Issue 33, p 638, 1978.

[160] S G Croll, *The Origin of Residual Internal Stress in Solvent-Cast Thermoplastic Coatings,* Journal of Applied Polymer Science, Vol. 23, issue 3, pp. 847-858, 1979.

[161] D Y Perera and D V Eynde, *Consideration on a Cantilever(Beam) Method For Measuring the Internal Stress in Organic Coatings,* Journal of Coatings Technology, Vol. 53, No 677, pp. 39, 1981.

[162] D Y Perera and D V Eynde, *Changes in Composition and Characteristics of Latex Paints Applied on Porous Inorganic Substrated,* Journal of Coatings Technology, Vol.73, pp. 919., 2001.

[163] P J Hine, SE L Muddarris and D E Packham, Journal of Adhesion Science and Technology, Vol. 1, pp 69-78, 1987.

[164] A A Roche, M Aufray and J Bouchet, *The Role of the Residual Stresses of the Epoxy-Aluminium Interphase on the Interfacial Fracture Toughness,* J. Adhesion, Vol. 82, pp 867-886, 2006.

[165] H Orsini and F Schmit, *Influence of Residual Thermal Stresses on the Fracture Behaviour of Hybrid Bonded Joints,* Journal of Adhesion, Vol. 43, issue 1-2, pp 55-68, 1993.

[166] M D Thouless and H M Jensen, *The Effect of Residual Stresses on Adhesion Measurements,* Journal of Adhesion Science and Technology, Vol. 8, issue 6, pp 579-586, 1994.

[167] D R Mulville and R N Vaishnav, *Interfacial Crack Propagation,* Journal of Adhesion, Vol. 7, issue 3, pp 215-233, 1975.

[168] G Yan, *Internal Stress Development in Marine Coatings,* MPhil thesis, Department of Mechanical, Materials and Manufacturing Engineering, University of Newcastle upon Tyne, 1997.

[169] M Shimbo, M Ochi nad Y Shigeta, *Shrinkage and Internal Stress During Curing of Epoxide Resins,* Journal of Applied Polymer Science, Vol. 26, issue 7, pp. 2265-2277, 1981.

[170] M Shimbo and N Nishitani, *Mechanical Properties of Acid-Cured Epoxy Resins with Different Network Structures,* Journal of Applied Polymer Science, Vol. 29, issue 5, pp. 1709-1721, 1984.

[171] M Shimbo, M Ochi and K Arai, *Internal Stress of Curred Epoxide Resin Coatings Having Different Network Chains,* Journal of Coatings Technology, Vol. 56, pp. 45-51, 1984.

[172] M Shimbo, M Ochi and K Arai, *Effect of Solvent and Solvent Concentration on the Internal Stress of Epoxide Resin Coatings,* Journal of Coatings Technology, Vol. 57, pp. 93-99, 1985.

[173] M Ochi, K Yamashita and M Shimbo, *The Mechanism for Occurrence of Internal Stress During Curing Epoxide Resins,* Journal of Applied Polymer Science, Vol. 43, pp. 2013-2019, 1991.

[174] L M Robeson and M S Vratsanos, *Mechanical Characteristics of Emulsion Polymer Blends,* Polymeric Materials Science and Engineering, Vol. 80, pp. 565-566, 1999.

[175] D Y Perera and D V Eynde, *Moisture and Temperature Induced Stresses (Hygrothermal Stresses) in Organic Coatings,* Journal of Coatings Technology, Vol. 59, pp. 55-63, 1987.

[176] O Negele and W Funke, *Internal Stress and Wet Adhesion of Organic Coatings,* Progress in Organic Coatings, Vol. 28, issue 4, pp. 285-289, 1996.

[177] A F Abdelkader and J R White, *Influence of Relative Humidity on the Development of Internal Stresses in Epoxy Resins Based Coatings,* Journal of Materials Science, Vol. 37, No.22, pp. 4769-4773, 2002.

[178] S G Croll, *Internal Stress in a Solvent-Cast Thermoplastic Coating,* Journal of Coatings Technology, Vol. 50, pp. 33-38, 1978.

[179] R R Myers, *Relaxation During the Formation of Films,* Journal of Polymer Science, Polymer Symposia, No. 35, pp. 3-21, 1971.

[180] V J Parks and A J Durelli, *Photoelastic Analysis of Plates Subjected to Restrained Shrinkage,* Journal of Applied Mechanics, Vol. 32, issue 3, pp. 504-510, 1965.

[181] Y Niitsu, K Ichinose and K Ikegani, *Stress Measurements of Transparent materials by Polarizes Laser,* JSME International Journal, Series A: Solid Mechanics and Material Engineering, Vol. 38, issue 1, pp. 68-72, 1995.

[182] R M O'Brien, S A Brown, G B Bufkin and J R Grawe, *Use of Thiirane-Functional Monomers as a Means of Developing Crosslinkable Emulsions,* Journal of Coatings Technology, Vol. 53, pp. 49-58, 1985.

[183] R N O'Brien and W Michalik, *Laser Interferometry Method for Internal Stress Measurement in Coatings,* Journal of Coatings Technology, Vol. 58, p 735, 1986.

[184] D R Bauer, *How to Calculate Crosslink Structure in Coatings,* Journal of Coatings Technology. Vol. 60, pp. 53-66, 1988.

[185] A J Perry, *The Residual-Stress in Thin Films Deposited onto Cemented Carbide by High-Rate Reactive Sputering,* Surface and Coatings Technol., Vol. 39, pp387, 1989.

[186] D S Rickerby and S J Bull, *High-Temperature X-Ray-Diffraction Studies on Physical Vapor-Deposited TiN,* Surface and Coatings Technol., Vol. 39, issue 13, pp 397, 1989.

[187] W H Burrows, *Molecular Science in Surface Coatings,* Journal of Paint Technology, Vol. 41, pp. 144-166, 1969.

[188] D M Vaessen, A V McCormick and L F Francis, *Effects of Phase Separation on Stress Development in Polymeric Coatings,* Polymer, Vol. 43, issue 8, pp. 2267-2277, 2002.

[189] C J Martinez and J A Lewis, *Shape Evolution and Stress Development During Latex-Silica Film Formation,* Langmuir, Vol. 18, pp. 4689-4698, 2002.

[190] M Lu, S Y Tam, P R Schunk and C J Brinker, *Thin Films-Stresses and Mechanical Properties VIII,* Materials Research Society, Pittsburgh, USA, 2000.

[191] K S Park, Y D Kwon and D Kim, *Theoretical and Experimental Analysis on the Thickness-Controlled Residual Stress During Drying of Solvent-Absorbed Polymer Films,* Polymer Journal (Tokyo, Japan), Vol. 33, issue 7, pp. 503-508, 2001.

[192] B S Berry and W C Pritchet, *Elastic and Viscoelastic Behaviour of a Magnetic Recording Type,* IBM Journal of Research Development, Vol. 32, pp. 682-694, 1984.

[193] H M Tong and K L Saenger, *New Characterization Techniques for Thin Polymer Films,* John Wiley & Sons, London, UK, 1990.

[194] J H Jou. L Hsu, P T Huang, R Huang and W P Shen, *Bending beam Measurement of Moisture Diffusion in Polyimide Films on Silicon Substrate,* Polymer Journal (Tokyo, Japan), Vol. 23, issue 9, pp. 1123-1133, 1991.

[195] D Y Perera and M Oosterbroek, *Hygrothermal Stress Evolution During Weathering in Organic Coatings,* Journal of Coatings Technology, Vol. 66, pp. 82-88, 1994.

[196] D F Stamatialis, M Sanopoulou and I Raptis, *Swelling and Dissolution Behavior of Poly(Methyl Methacrylate) Films in Methyl Ethyl Ketone/Methyl Alcohol Mistures Studied by Optical Techniques,* Journal of Applied Polymer Science, Vol. 83, issue 13, pp. 2823-2834, 2002.

[197] G S Stoney, *The Tension of Metallic Films Deposited by Electrolysis,* Proc. Royal Soc. London, Series A 82, p. 172, 1909.

[198] S Senderoff and A Brenner, *Calculation of the stress in electrondeposits from the curvature of plated strip,* J. Res. Of the Nat. Bureau of Stand., Vol. 42, 1949.

[199] Y Inoue and Y Kobatake, *Effects of Fillers on Residual Stresses in Coatings,* Kolloid-Zeitschrift, pp. 18-24, 1958.

[200] S P Timoshenko, *Analysis of Bi-Metal Thermostats,* Journal Opt. Soc. Am., Vol. 11, pp. 233-255, 1925.

[201] A Brenner and S Senderoff, *Calculation of Stress in Electrodeposits from the Curvature of a Plated Strip,* Journal of Research and National Burro of Standards, Vol. 42, pp. 105-123, 1949.

[202] C C Chiu, *Determination of the Elastic Modulus and Residual Stresses in Ceramic Coatings Using a Strain Gage,* Journal of the American Ceramic Society, Vol. 73, pp. 1999-2005, 1990.

[203] M Benabdi and A A Roche, *Mechanical Properties of Thin and Thick Coatings Applied to Various Substrates, Part II. Young's Modulus Determination of Coating Materials,* Journal of Adhesion Science and Technology, Vol.11, issue 3. pp. 373-391, 1997.

[204] M Ohring, *The Materials Science of Thin Films,* Academic Press, New York, USA, 1992.

[205] J R White, Polym. Test. Vol. 4, p 165, 1984. [Also appeared as Chapter 8 in *Measurements Technique for Polymeric Solids,* edited by R. P. Brown and B E Read, Elsevier, Barking, UK, 1984.]

[206] A F Abdelkader and J R White, *Curing Characteristics and Internal Stresses in Epoxy coatings: Effect of Crosslinking Agent,* J. Mat. Sci., Vol. 40, pp 1843-1854, 2005.

[207] D T Llewellyn and R C Hudd, *Steels: Metallurgy and Applications,* Butterworth-Heinemann, London, UK, 1998.

[208] W F Smith and J Hashemi, *Foundations of Materials Science and Engineering*, McGraw-Hill, London, UK, 2006.

[209] Standard ISO 8401:1994, *Corrosion protection of metals*

[210] S C Dexter, *ASM Metals Handbook, Volume 13: Corrosion*, Materials Park, ASM International, pp 893-902, Ohio, USA, 1987.

[211] G Yan and J R White, *Residual Stresses in Marine Coatings under Simulated Service Conditions,* Polymer Engineering and Science, Vol 39, Issue 10, pp 1866-1879, 1999.

[212] H Hatakeyama and T Hatakeyama, *Interaction between Water and Hydrophilic Polymers,* Thermochimica Acta, Vol 308, Issues 1-2, pp 3-22, 1998.

[213] P Blasi, SS D'Souza, F Selmin and P P DeLuca, *Plasticizing Effect of Water on Poly(lactide-co-glycolide),* Journal of Controlled Release, Vol 108, Issue 1, pp 1-9, 2005.

[214] P Iredale, *Investigation of Crack Development in Epoxy Coatings under Tensile Loading,* School of Mechanical and Systems Engineering, Newcastle University, final undergraduate project partially supervised by M Vicevic, 2007.

[215] K C Dao and D J Dicken, *Fatigue Failure Mechanisms in Polymers,* Polymer Engineering and Science, Vol 27, No 4, pp 271-276, 1987.

[216] S Putic, M Stamenovic, B Bajceta, P Stajcic and S Bosnjak, *The Influence of High and Low Temperatures on the Impact Properties of Glassy-Epoxy Composites,* Journal of Serbian Chemical Society, Vol 72, Issue 7, pp 713-722, 2007.

[217] M G Kim, S G Kang, C G Kim and C W Kong, *Tensile Response of Graphite/Epoxy Composites at Low Temperatures,* Composite Structures, Vol 79, Issue 1, pp 84-89, 2007.

[218] A A Khalid, *The Effect of Testing Temperature and Volume Friction on Impact Energy of Composites,* Materials and Design, Vol 27, Issue 6, pp 499-506, 2006.

[219] G C Sih and C K Chao, *Fatigue Initiation in Unnotched Specimens Subjected to Monotonic and Cyclic Loading,* Journal of Theoretical and Applied Fracture Mechanics, Vol 2, Issue 1, pp 67-74, 1984.

[220] G Yan, M El-Hadik, H Aglan, P Faughnan and C Bryan, *Fatigue Crack Growth Analysis of Polymonochlorotrifluoroethylene (CTFE),* Journal of Elastomers and Plastics, Vol 31, pp 96-129, 1999.

[221] A Nádai, *Theory of Flow and Fracture of Solids* (Vol. 1 ed.), McGraw-Hill, New York, USA, 1950.

[222] L E Nielsen, *Fatigue Behaviour of Some Filled Polymers,* Journal of Composite Mterials, Vol 9, pp 149-156, 1975.

[223] J A Sauer and G C Richardson, *Fatigue of Polymers,* International Journal of Fracture, Vol 16, pp 499-532, 1980.

[224] A Leyland and A Matthews, *On the Significance of the H/E Ratio in Wear Control: a Nanocomposite Coating Approach to Optimised Tribological Behaviour,* Wear, Vol 246, Issue 1-2, pp 1-11, 2000.

[225] T Y Tsui and G M Pharr, *Substrate Effects on Nanoindentation Mechanical Property Measurements of Soft Films on hard Substrates,* Journal of Materials Research, Vol 14, Issue 1, pp 292, 1999.

[226] J C Rowlands and D J Chuter, *A.C. Impedance Measurements on Marine Paint Systems,* Corrosion Science, Vol 23, Issue 4, pp 331-340, 1983.

[227] G Georgiou, *Residual Stresses of Marine Coatings,* School of Mechanical and Systems Engineering, Newcastle University, final undergraduate project partially supervised by M.Vicevic, 2007.

APPENDICES

APPENDIX 3.1.

Marine shop primers

Primer is a first coat on a substrate usually applied on marine structures with the purpose to protect the steel surfaces during the time of building to prevent them from rusting. Marine shop primers are also known by a variety of other more descriptive titles, such as preconstructive primers, prefabrication primers, etch-primers, shop-primers, wash-primers, etc. Primers need to have good adhesion on the substrate, to give protection of the substrate surface (corrosion protection) and to have good adhesion to top coatings. Some components are given in Figure A3.1.

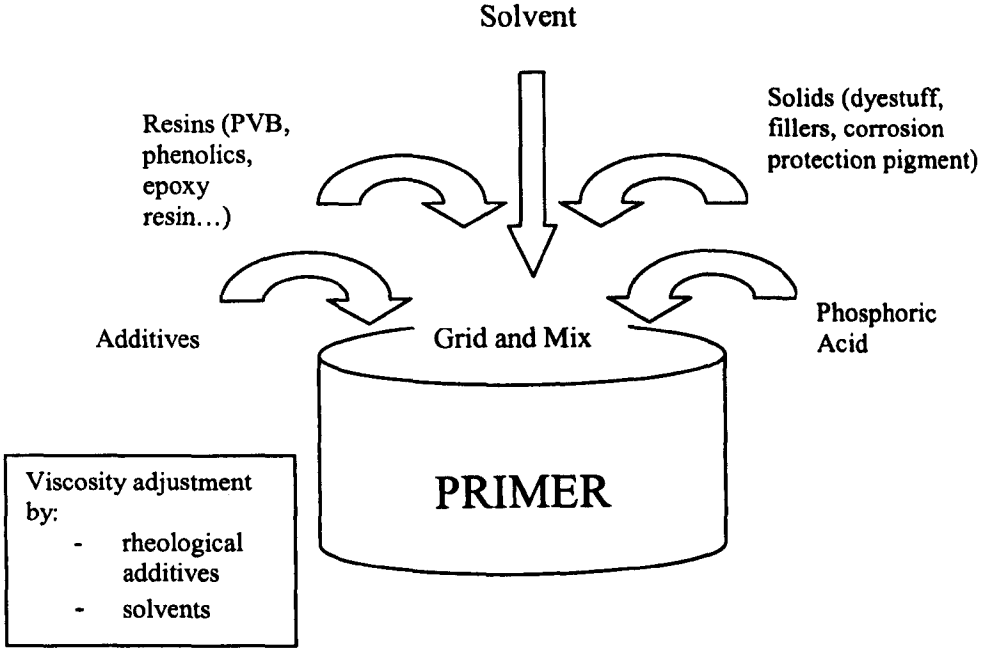

Figure A3.1. Composition of primers

Technical data of applied shop primer is given in Table A3.1. Instructions of EN ISO 12944-Part 4 were followed throughout the application procedure.

Table A3.1. Technical Data for PVB etch primer

Technical Data	
Composition	PVB binder, fillers, colouring pigments and corrosion protecting pigments
Colour	gray
Delivery viscosity	25 - 35 DIN53211 4mm 20°C
Density	1.11 kg/m^3
Solid content volume	51-52 volume %, by colour
Theoretical covering rate	~14 m^2kg/ 15µm

APPENDIX 3.2.

Electron Scanning Environmental Microscopy

At all stages of sample preparation, ageing, conditioning and fracture testing, surface observations were made on an optical microscope. Selected samples were studied in an environmental scanning electron microscope (ESEM). The advantage of an electron microscope compared to a light microscope is its much greater resolution. The resolution in a microscope is directly proportional to the wavelength of the radiation being employed. In a conventional light microscope, the best resolution is about 0.2 μm [4], which is largely dictated by the wavelength of visible light. In electron microscopy, electrons are used to form images, not visible light. Since electrons have much smaller wavelengths than visible light, the resolution is usually less than 10 nm, easily 20 times better than the best light microscope. Furthermore, electron microscopes have a much better depth of field than light microscopes.

A scanning electron microscope uses a focused beam of high-energy electrons to scan in a raster-like manner across the surface of the sample. The beam diameter sets a limit on the resolution that is much greater than the electron beam wavelength, but 10 nm resolution is easily achieved. This beam interacts with the sample surface to produce a large number of secondary electrons, which are collected by a detector and eventually converted into a magnified image on a monitor. The contours of the surface of the specimen are discernable due to the fact that electrons that were emitted from a surface facing away from the detector are partly absorbed by the specimen itself. This results in shadows, or a gradation in the grey scale, which the human brain processes as "features". The efficiency of recording electron collection depends on the local orientation of the sample surface, and the efficiency of secondary electron production depends on the atomic number of the atoms bombarded by the primary beam.

The production of the focused beam of electrons is performed by an electron gun. This usually consists of a cathode constructed of a tungsten filament housed in a specially constructed cylinder, an anode plate, and various electromagnetic lenses. The filament is negatively charged by connecting it to the negative pole of a high-voltage power supply, and the anode plate is grounded. This results in a large

potential difference between the filament and the anode, called the 'accelerating voltage'. This voltage is usually between 5 and 30 keV. When the filament is heated, a flow of electrons is produced that travel towards the anode plate under the effect of the potential difference.

In a conventional light microscope, glass lenses focus visible light photons. Electrons, however, being charged particles, can be deflected and therefore focused by magnetic fields [5]. The 'lenses' used in electron microscopes are actually electromagnetic. At least two such lenses are employed in the column of the electron gun in order to focus the beam of electrons at a precise spot on the specimen. After the last lens, and just before the specimen, will be an aperture to control the spot size, and hence the resolution of the beam. The aperture also helps to reduce spherical aberrations in the lens.

When the focused beam of electrons impinges on the surface of the specimen, several possible interactions can take place, thus producing a discrete volume of excitation within the specimen. For imaging, the two types of interaction of most practical significance are the production of either elastically or inelastically scattered electrons. An elastically scattered electron is one that retains all (or nearly all) of its original energy. An inelastically scattered electron is one that has lost much of its original energy due to interactions within the specimen. In scanning electron microscopy, elastically scattered electrons are referred to as 'back-scattered electrons', while inelastically scattered electrons are referred to as 'secondary electrons'. Back-scattered electrons have more energy than secondary electrons, and can escape from a zone of penetration within the sample that is deeper than that from which the low energy secondary electrons can escape, and hence are not quite as sensitive to surface features. For both types of electrons, at any given acceleration voltage, the depth of penetration is also affected by the atomic number of the element(s) making up the specimen. Higher-atomic-number elements scatter electrons more readily and the depth of penetration will therefore be reduced.

The primary advantages of the ESEM compared to SEM, lie in permitting the microscopist to vary the sample environment through a range of pressures, temperatures and gas compositions [6]. The Environmental SEM retains all of the

performance advantages of a conventional SEM, but removes the high vacuum constraint on the sample environment. Wet, oily, dirty, non-conductive samples may be examined in their natural state without modification or preparation. The ESEM offers high resolution secondary electron imaging in a gaseous environment of practically any composition, at pressures as high as 7 kPa, and temperatures as high as 1500 °C.

APPENDIX 4.1.

Hardness Measurements During Soaking Period in De-Ionized Water

Table A4.1. Hardness values during soaking period

Time [hours]	Hardness [HV]		
	Coating 'A'	Coating 'B'	Coating 'C'
0	150.8	32.8	16.86
1	140.87	26.89	12.92
2	120.21	29.85	11.06
5	110.53	24.62	8.72
6	109.32	23.92	8.06
24	105.19	26.53	8.16

APPENDIX 4.2.

Calculation of Dry Film Thickness

Coating thickness for every shim was calculated from the difference between the average coated shim thickness and the uncoated steel thickness. As a standard statistical method, all shims were measured by micrometer at six different places and then the average value was taken from those measurements. The steel thickness was double checked by micrometer as well.

Table A4.2. Coating thickness measurements and calculations for shims 150 mm length (COATING 'A')

Shim No	Coated Shim Thickness-measurements [mm]			Average Shim Thickness [mm]	Steel Thickness [mm]	Coating Thickness [µm]
1.1A	1.03	1.02	1.13	1.07	0.21	860
	1.07	1.07	1.10			
2.1A	0.98	1.03	1.10	1.06	0.13	930
	1.16	1.10	0.97			
3.1A	1.11	1.13	1.14	1.10	0.14	960
	1.09	1.12	1.03			
Average				1.08	0.16	917
1.2A	1.01	1.03	1.02	1.04	0.21	830
	1.05	1.09	1.06			
2.2A	1.04	1.05	1.07	1.08	0.22	860
	1.11	1.11	1.09			
3.2A	1.04	1.12	1.11	1.09	0.24	850
	1.14	1.10	1.04			
Average				1.07	0.22	847
1.3A	1.21	1.23	1.25	1.22	0.32	900
	1.24	1.24	1.17			
2.3A	1.17	1.18	1.22	1.19	0.32	870
	1.20	1.21	1.18			
3.3A	1.19	1.21	1.27	1.23	0.34	890
	1.28	1.25	1.20			
Average				1.21	0.33	887

Table A4.3. Coating thickness measurements and calculations for shims 150 mm length(COATING 'B')

Shim No	Coated Shim Thickness-measurements [mm]			Average Shim Thickness [mm]	Steel Thickness [mm]	Coating Thickness [μm]
1.1B	1.03	1.10	1.11	1.08	0.11	970
	1.14	1.11	1.03			
2.1B	0.95	1.01	1.09	1.06	0.12	940
	1.13	1.08	1.09			
3.1B	0.95	1.08	1.09	1.06	0.11	950
	1.14	1.08	1.03			
Average				*1.07*	*0.11*	*953*
1.2B	1.05	1.14	1.12	1.15	0.25	900
	1.17	1.20	1.25			
2.2B	0.98	1.04	1.08	1.07	0.21	860
	1.10	1.12	1.08			
3.2B	1.14	1.15	1.21	1.16	0.26	900
	1.19	1.19	1.10			
Average				*1.13*	*0.24*	*887*
1.3B	1.29	1.25	1.35	1.33	0.33	1000
	1.35	1.34	1.41			
2.3B	1.22	1.31	1.35	1.32	0.32	1000
	1.34	1.35	1.34			
3.3B	1.36	1.35	1.39	1.35	0.33	1020
	1.33	1.37	1.31			
Average				*1.33*	*0.33*	*1007*

Table A4.4. Coating thickness measurements and calculations for shims 150 mm length(COATING 'C')

Shim No	Coated Shim Thickness-measurements [mm]			Average Shim Thickness [mm]	Steel Thickness [mm]	Coating Thickness [µm]
1.1C	0.83	0.92	0.97	0.92	0.12	800
	0.95	0.93	0.93			
2.1C	0.95	0.90	0.89	0.90	0.12	780
	0.88	0.90	0.89			
3.1C	0.87	0.89	0.99	0.94	0.13	810
	0.94	0.94	0.99			
Average				*0.92*	*0.12*	*797*
1.2C	1.11	1.15	1.08	1.07	0.21	860
	1.03	1.05	0.98			
2.2C	0.98	0.93	0.97	0.98	0.25	730
	0.97	1.03	1.00			
3.2C	1.07	1.04	1.03	1.00	0.22	780
	0.97	0.94	0.96			
Average				*1.02*	*0.23*	*790*
1.3C	1.06	1.07	1.11	1.11	0.36	750
	1.12	1.13	1.18			
2.3C	1.17	1.14	1.12	1.12	0.33	790
	1.09	1.10	1.08			
3.3C	1.07	1.08	1.12	1.15	0.38	770
	1.17	1.21	1.23			
Average				*1.13*	*0.36*	*770*

APPENDIX 4.3.

Young's Modulus and Poisson ratio for the coatings and steel substrate

Table A4.5. Young's Modulus and Poisson ratio for the coatings

Coating Type	Young's Modulus [GPa]
A	4.8
B	4.7
C	6.1

Poisson's ratio for the coatings 0.4 (literature value for epoxy coatings)

Poisson's ratio for a substrate (steel) 0.33 (literature value)

APPENDIX 4.4.

Internal Stresses, shims 150 mm length, different substrate thicknesses

Table A4.6. Internal stress in the coating **'A'** for shims with three different thicknesses, 150mm length of shims

COATING A	Steel Thickness [mm]		
	0.1	**0.2**	**0.3**
Internal Stress in the Coating σ_c [MPa]	5.2	16.4	13.5
	4.4	16.9	12.4
		16.8	13.7
		17.8	
AVERAGE	***4.8***	***17.0***	***13.2***

Table A4.7. Standard deviation, Coefficient of variation and Standard error for internal stress and radius measurements for shims coated with type **'A'** coating (150mm length)

	Radius			*Internal Stress*		
Steel Thickness	**0.1mm**	**0.2mm**	**0.3mm**	**0.1mm**	**0.2mm**	**0.3mm**
Standard Deviation	0.1m	0.01m	0.02m	0.6MPa	0.6MPa	0.7MPa
Coefficient of Variation [%]	14.2%	3.2%	3.1%	11.8%	3.6%	5.3%
Standard Error	0.1m	0.01m	0.01m	0.4MPa	0.3MPa	0.4MPa

Table A4.8. Internal stress in the coating **'B'** for shims with three types of steel thickness, 150mm length of shims

COATING B	**Steel Thickness [mm]**		
	0.1	**0.2**	**0.3**
Internal Stress in the Coating σ_c [MPa]	4.6	15.7	12.2
	6.5	16.9	12.6
	5.6	17.8	13.6
AVERAGE	***5.6***	***16.8***	***12.8***

Table A4.9. Standard deviation, Coefficient of variation and Standard error for internal stress and radius measurements for shims coated with type **'B'** coating (150mm length)

	Radius			***Internal Stress***		
Steel Thickness	**0.1mm**	**0.2mm**	**0.3mm**	**0.1mm**	**0.2mm**	**0.3mm**
Standard Deviation	0.14m	0.04m	0.03m	0.9MPa	1.0MPa	0.7MPa
Coefficient of Variation [%]	16.49%	12.3%	5.38%	16.93%	6.18%	5.71%
Standard Error	0.08m	0.02m	0.02m	0.5MPa	0.6MPa	0.4MPa

Table A4.10. Internal stress in the coating **'C'** for shims with three types of steel thickness

COATING C	**Steel Thickness [mm]**		
	0.1	**0.2**	**0.3**
Internal Stress in the Coating σ_c [MPa]	2.6	4.5	1.8
	2.5	4.5	1.6
	2.6	2.5	1.8
AVERAGE	***2.6***	***3.8***	***1.8***

Table A4.11. Standard deviation, Coefficient of variation and Standard error for internal stress and radius measurements for shims coated with type **'C'** coating (150mm length)

	Radius			***Internal Stress***		
Steel Thickness	**0.1mm**	**0.2mm**	**0.3mm**	**0.1mm**	**0.2mm**	**0.3mm**
Standard Deviation	0m	0.6m	0m	0.7MPa	1.2MPa	0.1MPa
Coefficient of Variation [%]	0%	34.6%	0%	27.5%	30.5%	6.3%
Standard Error	0 m	0.4m	0m	0.4MPa	0.7MPa	0.1MPa

APPENDIX 4.5.

Coating Thickness Calculations for shims 250mm length

Table A4.12. Coating thickness calculations and measurements for shims 250 mm length

Type of Coating	Shim Number	Shim Thickness Measurements [mm]			Average Shim Thickness [mm]	Steel Thickness [mm]	Coating Thickness [μm]
Coating A	1	1.24	1.29	1.38	1.31	0.37	940
		1.40	1.29	1.26			
	2	1.29	1.36	1.37	1.34	0.37	970
		1.44	1.36	1.23			
	3	1.27	1.20	1.30	1.29	0.37	920
		1.37	1.32	1.32			
	4	1.27	1.32	1.37	1.32	0.38	940
		1.40	1.41	1.17			
	5	1.19	1.22	1.28	1.24	0.36	880
		1.29	1.28	1.19			
	6	1.14	1.17	1.29	1.23	0.35	880
		1.28	1.29	1.22			
	Average				*1.29*	*0.37*	*922*
Coating B	7	1.08	1.04	1.05	1.08	0.36	720
		1.14	1.15	1.04			
	8	1.11	1.04	1.09	1.11	0.36	740
		1.15	1.16	1.10			
	9	0.99	1.04	1.12	1.07	0.37	700
		1.13	1.17	0.98			
	10	0.98	1.05	1.10	1.06	0.34	720
		1.12	1.13	0.97			
	11	1.06	1.00	1.11	1.08	0.35	730
		1.14	1.12	1.04			
	12	0.97	1.10	1.10	1.08	0.35	730
		1.15	1.13	1.03			
	Average				*1.08*	*0.35*	*723*
Coating C	13	0.94	0.95	1.04	0.95	0.36	590
		1.03	0.92	0.84			
	14	0.90	1.00	1.01	0.99	0.36	630
		1.02	1.00	1.03			
	15	1.00	1.04	1.04	0.99	0.36	630
		1.03	0.97	0.7			
	16	1.00	1.01	1.00	0.97	0.36	610
		1.02	0.91	0.88			
	17	0.94	1.02	1.03	0.99	0.37	620
		1.03	1.02	0.91			
	18	0.93	0.97	1.02	0.99	0.37	620
		1.03	1.01	0.97			
	Average				*0.98*	*0.36*	*617*

Table A4.13. Standard deviation, Coefficient of variation and Standard error for internal stress and radius measurements for shims 250mm length

	Coating A		Coating B		Coating C	
	Radius	**Internal Stress**	**Radius**	**Internal Stress**	**Radius**	**Internal Stress**
Standard Deviation	0.01m	3.4MPa	0.08m	1.98MPa	3.7m	1.1MPa
Coefficient of Variation [%]	14.5%	16.9%	14.81%	12.41%	91.7%	92.6%
Standard Error	0.02m	1.4MPa	0.02m	0.81MPa	1.5m	0.4MPa

APPENDIX 4.6

Nano-indentor measurements for Young Modulus and Hardness with applied load value for each type of the coatings

COATING A Indent	Maximum Load [μN]	Young Modulus [GPa]	Hardness [GPa]
1	203.7	355.2	3.6
2	682.2	7.6	0.4
3	983.7	6.3	0.4
4	1290.3	6.6	0.4
5	91.5	6.3	0.4
6	579.8	6.3	0.4
7	1085.1	6.5	0.3
8	383.3	6.5	0.4
9	686.2	7.5	0.5
10	1291.9	6.9	0.4
Average	***786.1***	***6.7***	***0.4***

COATING B Indent	Maximum Load [μN]	Young Modulus [GPa]	Hardness [GPa]
1	129.7	6.8	0.3
2	185.7	7.2	0.4
3	227.3	6.2	0.3
4	265.1	5.6	0.2
5	384.1	8.5	0.4
6	413.7	2.6	0.3
7	567.9	6.6	0.3
8	644.9	13.6	0.7
9	673.1	8.9	0.3
10	714.7	5.6	0.2
11	763.1	5.3	0.3
12	930.7	8.0	0.3
Average	***524.6***	***7.1***	***0.3***

COATING C Indent	**Maximum Load [μN]**	**Young Modulus [GPa]**	**Hardness [GPa]**
1	85.1	4.0	0.3
2	132.3	4.0	0.2
3	182.7	5.6	0.3
4	222.2	3.8	0.2
5	283.3	5.5	0.4
6	304.5	2.8	0.1
7	359.4	3.1	0.2
8	397.2	2.5	0.1
9	456.1	3.4	0.2
10	80.7	3.6	0.2
11	124.3	3.1	0.2
12	184.7	5.3	0.4
13	216.8	3.2	0.2
14	280.5	5.6	0.3
15	329.4	6.2	0.3
16	367.6	3.9	0.2
17	406.1	2.9	0.2
18	444.2	2.3	0.1
19	508.5	3.5	0.2
20	563.6	4.2	0.2
21	603.1	3.1	0.2
Average	***322.4***	***3.9***	***0.2***